UNIVERSITY OF Southampton

University of Southampton Research Repository
ePrints Soton

Copyright © and Moral Rights for this thesis are retained by the author and/or other copyright owners. A copy can be downloaded for personal non-commercial research or study, without prior permission or charge. This thesis cannot be reproduced or quoted extensively from without first obtaining permission in writing from the copyright holder/s. The content must not be changed in any way or sold commercially in any format or medium without the formal permission of the copyright holders.

When referring to this work, full bibliographic details including the author, title, awarding institution and date of the thesis must be given e.g.

AUTHOR (year of submission) "Full thesis title", University of Southampton, name of the University School or Department, PhD Thesis, pagination

http://eprints.soton.ac.uk

Declaration

Except where reference is made to sources, the research presented in this thesis is original work of the author. It has not been submitted, in part or in whole, for any other degree. All figures have been reproduced with copyright permission.

University of Southampton

SYNTHESIS AND PROPERTIES OF MONO- AND BI-METALLIC COMPLEXES WITH NEUTRAL GROUP 16 DONOR LIGANDS

by Luke Paul Ollivere

A Thesis Submitted for
the Degree of Doctor of Philosophy

Department of Chemistry

March 2013

UNIVERSITY OF SOUTHAMPTON
ABSTRACT
FACULTY OF NATURAL AND ENVIROMENTAL SCIENCES
CHEMISTRY
Doctor of Philosophy

SYNTHESIS AND PROPERTIES OF MONO- AND BI-METALLIC COMPLEXES WITH NEUTRAL GROUP 16 DONOR LIGANDS

By Luke Ollivere

The novel tetradentate ligands $C(CH_2SeCH_3)_4$ and $C_6H_2(CH_2ECH_3)_4$ (E= S, Se, Te) were prepared and characterised by multinuclear NMR (^1H, $^{13}C\{^1H\}$, $^{77}Se\{^1H\}$ and $^{125}Te\{^1H\}$), IR spectroscopy, mass spectrometry, elemental analysis and in some cases single crystal X-ray diffraction. Synthesis of $C(CH_2SeCH_3)_4$ was shown to produce the cyclopropyl ligand $(CH_2)_2C(CH_2SeCH_3)_2$ and dimethyl selenide as side products. The attempted synthesis of $C(CH_2TeCH_3)_4$ yielded only $(CH_2)_2C(CH_2TeCH_3)_2$ and dimethyl telluride.

The metal carbonyl reagents $[Mo(CO)_4(nbd)]$, $[W(CO)_4(tmpa)]$ and $[Mn(CO)_5Cl]$ were reacted with a series of ligands to form both monometallic and homo-bimetallic carbonyl complexes. Monometallic species containing each of the metal centres were produced by reacting the bidentate ligands; $C_6H_4(CH_2EMe)$ (E= S, Se) and $(CH_2)_2C(CH_2EMe)_2$ (E= Se, Te) under appropriate conditions. Both monometallic and homo-bimetallic complexes were produced by reacting the metal reagents with tetradentate ligands $C(CH_2EMe)_4$ and 1,2,4,5-$C_6H_2(CH_2EMe)_4$ (E= S, Se). These compounds were characterised using multinuclear NMR (^1H, $^{13}C\{^1H\}$, ^{55}Mn, $^{77}Se\{^1H\}$ and ^{95}Mo), IR spectroscopy, APCI mass spectrometry, elemental analysis and single crystal X-ray diffraction. Crystal structures of $[Mo(CO)_4\{o\text{-}C_6H_4(CH_2SeMe)_2\}]$, $[Mo(CO)_4\{\mu\text{-}C_6H_4(CH_2SMe)_4\}Mo(CO)_4]$, $[Mo(CO)_4\{C_6H_4(CH_2SMe)_4\}]$, $[Mo(CO)_4\{C_6H_4(CH_2SeMe)_4\}]$, $[Mn(CO)_3Cl\{\mu\text{-}C_6H_4(CH_2SMe)_4\}Mn(CO)_3Cl]$, $[W(CO)_4\{C(CH_2SMe)_4\}]$, $[Mo(CO)_4\{\mu\text{-}C(CH_2SMe)_4\}Mo(CO)_4]$ and $[Mn(CO)_3Cl\{C(CH_2SMe)_4\}]$ and *fac*-$[Mn(CO_3)Cl\{(CH_2)C(CH_2TeMe)_2\}]$ have been determined. Examples of both *meso* and *DL* isomers can be seen in these structures and does not seem to be driven by ligand type or which metal centre is present. Monometallic carbonyl compounds were shown to dissociate in solution making them unsuitable for production of hetero-bimetallic species.

$\{MCl(\eta^6\text{-arene})\}^+$ (M= Ru, Os) fragments were shown to form stable monometallic and homo-bimetallic complexes when reacted with the tetradentate ligands $C(CH_2EMe)_4$ and $C_6H_2(CH_2EMe)$ (E= S, Se). $[\{OsCl(\eta^6\text{-}p\text{-cymene})\}_2\{\kappa^2\kappa'^2\text{-}C(CH_2EMe)_4\}]^{2+}$ (E= S/Se) showed slow pyramidal inversion, as evidenced by multinuclear NMR studies, with individual invertomers being observed. The distribution of each invertomer was unequal, with the dominant form being *meso*. Crystal structures of $[RuCl(\eta^6\text{-}p\text{-cymene})\{\kappa^2\text{-}C(CH_2EMe)_4\}][PF_6]$, $[RuCl(\eta^6\text{-}p\text{-cymene})\{\kappa^2\text{-}1,2,4,5\text{-}C_6H_2(CH_2SMe)_4\}][BPh_4]$, $[RuCl(\eta^6\text{-}p\text{-cymene})\{\kappa^2\text{-}1,2,4,5\text{-}C_6H_2(CH_2SeMe)_4\}][BPh_4]$, $[\{RuCl(\eta^6\text{-}p\text{-cymene})\}_2\{\kappa^2\kappa'^2\text{-}1,2,4,5\text{-}C_6H_2(CH_2SMe)_4\}][PF_6]_2$ and $[\{RuCl(\eta^6\text{-}p\text{-cymene})\}\{(CH_2)_2C(CH_2SMe)_4\}][PF_6]_2$ have been determined. In each case the EMe groups were present as a *meso* invertomer with both methyl groups directed away from the arene ligand. A monometallic osmium complex was shown to be a suitable starting material for production of the hetero-bimetallic compound, $[\{OsCl(\eta^6\text{-}p\text{-cymene})\}\{PtCl_2\}\{\kappa^2,\kappa'^2\text{-}C(CH_2SeMe)_4\}][PF_6]$.

A series of Group 13 complexes were produced by reacting $GaCl_3$ and $InCl_3$ with $C_6H_4(CH_2SMe)_4$, $C_6H_4(CH_2SEt)$, $(CH_2)_2C(CH_2EMe)_2$ (E= Se, Te), $C(CH_2EMe)_4$ and 1,2,4,5-$C_6H_2(CH_2EMe)_4$ (E= S, Se). $GaCl_3$ formed compounds with tetrahedral geometry, $InCl_3$ produced compounds with octahedral geometries and variable stoichiometries. $[(GaCl_3)_2o\text{-}C_6H_4(SMe)_2]$ undergoes further reaction in solution yielding $[o\text{-}C_6H_4(SMeCH_2Cl)_2][GaCl_4]_2$. Crystal structures of $[o\text{-}C_6H_4(SMeCH_2Cl)_2][GaCl_4]_2$, $[(GaCl_3)_2\{o\text{-}C_6H_4(CH_2SEt)_2\}_3]$, $[(InCl_3)_4\{o\text{-}C_6H_4(CH_2SEt)_2\}_3]$ have been determined.

Acknowledgements

I would like to thank Prof. Gillian Reid for all her constant support, advice and time she has willingly given up during my write up and lab time. I am also very grateful Prof. William Levason who has given up considerable amounts of time over the past few years, always providing guidance and useful insights. Acknowledgements must also go to Dr. Mark Light and Dr. Mike Webster for support and guidance when modelling tricky crystallographic data. I also owe thanks to Prof. William Levason and Prof. Gillian Reid for obtaining multinuclear NMR data. The EPSRC must also be acknowledged for the funding of this project.

I would also like to thank the entire Levason and Reid research group past and present in particular I'd like to mention Dr. Zhang for advice with problematic crystals and generally making my time in the lab very enjoyable. I am also grateful Dr. Jolleys for all the proof reading and putting me up during my write up.

I also owe a extra big thank you to JJ for all her advice during the formatting and generally putting up with me during my write up. I should also mention my friends Keith, Kim, Lewis, Frank, Chris and Julian for all there support and encouragement.

Finally I'd like to thank my parents for everything over the past few years, I couldn't have done it without you.

Contents

CHAPTER 6: Synthesis and characterisation of gallium(III) and indium(III) chloride complexes with geometrically constrained thio- and seleno-ether ligands

List of figures

CHAPTER 1

CHAPTER 2

CHAPTER 3

CHAPTER 4

CHAPTER 5

CHAPTER 6

List of tables

CHAPTER 1

CHAPTER 2

CHAPTER 3

CHAPTER 4

CHAPTER 5

CHAPTER 6

List of abbreviations

Substituent Groups

Me	Methyl
Et	Ethyl
Ph	Phenyl
^{n}Bu	n-Butyl
R	Alkyl or aryl
Cp	cyclopentadienyl

Solvents

EtOH	Ethanol
MeOH	Methanol
thf	Tetrahydrofuran
Et_2O	Diethyl ether
MeCN	Acetonitrile

Techniques

IR	Infrared
NMR	Nuclear Magnetic Resonance
ES^+	Electrospray Mass Spectrometry
APCI	Atmospheric Pressure Chemical Ionisation

Spectroscopy

sh	shoulder
s	strong
m	medium

w	weak
br	broad
Hz	Hertz
δ	Chemical shift (in parts per million, ppm)
J	Coupling constant
m	Multiplet
s	Singlet
d	Doublet

Miscellaneous

nbd	Norbornadiene, bicycle[2.2.1]hepta-2,5-diene
TMPA	N,N,N’,N’-Tetramethyl-1,3-propanediamine
mmol	Millimoles
[8]aneSe_2	1,5-diselenacyclooctane
[14]aneS_4	1,4,8,11-tetrathiacyclododecane
[16]aneS_4	1,5,9,13-tetrathiacyclohexadecane
[16]aneSe_4	1,5,9,13-tetraselenacyclohexadecane

CHAPTER 1

Introduction

1.1 Coordination chemistry and hetero bimetallic complexes

Hetero bimetallic complexes are compounds containing two different metal centres, and are of interest in many areas of chemistry. Mixed metal species have many practical applications; however, production of bimetallic compounds such as these is rarely straightforward.

Bimetallic complexes have many applications in many different areas of chemistry including mixed metal catalysts, metalloenzyme models, molecular magnets and as reagents for producing alloys. The behaviour of these complexes is determined by the combination of metal atoms, the structure of the ligand and donor atom types.[1] A wide range of mixed metal compounds have been reported for their catalytic activity.[2-6]

Mixed metal catalysts have different electronic and chemicals properties when compared to monometallic materials often having better selectivity, activity and stability. During the 1960's bimetallic catalysts gained commercial interest in the hydrocarbon industry as they displayed far greater activities than monometallic catalysts.[7] These findings prompted extensiveresearch into synthesis of bimetallic compounds and possible applications . Currently bimetallic catalysts are used in many catalytic and electrocatalytic processes[8] such as hydrodesulfurisation and hydrogenation.[9-11]

1.2 Hydrodesulfurisation

Hydrodesulfurisation (removal of sulfur compounds from hydrocarbon fuel stocks) is one of the key chemical processes in the petroleum industry. Transition metal bimetallic catalysts have been extensively studied for several decades for removal of organo-sulfur compounds.[12-14]

Upon fuel combustion sulfur compounds produce noxious sulfur oxides which are considered to be a major cause of air pollution. Currently molybdenum sulfide-based heterogeneous catalysts often with cobalt or nickel promoters are used.[15] These catalysts remove most thiophenes, benzothiophenes and dibenzothiophenes however; removal of their derivatives still remains a challenge. Improving the current industrial catalysts

requires increased efficiency of removal of these problematic compounds which has led to increased commercial interest into new catalytic systems for hydrodesulfurisation.[16-18]

Many mixed metal sulfide compounds have been investigated to provide further insight into the C–S bond activation and cleavage of organosulfur compounds present during the catalytic process.[15, 17]

1.3 Metalloenzymes and bimetallic biological molecules

Many bioorganometallic enzymes that perform essential reactions in nature contain bimetallic active sites. While these reactions have been replicated in chemical industry most methods are not as efficient or environmentally friendly as the equivalent reactions in nature. Most of these reactions are catalysed with enzymes containing bimetallic active sites. Some examples of such enzymes can be seen in the reversible oxidation of dihydrogen and the reduction of nitrogen to ammonia both of which are essential reaction in nature.

The reduction of nitrogen to ammonia is catalysed by nitrogenase enzymes. All nitrogenases enzymes contain iron and sulfur clusters as well as a hetero metallic active site such as FeMoCo.[19] Oxidation of dihydrogen is catalysed by [NiFe] hydrogenase enzyme which contains several metallic sites such as Ni-Fe, Fe-Fe and Fe/S clusters this allows the enzyme to pass through various oxidation states during the reaction.[20]

Chemical industry cannot replicate these reactions as efficiently as enzymes consequently, this is an area of great interest in chemical research.[19, 20] Modelling the active site and synthetically producing chemically similar hetero metallic compounds may help understanding of these processes and led to production of more efficient catalysts.

Most of the industrial methods for production of mixed metal catalysts require synthesis of hetero bimetallic precursors in high purity however; synthesis of mixed metal complexes is often problematic. This thesis aims to develop new synthetic routes for production of hetero bimetallic complexes with Group 16 ligands, which could be used as metal precursors in production of mixed metal catalysts.

1.4 Synthesis of hetero-bimetallic complexes

Synthesis of hetero-bimetallic complexes is still a relatively new area of chemistry.[21] Most early reports of hetero-bimetallics were complexes containing two metal atoms bridged *via* a halide atom[21] or containing a cluster of two metals.[22, 23] An example of a ruthenium and molybdenum containing hetero-bimetallic molecule is shown below in figure 1.1.

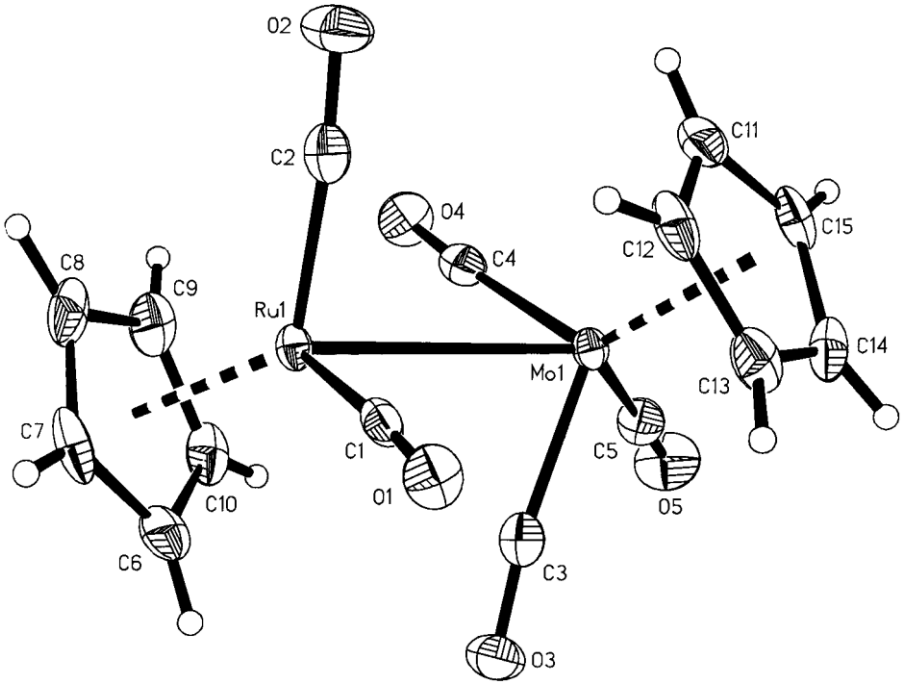

Figure 1.1 Structure of $[Cp(CO)_3Mo\text{-}Ru(CO)_2Cp]$.[24]

The structure of $[Cp(CO)_3Mo\text{-}Ru(CO)_2Cp]$ contains a ruthenium atom bonded directly to a molybdenum atom. Several similar examples of ruthenium/tungsten and ruthenium/chromium mixed metal species have also been isolated and characterised.[2, 25, 26]

Although these types of mixed metal compounds have been successfully produced, the synthesis often requires chromatographic separation and purification steps leading to low yields. These compounds have also been shown to be highly susceptible to cleavage at the metal-metal bond when exposed to UV light, oxygen and halides.[24]

Examples of complexes with two metal centres linked *via* an organic framework are less common than halide bridged complexes, however, some systems have been studied.[27, 28] A variety of mixed metal manganese carbonyl complexes, with ruthenium, iron, osmium and rhenium linked *via* various arene ligands have been produced and characterised.[27] The structure of a manganese carbonyl and ruthenium complex is shown below.

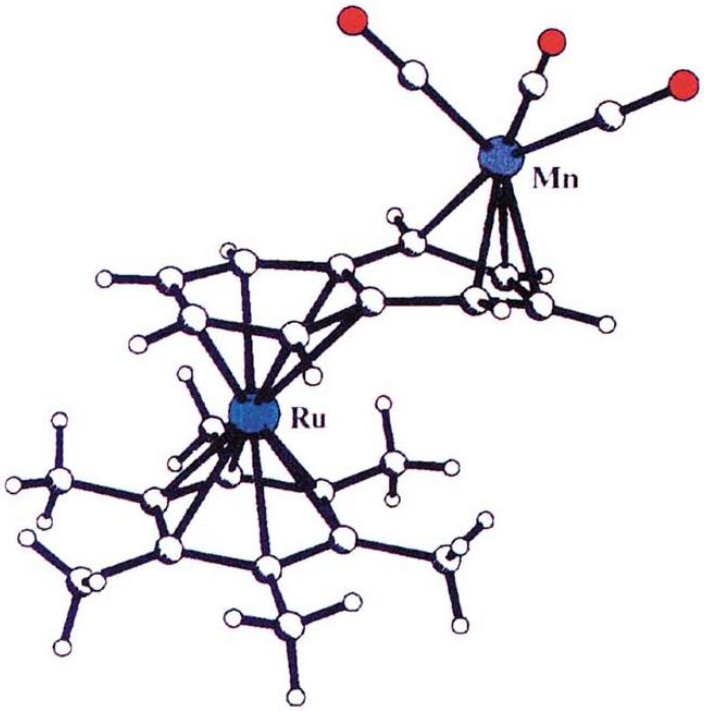

Figure 1.2 Structure of $[(C_{12}H_{18})Ru\ (C_{10}H_8)Mn(CO)_3]^+$ cation.[27]

These arene-manganese carbonyl complexes have been studied extensively, often the synthetic routes produce stable compounds in good yields. Anti-facial bimetallic complexes (shown in figure 1.2) are highly polar; a characteristic that could be applied to several different areas of chemistry. Sulfur containing mixed metal species have also been produced by reducing a sulfur/ruthenium complex in the presence of a manganese tricarbonyl reagent.[27]

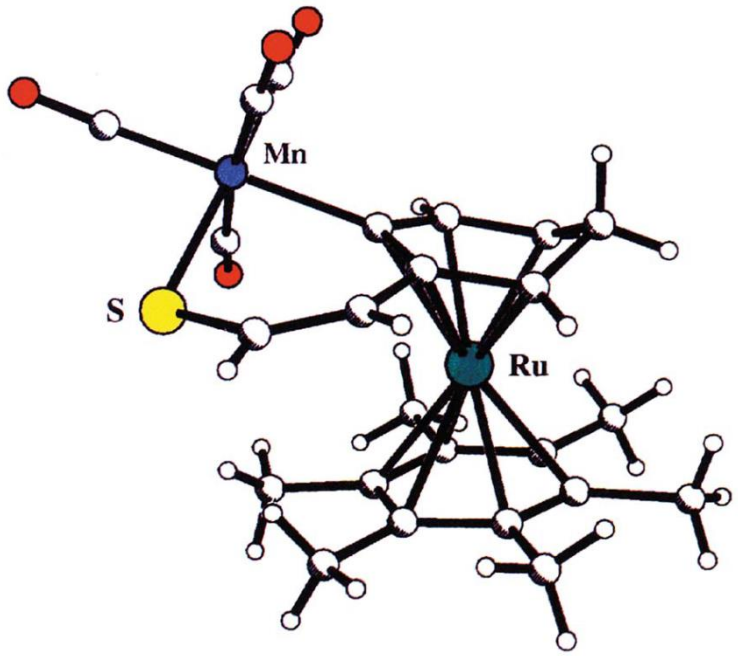

Figure 1.3 Structure of a sulfur containing heterobimetallic complex.[27]

Although this synthetic route has produced a hetero-bimetallic complex containing a Group 16 atom, the method is not suitable for producing compounds containing selenium or tellurium.

Another example of hetero-bimetallic complexes linked *via* an organic ligand report several molybdenum/tungsten complexes linked *via* bidentate alkyl- and arylamide ligands.[28] These complexes were prepared by first synthesising and purifying the monometallic complexes before reacting with a second different metal precursor. This approach could be modified to incorporate multi-dentate ligands with different donor atoms.

Complexes containing group 16 ligands, linking two different metals are uncommon, producing a bimetallic complex requires careful choice of conditions and reagents.

1.5 Chalogenoether ligands and transition metal complexes

In order to produce a hetero bimetallic species the metal centres must be introduced stepwise. The first reaction produces a monometallic species, leaving two uncoordinated donor atoms available for the second reaction. These considerations must be taken into

account when selecting appropriate ligands. The ligands used must be symmetrical and tetradentate, with two donors available for each reaction. Each ligand must also have a semi rigid organic backbone to prevent more than two donor atoms chelating to each metal centre at any one time. With these considerations in mind two ligand frameworks were chosen.

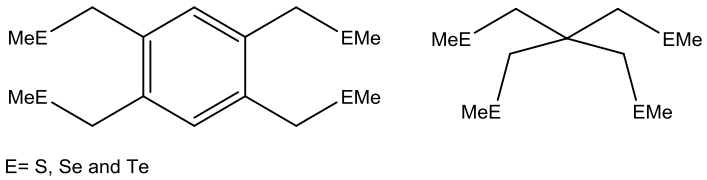

Figure 1.4 Chalogenoether ligands.

Synthesis of thio- seleno- and telluro-ethers of both the ligand types in figure 1.4 were attempted however, $C(CH_2TeCH_3)_4$ was not isolated, full details are given in Chapter 2.

Experimental conditions for production of these ligands were based on similar ligands previously reported.[29-31] Thioether ligands have been well established with many examples available in the literature. Fewer selenoether ligands have been discussed however, several examples of similar ligands could be found to determine experimental conditions.[29] Even fewer telluroether ligands can be found in the literature presumably due to the sensitivity of the ligands making isolation of pure product difficult.[31]

Several thioether ligands similar to the tetrabenzyl compound; $1,2,4,5\text{-}C_6H_2(CH_2SCH_3)_4$ shown in figure 1.4 have been reported.[32] Ligands such 1,2,4,5-tetrakis(2-pyridylsulfanylmethyl)benzene were produced from reacting 1,2,4,5-tetrakis(bromomethyl)benzene with 2-mercaptopyridine in acetonitrile.[32] Each of the ligands were produced in moderate yields and high purity; the structure of 1,2,4,5-tetrakis(2-pyridylsulfanylmethyl)benzene is shown below.

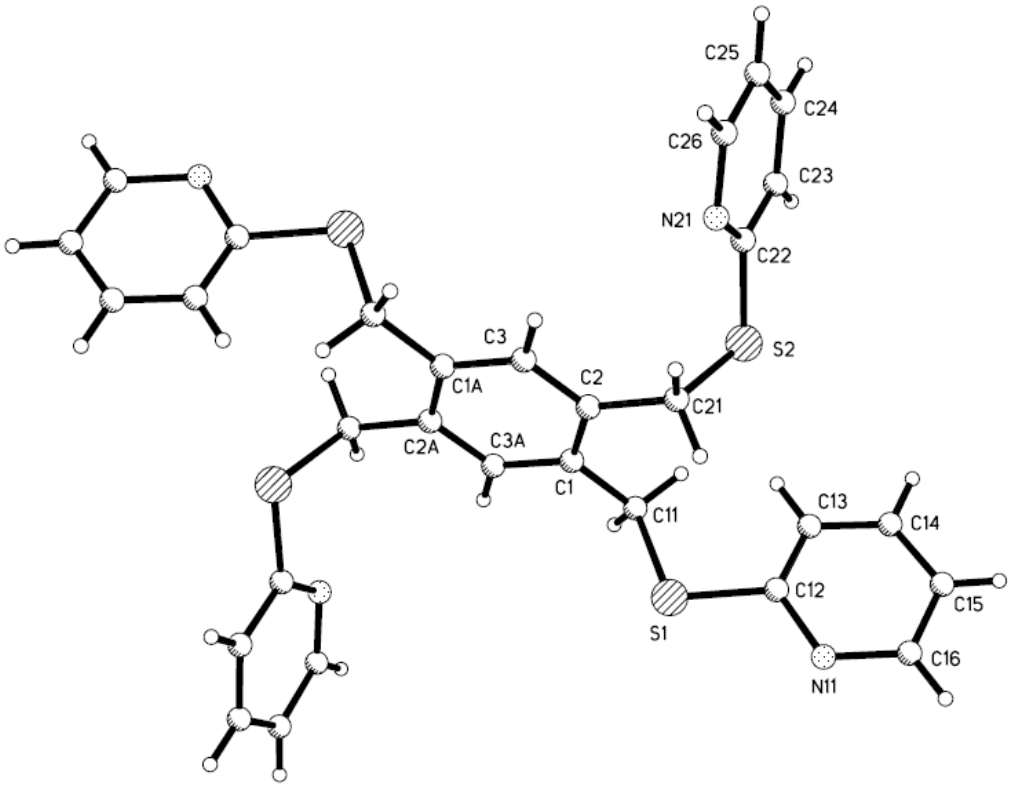

Figure 1.5 Structure of 1,2,4,5-tetrakis(2-pyridylsulfanylmethyl)benzene.[32]

Ligands with a similar structure to 1,2,4,5-$C_6H_2(CH_2SCH_3)_4$ have been shown to form complexes with a variety of transition metals.[11, 33, 34] Examples of complexes containing the spirocyclic ligand, $C(CH_2ECH_3)_4$, have not been reported, consequently, simpler ligand systems must be considered when predicting behaviour of these complexes.

A number of thioether compounds with simple bidentate ligands have been reported, such as, $[W(CO)_4\{CH_3S(CH_2)_2SCH_3\}]$[35] and $[Mo(CO)_4\{CH_3S(CH_2)_2SCH_3\}]$.[35] Although slightly simpler ligand systems these preparations were used when determining experimental conditions producing molybdenum and tungsten carbonyl complexes. Ruthenium(II) has also been shown to form the thioether complexes $[RuCl_2\{o\text{-}C_6H_4(CH_2SCH_3)_2\}_2]$ and $[\{RuCl_2(p\text{-cymene})\}_2\{\mu\text{-}o\text{-}C_6H_4\text{-}(CH_2SCH_3)_2\}]$ with octahedral and distorted tetrahedral geometry, respectively.[29]

The selenoether complexes, $[Mn(CO)_3Cl\{CH_3Se(CH_2)_2SeCH_3\}]$[36] and $[W(CO)_4\{CH_3Se(CH_2)_2SeCH_3\}]$[35] have been reported and the preparations considered during experimental procedures. Similar macrocyclic complexes such as

$[MnBr(CO)_3([8]aneSe_2]$ and $[W(CO)_4([8]aneSe_2]$ have also been discussed and characterised.[37]

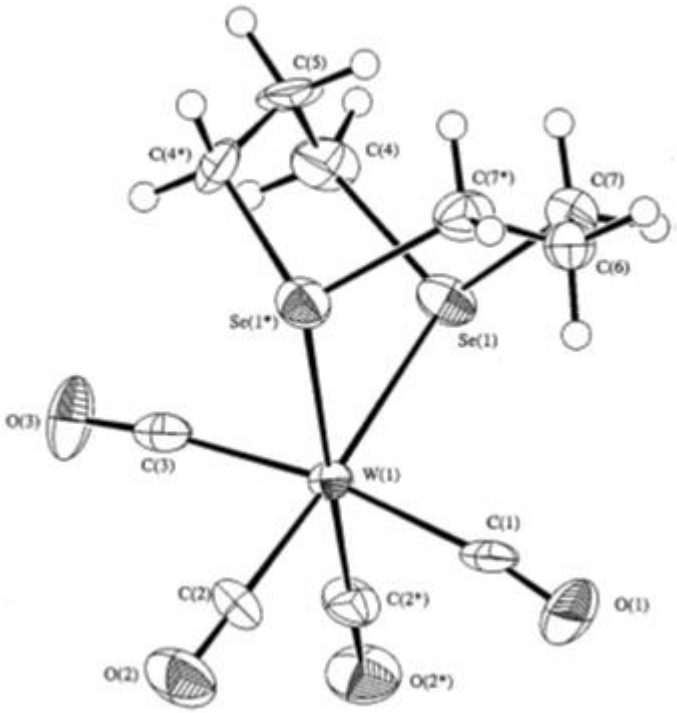

Figure 1.6 Structure of $[W(CO)_4([8]aneSe_2]$[37]

Telluroethers such as $[Mo(CO)_4\{CH_3Te(CH_2)_2TeCH_3\}]$[35], $[W(CO)_4\{o\text{-}C_6H_4(CH_2TeCH_3)\}]$[38] and $[Mn(CO)_3Cl\{o\text{-}C_6H_4(CH_2TeCH_3)\}]$[38] have been reported and structurally characterised see figure 1.7.

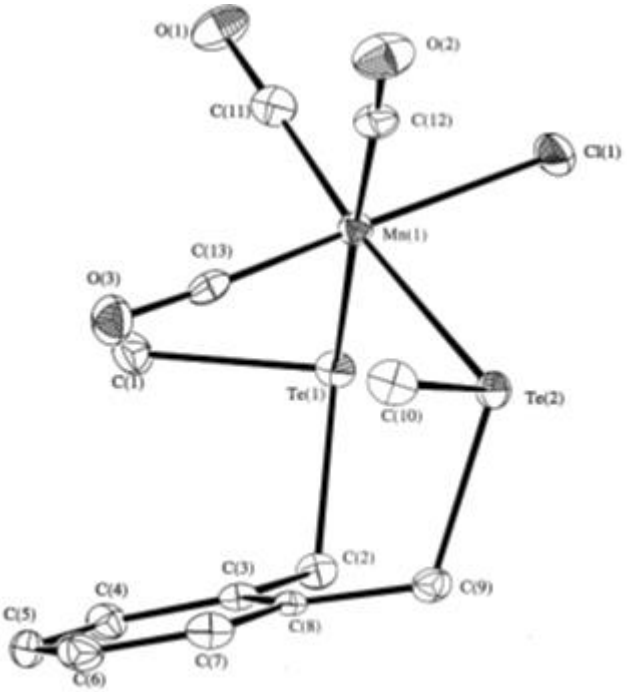

Figure 1.7 Structure of $[Mn(CO)_3Cl\{o\text{-}C_6H_4(CH_2TeCH_3)\}]$[38]

Each of the compounds discussed above either provided spectroscopic data for comparison or were used when determining experimental conditions.

1.6 Metal ligand bonding

Chalcogenoether ligands are defined as Group 16 atoms bonded to two carbon atoms.[29] Group 16 elements have the ground state electronic configuration $ns^2\ np^4\ nd^0$, two electrons are used to bond to alkyl groups leaving four electrons in the non-bonding orbitals.

Thioethers contain sp^3 hybridised sulfur atoms with two lone pairs available to form covalent bonds to metal atoms. If only one pair forms an M-S bond then the non-bonded lone pair can affect the M-S bond in several ways; it could weaken the M-S bond by causing stereoelectronic repulsion with the electron-rich metal center hence weakening the overall bond. A second possibility is that the remaining lone pair could form a σ-bond to a second metal center, producing a bridged complex. Finally, if sulfur is bonding with an early (electron poor) transition metal with free d-orbitals then it is

possible that the second lone pair participates in π-donation from a p-orbital, consequently re-hybridising sulfur to sp^2.

The metal to ligand π-acceptor system of Group 15 ligands proposed by Chatt can be applied to chalcogens, with vacant d-orbitals of appropriate energy and correct symmetry. Similarly, the Orpen-Connelly model could be applied using the E-C σ^* orbitals.[39] Applying the Chatt model however, utilises high energy empty d-orbitals on the chalcogenoether consequently, the Orpen-Connelly model is favoured.

Most previous research of chalcogenoethers has concentrated on transition metal complexes; some main group systems have been studied but are not as common.[40] Metal ligand bond strengths depend on the size and electronegativity of the donor atoms, electronegativity decreases and orbital size increases down the Group so it is natural to assume that the metal ligand bond strength decreases down the group; M-S > M-Se > M-Te. This assumption however, has been shown to be incorrect. Molecular orbital calculations based on a series of ligand exchange experiments by Schumann proposed that M-E bond strengths increase down Group 16, M-Te > M-Se > M-S where M is a low valent transition metal, this can be attributed to decreasing electronegativity of donor atoms down the group causing increased σ-donation. During later work, investigating transition metal carbonyl species, measurements of ν(CO) force constants and $^{77}Se/^{125}Te$ NMR coordination shifts, confirmed Schumann's proposal.[35, 41-43] However, data collected from transition metal halide complexes, show the order of M-E bond strengths to be M-Se > M-Te > M-S, suggesting the order of donor ability for Group 16 ligands is dependent on the metal and oxidation state.[44] Increasing oxidation state causes metals to harden and orbitals contract. Consequently, soft telluroethers are unable to bind to metals with a medium or high oxidation. This is evident from there being many reported thio- and selenoether complexes with Pt(IV), Ru(III), and Os(IV) and no examples of telluroethers available.[40]

Donor strength in Group 16 varies according to the metal acceptor, when interacting with low valent metal centres the order is S > Se > Te however, in case of high or medium oxidation state metals the order is changed to Se > S > Te. This behaviour is not seen is Group 15 where donation always appears to be P > As > Sb.

1.7 Pyramidal inversion

A chalcogenoether bonded to a metal using one lone pair adopts a pseudo tetrahedral geometry. For the κ^2 coordinated ligand fragments discussed in Chapters 3, 4 and 5 the possible invertomers are shown below in figure 1.8.

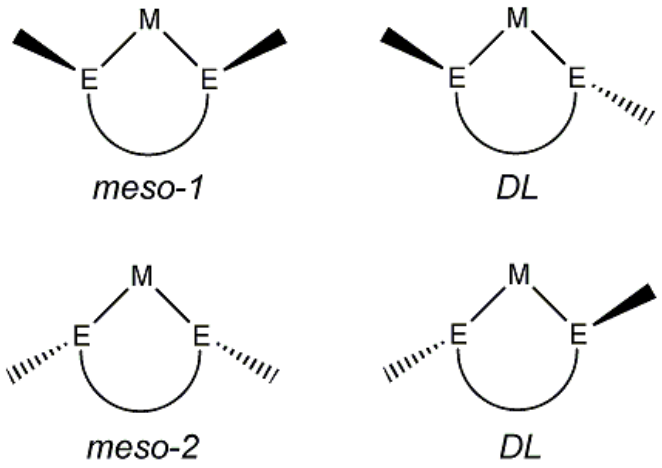

Figure 1.8 The four possible conformations for bi-dentate chalcogenoethers bound to a metal.

X-ray diffraction studies show chalcogen atoms present in a pyramidal environment when coordinated. Assuming sulfur, selenium and tellurium adopt this geometry then the bond angles will be approximately tetrahedral, with a sp^3 electron lone pair. Consequently, there is a potential for all coordinated chalcogen atoms discussed in this thesis to undergo an inversion process.

Typically inversion is studied by NMR spectroscopic methods.[45] When a metal complex is inverting "fast" on the NMR timescale, an averaged resonance is observed. In "slow" inverting systems, separate resonances may be observed for each invertomer.[46] In order to understand the factors affecting the rate of inversion, energy barriers are measured by microwave techniques.[45] These values can allow the comparison different complexes while varying the donor type, metal center and ligand structure.

Several factors are known to affect the inversion process of complexes. These are often mutually counteracting effects making prediction of behavior complicated. The presence of different donor atoms affects the inversion energy, the energy barrier increases down

Group 16, Te > Se > S.[47] This effect is demonstrated when comparing the coalescence temperatures of different platinum containing complexes.[45]

trans-$[PtI_2(SEt_2)_2]$	275 K
trans-$[PtI_2(SeEt_2)_2]$	363 K
trans-$[PtI_2(TeEt_2)_2]$	378 K

Coalescence temperature is the temperature at which the observed peaks for *meso* and *DL* forms have merged in one average resonance.

Coordination of different metal centres also affects the energy barrier for inversion, the introduction of a metal will lower a chalcogen atoms inversion energy. Presence of a metal will decrease the *s* character of the lone pair ground state, due to the electropositive nature of the metal atom. Consequently, less energy is required to allow the lone pair to the transition state. Metal atoms also reduce the energy barrier of inversion by stabilizing the planar transition state due to (*p-d*)π conjugation. The induction of different metal centers to Group 16 compounds has been shown to greatly decrease the energy barrier for inversion. The lower energy barriers in these complexes is most likely due electronegativity of the metals. This effect can be seen by comparing series of chromium, molybdenum and tungsten compounds with the same selenoether ligand. The inversion energies recorded the complexes follow the variations shown in electronegativity.

Compound	**Inversion Energy $\Delta G^{\ddagger}$/ kJ mole^{-1}**	**Allred-Rochow Metal Electronegativity**
$[Cr(CO)_4\{CH_3SeCH_2C(CH_3)_2CH_2SeCH_3\}]$	61.6	1.56
$[Mo(CO)_4\{CH_3SeCH_2C(CH_3)_2CH_2SeCH_3\}]$	56.6	1.30
$[W(CO)_4\{CH_3SeCH_2C(CH_3)_2CH_2SeCH_3\}]$	62.9	1.40

Table 1.1 Inversion energies for analogues compound of Cr, Mo and W.[45]

Ligand structure has also been shown to affect the activation energy in two ways. Firstly the presence unsaturated carbon atoms reduces the inversion energy, the less saturated the ligand lower the inversion energy required.[48] Secondly ligand ring size, the greater the chelate ring size the lower the inversion energy; six-membered chelate rings require 5-15 kJ mole^{-1} less energy than the corresponding five-membered ring.[45]

The final factor contributing to differences in inversion energy is the *trans* influence. Studies have shown the presence of less electronegative substituents *trans* to the chalcogen atom lowers the activation energy.[45]

This study did not set out to investigate the pyramidal inversion process which is well understood and has been previously discussed in detail.[45] However, the consequences of different inversion rates are evident in the NMR data.

1.8 Characterisation techniques

Multinuclear NMR spectroscopy (^{1}H, ^{13}C{^{1}H}, ^{55}Mn, ^{71}Ga,^{77}Se{^{1}H}, ^{95}Mo,^{125}Te{^{1}H} and ^{195}Pt) has been used extensively to characterise the compounds described in this research.

Nucleide	Spin I	Natural abundance A (%)	Receptivity R^c	Frequency Ξ (MHz)*	Nuclear electric quadrupole moment Q (10^{-28} m^2)
^{1}H	1/2	99.99	5.67×10^{3}	100	-
^{13}C	1/2	1.11	1.00	25.14	-
^{33}S	3/2	0.76	0.097	7.67	-6.4×10^{-2}
^{55}Mn	5/2	100	9.94×10^{2}	24.67	0.40
^{71}Ga	3/2	39.60	3.22×10^{2}	3.49	0.11
^{77}Se	1/2	7.58	3.02	19.07	-
^{95}Mo	5/2	15.72	2.92	6.52	-0.015
^{99}Ru	5/2	12.72	0.815	4.61	7.6×10^{-2u}
^{115}In	9/2	95.72	1.92×10^{3}	22.04	0.86
^{125}Te	1/2	6.99	12.8	31.54	-
^{183}W	1/2	14.40	5.89×10^{-2}	4.16	-
^{187}Os	1/2	1.64	1.15×10^{-3}	2.28	-
^{195}Pt	1/2	33.80	19.9	21.50	-

* Resonance frequency for nucleus in a magnetic field such that the protons in TMS resonate at exactly 100 MHz.

Table 1.2 List of possible NMR nuclei.

Receptivity or R can be used to compare different nuclei. It is defined as a product of the natural abundance and the sensitivity at a constant field. This value is commonly compared to the receptivity of carbon-13, to give R^c. Comparing values of R^c allows an assessment of different nucleide sensitivity.

$$R^c = |\gamma^3| AI(I+1)/(\gamma_c{}^3 A_c 3/4)$$

Equation 1.1 γ = magnetogyric ratio, I = Spin, A= Natural abundance.[49]

R^c provides a helpful method for comparing different nuclei however, it is less useful when considering quadrupolar nuclei ($I > 1/2$) due line broadening.

Depending on the nuclei studied, the chemical shifts (δ in ppm) are reported relative to a standard reference chemical. Each chemical shift is related to the difference in shielding between the reference and sample, the equation for calculating chemical shift is show in equation 1.2, individual references for each nuclei are discussed below. Coordination shift refers to the difference in chemical shift after free ligand has formed a complex.

$$\delta = (\nu_{sample} - \nu_{reference}) / \text{oscillator frequency (Hz)} \times 10^6$$

Equation 1.2 δ = chemical shift, ν = frequency.

For any nuclei with spin = 1/2, the number of peaks produced by spin spin couplings can be given by the equation.

$$\text{No. of peaks} = 2nI+1$$

Equation 1.3 n = number of equivalent nuclei being coupled, I = spin.

The number of peaks observed can be expressed in a diagram similar to Pascals triangle (see figure 1.9) the values on each row denote the area under each peak, so when n = 2 the values 1 2 1 would be displayed as a triplet; three peaks with the middle peak twice the size of the other two.

n	*I* = ½									
0					1					
1				1		1				
2			1		2		1			
3		1		3		3		1		
4	1		4		6		4		1	

Figure 1.9 Number of resonances where *I*= 1/2

Nuclei with spin greater than half are treated the same; however using equation 1.3 with these values produces very complicated spectra.

n	*I* = 1							
0				1				
1			1	1	1			
2		1	2	3	2	1		
3	1	3	6	7	6	3	1	

Figure 1.10 Number of resonances where *I*= 3/2

Nuclei with spin greater than 1/2 are considered quadrupolar. These nuclei have an ellipsoidal distribution of charge which is measured as electric quadrupole moment or Q (a measurement of the cross section of the nucleus), values for Q are detailed in table 1.2. Positive values for Q show the nucleus lengthening in the direction of its spin angular momentum and negative values show the nucleus flattening. The unit for Q is 10^{-28} m^2 = 1 barn.

Quadrupolar nuclei with *I*= *n*/2 produce magnetic and electric fields, asymmetry of distribution in charge within a nucleus causes molecules to have an electric field gradient (*efg*), the energy of a quadrupolar nucleus is determined from the orientation of the efg.

When a molecule is placed in a magnetic field so that the nuclear spin is quantised along the magnetic field direction rather than the efg symmetry axis, the nuclear magnetic energy levels depend on both the efg and the applied field. Changes in the efg, due to molecular

motion in solution produce transitions to different excited states known as quadrupolar relaxation. Short relaxation times leads to line broadening, long relaxation times can lead to time consuming data collection.

As NMR data is collected from a series of repeat scans equilibrium must be reached before the next scan otherwise the data will be unusable. Equally if the relaxation time is too short, then the solution must be cooled to prevent the resonances broadening out of existence.

The relaxation processes is an exponential relationship between the number of excited nuclei compared to the number at thermal equilibrium, the number of excited nuclei can be expressed as:

$$n_t = n_0 \exp(-t / T)$$

n = Excess of excited nuclei
t = Time after excitation
T = Time constant specific to this system

Equation 1.4 Number of excited nuclei at time t, where $n = n_0$ at $t = 0$.

As T is a constant specific to individual systems, the relaxation rate of the system can be considered as T^{-1}.

The spin lattice relaxation time (T_1), is the rate at which magnetisation in the direction of the applied field (z plane) returns to equilibrium after excitation. T_1 can therefore be considered to be longitudinal relaxation time. Transverse relaxation time (T_2) is defined as the rate at which magnetisation is lost in the xy plane. The relationship between T_2 and line broadening can be expressed as:

$$W_{1/2} = 1/\pi T_2$$

$W_{1/2}$= line width at half height

Equation 1.5 Relationship of line width and T_2.

By measuring $W_{1/2}$ a value for T_2 can be obtained for a particular system.

There are several possible nuclei with *I*= 1/2 that could be studied during this research some more suitable than others. ^{1}H and ^{13}C{^{1}H} NMR measurements were routinely performed on all soluble compounds, ^{77}Se, ^{125}Te and ^{195}Pt measurements however required more specialist sample preparation and data collection.

The ^{77}Se nucleus has *I*= 1/2 and a sensitivity better than ^{13}C nucleus, these attributes make it ideal for studying the selenoether complexes. It has been studied extensively and a comprehensive range of δ (^{77}Se) values has been established for both ligands and complexes. Coordination shifts are easily recognisable with some as large as 50 ppm. Chemical shifts are typically referenced to neat dimethylselenide.[49]

^{125}Te nucleus also has *I*= 1/2 and better sensitivity than ^{13}C nucleus, it shows large coordination shifts sometimes >100 ppm and was used where possible to characterise complexes. Chemical shifts are referenced to neat dimethyltelluride.[49]

^{183}W NMR measurements were not implemented during this study although the nucleus has *I*= 1/2, but a low resonance frequency and poor receptivity make it unsuitable. The tungsten carbonyl systems discussed in chapter 3 also have very long the relaxation times, making routine study of this nucleus, especially in compounds of modest solubility and high M.Wt. a very time consuming process.

^{195}Pt nucleus has *I*= 1/2 and a lot better sensitivity than other nuclei with *I*= 1/2 discussed in this chapter, and a large range of chemical shifts. This is typically indicative of the oxidation state of the Pt centre, donor set and geometry. Coupling to other active nuclei such as ^{77}Se is often observed in the spectrum. Chemical shifts are referenced to 1 mol dm^{-3} $Na_2[PtCl_6]$ in D_2O.[49]

^{187}Os nucleus has low natural abundance and poor receptivity making it highly unsuitable for study.

^{33}S, ^{55}Mn, ^{71}Ga, ^{95}Mo, ^{99}Ru and ^{115}In all have *I*> 1/2 and as a consequence it is more challenging to record spectra from these nuclei.

^{33}S nucleus is a naturally occurring isotope (*I*= 3/2) however, the very low natural abundance and poor receptivity (R^{c}) makes it unsuitable for study.

^{55}Mn nucleus has *I*= 5/2, is inherently highly sensitive, but as a consequence of the moderate quadrupole moment resonances may not be observable in low symmetry environments due to fast quadrupolar relaxation (extreme line broadening). For the same reason, spin-spin couplings to other nuclei are very rarely observed. Broad peaks with poor signal to noise are often observed and consequently data collection can be a very time consuming process. The accepted zero reference ($\delta = 0$) is external $KMnO_4$ in water.[49]

^{71}Ga NMR mesurements were collected where possible – again the quadrupolar nucleus meant data collect often contained broad peaks, Chemical shifts are referenced to $[Ga(H_2O)_6]^{3+}$.[49]

^{95}Mo nucleus has *I*= 5/2 and was used to study all molybdenum containing species. It has small quadrupole moment, a very wide chemical shift range and usually produced relatively sharp resonances. $[MoO_4]^{2-}$ in water at pH = 11 is the accepted zero reference.[49]

^{115}In nucleus is unsuitable for study in high symmetry enviroments due a large quadrupole moment.

Single crystal X-ray diffraction

X-ray crystallography was applied where possible on all crystalline products collected. The additional structural data collected such as bond angles and lengths was vital in order to fully characterise a complex. Although it provides information not available from other techniques, several factors must be considered when discussing this data. Firstly only a single crystal is analysed, the bulk of the sample may contain several products or unreacted starting materials. Secondly the sample must form a single crystal, some products discussed in this research had low melting points, others were too sensitive and decomposed before a single crystal could be isolated. Finally X-ray diffraction relies scattering of X-ray by electrons hence, heavier atoms containing lots of electrons are more readly located. Consequently, when considering a compound containing heavy elements such as tungsten or osmium the diffraction of lighter atoms is less well defined. Although providing unique structural data other techniques must be performed in conjunction when analysing a product.

Vibrational spectroscopy

Infra-red spectroscopy was routinely used throughout this research to provide evidence for the identity of products. Metal carbonyl complexes show strong absorptions at high frequency ~2000cm^{-1}; solution IR spectroscopy also allowed reactions to be monitored, as well as determining the geometry of the metal centre *via* application of group theory.

The use of solution IR spectroscopy was fundamental to the characterisation of carbonyl containing compounds as it allowed the products to be monitored throughout a reaction. The tetracarbonyl complexes *cis*-[M(CO)$_4${L}] (M = Mo, W, L = Ligand) which have local C_{2v} symmetry, are predicted to exhibit four IR active CO stretching vibrations ($2A_1 + B_1 + B_2$).

For tricarbonyl complexes [Mn(CO)$_3$Cl{L}] assuming *fac* coordination, each complex will have a C_s local symmetry. Each compound is predicted to show three strong absorptions (A' + 2A").

Raman spectroscopy provided structural information during characterisation of gallium and indium complexes. The number of vibrational modes can be determined *via* group theory however, different selection rules exist in Raman spectroscopy compared to Infra-red. Consequently, vibrational modes can be; only Raman active, only IR active or both.

Mass spectrometry

Where possible, mass spectrometry was performed on each product. The sample is ionised and values for mass/charge of fragments and the parent ion recorded. The parent ion is usually defined as, $[M]^+$ where M is the mass of the mass of the ion. Several different ionisation techniques were employed during this study dependant on the compound being tested.

Electrospray ionisation (ESI) was used routinely to produce ions of compounds during this study. It produces fewer fragments than other techniques and consequently, was used to characterise most complexes. Atmospheric-pressure chemical ionisation (APCI) was used extensive during analysis of metal carbonyl complexes; it is considered to be a harder ionisation technique than electrospray ionisation, producing more fragments from the parent ion. Many compounds tested contain elements such as selenium and tellurium

with distinct isotope patterns; consequently ions containing these elements are easily recognisable.

1.9 Aims of study

Attempt to synthesise a new range tetradentate chalogenoether ligands with a semi rigid organic frameworks capable of binding to two different metal centres. Also to develop new synthetic routes for production selenium and tellurium analogues of known thioether ligands.

To prepare and characterise a range of mono- and bi-metallic complexes with a variety of transition metal centres, while comparing the properties such as coordination geometry, stability and sensitivity

To compare the suitability of different donor atoms and metal centres with a view to developing synthetic routes for production of hetero bimetallic molecules, by investigating possible reaction conditions for optimising yields and purity.

To investigate the ligating properties of new ligands with p-block Lewis acid centres from group 13 (Ga^{III} and In^{III}), focusing on how differences in the ligand structure affect coordination geometry of the complexes formed.

1.10 References

1. *Comprehensive Coordination Chemistry II*, ed. J. A. McCleverty and T. J. Meyer, Elsevier, Oxford, vol. 9, Oxford, 2004.
2. S. A. R. Knox, *J. Organomet. Chem.*, 1990, **400**, 225.
3. M. Cazanoue, L. Noel, J. J. Bonnet and R. Mathieu, *Organometallics*, 1988, **7**, 2480.
4. D.-K. Hwang, Y. B. Chi, S.-M. Peng and G.-H. Lee, *Organometallics*, 1990, **9**, 2709.
5. R. D. Adams, J. E. Babin and M. Tasi, *Organometallics*, 1988, **7**, 219.
6. H. Adams, N. A. Bailey, S. R. Gay, T. Hamilton and M. J. Morris, *J. Organomet. Chem.*, 1995, **493**, C25.
7. J. Sinfelt, *Acc. Chem. Res*, 1977, **10**, 15.
8. W. Yu, M. D. Porosoff and J. G. Chen, *Chem. Rev.*, 2012, **112**, 5780.
9. M. R. Dubois, *Chem. Rev.*, 1989, **89**, 1.
10. U. Riaz, O. J. Curnow and M. D. Curtis, *J. Am. Chem. Soc.*, 1994, **116**, 4357.
11. S. J. Loeb, G. K. H. Shimizu and J. A. Wisner, *Organometallics*, 1998, **17**, 2324.
12. R. Tan and D. Song, *Organometallics*, 2011, **30**, 1637.
13. S. Kundu, W. W. Brennessel and W. D. Jones, *Organometallics*, 2011, **30**, 5147.
14. M. R. Grochowski, T. Li, W. W. Brennessel and W. D. Jones, *J. Am. Chem. Soc.*, 2010, **132**, 12412.
15. L. Wang, W. He and Z. Yu, *Chem. Soc. Rev.*, 2013, **42**, 599.
16. G. M. Dhar, B. N. Srinivas, M. S. Rana, M. Kumar and S. K. Maity, *Catal. Today*, 2003, **86**, 45.
17. H. M. Wang and E. Iglesia, *J. Catal.*, 2010, **273**, 245.
18. S. Brunet, D. Mey, G. Perot, C. Bouchy and F. Diehl, *Appl. Catal. A*, 2005, **278**, 143.
19. L. M. Rubio and P. W. Ludden, *Annual Review of Microbiology*, 2008, **62**, 93.
20. H. Ogata, W. Lubitz and Y. Higuchi, *Dalton Trans.*, 2009, 7577.
21. R. A. Head and J. F. Nixon, *J. Chem. Soc., Dalton Trans.*, 1978, 909.
22. M. A. Kondratenko, B. Malezieux, M.Gruselle, D. Bonnet-Delpon and J. P. Begue, *J. Organomet. Chem.*, 1995, **487**, C15.
23. M. Elrington, N. N. Greenwood, J. D. Kennedy and M. Thornton-Pett, *J. Chem. Soc. Chem. Com.*, 1984, 1398.
24. T. Straub, M. Haukka and T. A. Pakkanen, *J. Organomet. Chem.*, 2000, **612**, 106.
25. R. L. Beddoes, E. S. Davies, M. Helliwell and M. W. Whiteley, *J. Organomet. Chem.*, 1991, **421**, 285.

26. J. P. Collman, S. T. Harford, P. Maldivi and J. C. Marchon, *J. Am. Chem. Soc.*, 1998, **120**, 7999.

27. D. A. Sweigart, C. A. Dullaghan and S. Sun, *J. Chem. Soc., Dalton Trans.*, 1996, 4493.

28. G. Denti, C. J. Jones, J. A. McCleverty, B. D. Neaves and S. J. Reynolds, *J. Chem. Soc., Chem. Commun.*, 1983, 474.

29. W. Levason, M. Nirwan, R. Ratnani, G. Reid, N. Tsoureas and M. Webster, *Dalton Trans.*, 2007, 439.

30. K. Brodersen, W. Roelz, G. Jordan, R. Gerbeth and J. Ellerman, *Chem. Ber*, 1978, **111**, 132.

31. E. G. Hope, T. Kemmitt and W. Levason, Organometallics, 1988, 7, 78.

32. D. A. McMorran and P. J. Steel, Tetrahedron, 2003, 59, 3701.

33. F. K. Gormley, J. Gronbach, S. M. Draper and A. P. Davis, Dalton Trans., 2000, 173.

34. D. B. Cordes and L. R. Hanton, Inorg. Chem., 2007, 46, 1634.

35. A. J. Barton, W. Levason and G. Reid, J. Organomet. Chem., 1999, 579, 235.

36. J. Connolly, M. K. Davis and G. Reid, *J. Chem. Soc., Dalton Trans.*, 1998, 3833.

37. M. K. Davies, M. C. Durrant, W. Levason, G. Reid and R. L. Richards, *J. Chem. Soc., Dalton Trans.*, 1999, 1077.

38. W. Levason, B. Patel, G. Reid and A. J. Ward, *J. Organomet. Chem.*, 2001, **619**, 218.

39. A. G. Orpen and N. G. Connelly, *J. Chem. Soc., Chem. Commun.*, 1985, 1310.

40. W. Levason, G. Reid and S. D. Orchard, *Coord. Chem. Rev.*, 2002, **225**, 159.

41. H. Schumman, A. M. Arif, C. Rheingold, C. Janiak and R. Hoffmann, *Inorg. Chem.*, 1991, **30**, 1618.

42. W. Levason, S. D. Orchard and G. Reid, *Organometallics*, 1999, **18**, 1275.

43. W. Levason, S. D. Orchard and G. Reid, *J. Chem. Soc., Dalton Trans.*, 1999, 823.

44. E. G. Hope and W. Levason, *Coord. Chem. Rev.*, 1993, **122**, 109.

45. E. W. Abel, S. K. Bhargava and K. G. Orrell, *The Stereodynamics of metal complexes of Sulfur-, Selenium-, and Tellurium-containing ligands*, Progress in Inorganic Chemistry, Interscience, vol. 32, 1984.

46. D. H. Brown, R. J. Cross and R. Keat, *J. Chem. Soc., Dalton Trans.*, 1980, 871.

47. E. Abel, K. G. Orrell, S. P. Scanlan, D. Stephenson, T. Kemmitt and W. Levason, *J. Chem. Soc., Dalton Trans.*, 1991, 591.

48. F. R. Hartley, S. G. Murray, W. Levason, H. E. Soutter and C. A. McAuliffe, *Inorg. Chim. Acta.*, 1979, **35**, 265.

49. J. Mason, *Multinuclear NMR*, Plenum Press, New York, 1987.

CHAPTER 2

Ligand synthesis and characterisation

2.1 Introduction

This chapter describes the synthesis of thio- seleno- and telluro-ether ligands, with several different organic backbones. As expected, varying either the chalcogen or the ligand architecture resulted in different behaviour being observed. Once produced in high purity the seleno- and telluro-ether ligands were then reacted with iodomethane or iodine to form stable derivatives allowing further comparisons between the species.

The target of preparing heterobimetallic molecules was discussed in the Chapter 1. To produce these compounds; several factors must be considered when selecting the appropriate ligand type. Each ligand must be capable of coordinating to two different metal centres. Ideally each ligand also has a rigid carbon framework between the donor atoms, to prevent tetradentate monometallic chelation. In order to produce hetero bimetallic complexes, each metal must be attached to the ligand in a stepwise sequence of reactions to prevent formation of homo bimetallic complexes see figure 2.1.

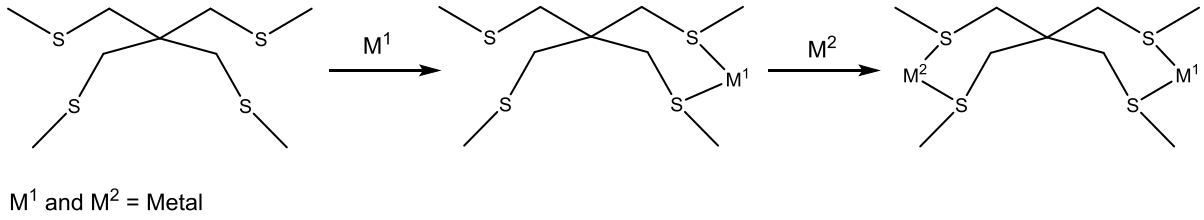

Figure 2.1 Stepwise addition of two different metals to a ligand.

This approach requires tetradentate ligands with architectures incapable of tetradentate monometallic chelation. With this in mind, two ligand types were chosen, based upon either a spirocyclic framework; $C(CH_2EMe)_4$, or a tetrasubstituted aromatic backbone $1,2,4,5\text{-}C_6H_2(CH_2EMe)_4$ (E = S, Se and Te). Seven ligands based on these frameworks were successfully synthesised (see figure 2.2), but although the telluroether ligands were attempted, they were found to be highly sensitive and it was difficult to isolate a pure sample. Experimental conditions and spectroscopic data from these attempted products are detailed in the results section.

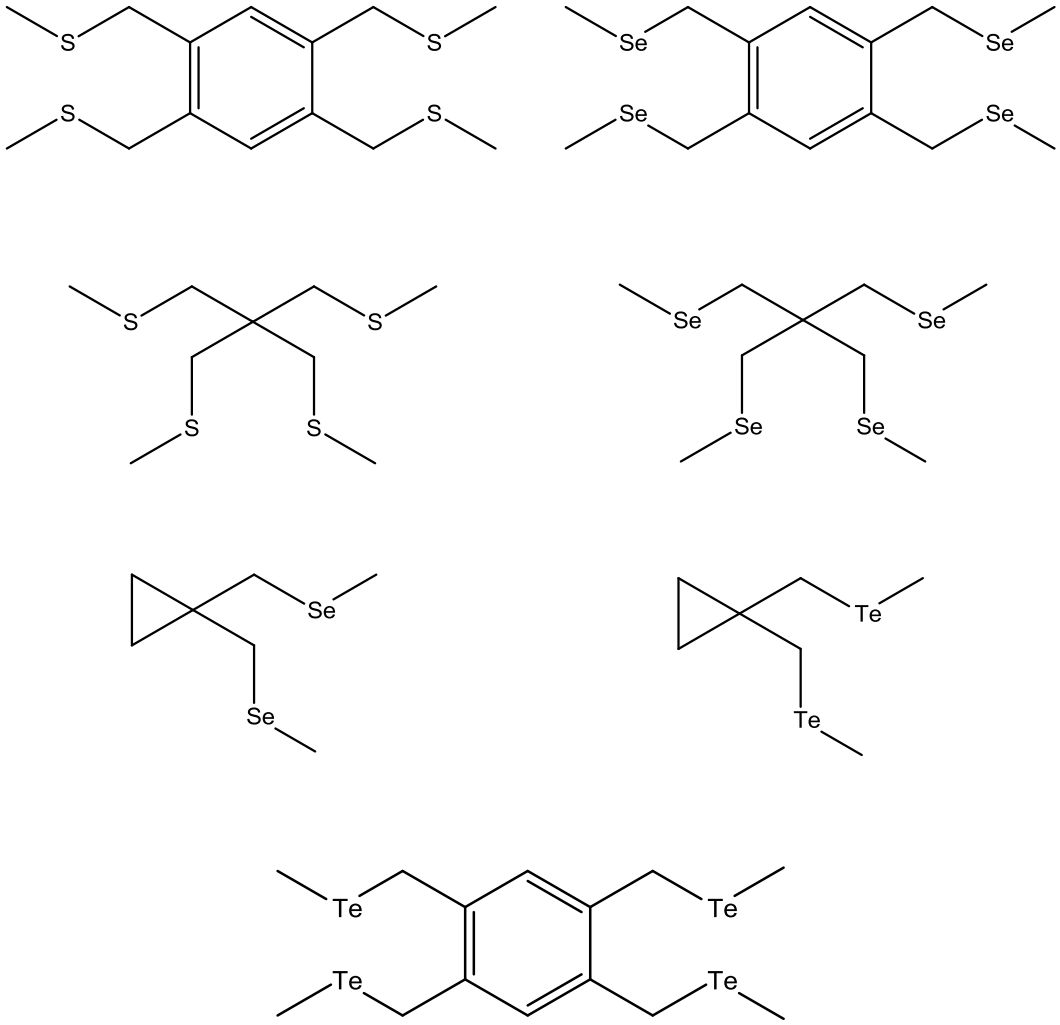

Figure 2.2 Ligands successfully synthesised.

2.2 Results

2.2.1 General synthesis

The thioether ligands $C(CH_2SMe)_4$ and 1,2,4,5-$C_6H_2(CH_2SMe)_4$ were produced in good yield (90 %) from reacting the appropriate organo-bromide with NaSMe in EtOH. These reactions were performed in a dry nitrogen environment. Seleno- and telluroether ligands $C(CH_2SeMe)_4$, 1,2,4,5-$C_6H_2(CH_2SeMe)_4$, $(CH)_2C(CH_2SeMe)_2$ and $(CH)_2C(CH_2TeMe)_2$ were produced in lower yields, by reacting freshly ground selenium or tellurium in THF with MeLi at -77 °C to form MeELi which was then reacted with the appropriate bromide

reagent. The use of alkyl lithium regents meant the method was highly sensitive and required strict Schlenk procedures throughout the method. An overview of ligands produced is shown below and details of reaction conditions are reported in the Experimental Section 2.4.

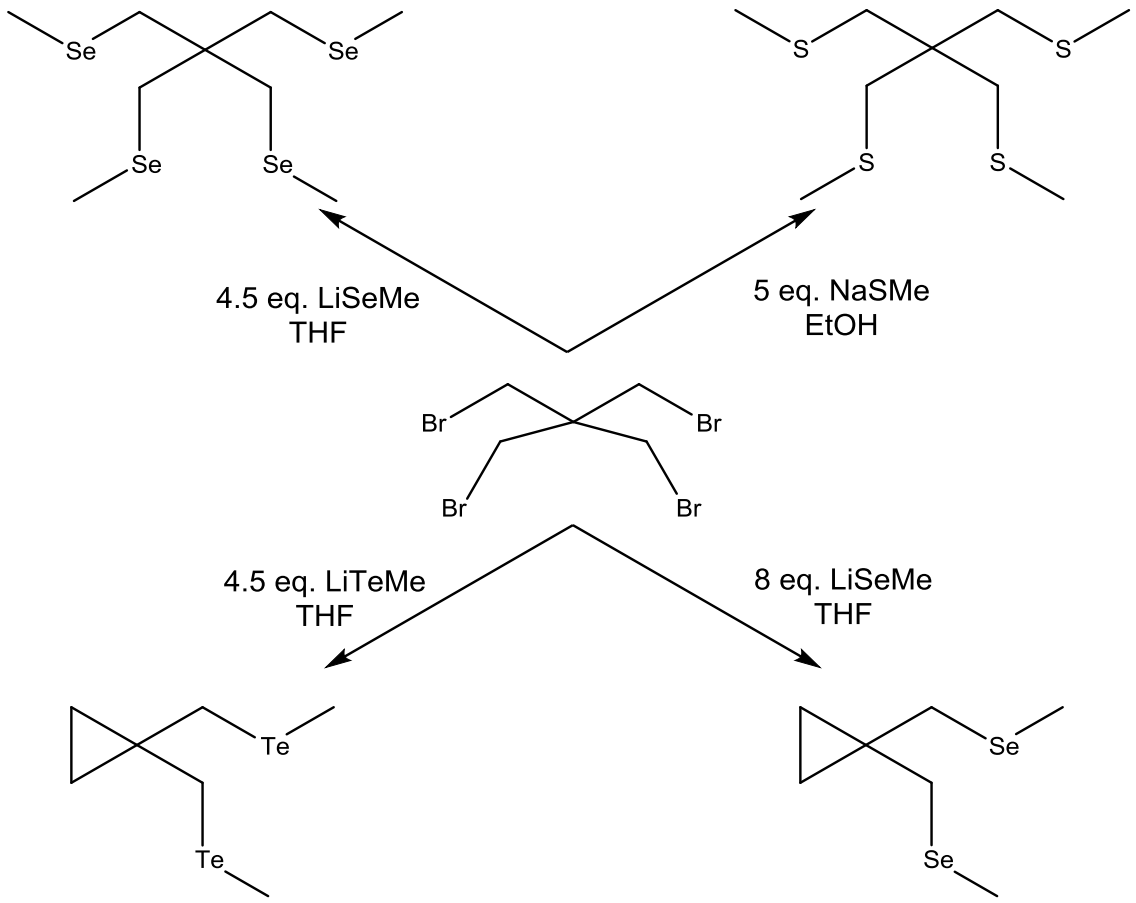

Figure 2.3 General reaction scheme for synthesis of spirocyclic ligands.

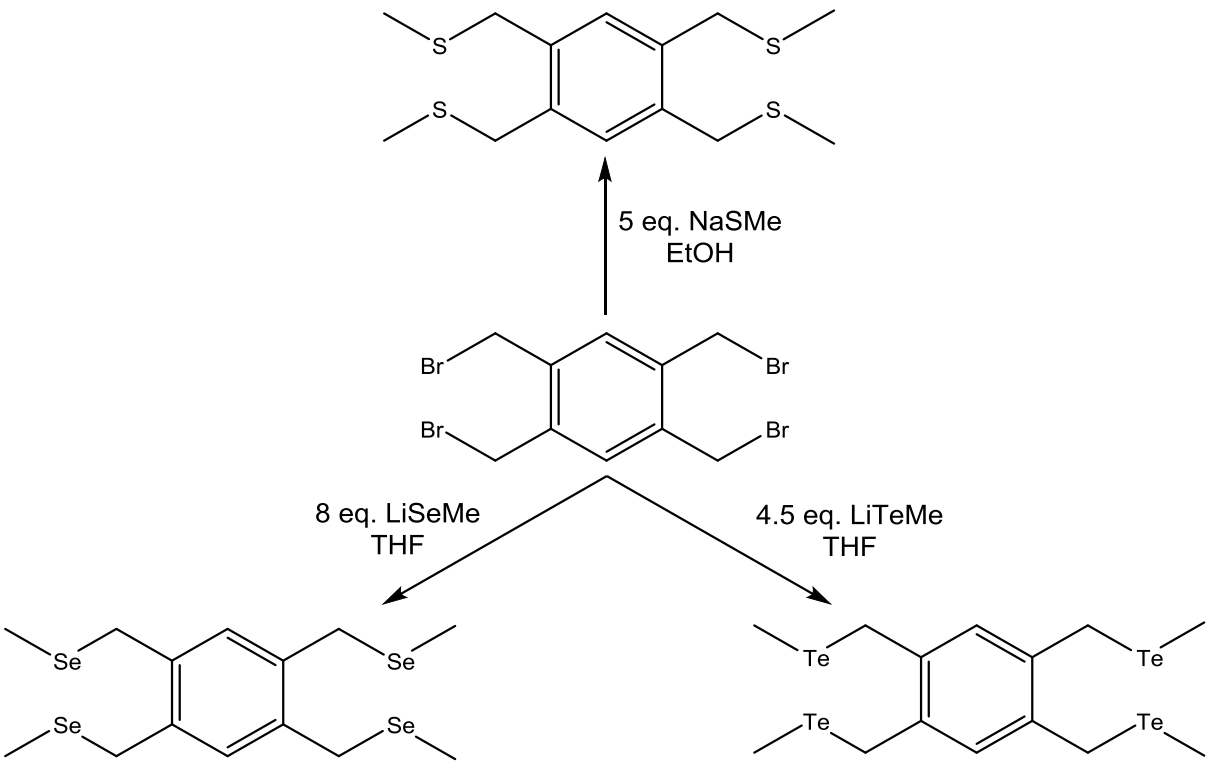

Figure 2.4 General reaction scheme for synthesis of tetrabenzyl ligands.

The ligands produced decomposed more readily down group 16, presumably due to the weaker C-E bonds present in seleno- and telluro-ethers. The tellurium ligands produced were highly unstable and require storage under nitrogen in the freezer. This sensitivity was also reflected in the synthesis, where the tellurium ligand was not allowed above room temperature throughout the procedure. Any further reactions with tellurium were carried within a few days of the initial synthesis, as signs of decomposition were observed on samples kept for longer than a week even with careful storage.

Each ligand was reacted with an excess of iodomethane or iodine, the reaction in most cases occurred immediately to form a solid which was then collected by filtration. The products from each reaction were poorly soluble but not air sensitive, allowing further characterisation each of ligand.

2.2.2 Characterisation

Each of the ligands was characterised with a variety techniques including multinuclear NMR, mass spectrometry, microanalysis and single crystal X-ray diffraction.

^{1}H NMR spectroscopy was essential during characterisation and usually easy to interpret due to the purity and high solubility of the compounds.

Multinuclear NMR spectroscopy was performed on all selenium and tellurium containing compounds, revealing single, sharp resonances observed for all ligands. Selenium-77 NMR spectroscopy was an important technique confirming the presence of the two selenium species formed during the synthesis of $C(CH_2SeMe)_4$ and was later revealed to be both $C(CH_2SeMe)_4$ and $(CH)_2C(CH_2SeMe)_2$ ligands. While investigating the synthesis of 1,2,4,5-$C_6H_2(CH_2TeMe)_4$, *in situ* ^{125}Te NMR data were collected, which proved very useful when monitoring the formation of the ligand.

Chemical ionisation mass spectroscopy showed a parent ion at the expected mass for all thio- and seleno-ethers. Less conclusive data were collected for the telluroether ligands, probably due to decomposition before/during data collection. Selenium and tellurium produce characteristic isotope patterns which is useful when establishing the number of chalcogen atom in each fragment.

Due to poor solubility, the methiodides and iodide compounds required d_6-DMSO for NMR spectroscopic studies. Other methods of characterisation were also restricted by poor solubility. Where possible MS data were collected, full characterisation data are detailed in the Experimental Section 2.4.

2.2.3 Spirocyclic Ligands

The spirocyclic ligand $C(CH_2SMe)_4$ was produced in good yield by reacting NaSMe with $C(CH_2Br)_4$ in refluxing ethanol as in the literature procedure.[1] Synthesis of $C(CH_2SeMe)_4$ had been previously reported in poor yield (~10%) by reacting of LiSeMe with $C(CH_2Br)_4$ in THF.[2] This reaction was examined under a variety of conditions and reactant ratios in order to optimise the yield. A reaction of LiSeMe with $C(CH_2Br)_4$ in a 4.5 : 1 molar ratio in hot THF, stirred for 15 h gave a good yield (~55 %) of $C(CH_2SeMe)_4$. An example of ^{1}H NMR spectrum of $C(CH_2SeCH_3)_4$ is show in figure 2.5.

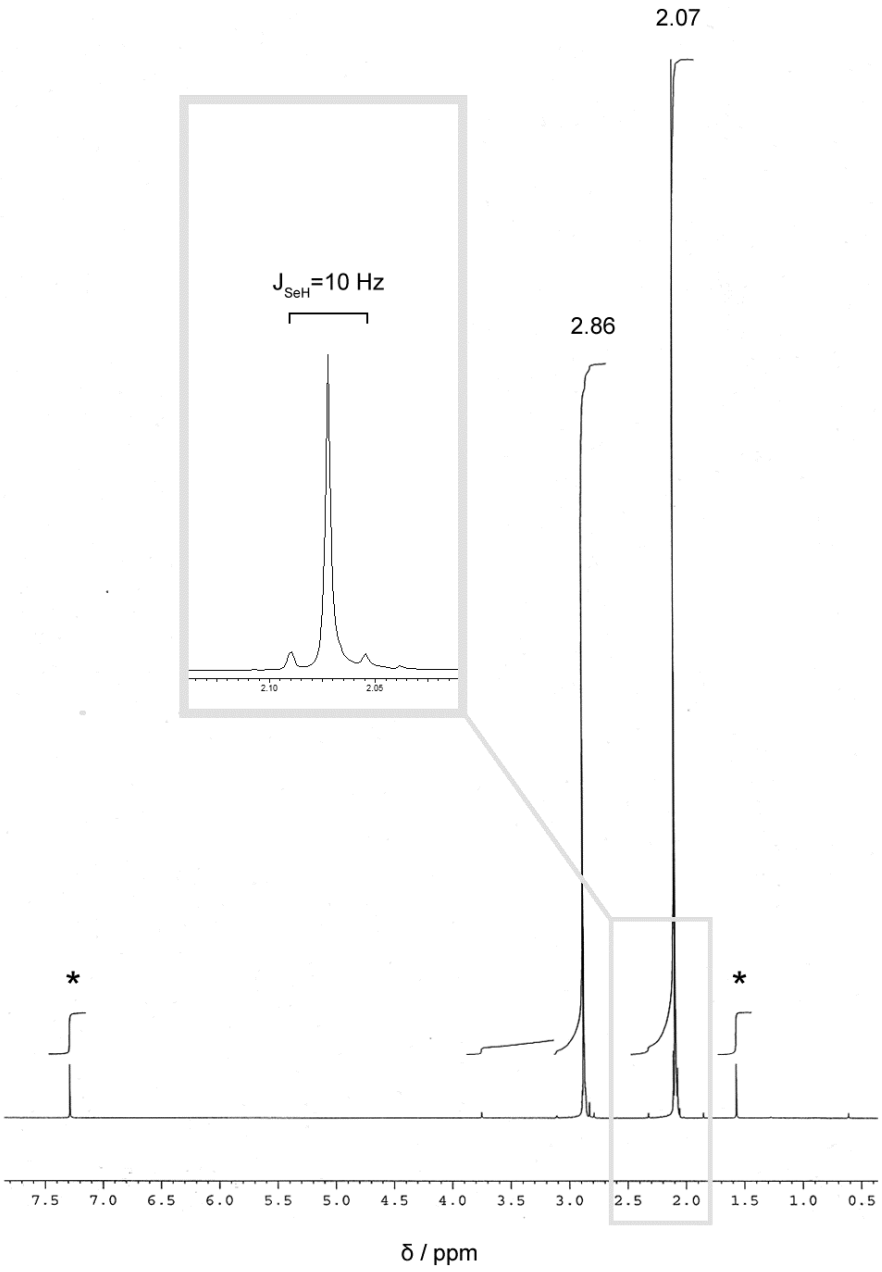

* Assigned to H_2O and $CDCl_3$

Figure 2.5 ^{1}H NMR spectrum of $C(CH_2SeCH_3)_4$ recorded in $CDCl_3$.

Only two resonances are observed in the spectrum of the ligand due to high purity of the sample. The two peaks at 2.07 and 2.86 are assigned to the CH_2 and CH_3 groups respectively. Full assignment of all data is given in the Experimental Section. Selenium-77 satellites, two small evenly spaced peaks either side of the main resonance are also observed in this spectrum, indicating the presence of neighbouring selenium atom.

$^{13}C\{^{1}H\}$ NMR data were collected for each ligand, full assignments for each product is reported in the Experimental Section 2.4. An example spectrum for one ligand is shown below.

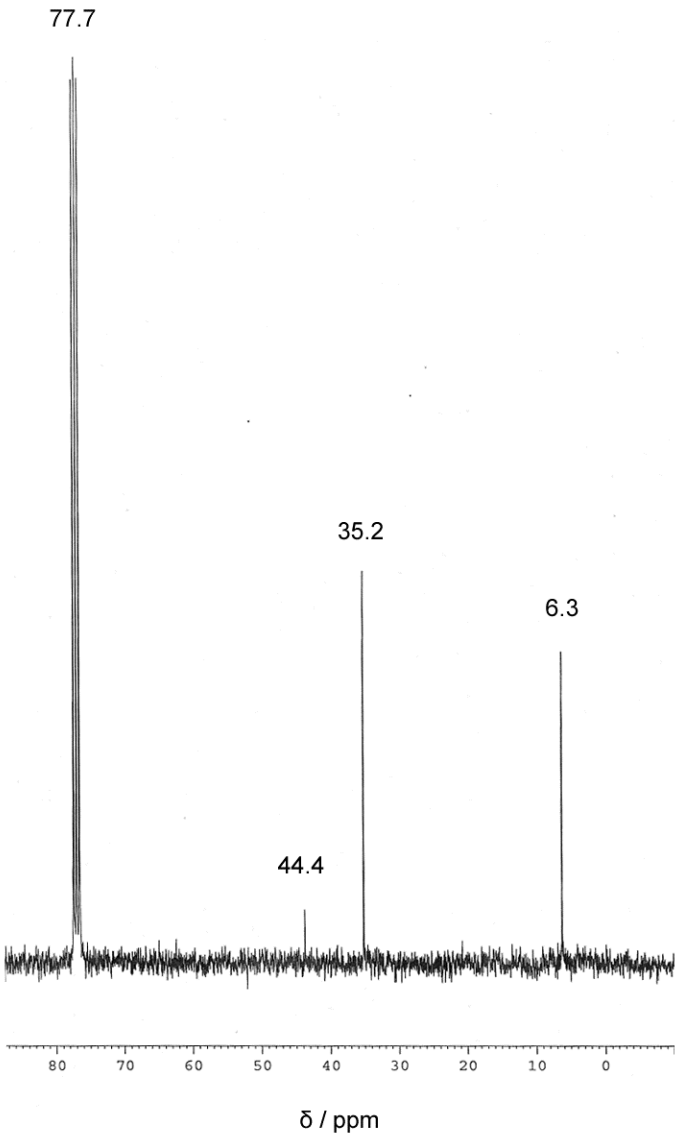

Figure 2.6 $^{13}C\{^{1}H\}$ NMR spectrum of $C(CH_2SeCH_3)_4$ recorded in $CDCl_3$ (77.7 ppm).

The three resonances observed at 6.3 ppm, 35.2 ppm and 44.4 ppm can be assigned to CH_3, CH_2 and the quaternary carbon respectively. Most NMR data collected for each ligand was unexceptional and assignment is straight forward, the symmetrical structures give rise to simple spectra for the ligand themselves.

Increasing the LiSeMe to $C(CH_2Br)_4$ molar ratio to 8 : 1 in refluxing THF produced the cyclopropane derivative $(CH_2)_2C(CH_2SeMe)_2$ in ~90 % yield, and under a variety of other conditions mixtures of the two are produced. Reacting different ratios of LiTeMe and $C(CH_2Br)_4$ in THF only produced the cyclopropyltelluroether, $(CH_2)_2C(CH_2TeMe)_2$ confirmed by spectroscopic analysis.[3]

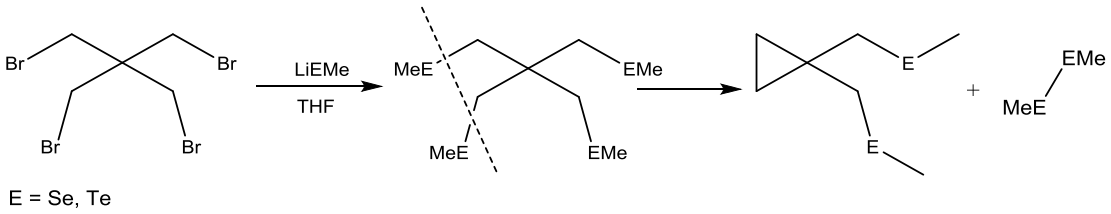

Figure 2.7 Synthesis of $(CH_2)_2C(CH_2EMe)_2$.

2.2.4 Tetra-benzyl ligands

Reacting an excess of NaSMe in ethanol, or LiSeMe in THF, with 1,2,4,5-$C_6H_2(CH_2Br)_4$ gave excellent yields (>85 %) of the 1,2,4,5-$C_6H_2(CH_2EMe)_4$ (E= S, Se), both of which are air-stable crystalline solids. Spectroscopic data for both ligands are unexceptional details of the full characterisation are shown in the Experimental Section 2.4.

The crystal structures of 1,2,4,5-$C_6H_2(CH_2SMe)_4$ and 1,2,4,5-$C_6H_2(CH_2SeMe)_4$ were determined (figures 2.8 and 2.9, table 2.5). The structure of 1,2,4,5-$C_6H_2(CH_2SMe)_4$ has similar dimensions to those of *o*-$C_6H_4(CH_2SMe)_2$.[4] Each sulfur atom is directed away from the neighbouring CH_2SMe group, presumably to minimise lone pair repulsions. In comparison the structure of the tetraselenoether ligand, although it is not isomorphous with the tetrathioether, has a very similar molecular structure. In both cases the CH_2EMe groups on adjacent ring carbon atoms are on opposite sides of the plane of the aromatic ring.

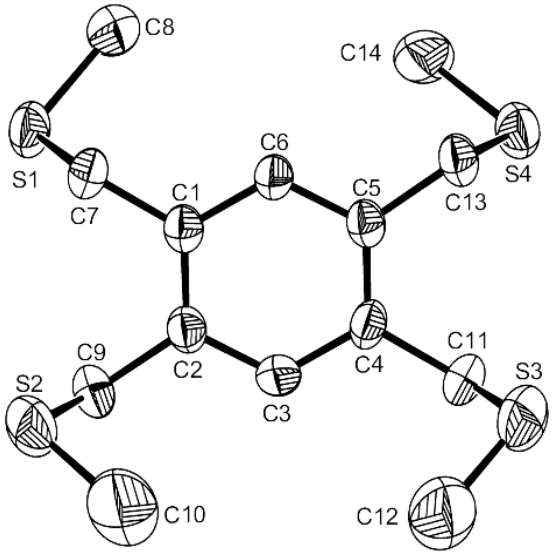

Figure 2.8 Crystal structure of 1,2,4,5-$C_6H_2(CH_2SMe)_4$ showing the numbering scheme adopted. Ellipsoids are drawn at the 50% probability level and H atoms have been omitted for clarity.

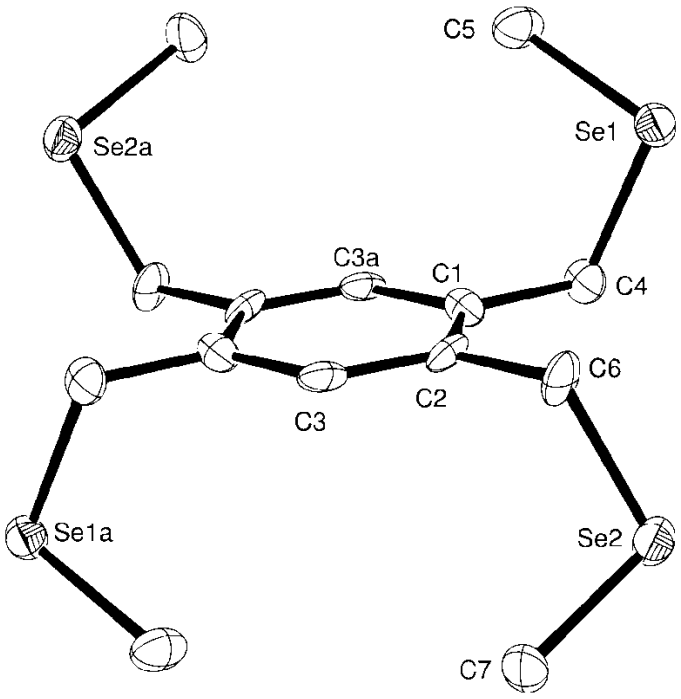

Figure 2.9 Crystal structure of 1,2,4,5-$C_6H_2(CH_2SeMe)_4$ showing the numbering scheme adopted. Ellipsoids are drawn at the 50% probability level and H atoms have been omitted for clarity. Symmetry operation: a = 1–x, 2–y, –z.

1,2,4,5-$C_6H_2(CH_2SMe)_4$			
S1–C7	1.815(4)	S2–C9	1.811(5)
S1–C8	1.801(4)	S2–C10	1.787(7)
S3–C11	1.833(5)	S4–C13	1.815(4)
S3–C12	1.770(8)	S4–C14	1.786(4)
C7–S1–C8	100.4(2)	C9–S2–C10	99.9(3)
C11–S3–C12	102.7(3)	C13–S4–C14	101.2(2)
1,2,4,5-$C_6H_2(CH_2SeMe)_4$			
Se1–C4	1.971(9)	Se2–C6	1.974(8)
Se1–C5	1.940(8)	Se2–C7	1.947(9)
C4–Se1–C5	99.0(4)	C6–Se2–C7	97.5(4)
C1–C4–Se1	115.4(5)	C2–C6–Se2	112.6(6)

Table 2.1 Selected bond lengths (Å) and angles (°) for 1,2,4,5-$C_6H_2(CH_2SMe)_4$ and 1,2,4,5-$C_6H_2(CH_2SeMe)_4$.

2.2.5 Tetrabenzyltelluroether ligands

The synthesis of 1,2,4,5-$C_6H_2(CH_2TeMe)_4$ was attempted several times under a range of reaction conditions with varying levels of success (figure 2.10). The ligand was found to be highly sensitive and difficult to isolate as a pure sample.

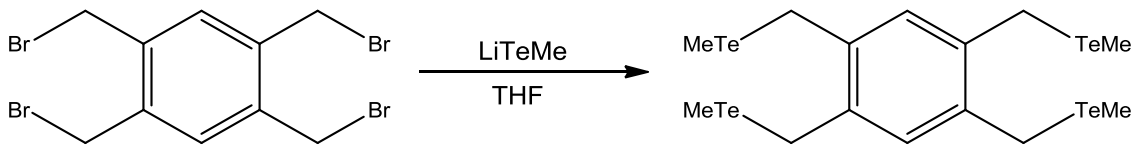

Figure 2.10 Attempted synthesis of 1,2,4,5-$C_6H_2(CH_2TeMe)_4$.

The pure ligand is a poorly soluble, deep red solid which turns to oil immediately when exposed to air; storing in a foil wrapped Schlenk at -18 °C prevented decomposition. However, further reactions and characterisation were performed immediately due to the ligand's short shelf life.

Several different reaction conditions were attempted to optimise the synthesis; the ratio of LiTeMe to 1,2,4,5-$C_6H_2(CH_2Br)_4$ was varied from 8 eq. to 4.5 eq. ^{125}Te NMR data showed increasing the concentration of LiTeMe produced lower purity products with several tellurium containing species. Increasing the reaction time before hydrolysing with NaCl solution was also found to have a detrimental effect on yield and purity of the product. Performing ^{125}Te NMR measurements on *in situ* samples meant the tellurium species could be monitored during the reaction, helping determine when the reaction had reached completion. The optimised method is detailed in the Experimental Section 2.4.

Once isolated the ligand was characterised spectroscopically. However, poor solubility and sensitivity meant some techniques were more problematic than others. The ^{1}H NMR spectrum is illustrated in figure 2.11.

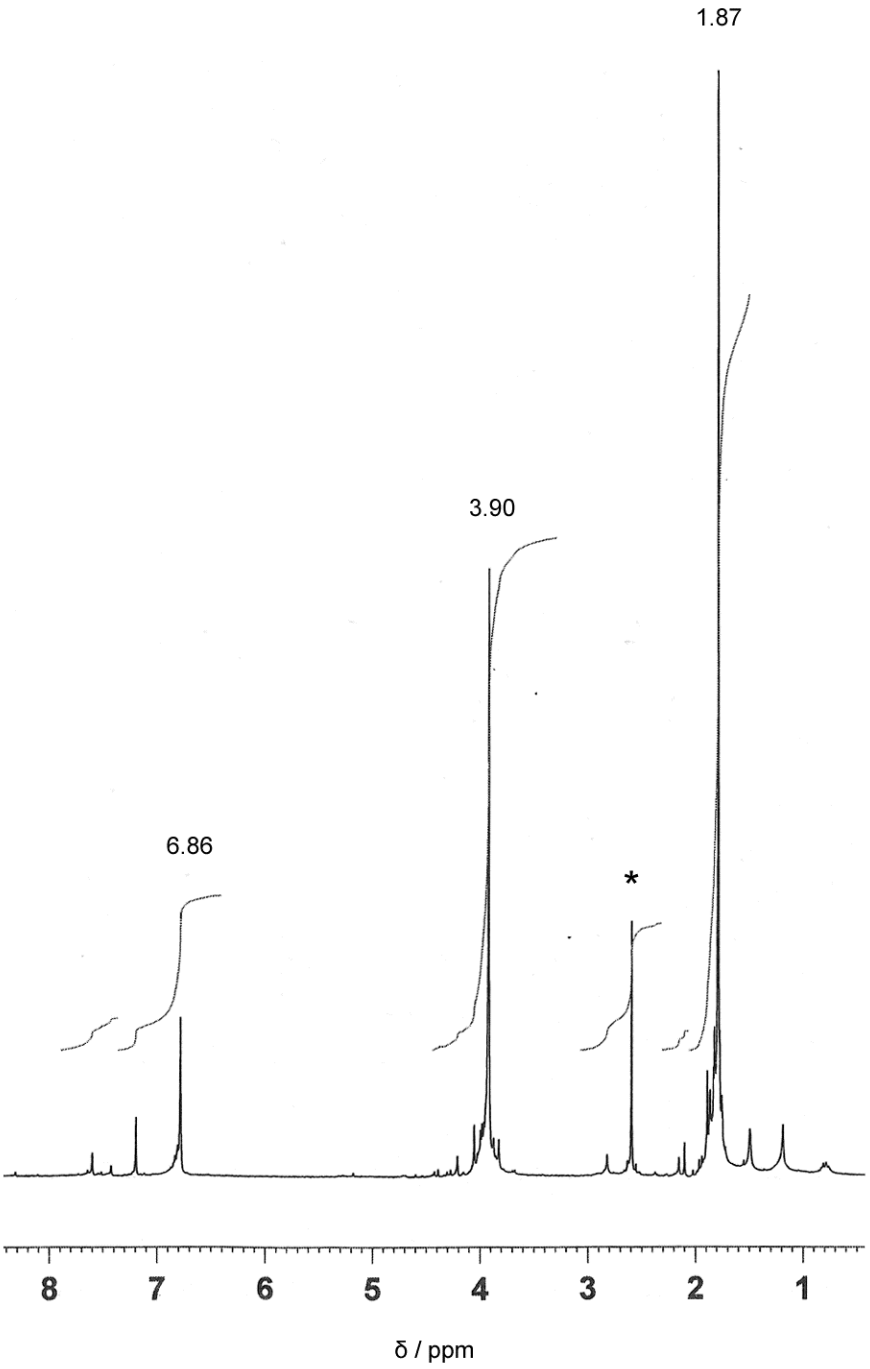

* Assigned to unknown impurity.

Figure 2.11 ^{1}H NMR of 1,2,4,5-$C_6H_2(CH_2TeCH_3)_4$ recorded in $CDCl_3$.

Three major resonances are observed on the spectra at 1.87, 3.90 and 6.86 ppm which may be assigned to TeMe, CH_2 and aromatic CH groups respectively. An impurity can be seen at 2.56 ppm and was still present in the spectra after a second stage of purification,

microanalysis of the same sample showed no significant impurities present. This suggests minor amounts of decomposition occur when dissolved in the NMR solvent. Selected NMR data from the literature are shown in table 2.2.

Compound	δ (TeMe) ^{1}H NMR/ ppm	δ ^{125}Te{^{1}H} / ppm
1,2,4,5-$C_6H_2(CH_2TeCH_3)_4$	1.87	260
o-$C_6H_4(TeCH_3)_2$[a]	2.03	372

[a] Comparative data from literature[5]

Table 2.2 Comparative NMR data recorded in $CDCl_3$.

Large variations in chemical shifts are observed in ^{125}Te{^{1}H} NMR data due to the inherently wide chemical shift range and solvent effects. The *o*-$C_6H_4(TeCH_3)_2$, while only a bidentate ligand, is the most comparable example available. Although the difference in shifts is relatively large, the ^{125}Te{^{1}H} NMR spectrum of 1,2,4,5-$C_6H_2(CH_2TeMe)_4$ only showed a single resonance, confirming the presence of only one tellurium containing species. The ^{1}H NMR spectrum compares well to the expected values based on the literature data for *o*-$C_6H_4(TeCH_3)_2$. Considering of the new ligand structure, the spectrum only shows very small variation in chemical shift.

All attempts at reacting 1,2,4,5-$C_6H_2(CH_2TeMe)_4$ with MeI and I_2 produced insoluble solids which could not be identified. Attempts to form complexes with transitions metals also resulted in intractable products.

2.2.6 Telluroethers and Organotellurium(IV) derivatives

As discussed, the reaction of MeSeLi and $C(CH_2Br)_4$ with a molar ratio of the reactants of 4.5 : 1 produced $C(CH_2SeMe)_4$.[6] Increasing the quantity of MeSeLi to a molar ratio to 8 : 1 produces $(CH_2)_2C(CH_2SeMe)_2$ in high yield (~90 %) (above). The corresponding reaction of MeTeLi with $C(CH_2Br)_4$ was reported to give only $(CH_2)_2C(CH_2TeMe)_2$.[3] A range of molar ratios and conditions were tested to see if the tetratelluroether $C(CH_2TeMe)_4$ could be obtained. However, various molar ratios of MeTeLi to $C(CH_2Br)_4$ (~4 : 1 through 8 : 1) and reaction temperatures of 200 K to ambient showed no $C(CH_2TeMe)_4$ present. ^{125}Te{^{1}H} NMR spectrum from the products showed two tellurium containing products;

$(CH_2)_2C(CH_2TeMe)_2$ ($^{125}Te\{^1H\}$ NMR $\delta = 63.1$) and Me_2Te_2. *In situ* samples were taken for $^{125}Te\{^1H\}$ NMR at various stages of the reaction to ascertain if $C(CH_2TeMe)_4$ was forming. This also failed to show any evidence of the tetratelluroether (since tellurium-125 chemical shifts are approximately additive with the substituents – the tetratelluroether is expected to have a resonance δ ~30).[3, 7]

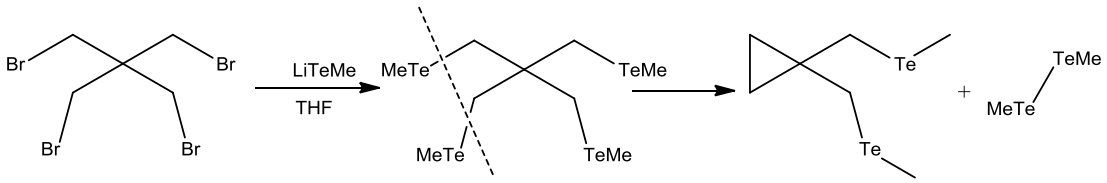

Figure 2.12 Attempted synthesis of $C(CH_2TeMe)_4$ resulting in production of $(CH_2)_2C(CH_2TeMe)_2$.

Two Te(IV) derivatives of the cyclopropyl ditelluroether were formed by reacting an excess of either MeI or I_2 (figure 2.13) with $(CH_2)_2C(CH_2TeMe)_2$, to produce $(CH_2)_2C(CH_2TeMe_2I)_2$ and $(CH_2)_2C(CH_2TeMeI_2)_2$ respectively see Experimental Section 2.4 for details.

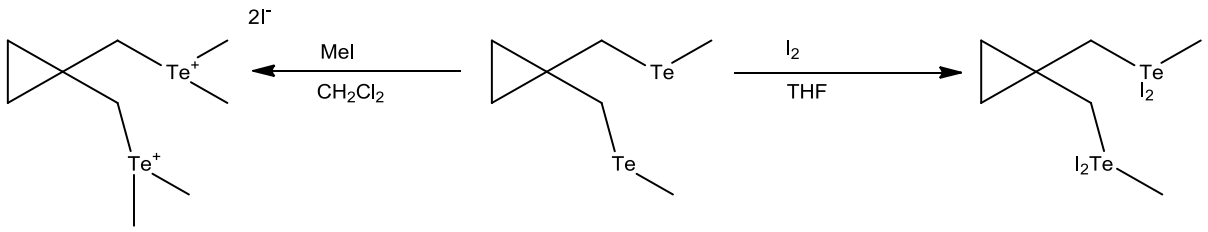

Figure 2.13 Te(IV) compounds formed by reacting an excess of MeI or I_2 with $(CH_2)_2C(CH_2TeMe)_2$.

Each of these compounds was fully characterised spectroscopically. The Te(IV) derivatives showed large, high frequency shifts in the tellurium-125 NMR spectra compared to the parent ligand, as expected.[3, 8] Crystals of $[(CH_2)_2C(CH_2TeMe_2]I_2$ were obtained from a solution of the product in dmso/MeOH cooled in the freezer. Although the crystal quality was poor, this structure (figure 2.14, table 2.5) provided conclusive proof of the ligand backbone.

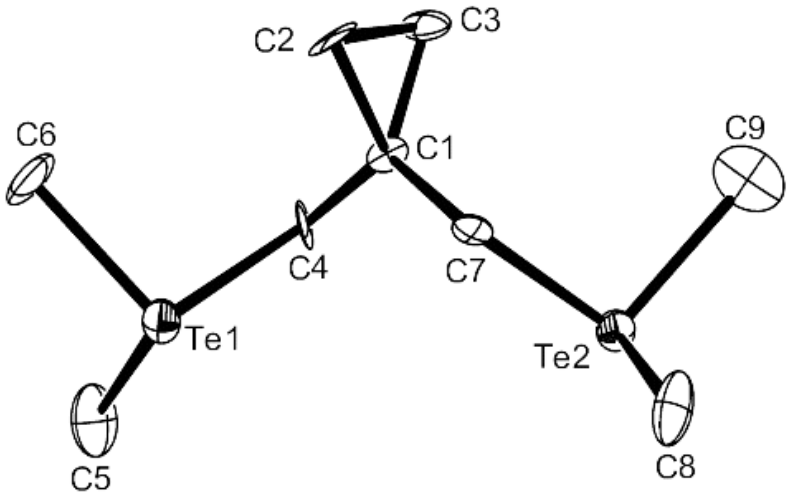

Figure 2.14 Structure of the cation in $[(CH_2)_2C(CH_2TeMe_2)_2]I_2$ showing the numbering scheme adopted. Ellipsoids are drawn at the the 50 % probability level and hydrogen atoms have been omitted for clarity.

The compound contains a ion pair consisting of a dicationic dimethylated ligand and iodide anions to provide charge balance. Secondary Te···I interactions in the range 3.803 – 3.568 Å, and pyramidal TeC_3 units can be seen in the structure, see figure 2.15. These interactions produce distorted square pyramidal and distorted octahedral geometries about Te1 and Te2 respectively.

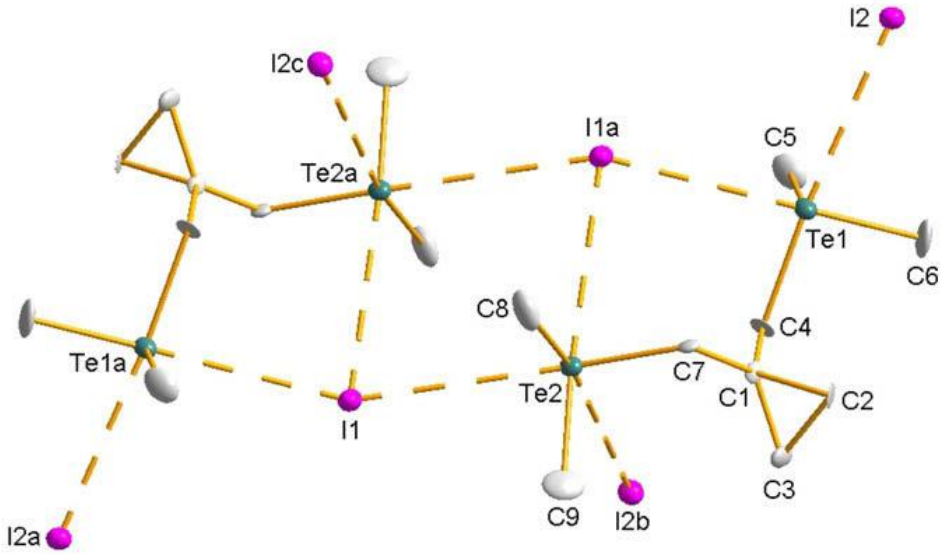

Figure 2.15 The extended structure $[(CH_2)_2C(CH_2TeMe_2)]I_2$ showing the long intermolecular Te···I (secondary) interactions.

Te1–C6	2.10(2)	Te2–C8	2.13(2)
Te1–C5	2.12(2)	Te2–C7	2.143(19)
Te1–C4	2.162(17)	Te2–C9	2.18(2)
Te1…I2	3.568	Te2…I1	3.803
Te1…I1’	3.594	Te2…I1’	3.695
		Te2…I2’’	3.692

Table 2.3 Selected bond lengths (Å) and angles (°) for $[(CH_2)_2C(CH_2TeMe_2)_2]I_2$.

The Te-C and Te-I distances shown in table 2.3, are similar to those in other telluronium salts.[9-11] However, detailed comparisons of bond lengths and angles cannot be justified due to the modest crystal quality.

2.2.7 Selenoethers and Organoselenium(IV) derivatives

The fragility of the C-Se bonds is demonstrated in the reaction of $(CH_2)_2C(CH_2SeMe)_2$ with MeI in warm acetone solution, in which the expected product; a methylated

selenonium salt $[(CH_2)_2C(CH_2SeMe_2)_2]I_2$, similar to those observed with other aliphatic diselenoethers[12] was not in fact produced.

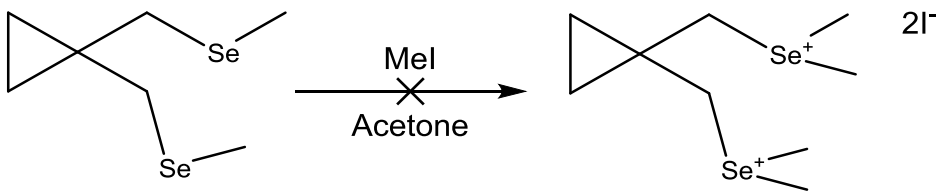

Figure 2.16 Expected product from reaction of $(CH_2)_2C(CH_2SeMe)_2$ with MeI

The main selenium containing product of this reaction was identified as $[Me_3Se]I$, ^{77}Se NMR spectroscopy showed a resonance at +256 ppm (lit.[13] +253 ppm). A major feature in the ES^+ mass spectrum was observed at m/z = 125 $[Me_3Se]^+$. Crystals were also obtained and confirmed the product to be $[Me_3Se]I$ by an X-ray study. This structure was previously reported[14] and is not a minor by product since the ^{77}Se NMR spectrum of the bulk product showed no other significant selenium species.

The reaction of *o*-$C_6H_4(CH_2SeMe)_2$ with MeI showed a similar rearrangement to that observed with the cyclopropyl selenoether. The expected product is shown in figure 2.17.

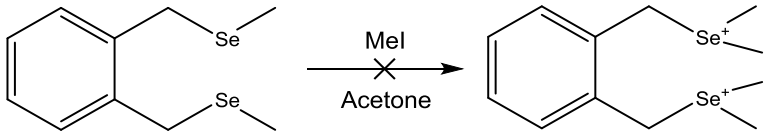

Figure 2.17 Expected product from reaction of *o*-$C_6H_4(CH_2SeMe)_2$ and MeI.

Two major products were observed from this reaction see figure 2.18; the selenonium species [*o*-$C_6H_4(CH_2)_2SeMe]I$ and $[Me_3Se]I$.

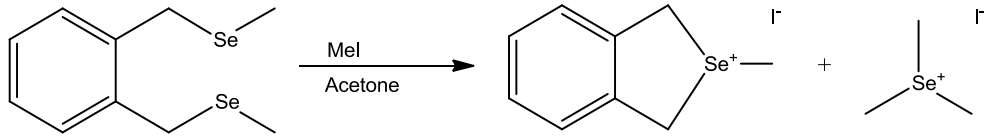

Figure 2.18 Observed products from reaction of *o*-$C_6H_4(CH_2SeMe)_2$ and MeI.

The cyclised selenonium cation has previously been obtained during reactions of this diselenoether with $GaCl_3$ or $InCl_3$.[15, 16] These products were isolated as [*o*-$C_6H_4(CH_2)_2SeMe$][MCl_4] (M = Ga or In). The tetracholorgallate salt was characterised by an X-ray structure, ES^+ mass spectrometry and the ^{77}Se NMR chemical shift data were consistent with those observed for the product of this reaction. Crystals of [*o*-$C_6H_4(CH_2)_2SeMe$]I were grown and the crystal structure determined (figure 2.19 and table 2.5).

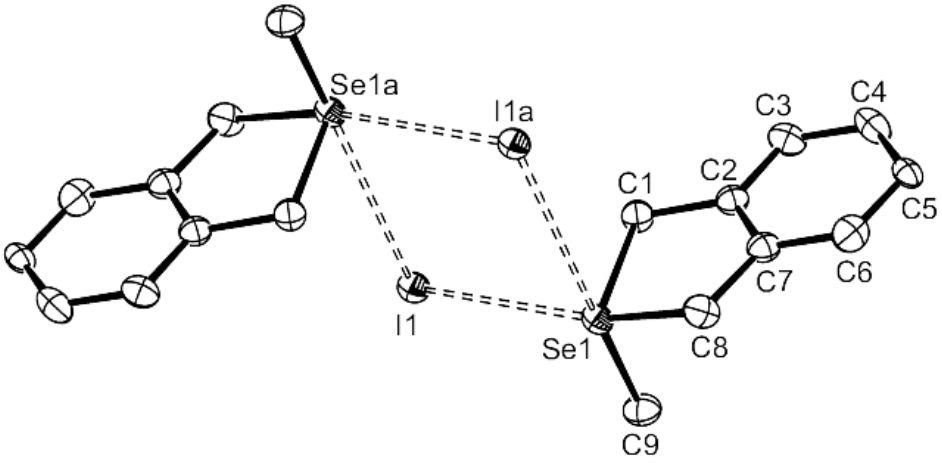

Figure 2.19 The structure of the centrosymmetric [*o*-$C_6H_4(CH_2)_2SeMe$]I showing the weakly associated dimer unit.

Se1–C9	1.940(3)
Se1–C1	1.949(3)
Se1–C8	1.961(3)
C9–Se–C1	97.28(13)
C9–Se1–C8	97.62(14)
C1–Se1–C8	91.00(12)
Se1···I1	3.589(1)
Se1···I1a	3.599(1)

Table 2.4 Selected bond lengths (Å) and angles (°) for $[C_6H_4(CH_2)_2SeMe]I$.

The structure of $[o\text{-}C_6H_4(CH_2)_2SeMe]I$ (figure 2.19) contains pyramidal selenium cations weakly linked into dimers *via* long Se···I···Se bridges forming approximately square pyramidal geometry. A possible mechanism for this rearrangement is shown in figure 2.20.

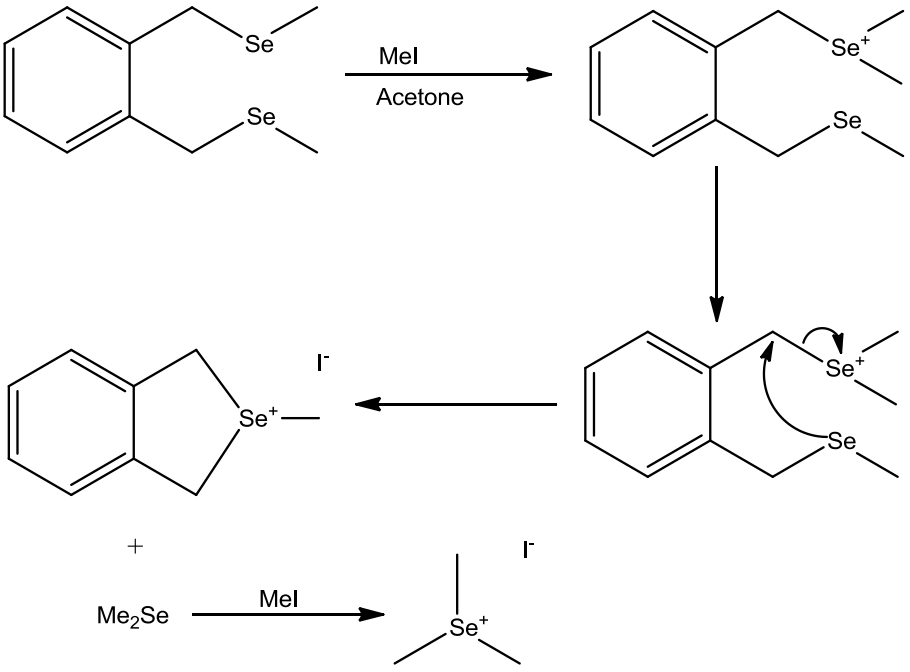

Figure 2.20 Possible mechanism for formation of $[o\text{-}C_6H_4(CH_2)_2SeMe]I$ and $[Me_3Se]I$.

Quaternisation of one selenium by MeI (or coordination to the Group 13 Lewis acid) will polarise the Se-$C_\alpha H_2$ bond, allowing the lone pair on the second selenium to attack the carbon forming a cyclic selenonium cation and eliminating Me_2Se (figure 2.20). The Me_2Se then reacts with further MeI to form $[Me_3Se]I$.

In contrast, the tellurium analogue behaved differently; *o*-$C_6H_4(CH_2TeMe)_2$ quaternises "normally" to form *o*-$C_6H_4(CH_2TeMe_2I)_2$ which has a dimer structure composed of a Te_4I_4 cubane core.[17]

It is clear from these observations that small differences in structure affect the balance between 'normal' quaternisation and elimination in these systems. It is possible that the Te-C bond is less polar, due the less electronegative tellurium centre and consequently the suggested mechanism (figure 2.20) is disfavoured.

2.3 Conclusions

A series of tetradentate chalcogenoether ligands has been produced in high purity and fully characterised. Tellurium containing ligands are highly sensitive and difficult to isolate. However, a new telluroether ligand was produced and spectroscopically characterised.

Synthesis of $C(CH_2SeCH_3)_4$ can produce cyclopropyl ligands dependant on the molar ratio of reactants. In contrast, $(CH_2)_2C(CH_2TeMe)_2$ and Me_2Te_2 are the only significant products of the reaction of $C(CH_2Br)_4$ with LiTeMe. Upon quaternisation with MeI the cyclopropyl unit in $(CH_2)_2C(CH_2SeMe)_2$ is cleaved, however, the tellurium analogue is unaffected.

Complex	$C_6H_2(CH_2SMe)_4$	$C_6H_2(CH_2SeMe)_4$	$[(CH_2)_2C(CH_2TeCH_3)_2]_2$	$[o\text{-}C_6H_4(CH_2)_2SeMe]I$
Formula	$C_{14}H_{22}S_4$	$C_{14}H_{22}Se_4$	$C_9H_{16}I_2Te_2$	$C_9H_{11}ISe$
M	318.56	506.16	637.25	325.04
Crystal system	Monoclinic	Triclinic	Monoclinic	Monoclinic
Space group	$P2_1/c$ (#14)	$Pbar1$ (#2)	$P2_1/n$ (#14)	$P2_1/n$ (#14)
a (Å)	9.6553(10)	9.172(3)	10.9852(15)	7.8050(10)
b (Å)	20.575(3)	9.618(4)	13.472(2)	11.2813(15)
c (Å)	9.2189(15)	11.742(6)	11.9328(15)	11.5214(15)
α (°)	90	107.83(2)	90	90
β (°)	113.249(7)	91.12(3)	114.696(10)	97.474(10)
γ (°)	90	116.92(2)	90	90
U (Å^3)	1682.7(4)	863.9(7)	1604.5(4)	1005.8(2)
Z	4	2	4	4
μ(Mo-Kα)/mm^{-1}	0.547	8.477	7.453	6.741
F(000)	680	484	1136	608
Total no. of reflections	22435	9140	13490	11656
Unique reflections	3122	3647	3583	2269
B_{eq}	0.048	0.086	0.102	0.024
No. of parameters, restraints	168, 0	167, 0	118, 17	100, 0
R_1[b] [$I_o > 2\sigma(I_o)$]	0.075	0.059	0.088	0.023
R_1 (all data)	0.106	0.114	0.163	0.025
wR_2[b] [$I_o > 2\sigma(I_o)$]	0.224	0.099	0.220	0.051
wR_2 (all data)	0.247	0.117	0.278	0.052

[a] Common items: temperature = 120 K; wavelength (Mo-Kα) = 0.71073 Å; θ(max) = 27.5°.

[b] $R_1 = \Sigma||F_o| - |F_c||/\Sigma|F_o|$. $wR_2 = [\Sigma w(F_o^2 - F_c^2)^2/\Sigma wF_o^4]^{1/2}$.

Table 2.5 Crystal data and structure refinement details[a].

2.4 Experimental

2.4.1 Synthesis

1,2,4,5-tetrakis(methylthiomethyl)benzene, 1,2,4,5-$C_6H_2(CH_2SMe)_4$

Liquid ammonia (150 mL) was condensed into a 500 mL three necked flask, equipped with condenser and pressure equalising addition funnel at –78 °C using a dry-ice/acetone slush bath. Sodium (0.76 g, 33.2 mmol) was added and the blue solution stirred for 10 min. under N_2. Dimethyldisulfide (1.5 mL 17.3 mmol) was added slowly, which discharged the blue colour. The NH_3 was left to evaporate under a stream of N_2, and the NaSMe dissolved in 100 mL of dry EtOH. 1,2,4,5-tetrakis(bromomethyl)benzene (3.0g, 6.67 mmol) was dissolved in warm degassed EtOH (250 mL), and added dropwise to the NaSMe solution. After half the solution was added the flask was heated to reflux and the addition completed. The mixture was heated to reflux overnight. The cooled reaction mixture was transferred to a separating funnel, and saturated aqueous $NaHCO_3$ (100 mL) added. The mixture was extracted with CH_2Cl_2 (3 × 200 mL) and the organic phase was collected, washed with 100 mL brine and dried over $MgSO_4$. Upon removal of most of the solvent, the product precipitated as a white solid which was collected by filtration, washed with hexane and dried under vacuum. A second crop of crystalline product was collected by combining the hexane washings with the CH_2Cl_2 mother-liquor and cooling at –30 °C. Overall yield: 1.85 g, 87 %. Anal. Found: C, 52.83; H, 6.79. Calc. for $C_{14}H_{22}S_4$: C, 52.78; H, 6.96 %. ^{1}H NMR ($CDCl_3$): 2.05 (s, 12[H], SMe), 3.81 (s, 8[H], CH_2), 7.13 (s, 2[H], aromatic CH) ppm. $^{13}C\{^1H\}$ NMR ($CDCl_3$): 15.6 (SMe), 35.2 (CH_2), 133.0 (CH), 135.2 (aromatic quaternary) ppm. CIMS: *m/z*= 319 $[M]^+$.

1,2,4,5-tetrakis(methylselenomethyl)benzene, 1,2,4,5-$C_6H_2(CH_2SeMe)_4$

Freshly ground selenium powder (3.5 g, 44.4 mmol) was added to dry THF (25 mL) in a dry three necked round-bottomed flask under nitrogen. The solution was then frozen (-196 °C) with liquid nitrogen. MeLi solution (27.8 mL of 1.6 M solution in diethyl ether, 44.4 mmol) was then added via syringe and the mixture was left to thaw for 40 min, then stirred at room temperature for 2 h. 1,2,4,5-tetrakis(bromomethyl)benzene (2.5 g, 5.55 mmol) was then added and the reaction mixture was refluxed for 1 h, cooled and

hydrolysed with NaCl solution (25 mL). The organic layer was then separated and the aqueous layer was extracted with diethyl ether (3 × 20 mL). The combined extracts were dried over $MgSO_4$, filtered and the solvent removed under high vacuum to yield a yellow powder. Yield: 2.44 g, 86 %. Anal. Found: C 33.26, H 4.17. Calc. for $C_{14}H_{22}Se_4$: C, 33.22; H, 4.38 %. ^{1}H NMR ($CDCl_3$): 1.96 (s, 12[H], SeMe), 3.85 (s, 8[H], CH_2), 7.01 (s, 2[H], CH) ppm. $^{13}C\{^{1}H\}$ NMR ($CDCl_3$): 4.84 (SeMe), 25.05 (CH_2), 132.8 (CH), 135.5 (aromatic quaternary) ppm. $^{77}Se\{^{1}H\}$ NMR (CH_2Cl_2): 150.7 ppm. CIMS: *m/z*= 505 $[M]^+$. Crystals were grown by evaporation from CH_2Cl_2 solution.

1,2,4,5-tetrakis(methyltelluromethyl)benzene, 1,2,4,5-$C_6H_2(CH_2TeMe)_4$

Freshly ground tellurium powder (1.96 g, 19.9 mmol) was added to dry degassed THF (25 mL) and stirred in a dry three necked round bottomed flask under nitrogen. The solution was then frozen (-196 °C) with liquid nitrogen. MeLi solution (12.4 mL of 1.6 M solution in diethyl ether, 24.9 mmol) was then added via syringe, and the mixture was allowed to warm to 0 °C for 2 h while stirring. When all of the tellurium has reacted, the pale yellow solution was then frozen (-196 °C) with liquid nitrogen. 1,2,4,5-tetrakis(bromomethyl)benzene (2.0 g, 4.48 mmol) in dry THF (30 mL) was added via syringe drop wise over 10 minutes. The flask was then warmed to (-78 °C) in an acetone slush bath and stirred for 2 h, the dark orange reaction mixture was hydrolysed with a degassed saturated NaCl solution (25 mL), after hydrolysis the flask was moved to a ice bath and allowed to separate into the dark red aqueous layer and a orange organic layer with a white precipitate. The product was then extracted from the aqueous layer with diethyl ether (5 x 50 mL). The combined extracts were transferred via cannula to a nitrogen purged Schlenk tube and dried over $MgSO_4$ for 30 minutes. The solution was then filtered and the solvent removed under high vacuum at room temperature to yield a red solid. The product was stored in a foil wrapped schlenk under nitrogen in the freezer. Yield: 1.2 g, 37 %. Anal. Found: C 27.58, H 3.36. Calc. for $C_{14}H_{22}Te_4$. ½Et_2O : C 26.64, H 3.66 %. ^{1}H NMR ($CDCl_3$): 1.87 (s, 12[H], TeMe), 3.9 (s, 8[H], CH_2), 6.86 (s, 2[H], aromatic CH) ppm.$^{13}C\{^{1}H\}$ NMR δ($CDCl_3$): -19.9 (CH_3), 4.0 (CH_2), 133.0 and 137.3 (aromatics) ppm. $^{125}Te\{^{1}H\}$ NMR ($CDCl_3$): 259.7 ppm.

1,1,1,1-tetrakis(methylthiomethyl)methane, $C(CH_2SMe)_4$[1]

This was synthesized in a way similar to that described for 1,2,4,5-tetrakis(methylthiomethyl)benzene above, starting from (5.0 g, 12.9 mmol) $C(CH_2Br)_4$, (1.42 g, 61.7 mmol) Na and (2.7 mL, 61.9 mmol) of Me_2S_2. After removal of volatiles the yellow liquid was distilled to yield the product as a colourless liquid. Yield: 3.05 g, 92 %. ^{1}H NMR ($CDCl_3$): 2.12 (s, 12[H], SMe), 2.81 (s, 8[H], CH_2) ppm. $^{13}C\{^1H\}$ NMR ($CDCl_3$): 17.5 (SMe), 40.8 (CH_2), 44.9 ($C_{quaternary}$) ppm. CIMS: *m/z*= 257 $[M]^+$.

1,1,1,1-tetrakis(methylselenomethyl)methane, $C(CH_2SeMe)_4$

Freshly ground selenium powder (2.8 g, 3.51 mmol) was added to dry THF (25 mL) and was stirred in a dry three necked round-bottomed flask under nitrogen. The solution was then frozen with liquid nitrogen. MeLi solution (21.9 mL of 1.6 M solution in diethyl ether, 3.51 mmol) was then added via syringe and left to thaw for 40 min, then stirred at room temperature for 2 h. Pentaerythrityl tetrabromide (3.0 g, 0.78 mmol) in THF (30 mL) was then added dropwise and the solution was stirred for 15 h before heating to 65 °C for 30 min. After cooling, the reaction mixture was hydrolysed with NaCl solution (25 mL). The organic layer was separated and the aqueous layer extracted via separation with diethyl ether (3 × 20 mL). The combined organic solutions were dried over $MgSO_4$, filtered and the solvent removed under vacuum to yield pale yellow oil. Kugelröhr distillation (110 °C, 0.1 mmHg) removed volatiles, and the residue is pure $(CH_2)C(CH_2SeCH_3)_2$. Yield: 1.91 g, 55 %. ^{1}H NMR ($CDCl_3$): 2.07 (s, 12[H], SeMe), 2.86 (s, 8[H], CH_2) ppm. $^{13}C\{^1H\}$ NMR ($CDCl_3$): 6.27 (SeMe), 35.2 (CH_2), 44.4 ($C_{quaternary}$) ppm.
$^{77}Se\{^1H\}$ NMR (CH_2Cl_2): 24.5 ppm. CIMS: *m/z*= 445 $[M]^+$.

1,1-bis(methylselenomethyl)cyclopropane, $(CH_2)_2C(CH_2SeCH_3)_2$

Freshly ground selenium powder (5 g, 6.25 mmol) was added to dry THF (25 mL) and stirred in a dry three necked round-bottomed flask under nitrogen. The solution was then frozen with liquid nitrogen. MeLi solution (39.0 mL of 1.6 M solution in diethyl ether, 6.45 mmol) was then added via syringe to the selenium and left to thaw for 40 min, then stirred at room temperature for 2 h. Pentaerythrityl tetrabromide (3.0 g, 0.781 mmol) in THF (30 mL) was then added to the solution and refluxed for 1 h. The flask was allowed to

cool and then hydrolysed with NaCl solution (25 mL). The product was then extracted via separation with diethyl ether (3 × 20 mL) dried over $MgSO_4$ filtered and the solvent and Me_2Se_2 removed under high vacuum to leave a pale yellow oil. Yield: 1.74 g, 87 %. ^{1}H NMR ($CDCl_3$): 0.61 (s, 4[H], CH_2 cyclopropyl), 2.10 (s, 8[H], SeMe), 2.82 (s, 4[H], CH_2) ppm. $^{13}C\{^1H\}$ NMR ($CDCl_3$): 5.3 (C-cyclopropyl), 15.0 (SeMe), 34.9 (CH_2) ppm. $^{77}Se\{^1H\}$ NMR (CH_2Cl_2): 58.6 ppm. GC-MS: *m/z*= 258 (RT. 5.2) $[M]^+$.

1,1-Bis(methyltellluromethyl)cyclopropane, $(CH_2)_2C(CH_2TeCH_3)_2$[3]

Freshly ground tellurium, powder (3.02 g, 29.3 mmol) was added to dry THF (25 mL) under nitrogen. The solution was then frozen with liquid nitrogen. MeLi solution (15.6 mL of 1.6 M solution in diethyl ether, 29.6 mmol) was then added via syringe and the mixture left to thaw for 40 min., then stirred at 0 °C for 2 h. The flask was then placed in an acetone slush bath (-78 °C) and pentaerythrityl tetrabromide (2.5 g, 6.5 mmol) in THF (30 mL) was added dropwise, then stirred for a further 2 h.. The reaction mixture was hydrolysed with saturated NaCl solution (25 mL). The product was extracted with diethyl ether (3 x 20 mL), the ether extract dried over $MgSO_4$, filtered, and the solvent and Me_2Te_2 removed under high vacuum to yield a dark red oil. 1.2g. (52 % on $C(CH_2Br)_4$). ^{1}H NMR ($CDCl_3$): 0.65 (s, 4[H], $CH_{2\ cyclopropyl}$), 1.87 (s, 6[H], TeMe), 2.80 (s, 4[H], CH_2Te) ppm. $^{13}C\{^1H\}$ NMR ($CDCl_3$): -22.0 (TeMe), 16.4 (CH_2Te), 17.7 (CH_2C), 22.3 ($C_{quaternary}$) ppm. $^{125}Te\{^1H\}$ NMR (CH_2Cl_2): 63.1 ppm.

Reaction of I_2 with $(CH_2)_2C(CH_2TeCH_3)_2$

1,1-Bis(methyldi-iodomethyltelluro)cyclopropane (0.19 g, 0.54 mmol) in dry degassed THF (20 mL) was stirred in a foil wrapped Schlenk tube, diiodine (0.27 g, 1.1 mmol) in dry degassed THF (20 mL) was added via a syringe and stirred for a further 2 h. The solvent was then reduced in volume to 5 mL before adding dry diethyl ether (10 mL). The dark red solid was collected via a filter canulla and dried *in vacuo*. Yield: 0.41 g (51 %). Anal: Calc. for $C_7H_{14}I_4Te_2$: C, 9.8; H, 1.6. Found: C, 10.2; H, 1.6 %. ^{1}H NMR (d^6- dmso- poorly soluble and solvent resonance partially obscures signal):
0.99 (s, 4[H], $CH_{2\ cyclopropyl}$), 2.65 (s, 12[H], TeMe), 3.12 (br, 4[H], CH_2Te) ppm.
$^{125}Te\{^1H\}$ NMR (d^6-dmso): 598 ppm.

Reaction of MeI with $(CH_2)_2C(CH_2SeMe)_2$

1,1,bis(methylselenomethyl)cyclopropane (0.2 g, 0.78 mmol) was placed in a Schlenk tube 10 mL of degassed acetone was added via syringe an excess of iodomethane (2.5 mL) in degassed acetone (10 mL) and heated to 40 °C for 2 h. The white precipitate was collected *via* filter canulla and dried under high vacuum to yield a white solid. The filtrate was refrigerated for 2 days when large dark yellow crystals formed. Yield: 0.16 g (41 % based upon Se). ^{1}H NMR (D_2O): 2.7 s, Lit.[18] (D_2O) 2.7 ppm. ^{77}Se{^{1}H} NMR (dmso): 256, Lit.[1] 253 ppm. ES$^+$ MS *m/z* = 125 $[Me_3Se]^+$. The structure was solved and showed to be $[Me_3Se]I$ (orthorhombic, P*nma*, a = 13.960, b = 7.944, c = 6.158Å), which is in excellent agreement with the literature data.[2]

Reaction of MeI with *o*-$C_6H_4(CH_2SeMe)_2$

o-$C_6H_4(CH_2SeMe)_2$ (0.2 g, 0.66 mmol) was placed in a Schlenk tube 10 mL of degassed acetone was added via syringe an excess of iodomethane (2.5 mL) in degassed acetone (10 mL) and heated to 40 °C after 2 h. The white precipitate was collected *via* filter canulla and dried under high vacuum. Crystals were grown by placing the filtrate in the freezer for a week. Yield: 0.12 g, 88 % (when calculated for selenophene derivative). ^{1}H NMR ($CDCl_3$): 1.95 (s, [3H], Me), 4.25 (s, [4H], CH_2), 7.1 (m [4H] (C-$H_{aromatic}$) ppm. ^{77}Se{^{1}H} NMR ($CDCl_3$) 406 ppm. ES MS$^+$ *m/z* = 199 $[C_9H_{11}Se]^+$. The filtrate from this reaction also contained large amounts of $[Me_3Se]I$ ^{77}Se{^{1}H} NMR (acetone): 259 ppm. ES$^+$ MS *m/z* = 125 $[Me_3Se]^+$.

Reaction of MeI with $(CH_2)_2C(CH_2TeCH_3)_2$

1,1-Bis(methyltelluromethyl)cyclopropane (0.10g, 0.28 mmol) was stirred with an excess of iodomethane (1.5 mL) in CH_2Cl_2 (20 mL) for 30 min.. The yellow product solid was collected and dried *in vacuo*. Yield: 0.13 g (77 %) Anal: Calc. for $C_9H_{20}I_2Te_2$ C, 17.0; H 3.2. Found: C, 16.8; H, 3.1 %. ^{1}H NMR (d^6- dmso): 0.92 (s, 4[H], $CH_{2\ cyclopropyl}$), 2.25 (s, 12[H], TeMe), 3.20 (s, 4[H], CH_2Te) ppm. ^{125}Te{^{1}H} NMR (N,N-dimethylformamide-d^6-acetone): 470.8 ppm. ES$^+$-MS: *m/z* = 511 $[M-I]^+$. Crystals were grown by cooling a dmso/ methanol solution of the compound at 255 K.

2.4.2 X-ray crystallography

Details of crystallographic data collection and refinement are given in table 2.5. The crystallisation details are provided in the Experimental Section 2.4. Data collection used a Nonius Kappa CCD diffractometer fitted with monochromated Mo Kα X-radiation (λ = 0.71073 Å), and with the crystals held at -153 °C in a dinitrogen gas stream. Structure solution and refinement were straightforward,[19-21] except as described below, and hydrogen were introduced into the models in calculated positions using the default C-H distances. The diffraction data for $[(CH_2)_2C(CH_2TeCH_3)_2]I_2$ was modelled by Dr. M. Webster. The modest quality crystal data needed several SHELXL DELU commands to restrain the anisotropic atomic displacement parameters (adp).

2.5 References

1. K. Brodersen, W. Roelz, G. Jordan, R. Gerbeth and J. Ellerman, *Chem. Ber.*, 1978, **111**, 132.
2. D. J. Gulliver, E. G. Hope, W. Levason, S. G. Murray, D. M. Potter and G. L. Marshall, *J. Chem. Soc., Perkin Trans. II*, 1984, 429.
3. E. G. Hope, T. Kemmitt and W. Levason, *Organometallics*, 1988, **7**, 78.
4. W. Levason, M. Nirwan, R. Ratnani, G. Reid, N. Tsoureas and M. Webster, *Dalton Trans.*, 2007, 439.
5. W. Levason and T. Kemmitt, *Organometallics*, 1989, **8**, 1303.
6. W. Levason, L. P. Ollivere, G. Reid, N. Tsoureas and M. Webster, *J. Organomet. Chem.*, 2009, **694**, 2299.
7. D. H. O'Brien, N. Deren, C. K. Huang, K. J. Irgolic and F. F. Knapp, *Organometallics*, 1983, **2**, 305.
8. N. P. Luthra and J. D. Odom, eds. S. Patai and Z. Rappoport, Wiley, NY, 1986, vol. 1, p. 189.
9. R. K. Chadha and J. E. Drake, *J. Organomet. Chem.*, 1986, **299**, 331.
10. Z.-L. Zhou, Y.-Z. Huang, Y. Tang, Z.-H. Chen, L.-P. Shi, X.-L. Jin and Q.-C. Yang, *Organometallics*, 1994, **13**.
11. N. J. Hill, W. Levason, G. Reid and A. J. Ward, *J. Organomet. Chem.*, 2002, **642**, 186.
12. R. J. Shine, in *Organic Selenium Compounds*, eds. D. L.Klayman and W. H. H. Gunther, Wiley, NY, 1973, ch. 6.
13. W. McFarlane and R. J. Wood, *J. Chem. Soc.*, 1972, 1397.
14. R. Pietschnig, S. Spirk, G. N. Rechberger and K. Merz, *Inorg. Chim. Acta.*, 2008, **361**, 1958.
15. S. D. Reid, A. L. Hector, W. Levason, G. Reid, B. J. Waller and M. Webster, *Dalton Trans.*, 2007, 4769.
16. C. Gurnani, W. Levason, R. Ratnani, G. Reid and M. Webster, *Dalton Trans.*, 2008, 6274.
17. W. Levason, B. Patel, G. Reid and A. J. Ward, *J. Organomet. Chem.*, 2001, **619**, 218.
18. A. J. Barton, W. Levason and G. Reid, *J. Organometal. Chem.*, 1999, **579**, 235.
19. G. M. Sheldrick, SHELXS-97, Program for Crystal Structure Solution, University of Göttingen, Germany, 1997.
20. G. M. Sheldrick, SHELXL-97, Program for Crystal Structure Refinement, University of Göttingen, Germany, 1997.
21. H. D. Flack, *Acta Crystallogr.*, 1983, **39**, 876.

CHAPTER 3

Synthesis and characterisation of homo-bimetallic complexes based upon metal carbonyls

3.1 Introduction

The aim of this chapter was to investigate the coordination chemistry of a series of Group neutral 16 donor ligands, specifically described in Chapter 2, with Group 6 and 7 metal carbonyls. There have been detailed studies of mono- and bi-dentate Group 16 ligands and also macrocyclic analogues with metal carbonyls. However, polydentates especially ligands which cannot bind all donors to a single metal centre have not been studied.[1, 2] This Chapter describes some chemistry of this last class, which are also potentially suitable for assembling homo- or hetero-nuclear bimetallic complexes. There is particular interest in hetero-bimetallic molecules of this type as catalysts and biomolecules. Figure 3.1 shows the ligands used in this work and examples of chelation of one metal centre to each ligand.

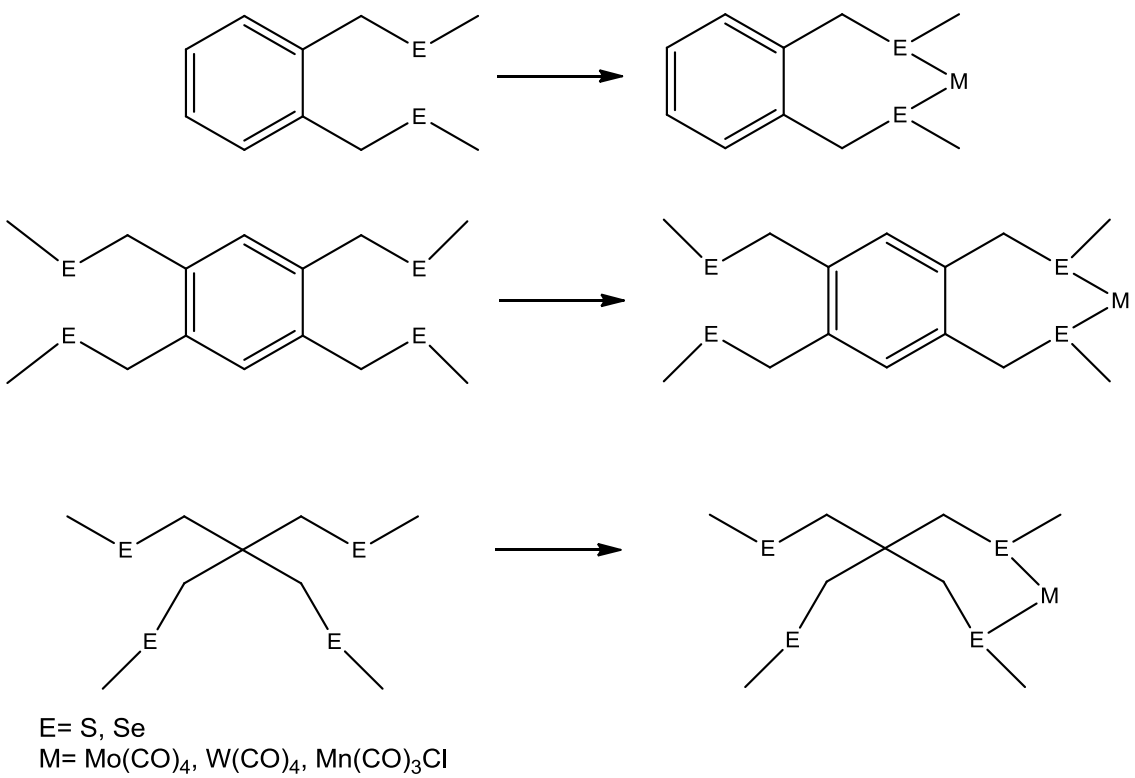

Figure 3.1 The three ligand types binding to a single metal centre.

Hetero-bimetallic molecules require a multidentate ligand capable of binding to two different metal centres; the synthesis of a mono-metallic complex must be in high purity in order to successfully attach a second metal.

Similar tetra dentate thioether ligands; 1,2,4,5-$C_6H_2(CH_2S(CH_2)_4CH_3)_4$ have been shown to form a molybdenum tetracarbonyl complex by stirring $[Mo(CO)_4(MeCN)_3]$ and the ligand in THF at 0 °C for 12 h.[3] This method however, required column chromatography to separate the complex from free ligand and although isolating some crystals the bulk material was not pure. $[Mo(CO)_4\{\mu\text{-}C_6H_2(CH_2S(CH_2)_4CH_3)_4\}]$ has been structurally characterised and is displayed in figure 3.2 the spectroscopic data from this compound will be used throughout this chapter to compare data collected from new thioether molydenium species.

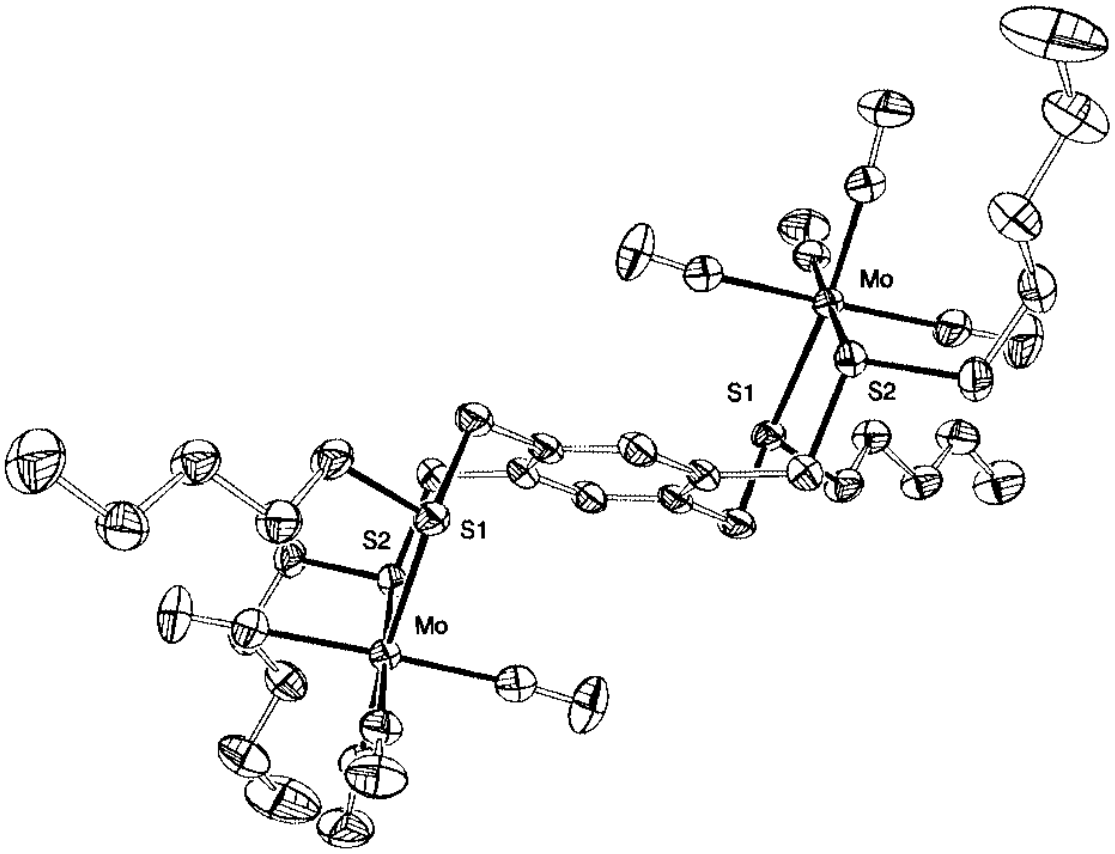

Figure 3.2 Structure of $[Mo(CO)_4\{\mu\text{-}C_6H_2(CH_2S(CH_2)_4CH_3)_4\}]$ ellipsoids are drawn at the 50% probability level and H atoms have been omitted for clarity.[3]

3.2 Results

3.2.1 Synthesis

Some of the compounds described in this chapter decomposed readily in solution and required careful synthetic techniques to obtain pure samples for characterisation.

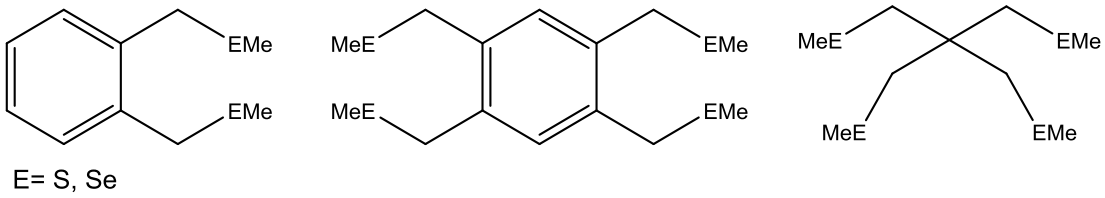

Figure 3.3 Structures of the three ligand types used in this chapter.

The ligands 1,2,4,5-$C_6H_2(CH_2SMe)_4$ and 1,2,4,5-$C_6H_2(CH_2SeMe)_4$ are expected to form seven-membered chelate rings, and for comparison, complexes of the simpler bidentates *o*-$C_6H_4(CH_2EMe)_2$ were synthesised. In contrast the spirocyclic ligands $C(CH_2SMe)_4$ and $C(CH_2SeMe)_4$ are expected to form six-membered chelate rings and these complexes were compared with complexes of $MeE(CH_2)_3EMe$.[4, 5]

The complexes [$Mo(CO)_4$(*o*-$C_6H_4(CH_2SMe)_2$)], [$W(CO)_4$(*o*-$C_6H_4(CH_2SMe)_2$)], [$Mo(CO)_4$(*o*-$C_6H_4(CH_2SeMe)_2$)] and [$W(CO)_4$(*o*-$C_6H_4(CH_2SeMe)_2$)] were produced in high yields by reacting the ligand with [$Mo(CO)_4$(nbd)] or [$W(CO)_4$(tmpa)] respectively. The compounds were air-stable yellow crystalline solids with spectroscopic properties (below) consistent with *cis*-tetracarbonyls.[4-6]

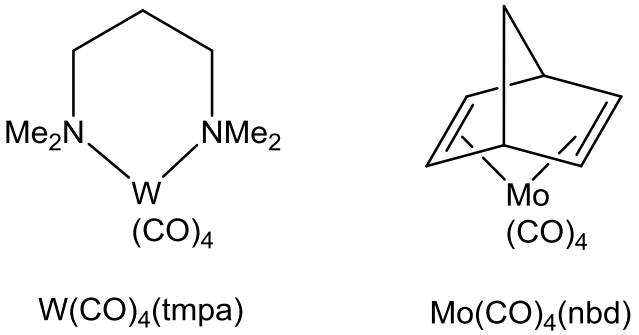

$W(CO)_4(tmpa)$ $Mo(CO)_4(nbd)$

Figure 3.4 Metal precursors $[Mo(CO)_4(nbd)]$ and $[W(CO)_4(tmpa)]$ synthesised from literature methods.[7, 8]

$[Mn(CO)_3Cl\{L\}]$ (L = *o*-$C_6H_4(CH_2SMe)_2$ or *o*-$C_6H_4(CH_2SeMe)_2$) were synthesised by reacting the ligand and $[Mn(CO)_5Cl]$. They show similar properties to other examples with Group 16 donors, but were poorly soluble in halocarbon solvents.[5]

Reacting $[Mo(CO)_4(nbd)]$ with 1,2,4,5-$C_6H_2(CH_2SMe)_4$ in a 1:1 molar ratio in toluene/CH_2Cl_2 produced a yellow-brown solid. ^{1}H NMR spectroscopy showed this product to be a mixture of $[Mo(CO)_4\{1,2,4,5\text{-}C_6H_2(CH_2SMe)_4\}]$ and $[Mo(CO)_4\{\mu\text{-}1,2,4,5\text{-}C_6H_2(CH_2SMe)_4\}Mo(CO)_4]$. The monometallic $[Mo(CO)_4\{1,2,4,5\text{-}C_6H_2(CH_2SMe)_4\}]$ could be extracted with diethyl ether from the crude material to produce a pure sample of the yellow solid. The less soluble bimetallic $[Mo(CO)_4\{\mu\text{-}1,2,4,5\text{-}C_6H_2(CH_2SMe)_4\}Mo(CO)_4]$ could then be recrystallised from THF. Usually trace amounts of the other complex or free ligand could be observed by ^{1}H and $^{13}C\{^1H\}$ NMR, suggesting these compounds are prone to rearrangement. The structures of both complexes were determined by X-ray crystallography. Pure samples of the corresponding tungsten complexes could not be isolated, due to very poor solubility and seemed to rearrange readily. The selenoether complexes $[Mo(CO)_4\{1,2,4,5\text{-}C_6H_2(CH_2SeMe)_4\}]$ and $[Mo(CO)_4\{\mu\text{-}1,2,4,5\text{-}C_6H_2(CH_2SeMe)_4\}Mo(CO)_4]$ however, could be prepared in high purity under direct conditions.

Reacting $[Mn(CO)_5Cl]$ with 1,2,4,5-$C_6H_2(CH_2SMe)_4$ in either a 1:1 or 2:1 molar ratio in hot CH_2Cl_2 only produced yellow crystals of $[Mn(CO)_3Cl\{1,2,4,5\text{-}C_6H_2(CH_2SMe)_4\}]$, using higher molar ratios caused decomposition and significant amounts of $Mn_2(CO)_{10}$

identified crystallographically. Interestingly, crystals obtained from a solution of the 1:1 complex were identified by the X-ray structure determination as the dinuclear species $[Mn(CO)_3Cl\{\mu\text{-}1,2,4,5\text{-}C_6H_2(CH_2SMe)_4\}Mn(CO)_3Cl]$, although this could not be isolated in bulk. Most probably this is a result of rearrangement in solution and deposition (crystallisation) of the less soluble species.

Complexes of $C(CH_2SMe)_4$ and $C(CH_2SeMe)_4$ were found to be more soluble in non-polar solvents, consequently synthesis and characterisation was less challenging than corresponding complexes of $1,2,4,5\text{-}C_6H_2(CH_2SMe)_4$ and $1,2,4,5\text{-}C_6H_2(CH_2SeMe)_4$. The monometallic complexes $[Mo(CO)_4\{C(CH_2SMe)_4\}]$, $[W(CO)_4\{C(CH_2SMe)_4\}]$, $[Mn(CO)_3Cl\{C(CH_2SMe)_4\}]$ and bimetallic $[(CO)_4Mo\{\mu\text{-}C(CH_2SMe)_4\}Mo(CO)_4]$ were all produced in high yields by reaction of the appropriate ligands with $[Mo(CO)_4(nbd)]$, $[W(CO)_4(tmpa)]$ and $[Mn(CO)_5Cl]$ respectively. They are air-stable yellow crystalline solids isolated in good yields and fully characterised.

3.2.2 Spectroscopy

The spectroscopic properties of Groups 6-10 metal carbonyl complexes with Group 15 or 16 donor ligands have been intensively studied, to establish trends and explore the metal-ligand bonding. Although very careful comparisons show relatively systematic changes of the spectral data with metal, donor type (S or Se), chelate ring size, and organic substituents, the differences are often small. The measurements must of course be made under similar conditions, e.g. in the same solvent or at the same temperature.[4, 5] In this Chapter the spectroscopic data are used to characterise the new complexes, and are compared with literature data on the nearest available analogues to confirm the identity of the new complexes. Due to limitations in solubility and stability of some of the new complexes, it was not always possible to record data under identical conditions, this accounts for some small anomalies in the observed trends.

3.2.3 IR spectroscopy

As discussed in Chapter 1 tetracarbonyl complexes are predicted to exhibit four IR active CO stretching vibrations. In a few cases only three bands are observed which is attributable to a lack of resolution of one of the A_1 and the B_1 modes.[9] A typical spectrum of the

carbonyl region (1600-2200 cm^{-1}) of $[W(CO)_4\{o\text{-}C_6H_4(CH_2SCH_3)_2\}]$ is shown below. The two absorptions centred at *ca*. 1917, 1890 cm^{-1} were sometimes unresolved and seen as one broad peak, as illustrated in this example.

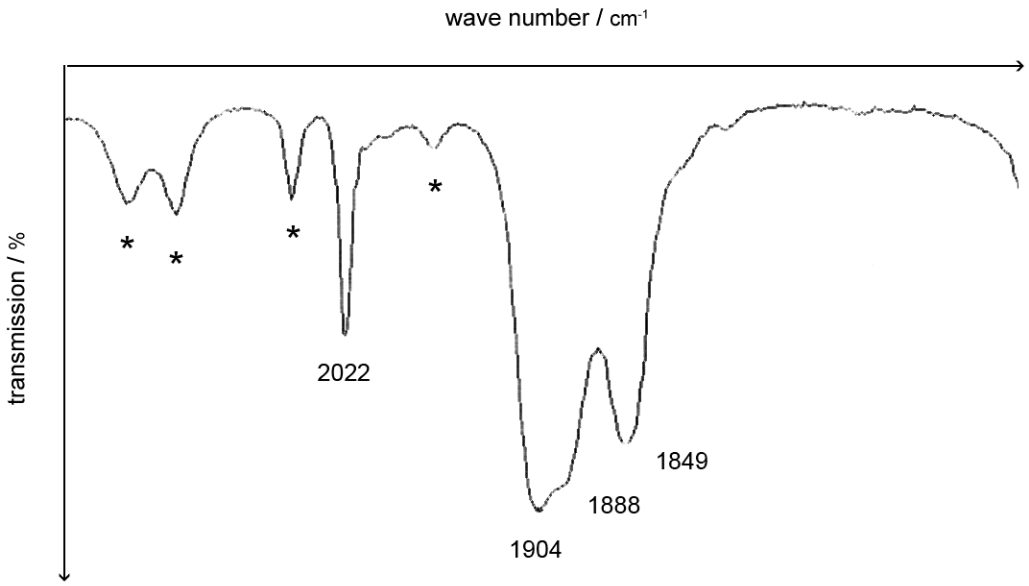

* Absorptions assigned to CH_2Cl_2

Figure 3.5 The carbonyl region (1600-2200 cm^{-1}) IR spectrum of $[W(CO)_4\{o\text{-}C_6H_4(CH_2SCH_3)_2\}]$ recorded in CH_2Cl_2.

Compound	ν_{CO}/cm^{-1}
$[Mo(CO)_4\{o\text{-}C_6H_4(CH_2SCH_3)_2\}]$	2028, 1915, 1895, 1853
$[W(CO)_4\{o\text{-}C_6H_4(CH_2SCH_3)_2\}]$	2022, 1904, 1888, 1849
$[Mo(CO)_4\{o\text{-}C_6H_4(CH_2SeCH_3)_2\}]$	2024, 1914, 1895, 1854
$[W(CO)_4\{o\text{-}C_6H_4(CH_2SeCH_3)_2\}]$	2018, 1904, 1886, 1850
$[Mo(CO)_4\{C_6H_2(CH_2SCH_3)_4\}]$	2036, 1927, 1884
$[Mo(CO)_4\{\mu\text{-}C_6H_2(CH_2SCH_3)_4\}Mo(CO)_4]$	2023, 1907, 1876, 1828
$[Mo(CO)_4\{C_6H_2(CH_2SeCH_3)_4\}]$	2024, 1917, 1895, 1856
$[Mo(CO)_4\{\mu\text{-}C_6H_2(CH_2SeCH_3)_4\}Mo(CO)_4]$	2025, 1914, 1893, 1829
$[Mo(CO)_4\{C(CH_2SCH_3)_4\}]$	2026, 1921, 1857
$[W(CO)_4\{C(CH_2SCH_3)_4\}]$	2010, 1900(sh), 1890, 1843
$[(CO)_4Mo\{\mu\text{-}C(CH_2SCH_3)_4\}Mo(CO)_4]$	2024, 1911, 1899, 1860
$[Mo(CO)_4\{C(CH_2SeCH_3)_4\}]$	2020, 1904, 1883, 1851
$[Mo(CO)_4\{o\text{-}C_6H_4(SCH_3)_2\}]$[a]	2028, 1917(s, br), 1870
$[Mo(CO)_4\{o\text{-}C_6H_4(SeCH_3)_2\}]$[a]	2025, 1914(s, br), 1870
$[W(CO)_4\{o\text{-}C_6H_4(SeCH_3)_2\}]$[a]	2019, 1901(s, br), 1866
$[Mo(CO)_4\{CH_3SCH_2CH_2CH_2SCH_3\}]$[a]	2023, 1910, 1895, 1856
$[W(CO)_4\{CH_3SCH_2CH_2CH_2SCH_3\}]$[a]	2018, 1897, 1890, 1852
$[Mo(CO)_4\{CH_3SeCH_2CH_2CH_2SeCH_3\}]$[a]	2020, 1908, 1895, 1855
$[Mo(CO)_4\{\mu\text{-}C_6H_2(CH_2S(CH_2)_4CH_3)_4\}]$[b]	2026, 1918(s), 1900(sh), 1864

[a] Comparative data recorded in CH_2Cl_2[4]

[b] Comparative data recorded in CH_2Cl_2 and hexane (1:1)[3]

Table 3.1 Solution IR spectroscopic data of C≡O region measured in CH_2Cl_2.

Data for complexes with aromatic-backboned ligands are comparable with literature data of $[M(CO)_4\{o\text{-}C_6H_4(SeCH_3)_2\}]$ (M= Mo, W), all but two absorptions are ±15 cm^{-1} which can be attributed to different donor atoms and ligand architecture, especially the smaller 5-membered ring. Complexes with a spirocyclic ligand are comparable to $[M(CO)_4\{CH_3ECH_2CH_2CH_2ECH_3\}]$ (M = Mo, W and E = S, Se), each complex shows

good correlation with the literature data. In two cases $[Mo(CO)_4\{\mu\text{-}C_6H_2(CH_2ECH_3)_4\}Mo(CO)_4]$ (E = S or Se) table 3.1 the lowest frequency carbonyl stretch was observed at ~ 1828 cm^{-1} some ~30 cm^{-1} lower than in the other complexes. The X-ray structure of the complex with E = S (below) shows one carbonyl group sitting over the aromatic backbone, and this probably accounts for the unusually low vibration frequency.

For tricarbonyl complexes $[Mn(CO)_3Cl\{L\}]$ each compound showed three strong absorptions as predicted from the point group discussed in Chapter 1. Table 3.2 gives solution IR data for each complex. The carbonyl region of a typical spectrum is shown below.

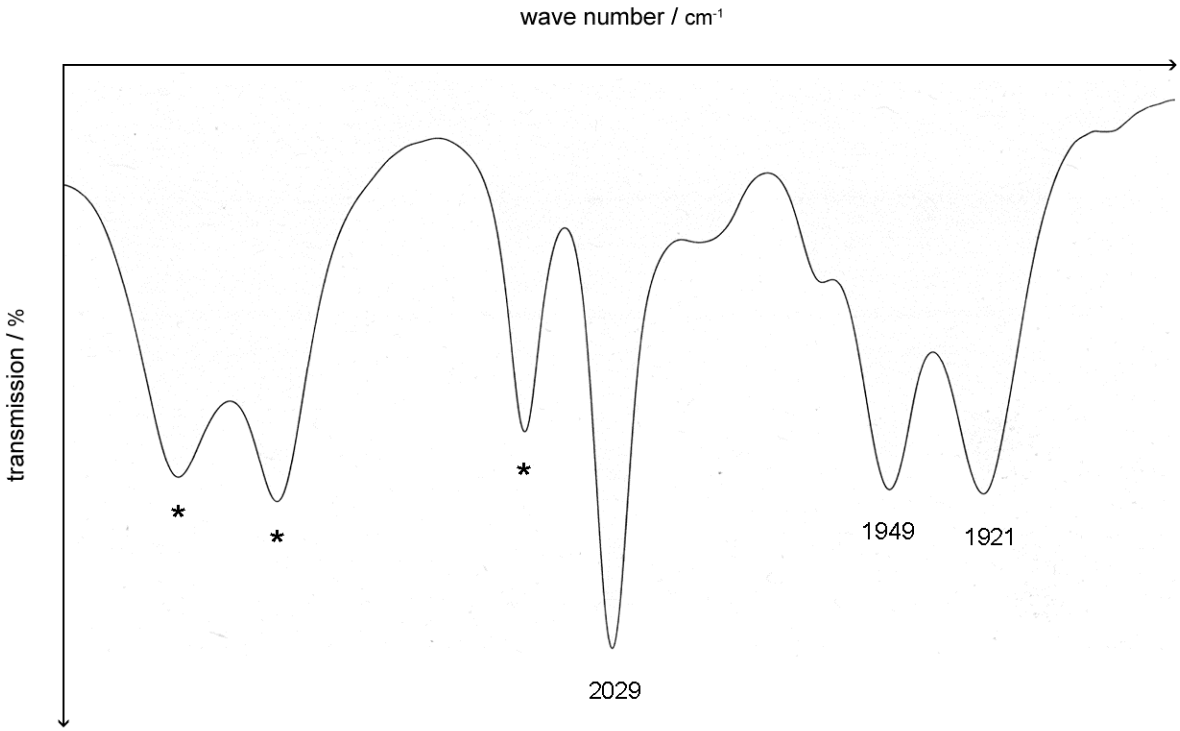

* Absorptions assigned to CH_2Cl_2

Figure 3.6 The carbonyl region (1600-2200 cm^{-1}) IR spectrum of $[Mn(CO)_3Cl\{o\text{-}C_6H_4(CH_2SeCH_3)_2\}]$ recorded in CH_2Cl_2.

Compound	ν_{CO}/cm^{-1}
$[Mn(CO)_3Cl\{o\text{-}C_6H_4(CH_2SCH_3)_2\}]$	2038, 1960 (vbr), 1910(sh)
$[Mn(CO)_3Cl\{o\text{-}C_6H_4(CH_2SeCH_3)_2\}]$	2030, 1949, 1921
$[Mn(CO)_3Cl\{C_6H_2(CH_2SCH_3)_4\}]$	2027, 1941, 1906
$[Mn(CO)_3Cl\{C(CH_2SCH_3)_4\}]$	2027, 1941, 1909
$[Mn(CO)_3Cl\{o\text{-}C_6H_4(SeCH_3)_2\}]^a$	2037, 1963, 1924
$[Mn(CO)_3Cl\{CH_3SeCH_2CH_2CH_2SeCH_3\}]^a$	2032, 1955, 1917

[a] Comparative data recorded in $CHCl_3$.[5]

Table 3.2 Solution IR spectroscopic data of C≡O region measured in CH_2Cl_2 unless stated otherwise.

$[Mn(CO)_3Cl\{CH_3SeCH_2CH_2CH_2SeCH_3\}]$ provides a useful comparison for complexes with a spirocyclic ligands, as they both form a 6-membered chelate ring after chelation to a metal centre. Each absorption is approximately 10 cm^{-1} higher compared to $[Mn(CO)_3Cl\{C(CH_2SCH_3)_4\}]$, these differences can be attributed to different donor atoms and solvent systems. Aromatic ligand complexes can be compared to data collected on $[Mn(CO)_3Cl\{o\text{-}C_6H_4(SeCH_3)_2\}]$, although only forming a 5-membered chelate ring after chelation, the similar ligand architecture provides a reasonable comparison. Each complex shows good correlation with the literature data.

3.2.4 NMR Spectroscopic studies

Multinuclear (^1H, $^{13}C\{^1H\}$, $^{77}Se\{^1H\}$, ^{55}Mn and ^{95}Mo) NMR spectroscopic studies were undertaken to give an insight in the character of these complexes in solution. The following section outlines the NMR spectroscopic data collected and discusses each nucleus in turn. The application of ^1H and $^{13}C\{^1H\}$ NMR spectroscopy was generally straightforward, the key points of note for these complexes was the presence or absence of fast pyramidal inversion in individual complexes. These two nuclei provide the clearest evidence to distinguish κ^2 from $\kappa^2\kappa'^2$ coordination modes and monitor the purity and solution stability of the various complexes. The other point of note is in the manganese complexes, the ^1H NMR resonances are often broadened by the proximity of the

quadrupolar manganese-55 nucleus; the $^{13}C\{^{1}H\}$ resonances of the carbonyl groups are also often very broad due to this effect, and individual resonances are sometimes not resolved, although the chalcogen ligand carbon resonances are usually quite sharp.

The ^{1}H NMR spectra of each complex was recorded at 300K in $CDCl_3$ and referenced internally to the solvent resonance. In the mono- and bimetallic complexes binding of two donor groups in the ligand is supported by a change in chemical shift of the associated resonances, whereas the resonances of the "free" donor groups are effectively unshifted – showing there is no communication between the free and bound donor units. This is expected since the linkers include saturated carbon groups. Most complexes produced with tetradentate ligands (1,2,4,5-$C_6H_2(CH_2SMe)_4$, 1,2,4,5-$C_6H_2(CH_2SeMe)_4$, $C(CH_2SMe)_4$ and $C(CH_2SeMe)_4$) were unstable in solution, freshly made samples in $CDCl_3$ showed clean ^{1}H NMR spectra but if left to stand for several hours a brown precipitate would form. ^{1}H NMR spectroscopy then identified the presence of free ligand and the complex; the precipitate however was identified.

The $^{13}C\{^{1}H\}$ NMR data were collected for all complexes and the carbonyl resonances are displayed in table 3.3.

Compound	**$\delta^{13}C\{^{1}H\}$/ppm**
$[Mo(CO)_4\{o\text{-}C_6H_4(CH_2SCH_3)_2\}]$	208.3(vbr)
$[W(CO)_4\{o\text{-}C_6H_4(CH_2SCH_3)_2\}]$[a]	201.9 (130 Hz), 206.2 (174 Hz)[g]
$[Mn(CO)_3Cl\{o\text{-}C_6H_4(CH_2SCH_3)_2\}]$	208.3(vbr)
$[Mo(CO)_4\{o\text{-}C_6H_4(CH_2SeCH_3)_2\}]$	207.4, 215.5
$[W(CO)_4\{o\text{-}C_6H_4(CH_2SeCH_3)_2\}]$[b]	201.6, 205.6
$[Mn(CO)_3Cl\{o\text{-}C_6H_4(CH_2SeCH_3)_2\}]$	217.0–220.5 (vbr)
$[Mo(CO)_4\{C_6H_2(CH_2SCH_3)_4\}]$	206.4, 215.6
$[Mo(CO)_4\{\mu\text{-}C_6H_2(CH_2SCH_3)_4\}Mo(CO)_4]$	206.4, 215.6
$[Mn(CO)_3Cl\{C_6H_2(CH_2SCH_3)_4\}]$	217.6(vbr)
$[Mo(CO)_4\{C_6H_2(CH_2SeCH_3)_4\}]$	211.4, 216.5
$[Mo(CO)_4\{\mu\text{-}C_6H_2(CH_2SeCH_3)_4\}Mo(CO)_4]$[c]	205.2, 217.7

Compound	$\delta^{13}C\{^1H\}$/ppm
$[Mo(CO)_4\{C(CH_2SCH_3)_4\}]$	206.4, 217.0
$[W(CO)_4\{C(CH_2SCH_3)_4\}]$	202.1, 208.0
$[(CO)_4Mo\{\mu\text{-}C(CH_2SCH_3)_4\}Mo(CO)_4]$	206.2, 216.4
$[Mn(CO)_3Cl\{C(CH_2SCH_3)_4\}]$	207.6, 217.6
$[Mo(CO)_4\{C(CH_2SeCH_3)_4\}]$	209.1, 215.1
$[Mo(CO)_4\{o\text{-}C_6H_4(SeCH_3)_2\}]$[d]	217.6, 205.8
$[Mo(CO)_4\{o\text{-}C_6H_4(SeCH_3)_2\}]$[d]	206.7, 218.0
$[W(CO)_4\{o\text{-}C_6H_4(SeCH_3)_2\}]$[d]	201 (v,br), 208.4 (165 Hz)[f]
$[Mo(CO)_4\{CH_3SCH_2CH_2CH_2SCH_3\}]$[d]	207.1, 217.0
$[W(CO)_4\{CH_3SCH_2CH_2CH_2SCH_3\}]$[d]	202.7 (126 Hz), 207.6 (156 Hz)[f]
$[Mo(CO)_4\{CH_3SeCH_2CH_2CH_2SeCH_3\}]$[d]	208.3, 216.8
$[Mn(CO)_3Cl\{o\text{-}C_6H_4(SeCH_3)_2\}]$[e]	218.8-221.7
$[Mn(CO)_3Cl\{CH_3SeCH_2CH_2CH_2SeCH_3\}]$[e]	216.7-223.1
$[Mo(CO)_4\{\mu\text{-}C_6H_2(CH_2S(CH_2)_4CH_3)_4\}]$[f]	215.2, 205.9

[a] Recorded in $CDCl_3$
[b] Recorded at 233 K
[c] Recorded in CD_3CN due to poor solubility
[d] Comparative data from literature in $CDCl_3$.[4]
[e] Comparative data from literature in $CDCl_3$.[5]
[f] Comparative data from literature in $CDCl_3$.[3]
[g] $^1J(^{183}W\text{-}^{13}C)$/Hz

Table 3.3 Selected $^{13}C\{^1H\}$ NMR spectroscopic data (for C=O ligands) recorded in CD_3Cl at ambient temperatures unless stated otherwise.

Carbonyl resonances for the metal complexes synthesised show good correlation to the literature data on comparable complexes. Again, when making detailed comparisons, it is necessary to note that solubility problems in some cases required different solvents (and small solvent shifts in the frequencies are expected). In some cases data were recorded at

different temperatures to take account of the effects of pyramidal inversion, again the resonances exhibit some temperature dependence in the chemical shifts.

^{77}Se {^{1}H} NMR data were collected for all selenium containing complexes; the data are displayed in table 3.4. The key features of selenium-77 NMR spectroscopy are discussed in Chapter 2.

Compound	δ^{77}Se{^{1}H}/ppm	Coordination shift[a]/ ppm
$[Mo(CO)_4\{o\text{-}C_6H_4(CH_2SeCH_3)_2\}]$	157.6	8.6
$[W(CO)_4\{o\text{-}C_6H_4(CH_2SeCH_3)_2\}]$[b]	115.8, 109.4	–33.2, –39.6
$[Mn(CO)_3Cl\{o\text{-}C_6H_4(CH_2SeCH_3)_2\}]$	147.8, 124.1, 122.5, 120.5.	–1.2, –24.9, –26.5, –28.5
$[Mo(CO)_4\{C_6H_2(CH_2SeCH_3)_4\}]$	151.8 uncoord, 154.9 coord	4.2
$[Mo(CO)_4\{\mu\text{-}C_6H_2(CH_2SeCH_3)_4\}Mo(CO)_4]$[c]	151.9(s)	1.2
$[Mo(CO)_4\{C(CH_2SeCH_3)_4\}]$	16.0(s) coord, 23.1(s) uncoord	–8.5
$[o\text{-}C_6H_4(CH_2SeCH_3)_2]$[d]	149.0	
$[C_6H_2(CH_2SeCH_3)_4]$	150.7	
$[C(CH_2SeCH_3)_4]$	24.5	

[a] Coordination shift = $\delta_{complex} - \delta_{ligand}$
[b] Recorded at 223 K
[c] Recorded in CD_3CN due to poor solubility
[d] Comparative data from literature[10]

Table 3.4 ^{77}Se{^{1}H} NMR spectroscopic data recorded in CD_2Cl_2 at ambient temperatures unless stated otherwise.

The ^{77}Se resonances from each complex showed a coordination shift when compared with the ligand data. $[Mo(CO)_4\{\mu\text{-}C_6H_2(CH_2SeCH_3)_4\}Mo(CO)_4]$ only shows a very small coordination shift of 1.2 ppm, however, the compound was poorly soluble and consequently its spectrum was recorded CD_3CN, and so is not directly comparable to the ligand data.

At ambient temperatures there are no ^{77}Se resonances observed in the spectrum of $[W(CO)_4\{o\text{-}C_6H_4(CH_2SeCH_3)_2\}]$. After lowering the temperature to 233 K two resonances

were observed (see figure 3.8) which reflects the slowing rate of pyramidal inversion at E. Inversion is a lower energy process in molybdenum so only a single resonance is present in spectra recorded at ambient temperatures. The possible invertomers for $[W(CO)_4\{o\text{-}C_6H_4(CH_2SeCH_3)_2\}]$ are shown in figure 3.7.

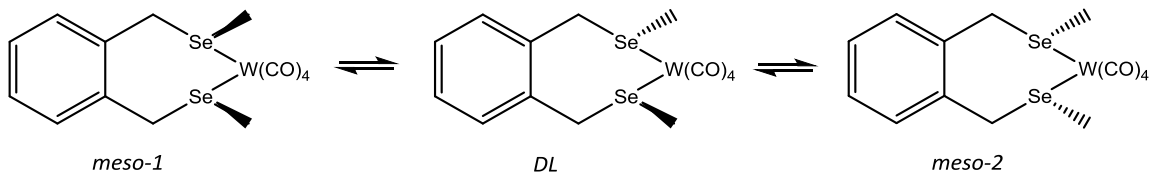

Figure 3.7 Possible invertomers of $[W(CO)_4\{o\text{-}C_6H_4(CH_2SeCH_3)_2\}]$.

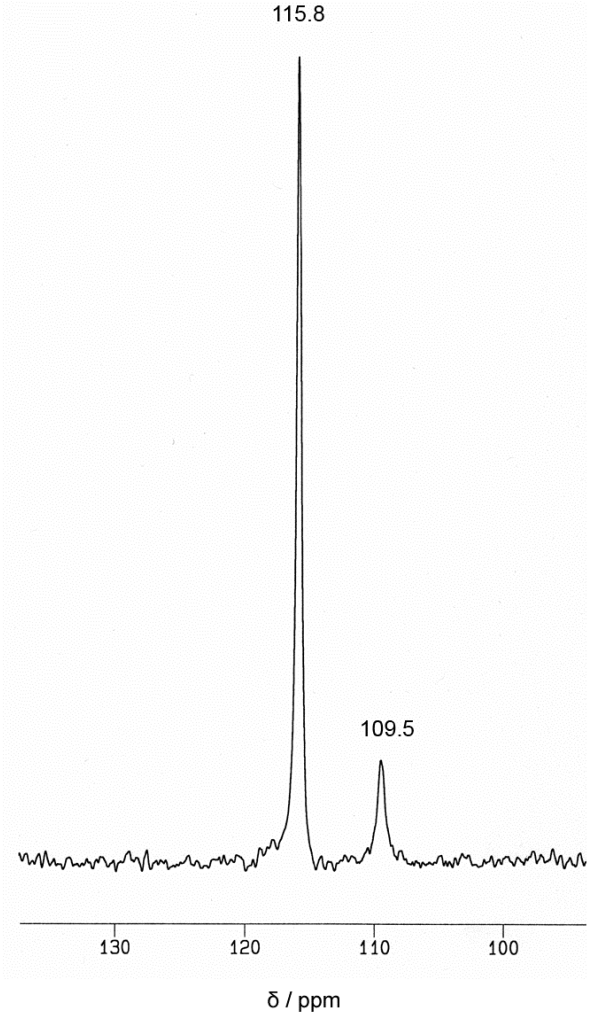

Figure 3.8 $^{77}Se\{^1H\}$ NMR spectrum of $[W(CO)_4\{o\text{-}C_6H_4(CH_2SeCH_3)_2\}]$ recorded in CH_2Cl_2 at -40 °C.

Manganese-55 NMR data were collected for all manganese containing complexes; the data are displayed in table 3.5. The relevant nuclear properties are detailed in Chapter 1.

Compound	**δ^{55}Mn/ ppm**
$[Mn(CO)_3Cl\{o\text{-}C_6H_4(CH_2SCH_3)_2\}]$	+45
$[Mn(CO)_3Cl\{o\text{-}C_6H_4(CH_2SeCH_3)_2\}]$	–42(major), –77(minor), –113 (minor)
$[Mn(CO)_3Cl\{C_6H_2(CH_2SCH_3)_4\}]$	+68
$[Mn(CO)_3Cl\{C(CH_2SCH_3)_4\}]$	–40
$[Mn(CO)_3Cl\{o\text{-}C_6H_4(SeCH_3)_2\}]$[a]	–247(minor), –311, –394
$[Mn(CO)_3Cl\{CH_3SeCH_2CH_2CH_2SeCH_3\}]$[a]	–175, –190(sh), –219(sh)

[a] Comparative data from literature[5]

Table 3.5 ^{55}Mn NMR spectroscopic data recorded at ambient temperatures and in CD_2Cl_2 unless stated otherwise.

Again fast pyramidal inversion, this time on the manganese NMR timescale will result in a single averaged resonance, whilst slow inversion results in resonances for each invertomer, although all three do not need to be present in detectable amounts.[11] (see table 3.5)

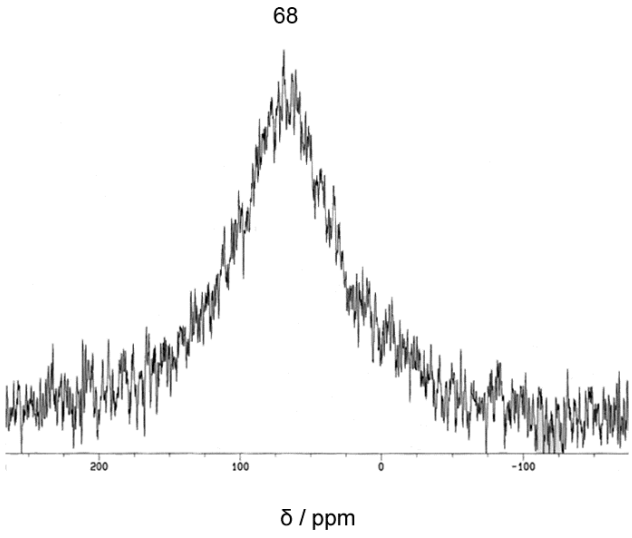

Figure 3.9 ^{55}Mn NMR spectrum of $[Mn(CO)_3Cl\{C_6H_2(CH_2SCH_3)_4\}]$ recorded at 295 K in CD_2Cl_2. An example of a "fast" inverting system.

$[Mn(CO)_3Cl\{o\text{-}C_6H_4(CH_2SCH_3)_2\}]$ showed a single ^{55}Mn resonance due to fast pyramidal inversion in the seven membered chelate ring. The corresponding selenoether has three broad overlapping ^{55}Mn resonances observed at room temperature, this can be attributed to a higher energy inversion process. Several invertomers are also seen in $^{77}Se\{^1H\}$ and $^{13}C\{^1H\}$ spectra.

In the Group 6 carbonyl complexes, ^{95}Mo and ^{183}W NMR spectroscopy was routinely applied in this study. The relevant nuclear properties are detailed in Chapter 1.The tungsten carbonyl systems have very long relaxation times, making routine study of this nucleus, especially in compounds of modest solubility and high M.Wt. a very time consuming process.[12]

^{95}Mo NMR data were much more easily obtained and were collected on all molybdenum containing complexes; the data is displayed in table 3.6. Each spectrum consisted of a single relatively sharp peak since all the molybdenum complexes reported in this chapter are undergoing fast inversion on the appropriate energy scale. A typical ^{95}Mo spectrum is shown below.

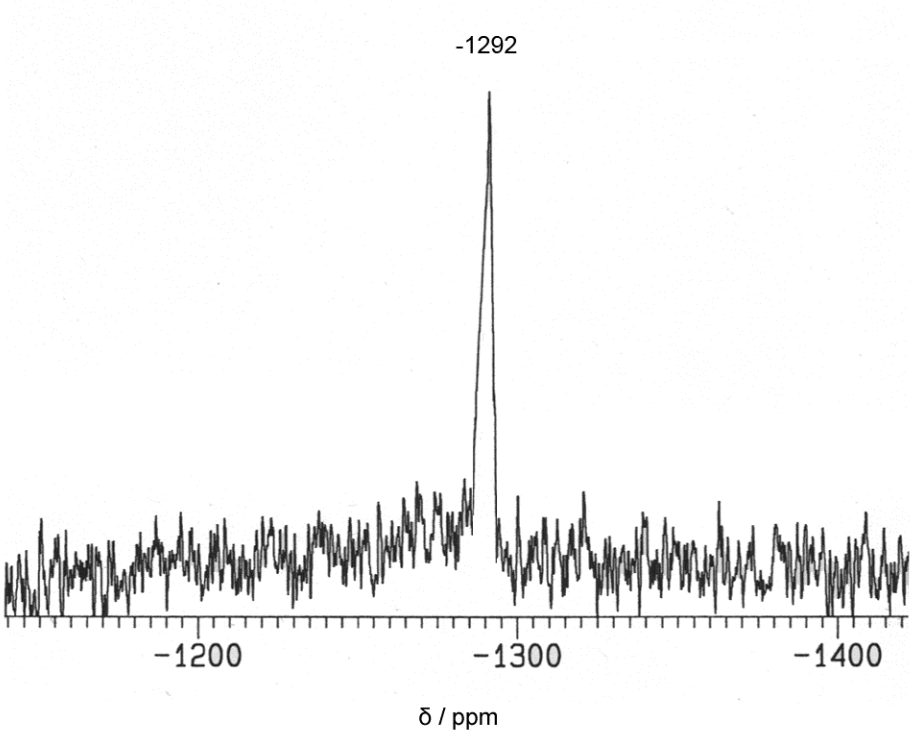

Figure 3.10 ^{95}Mo NMR spectrum of $[Mo(CO)_4\{o\text{-}C_6H_4(CH_2SCH_3)_2\}]$ recorded at 22 °C in CD_2Cl_2.

Compound	δ^{95}Mo/ ppm
$[Mo(CO)_4\{o\text{-}C_6H_4(CH_2SCH_3)_2\}]$	-1292
$[Mo(CO)_4\{o\text{-}C_6H_4(CH_2SeCH_3)_2\}]$	-1393
$[Mo(CO)_4\{C_6H_2(CH_2SeCH_3)_4\}]$	-1384
$[Mo(CO)_4\{\mu\text{-}C_6H_2(CH_2SeCH_3)_4\}Mo(CO)_4]$[a]	-1411
$[Mo(CO)_4\{C(CH_2SCH_3)_4\}]$	-1384
$[Mo(CO)_4\{C(CH_2SeCH_3)_4\}]$	-1450
$[Mo(CO)_4\{o\text{-}C_6H_4(SCH_3)_2\}]$[b]	-1375
$[Mo(CO)_4\{o\text{-}C_6H_4(SeCH_3)_2\}]$[b]	-1437
$[Mo(CO)_4\{CH_3SCH_2CH_2CH_2SCH_3\}]$[b]	-1294
$[Mo(CO)_4\{CH_3SeCH_2CH_2CH_2SeCH_3\}]$[b]	-1340

[a] Recorded in CD_3CN due to poor solubility.
[b] Comparative data from literature.[4]

Table 3.6 ^{95}Mo NMR spectroscopic data recorded at ambient temperatures and in CD_2Cl_2 unless stated otherwise.

The data show a good correlation with the literature data, both ligand types show a shift to lower frequency when changing donor atoms from sulfur to selenium. This is consistent with increasing σ-donation as Group 16 descends, the shifts are *ca*. 500 ppm above the frequency of $[Mo(CO)_6]$ (^{95}Mo = –1856 ppm). Again because of the quadrupolar nature of the nucleus spin-spin couplings are rarely seen.

3.2.5 X-Ray Crystallography

X-ray crystallographic data were collected for all crystals isolated during synthesis. Details of the data collection and refinement are given in table 3.15 and 3.16.

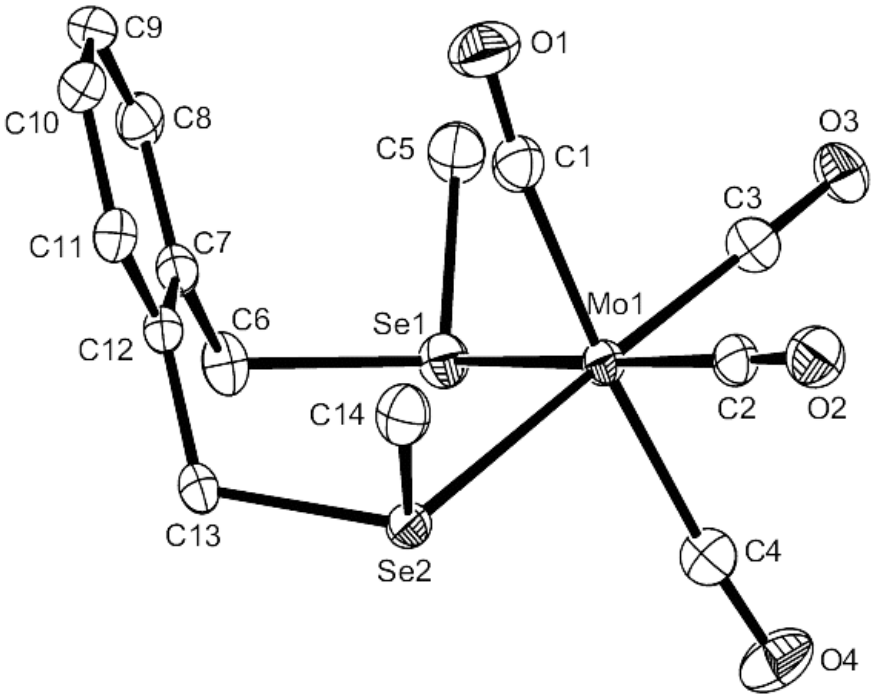

Figure 3.11 Structure of [Mo(CO)$_4${*o*-C$_6$H$_4$(CH$_2$SeMe)$_2$}] showing the numbering scheme adopted. Ellipsoids are drawn at the 50% probability level and H atoms have been omitted for clarity.

Mo1–Se1	2.6670(6)	Mo1–Se2	2.6799(7)
Mo1–C1	2.045(5)	Mo1–C3	1.963(4)
Mo1–C2	1.963(5)	Mo1–C4	2.053(5)
C1–Mo1–C2	87.54(18)	C2–Mo1–C4	87.28(18)
C1–Mo1–C3	86.96(18)	C3–Mo1–C4	90.44(18)
C2–Mo1–C3	88.96(18)	Se1–Mo1–Se2	96.059(17)
C6–Se1–C5	97.1(2)	C13–Se2–C14	96.74(18)
C1–Mo1–Se1	93.80(13)	C4–Mo1–Se1	91.17(12)
C1–Mo1–Se2	93.36(12)	C4–Mo1–Se2	88.99(12)

Table 3.7 Selected bond lengths (Å) and angles (°) for [Mo(CO)$_4${*o*-C$_6$H$_4$(CH$_2$SeMe)$_2$}].

The structure of $[Mo(CO)_4\{o\text{-}C_6H_4(CH_2SeMe)_2\}]$ (figure 3.11, table 3.15) shows a *meso-1* isomer, with both Me groups and the xylyl backbone on the same side of the $MoSe_2C_2$ plane. The ligand bite angle (Se–Mo–Se) is 96.06(2)°. Both Mo–C_{transC} bond lengths are longer than Mo–$C_{transSe}$ due to the *trans* influence. The σ-donor Group 16 ligand places more electron density on the metal and this results in stronger M-CO bonding trans to the Group 16 centre (i.e more π-backbonding).

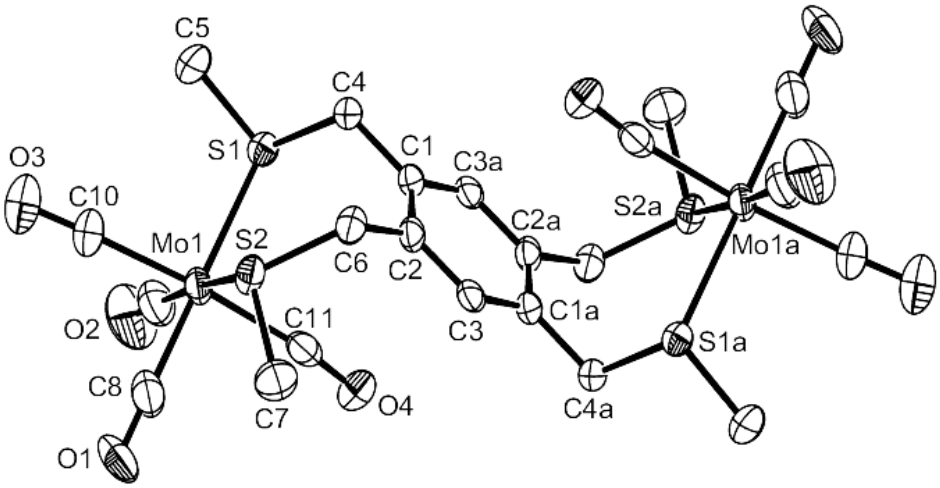

Figure 3.12 Structure of the centrosymmetric Mo1 centred molecule $[Mo(CO)_4\{\mu\text{-}1,2,4,5\text{-}C_6H_2(CH_2SMe)_4\}Mo(CO)_4]$ showing the numbering scheme adopted. Ellipsoids are drawn at the 50% probability level and H atoms have been omitted for clarity. Symmetry operation: a = –x, –y, 1–z. There is a second molecule in the asymmetric unit (Mo2 centred) with a similar structure, but showing some disorder at one SMe group.

Mo1–S1	2.5647(16)	Mo1–S2	2.5939(17)
Mo1–C8	1.962(7)	Mo1–C10	2.015(6)
Mo1–C9	1.942(7)	Mo1–C11	2.066(6)
C8–Mo1–C9	85.4(3)	C9–Mo1–C10	86.7(3)
C8–Mo1–C10	88.4(3)	C9–Mo1–C11	88.0(3)
C8–Mo1–C11	87.9(3)	S1–Mo1–S2	95.31(5)
C4–S1–C5	97.9(3)	C6–S2–C7	99.9(3)
C10–Mo1–S1	92.95(19)	C11–Mo1–S1	90.22(15)
C10–Mo1–S2	93.40(17)	C11–Mo1–S2	91.62(16)

Table 3.8 Selected bond lengths (Å) and angles (°) for $[Mo(CO)_4\{\mu\text{-}1,2,4,5\text{-}C_6H_2(CH_2SMe)_4\}Mo(CO)_4]$.

The structure of $[Mo(CO)_4\{\mu\text{-}1,2,4,5\text{-}C_6H_2(CH_2SMe)_4\}Mo(CO)_4]$ (figure 3.12, table 3.15) shows two $Mo(CO)_4$ groups coordinated to1,2,4,5-$C_6H_2(CH_2SMe)_4$ in an *anti*-arrangement, with one metal centre above and one below the plane of the aromatic ring. Both methyl groups have adopted *DL* conformations making the molecule centrosymmetric.

The structure of $[Mo(CO)_4\{\mu\text{-}C_6H_2(CH_2S(CH_2)_4CH_3)_4\}]$ (figure 3.2) from literature[3] also shows the two $Mo(CO)_4$ groups coordinated to the ligand in an *anti*-arrangement however, the alkyl groups have adopted *DL* and *meso* conformations. The bond lengths are not significantly different however, the bond angle for S-Mo-S (98.67°) is slightly wider.

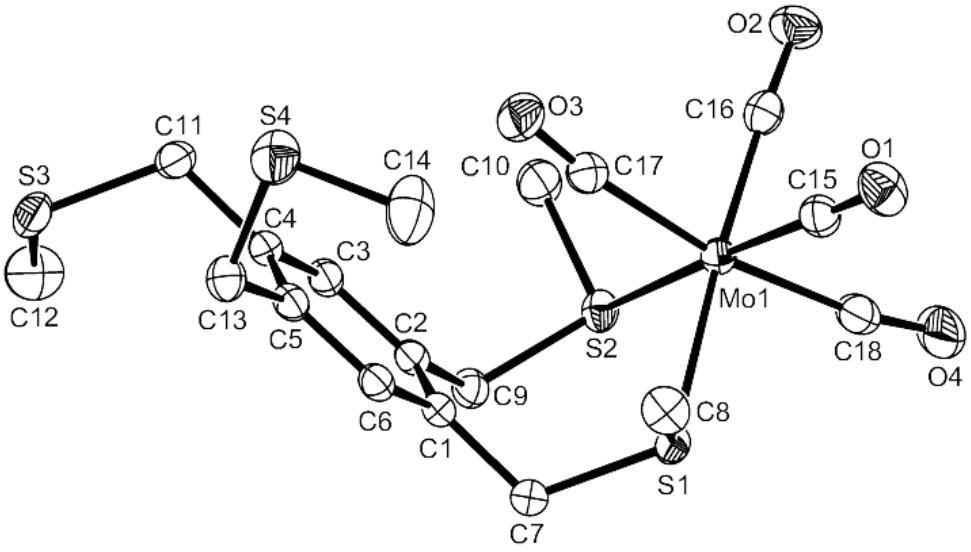

Figure 3.13 Structure of [Mo(CO)$_4${1,2,4,5-C$_6$H$_2$(CH$_2$SMe)$_4$}] showing the numbering scheme adopted. Ellipsoids are drawn at the 50% probability level and H atoms have been omitted for clarity.

Compared to [Mo(CO)$_4${1,2,4,5-C$_6$H$_2$(CH$_2$SMe)$_4$}] (figure 3.14) the only notable difference to [Mo(CO)$_4${μ-1,2,4,5-C$_6$H$_2$(CH$_2$SMe)$_4$}Mo(CO)$_4$] is that the *DL* conformation has a slightly wider (~3°) S1–Mo–S2 angle of 95.31(5)°.

The structure of [Mo(CO)$_4${1,2,4,5-C$_6$H$_2$(CH$_2$SMe)$_4$}] was determined (figure 3.14, table 3.15), the dithioether groups are present as the *meso*-1 isomer with the <S1–Mo–S2 = 91.89(2)°. Again the Mo–C$_{transS}$ bond lengths are shorter than Mo–C$_{transC}$.

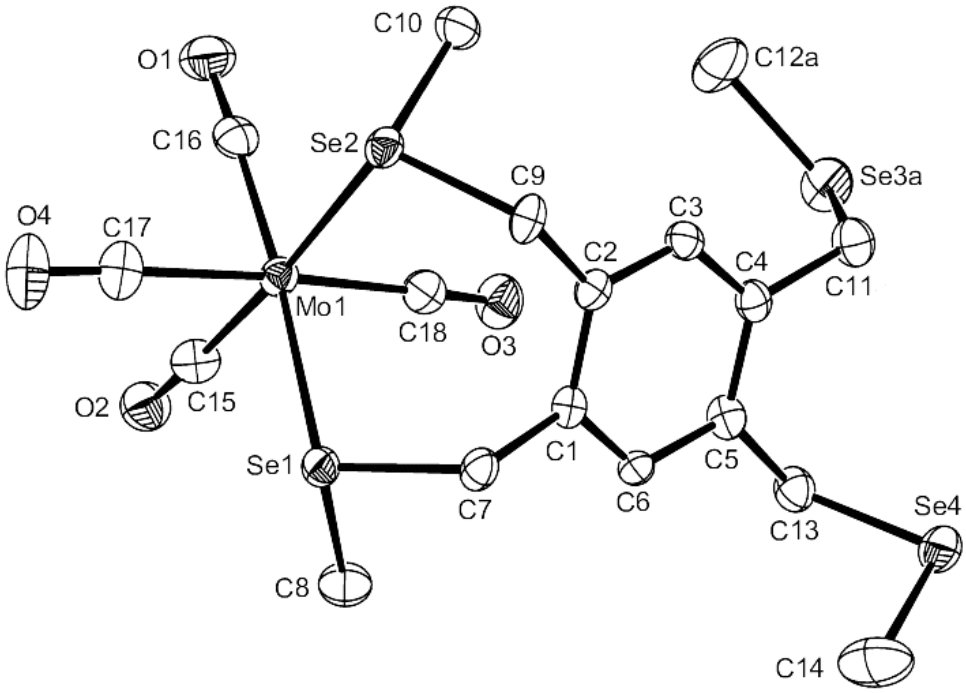

Figure 3.14 Structure of $[Mo(CO)_4\{1,2,4,5\text{-}C_6H_2(CH_2SeMe)_4\}]$ showing the numbering scheme adopted. Ellipsoids are drawn at the 50% probability level and H atoms have been omitted for clarity.

Mo1–Se1	2.6715(9)	Mo1–Se2	2.6871(10)
Mo1–C15	1.962(7)	Mo1–C17	2.040(7)
Mo1–C16	1.962(7)	Mo1–C18	2.053(7)
C15–Mo1–C16	86.1(3)	C16–Mo1–C17	87.2(3)
C15–Mo1–C17	82.6(3)	C16–Mo1–C18	90.2(3)
C15–Mo1–C18	88.2(3)	Se1–Mo1–Se2	90.72(3)
C7–Se1–C8	96.6(3)	C9–Se2–C10	96.7(3)
C17–Mo1–Se1	88.1(2)	C18–Mo1–Se1	94.4(2)
C17–Mo1–Se2	95.6(2)	C18–Mo1–Se2	93.4(2)

Table 3.10 Selected bond lengths (Å) and angles (°) for $[Mo(CO)_4\{1,2,4,5\text{-}C_6H_2(CH_2SeMe)_4\}]$.

$[Mo(CO)_4\{1,2,4,5\text{-}C_6H_2(CH_2SeMe)_4\}]$ structure was determined (figure 3.15, table 3.15) and like the $1,2,4,5\text{-}C_6H_2(CH_2SMe)_4$ analogue, contains the *meso-1* isomer of the ligand. There are no significant differences in M-C bond lengths when comparing the S and Se analogues suggesting similar electronic effects for each donor.

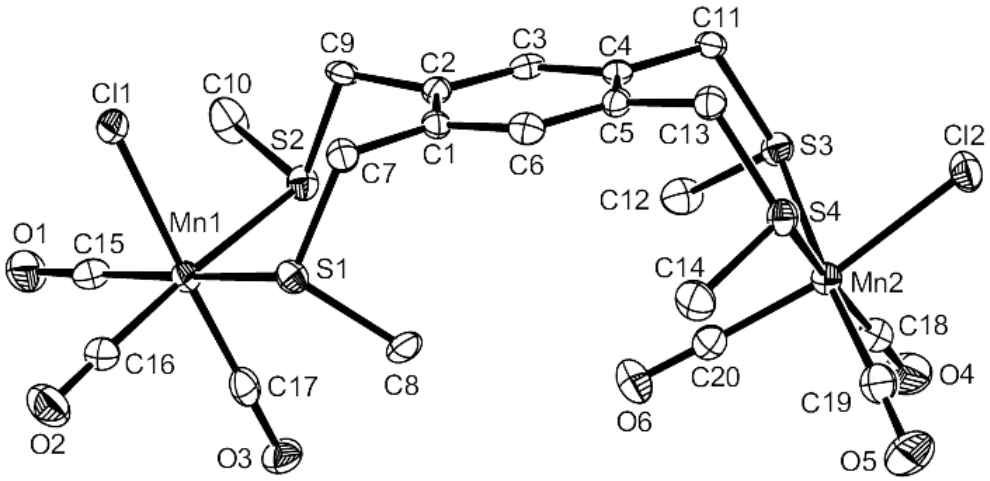

Figure 3.15 Structure of $[Mn(CO)_3Cl\{\mu\text{-}1,2,4,5\text{-}C_6H_2(CH_2SMe)_4\}Mn(CO)_3Cl]$ showing the numbering scheme adopted. Ellipsoids are drawn at the 50% probability level and H atoms have been omitted for clarity.

Mn1–S1	2.3908(11)	Mn2–S3	2.3709(11)
Mn1–S2	2.4005(11)	Mn2–S4	2.3675(11)
Mn1–Cl1	2.3781(11)	Mn2–Cl2	2.3892(11)
Mn1–C15	1.811(4)	Mn2–C18	1.810(4)
Mn1–C16	1.804(4)	Mn2–C19	1.812(4)
Mn1–C17	1.806(4)	Mn2–C20	1.795(4)
S1–Mn1–S2	92.69(3)	S3–Mn2–S4	103.61(4)
Cl1–Mn1–S1	89.09(4)	Cl2–Mn2–S3	82.51(4)
Cl1–Mn1–S2	90.37(4)	Cl2–Mn2–S4	81.51(4)
C15–Mn1–Cl1	85.75(12)	C18–Mn2–Cl2	95.11(12)
C16–Mn1–Cl1	93.13(12)	C19–Mn2–Cl2	95.25(12)
C–Mn1–C (ca. 90°)	87.1(2)–93.6(2)	C–Mn2–C (ca. 90°)	87.0(2)–93.2(2)

Table 3.11 Selected bond lengths (Å) and angles (°) for $[Mn(CO)_3Cl\{\mu\text{-}1,2,4,5\text{-}C_6H_2(CH_2SMe)_4\}Mn(CO)_3Cl]$.

$[Mn(CO)_3Cl\{\mu\text{-}1,2,4,5\text{-}C_6H_2(CH_2SMe)_4\}Mn(CO)_3Cl]$ was not synthesised directly but was isolated when purifying $[Mn(CO)_3Cl\{1,2,4,5\text{-}C_6H_2(CH_2SMe)_4\}]$. Crystals of the less soluble bimetallic complex were collected and the structure determined. The Mn metal centres (figure 3.15, table 3.15) unlike the dimolybdenum complex are coordinated *syn* with respect to the aromatic backbone, with methyl groups on one Mn bound in a *DL* conformation and bound in a *meso-1* form on the second. Very little difference can be seen in bond lengths within the molecule apart from the Mn-S distances with the *DL* unit being (~0.02 Å) longer than the *meso* group. The bite angle however, is quite different with 92.7(1)° for the *DL* versus 103.6(1)° for the *meso*. In each case the relatively bulky chlorine atom is directed away to the less hindered face on the molecule.

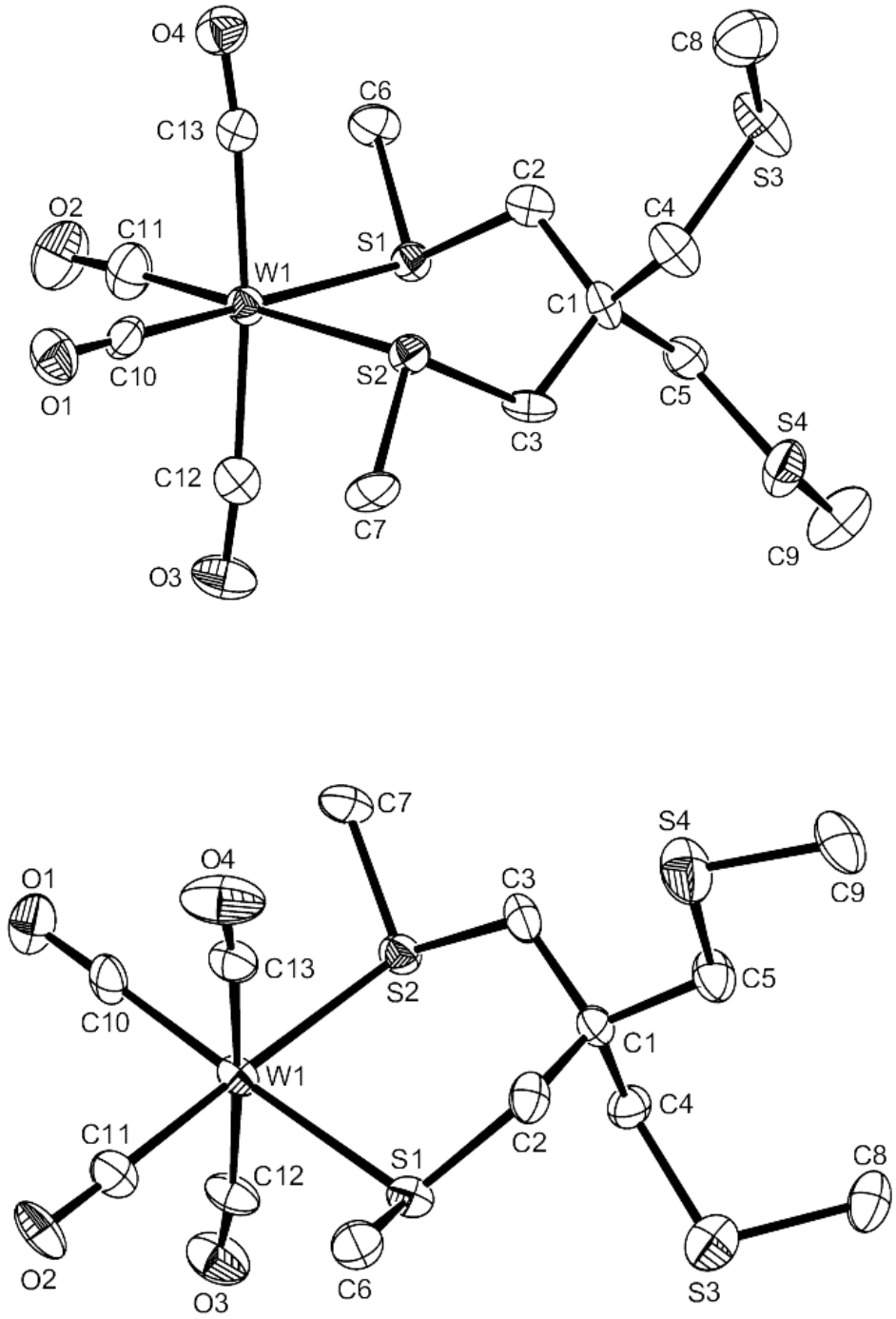

Figure 3.16 Structures of two conformational isomers of $[W(CO)_4(C(CH_2SMe)_4)]$ showing the numbering schemes adopted. Ellipsoids are drawn at the 50% probability level and H atoms have been omitted for clarity. (a) C atoms C6 and C7 are *DL* with respect to the WS_2 plane. (b) C atoms C6 and C7 are *meso* with respect to the WS_2 plane.

***DL* containing form**			
W1–S1	2.543(2)	W1–S2	2.554(2)
W1–C10	1.963(8)	W1–C12	2.035(9)
W1–C11	1.946(10)	W1–C13	2.034(8)
S1–W1–S2	83.88(6)	C10–W1–C13	89.3(3)
C10–W1–C11	91.6(4)	C11–W1–C12	89.3(4)
C10–W1–C12	87.7(3)	C11–W1–C13	86.1(4)
C12–W1–S1	93.8(2)	C13–W1–S1	89.4(2)
C12–W1–S2	89.2(2)	C13–W1–S2	95.6(2)
C2–S1–C6	98.7(4)	C3–S2–C7	98.7(4)
C4–S3–C8	98.3(5)	C5–S4–C9	98.4(5)
***meso* containing form**			
W1–S1	W1–S1	W1–S1	W1–S1
W1–C10	W1–C10	W1–C10	W1–C10
W1–C11	W1–C11	W1–C11	W1–C11
S1–W1–S2	S1–W1–S2	S1–W1–S2	S1–W1–S2
C10–W1–C11	C10–W1–C11	C10–W1–C11	C10–W1–C11
C10–W1–C12	C10–W1–C12	C10–W1–C12	C10–W1–C12
C12–W1–S1	C12–W1–S1	C12–W1–S1	C12–W1–S1
C12–W1–S2	C12–W1–S2	C12–W1–S2	C12–W1–S2
C2–S1–C6	C2–S1–C6	C2–S1–C6	C2–S1–C6

Table 3.12 Selected bond lengths (Å) and angles (°) for the two invertomers of $[W(CO)_4(C(CH_2SMe)_4)]$.

Crystals of $[W(CO)_4(C(CH_2SMe)_4)]$ were obtained from two separate preparations from a CH_2Cl_2/hexane solution, showing both *DL* and *meso* conformations (figure 3.16, table 3.16). It is very unusual to have X-ray structures of two invertomers of the same complex. Very unusually the two different forms were obtained from the same solvent system,

although in different batches both samples must be very similar in energy. Although the *meso* invertomer contained a small amount of disorder there were no significant differences in W–C and W–S bond lengths. The bite angle of the ligand (S1–W1–S2) however, is 3° wider in the *meso* form, which is similar to the different bond angles measured in $[Mn(CO)_3Cl\{\mu\text{-}1,2,4,5\text{-}C_6H_2(CH_2SMe)_4\}Mn(CO)_3Cl]$.

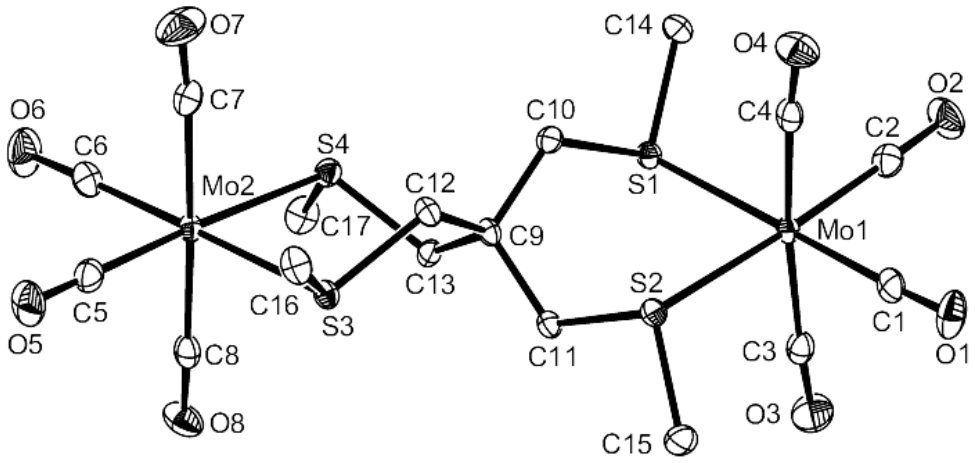

Figure 3.17 View of the structure of $[(CO)_4Mo(\mu\text{-}C(CH_2SMe)_4)Mo(CO)_4]$ with numbering scheme adopted. Thermal ellipsoids are shown at 50% probability and hydrogen atoms omitted.

Mo1–S1	2.5647(16)	Mo1–S2	2.5939(17)
Mo1–C8	1.962(7)	Mo1–C10	2.015(6)
Mo1–C9	1.942(7)	Mo1–C11	2.066(6)
C8–Mo1–C9	85.4(3)	C9–Mo1–C10	86.7(3)
C8–Mo1–C10	88.4(3)	C9–Mo1–C11	88.0(3)
C8–Mo1–C11	87.9(3)	S1–Mo1–S2	95.31(5)
C4–S1–C5	97.9(3)	C6–S2–C7	99.9(3)
C10–Mo1–S1	92.95(19)	C11–Mo1–S1	90.22(15)
C10–Mo1–S2	93.40(17)	C11–Mo1–S2	91.62(16)

Table 3.13 Selected bond lengths (Å) and angles (°) for $[Mo(CO)_4\{\mu\text{-}C_6H_2(CH_2SMe)_4\}Mo(CO)_4]$.

The dinuclear $[(CO)_4Mo(\mu\text{-}C(CH_2SMe)_4)Mo(CO)_4]$ (figure 3.17, table 3.16) has both pairs of methyl groups in the *DL* form, with both Mo environments very similar.

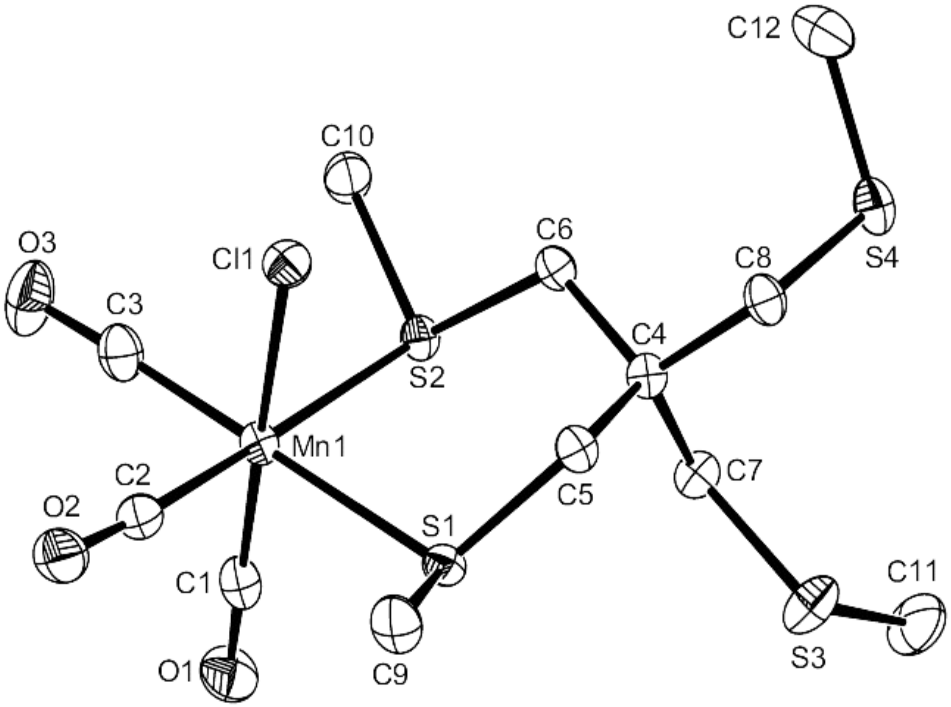

Figure 3.18 View of the structure of $[Mn(CO)_3Cl\{C(CH_2SMe)_4\}]$ with numbering scheme adopted. Thermal ellipsoids are shown at 50% probability and hydrogen atoms omitted.

The structure of $[Mn(CO)_3Cl\{C(CH_2SMe)_4\}]$ (figure 3.18, table 3.16) shows the ligand in a *meso-1* form with the methyl groups of the ligand directed to the same side of the MnC_2S_2 plane as the chlorine atom.

Mn1–S1	2.3763(5)	Mn1–S2	2.3823(6)
Mn1–C1	1.7946(15)	Mn1–C3	1.8117(15)
Mn1–C2	1.8153(15)	Mn1–Cl1	2.3789(6)
S1–Mn1–S2	85.506(17)	S1–Mn1–Cl1	91.724(16)
S2–Mn1–Cl1	89.775(13)	C1–Mn1–C3	91.54(7)
C1–Mn1–C2	92.47(6)	C2–Mn1–C3	87.67(6)
C5–S1–C9	98.18(7)	C6–S2–C10	97.57(7)
C–Mn1–S (ca. 90°)	86.74(5)–93.93(5)		

Table 3.14 Selected bond lengths (Å) and angles (°) for $[Mn(CO)_3Cl\{C(CH_2SMe)_4\}]$.

3.2.6 Attempted synthesis of hetero-bimetallics

The complexes described in this chapter show several examples of monometallic coordination and homo-bimetallic complexes. The synthesis of hetero-bimetallic complexes with these ligands in carbonyl systems was also attempted. $[W(CO)_4\{C(CH_2SCH_3)_4\}]$ was selected because it was readily prepared, expected to be inert to substitution of the tungsten, and had better solubility than the aromatic backboned ligand complexes. The complex was reacted separately under a variety of conditions with CoI_2 and $[Mo(CO)_4(nbd)]$. All attempts to incorporate cobalt show no evidence of a reaction, presumably reflecting the low affinity of the neutral thioethers for the hard labile Co(II) centre. The reactions involving molybdenum also failed, a complex mixture of products were obtained, along with much decomposition. It was concluded that these ligand/carbonyl systems were not well suited to prepare hetero-bimetallics, organo-ruthenium and -osmium systems however, may be more suitable due to the introduction of a counter ion and allowing greater control during the reaction these complexes are described in the next Chapter.

3.4 Conclusions

Monometallic and homo-bimetallic carbonyl complexes have been prepared and characterised with tetrathio- and tetraseleno-ether ligands. Single crystal x-ray

crystallography showed interesting structural data, most notably two samples of $[W(CO)_4\{C(CH_2SCH_3)_4\}]$ from the same solvent system, showed the ligand adopting *meso* and *DL* forms separately. The structure of the bimetallic molecule $[Mn(CO)_3Cl\{\mu\text{-}C_6H_2(CH_2SCH_3)_4\}Mn(CO)_3Cl]$ showed both *meso* and *DL* forms present on the same ligand. Spirocyclic ligand complexes were more soluble than aromatic linked systems, so appear to be better candidates for producing hetero-bimetallic species. However any attempt to attach a second metal centre resulted in rearrangement producing a non-carbonyl contain product. The poor solubility of 1,2,4,5-$C_6H_2(CH_2SMe)_4$ and 1,2,4,5-$C_6H_2(CH_2SeMe)_4$ complexes may contribute to the disproportionation observed with the crystallisation of the poorly soluble bimetallic species driven by low solubility. Although monometallic carbonyls can be produced in high purity they dissociate when left in solution or during further reaction, different metal systems need to be explored in order to allow the insertion of a second different metal.

Complex	[Mo(CO)$_4${*o*-C$_6$H$_4$(CH$_2$SeMe)$_2$}]	[Mo(CO)$_4${C$_6$H$_2$(CH$_2$SMe)$_4$}]	[Mo(CO)$_4${μ-C$_6$H$_2$(CH$_2$SMe)$_4$}Mo(CO)$_4$]	[Mn(CO)$_3$Cl{μ-C$_6$H$_2$(CH$_2$SMe)$_4$}Mn(CO)$_3$Cl]
Formula	$C_{14}H_{14}MoO_4Se_2$	$C_{18}H_{22}MoO_4S_4$	$C_{22}H_{22}Mo_2O_8S_4$	$C_{26}H_{22}Cl_2Mn_2O_8S_4$
M	500.11	526.54	734.52	667.40
Crystal system	Orthorhombic	Monoclinic	Triclinic	Monoclinic
Space group	*Pbcn* (#60)	$P2_1/n$ (#14)	*P*bar1 (#2)	$P2_1/c$ (#14)
a (Å)	27.939(6)	9.5685(15)	10.020(4)	12.772(2)
b (Å)	7.9549(10)	13.647(2)	10.040(4)	14.996(2)
c (Å)	14.676(3)	17.069(3)	14.683(6)	14.065(2)
α (°)	90	90	74.107(15)	90
β (°)	90	98.572(8)	76.174(15)	96.880(10)
γ (°)	90	90	88.089(15)	90
U (Å^3)	3261.7(10)	2203.9(6)	1378.8(10)	2674.4(7)
Z	8	4	2	4
μ(Mo-Kα)/mm^{-1}	5.278	0.994	1.255	1.490
F(000)	1920	1072	732	1352
Total no. of reflections	21685	41954	24815	31146
Unique reflections	3719	5074	6326	6126
R_{int}	0.066	0.040	0.053	0.109
No. of parameters	192	248	349	311
R_1[b] [$I_o > 2\sigma(I_o)$]	0.038	0.027	0.053	0.055
R_1 (all data)	0.056	0.037	0.083	0.092
wR_2[b] [$I_o > 2\sigma(I_o)$]	0.082	0.064	0.113	0.088
wR_2 (all data)	0.090	0.068	0.123	0.099

Table 3.15 Shows X-ray crystallographic data for complexes with *o*-$C_6H_4(CH_2SeMe)_2$ and 1,2,4,5-$C_6H_2(CH_2SMe)_4$

Complex	[Mo(CO)$_4${C$_6$H$_2$(CH$_2$SeMe)$_4$}]	[Mo(CO)$_4${μ-C(CH$_2$SMe)$_4$}Mo(CO)$_4$]	[W(CO)$_4${C(CH$_2$SMe)$_4$}] *anti* Me (*DL*)	[W(CO)$_4${C(CH$_2$SMe)$_4$}] *syn* Me (*meso*)	[Mo(CO)$_3$Cl{C(CH$_2$SMe)$_4$}]
Formula	$C_{18}H_{22}MoO_4Se_4$	$C_{17}H_{20}Mo_2O_8S_4$	$C_{13}H_{20}O_4S_4W$	$C_{13}H_{20}O_4S_4W$	$C_{12}H_{20}ClMnO_3S_4$
M	714.14	672.45	552.38	552.38	430.91
Crystal system	Monoclinic	Monoclinic	Monoclinic	Monoclinic	Monoclinic
Space group	$P2_1/n$ (#14)	$P2_1/c$ (#14)	Cc (#9)	$P2_1/n$ (#14)	$P2_1/c$ (#14)
a (Å)	9.7804(10)	14.607(2)	10.783(2)	10.5626(10)	11.205(3)
b (Å)	13.602(3)	10.0424(15)	21.010(5)	12.9810(15)	18.940(4)
c (Å)	17.285(3)	18.333(3)	8.7967(15)	14.0075(15)	8.8494(15)
α (°)	90	90	90	90	90
β (°)	98.852(10)	111.735(5)	106.853(10)	95.518(10)	91.266(6)
γ (°)	90	90	90	90	90
U (Å^3)	2272.2(7)	2498.1(7)	1907.2(7)	1911.7(4)	1877.6(7)
Z	4	4	4	4	4
μ(Mo-Kα)/mm^{-1}	7.005	1.376	6.506	6.491	1.294
F(000)	1360	1336	1072	1072	888
Total no. of reflections	23510	30458	8583	22551	31174
Unique reflections	5186	5714	3923	4376	4309
B_{eq}	0.057	0.044	0.057	0.030	0.026
No. of parameters	266	284	204	225	194
R_1[b] [$I_o > 2\sigma(I_o)$]	0.054	0.029	0.035	0.029	0.022
R_1 (all data)	0.085	0.046	0.040	0.032	0.028
wR_2[b] [$I_o > 2\sigma(I_o)$]	0.090	0.060	0.080	0.064	0.049
wR_2 (all data)	0.102	0.065	0.084	0.066	0.051

[a] Common items: temperature = 120 K; wavelength (Mo-Kα) = 0.71073 Å; θ(max) = 27.5°.

[b] $R_1 = \Sigma||F_o| - |F_c||/\Sigma|F_o|$. $wR_2 = [\Sigma w(F_o^2 - F_c^2)^2/\Sigma wF_o^4]^{1/2}$.

Table 3.16 X-ray crystallographic data for complexes with 1,2,4,5-$C_6H_2(CH_2SeMe)_4$ and $C(CH_2SMe)_4$.

3.5 Experimental

All preparations were performed under a nitrogen atmosphere using standard Schlenk techniques.

3.5.1 Synthesis

$[Mo(CO)_4\{o\text{-}C_6H_4(CH_2SMe)_2\}]$

$[Mo(CO)_4(nbd)]$ (nbd = norbornadiene), (0.085 g, 0.28 mmol) was dissolved in toluene (10 mL) and *o*-$C_6H_4(CH_2SMe)_2$ (0.055 g, 0.28 mmol) in toluene (5 mL) added. The mixture was stirred at 75 °C for 20 h, cooled, and the toluene removed *in vacuo*. The residue was dissolved in hot $CHCl_3$ (5 mL), filtered through Celite and n-pentane (5 mL) added. Refrigeration (–18 °C) for 3 days gave a yellow solid, which was filtered off, rinsed with n-pentane and dried in vacuo. Yield: 0.07 g, 62%. Anal. Found: C, 41.11; H, 3.89. Calc. for $C_{14}H_{14}MoO_4S_2$: C, 41.38; H, 3.47%. ^{1}H NMR ($CDCl_3$): 2.56(s) (6[H] SMe), 3.84(s) (4[H] CH_2), 7.1–7.3(m) (4[H] aromatic) ppm. $^{13}C\{^1H\}$ NMR (CH_2Cl_2/$CDCl_3$): 27.6 (SMe), 40.7 (CH_2), 129.7, 132.4, 134.2 (aromatic), 206.3, 215.7 (CO) ppm. ^{95}Mo NMR (CH_2Cl_2): –1292 ppm. APCI MS: found *m/z* 422; calc. $[M–Me]^+$ 423. IR (Nujol): υ(CO) 2020, 1904, 1878, 1833;
(CH_2Cl_2): ν(CO) 2028, 1915, 1895, 1853 cm^{-1}.

$[W(CO)_4\{o\text{-}C_6H_4(CH_2SMe)_2\}]$

Was prepared similarly to the molybdenum complex (section 3.5.1) using $[W(CO)_4(tmpa)]$ (tmpa = $Me_2N(CH_2)_3NMe_2$). Yield: 65%. Anal. Found: C, 32.54; H, 2.28. Calc. for $C_{14}H_{14}O_4S_2W\cdot 1/3CHCl_3$: C, 32.66; H, 2.74%. ^{1}H NMR ($CDCl_3$): 2.76(s) (6[H] SMe), 3.99 (s) (4[H] CH_2), 7.22–7.41(m) (4[H] aromatic) ppm. $^{13}C\{^1H\}$ NMR ($CDCl_3$): 28.8 (SMe), 41.9 (CH_2), 129.1, 132.1, 134.0 (aromatic), 201.9 (CO) ppm, $^1J_{WC}$ = 130 Hz, 206.2 CO, $^1J_{WC}$ = 174 Hz. APCI MS: found *m/z* 494, calc. $[M]^+$ 494. IR (CH_2Cl_2): ν(CO) 2022, 1904, 1888, 1849 cm^{-1}.

3.5.3 $[Mn(CO)_3Cl\{o\text{-}C_6H_4(CH_2SMe)_2\}]$

$[Mn(CO)_5Cl]$ (0.23 g, 1.01 mmol) was dissolved in CH_2Cl_2 (20 mL) and *o*-$C_6H_4(CH_2SMe)_2$ (0.2 g, 1.01 mmol) in toluene (20 mL) added. The mixture was stirred at 75 °C for 3 h, cooled, and the solvent removed *in vacuo*. The residue was dissolved in hot $CHCl_3$ (15 mL), cooled and the yellow solid filtered off, rinsed with $CHCl_3$ and dried in vacuo. Yield: 0.12 g, 32%. ^{1}H NMR ($CDCl_3$): 2.23(s) (6[H], SMe), 4.20(s) (4[H], CH_2), 7.5(m) (4[H], aromatic) ppm. $^{13}C\{^1H\}$ NMR ($CH_2Cl_2/CDCl_3$): 23.2 (SMe), 35.1 (CH_2), 129.1, 131.8, 134.0 (aromatic), 208.3(vbr) (CO) ppm. ^{55}Mn NMR (CH_2Cl_2): +45 ppm $w_{½}$= 9000 Hz.
IR (Nujol): υ(CO) 2038, 1960 (vbr), 1910(sh) cm^{-1}.

$[Mo(CO)_4\{o\text{-}C_6H_4(CH_2SeMe)_2\}]$

$[Mo(CO)_4(nbd)]$ (0.085 g, 0.28 mmol) was dissolved in toluene (10 mL) and *o*-$C_6H_4(CH_2SeMe)_2$ (0.082 g, 0.28 mmol) in toluene (5 mL) added. The mixture was stirred at 75 °C for 24 h, cooled and the toluene removed *in vacuo*. The residue was dissolved in hot $CHCl_3$ (5 mL), filtered through Celite and n-pentane (5 mL) added, which gave a yellow solid, which was filtered off, rinsed with n-pentane and dried *in vacuo*. Yield: 0.061 g, 53%. Anal. Found: C, 33.88; H, 2.90. Calc. for $C_{14}H_{14}MoO_4Se_2$: C, 33.62; H, 2.82%. ^{1}H NMR ($CDCl_3$): 2.93(s) (6[H], SeMe), 3.80(s) (4[H], CH_2), 7.1–7.3(m) (4[H], aromatic) ppm. $^{13}C\{^1H\}$ NMR ($CH_2Cl_2/CDCl_3$): 16.8 (SeMe), 31.3 (CH_2), 128.7, 131.6, 135.2 (aromatic), 207.4, 215.5 (CO) ppm. ^{95}Mo NMR (CH_2Cl_2): –1393 ppm. $^{77}Se\{^1H\}$ NMR (CH_2Cl_2): 157.6 ppm. APCI MS: found *m/z* 520, calc. $[M–Me]^+$ 519. IR (Nujol): υ(CO) 2015, 1913, 1879, 1834; (CH_2Cl_2): ν(CO) 2024, 1914, 1895, 1854 cm^{-1}. Crystals were grown by cooling a $CHCl_3$ solution in a freezer.

$[W(CO)_4\{o\text{-}C_6H_4(CH_2SeMe)_2\}]$

Was made similarly to the molybdenum complex (section 3.5.4) using $[W(CO)_4(tmpa)]$. Yield: 53%. Anal. Found: C, 25.07; H, 2.40. Calc. for $C_{14}H_{14}O_4Se_2W{\cdot}CHCl_3$: C, 25.47; H, 2.14%. ^{1}H NMR ($CDCl_3$): 2.56(s) (6[H], SeMe), 3.91(s) (4[H], CH_2), 7.1–7.3(m) (aromatic) ppm. $^{13}C\{^1H\}$ NMR ($CH_2Cl_2/CDCl_3$, 223 K): 17.9 (SeMe), 30.6 (CH_2), 128.0, 131.0, 133.8 (aromatic), 201.6, 205.6 (CO) ppm. $^{77}Se\{^1H\}$ NMR (CH_2Cl_2): (22 °C no resonance), 115.8, 109.4 (-50 °C) ppm. APCI MS: found *m/z* 590, calc. $[M]^+$ 590. IR

(CH_2Cl_2): ν(CO) 2018, 1904,
1886, 1850 cm^{-1}.

[$Mn(CO)_3Cl\{o\text{-}C_6H_4(CH_2SeMe)_2\}$]

[$Mn(CO)_5Cl$] (0.23 g, 1.32 mmol) was dissolved in $CHCl_3$ (50 mL) and *o*-$C_6H_4(CH_2SeMe)_2$ (0.39 g, 1.32 mmol) in $CHCl_3$ (20 mL) added. The mixture was refluxed for 3 h, cooled, and the solvent removed *in vacuo*. The residue was washed in hot $CHCl_3$ (3 × 15 mL). The resulting orange solid, was filtered and then dried in vacuo. Yield: 0.19g, 36%. Anal. Found: C, 30.66; H, 2.85. Calc. for $C_{13}H_{14}ClMnO_3Se_2.0.5CHCl_3$: C, 30.81; H, 2.78 %. ^{1}H NMR ($CDCl_3$): 2.2–2.5(br) (6[H], SeMe), 3.5–4.1 (br) (4[H], CH_2), 7.3–7.8(br) (4[H], aromatic) ppm. $^{13}C\{^1H\}$ NMR ($CH_2Cl_2/CDCl_3$): 14.8–15.9 (br, overlapping) (SeMe), 27.9–31.2 (br) (CH_2), 128.4, 129.9, 133.0, 135.2 (aromatic), 217.0–220.5 (vbr) (CO) ppm. $^{77}Se\{^1H\}$ NMR (CH_2Cl_2): 147.8, 124.1, 122.5, 120.5 ppm. ^{55}Mn NMR (CH_2Cl_2): –42(major), –77(minor), –113 (minor) ppm. IR (CH_2Cl_2): ν(CO) 2030, 1949, 1921 cm^{-1}.

[$Mo(CO)_4\{1,2,4,5\text{-}C_6H_2(CH_2SMe)_4\}$]

This complex was isolated as yellow crystals by diethyl ether extraction of the crude produce from the attempted synthesis of [$Mo(CO)_4\{\mu\text{-}1,2,4,5\text{-}C_6H_2(CH_2SMe)_4\}Mo(CO)_4$] and identified by the crystal structure (see section 3.2.5). ^{1}H NMR (CD_2Cl_2): 2.06(s) (6[H], SMe uncoord), 2.56(s) (6[H], SMe coord), 3.81(s) (4[H], CH_2 uncoord), 3.83(s) (4[H], CH_2 coord), 7.13(s) (2[H], aromatic) ppm. $^{13}C\{^1H\}$ NMR (CH_2Cl_2/CD_2Cl_2): 15.6 (SMe uncoord), 27.5 (SMe coord), 35.5 (CH_2 uncoord), 40.5 (CH_2 coord), 133.9, 134.9 135.2 (aromatic), 206.4 and 215.6 (CO) ppm. IR (CH_2Cl_2): ν(CO) 2036, 1927, 1884 cm^{-1}.

[$Mo(CO)_4\{\mu\text{-}1,2,4,5\text{-}C_6H_2(CH_2SMe)_4\}Mo(CO)_4$]

In an ampoule fitted with a Young's tap, [$Mo(CO)_4$(nbd)] (0.10 g, 0.33 mmol) suspended in dry toluene (15 mL) was added slowly 1,2,4,5-$C_6H_2(CH_2SMe)_4$ (0.106 g, 0.10 mmol) in CH_2Cl_2 (10 mL), the ampoule partially evacuated and placed in a thermostated oil bath at 100 °C for 3 h. Volatiles were removed under reduced pressure and the yellow-brown solid was extracted with dry Et_2O (3 × 30 mL) and filtered through Celite. The volume of the ether was reduced to 1/3 and the solution was placed at –30 °C to give a crop of the 1:1

complex. The ether insoluble portion was taken up in THF, filtered and the solution was layered with hexane to produce crystals of the 2:1 compound identified by an X-ray crystal structure. Yields variable (see section 3.2.1). ^{1}H NMR (CD_2Cl_2): 2.57(s) (12[H], SMe), 3.89(s) (8[H], CH_2), 7.10(s) (2[H], aromatic) ppm. $^{13}C\{^{1}H\}$ NMR (CH_2Cl_2/CD_2Cl_2): 27.5 (SMe), 40.7 (CH_2), 134.9, 137.6 (aromatic), 206.4 and 215.6 (CO) ppm. IR (Nujol): υ(CO) 2023, 1907,
1876, 1828 cm^{-1}.

$[Mn(CO)_3Cl\{1,2,4,5\text{-}C_6H_2(CH_2SMe)_4\}]$

1,2,4,5-$C_6H_2(CH_2SMe)_4$ (0.32 g, 1.0 mmol) and $[Mn(CO)_5Cl]$ (0.23 g, 1.0 mmol) were dissolved in CH_2Cl_2 (20 mL), the mixture was placed under partial vacuum and heated at 55 °C. After 2½ h at this temperature the ampoule was removed from the oil bath and the reaction mixture was left stirring overnight at room temperature. Volatiles were removed on a rotary evaporator and the yellow-brown oily residue was re-dissolved in CH_2Cl_2 (15 mL) and was filtered through Celite. The solvent from the bright yellow solution was then removed under vacuum and the residue was washed with n-pentane. It was then dissolved in a small amount of CH_2Cl_2 (2 mL) and n-pentane was added (20 mL) to precipitate a microcrystalline yellow solid, which was collected by filtration and dried under vacuum. Yield: 0.21 g, 43%. Anal. Found: C, 42.25; H, 4.66. Calc. for $C_{17}H_{22}ClMnO_3S_4$: C, 41.42; H, 4.50%. ^{1}H NMR ($CDCl_3$): 1.96(s) (6[H], SMe uncoord), 2.33(s) (6[H], SMe coord), 3.71(s) (4[H], CH_2 uncoord), 4.73(m) (4[H], coord), 7.05(s) (2[H], aromatic) ppm. $^{13}C\{^{1}H\}$ NMR ($CH_2Cl_2/CDCl_3$): 15.7 (SMe uncoord), 22.8 (SMe coord), 34.1 (CH_2 uncoord), 35.1 (CH_2 coord), 134.5, 133.1, 138.0 (aromatic), 217.6(vbr) (CO) ppm. ^{55}Mn NMR (CH_2Cl_2): +68 ppm. IR (Nujol): υ(CO) 2027, 1941, 1906 cm^{-1}.

Layering a CH_2Cl_2 of $[Mn(CO)_3Cl(1,2,4,5\text{-}C_6H_2(CH_2SMe)_4)]$ with n-pentane produced crystals identified as $[Mn(CO)_3Cl(\mu\text{-}1,2,4,5\text{-}C_6H_2(CH_2SMe)_4)Mn(CO)_3Cl]$ whose structure is described in section 3.2.5. Attempts to prepare the 2:1 complex directly gave a mixture of the 1:1 complex, ligand and $Mn_2(CO)_{10}$ (identified crystallographically see section 3.2.5).

$[Mo(CO)_4\{1,2,4,5\text{-}C_6H_2(CH_2SeMe)_4\}]$

$[Mo(CO)_4(nbd)]$ (0.11 g, 0.39 mmol) was dissolved in toluene (10 mL) and 1,2,4,5-$C_6H_2(CH_2SeMe)_4$ (0.2 g, 0.39 mmol) in toluene (5 mL) added. The mixture was stirred at 75 °C for 8 h, cooled and stirred overnight, and the toluene was removed *in vacuo*. The residue was dissolved in hot $CHCl_3$ (5 mL), filtered through Celite and n-pentane (10 mL) added. The flask was placed in the freezer overnight which gave a yellow solid, and crystals formed on the side of the flask (used for the X-ray crystallography); the solid was filtered off, rinsed with n-pentane and dried in vacuo. Yield: 0.06 g, 21%. Anal. Found: C, 30.31; H, 3.21. Calc. for $C_{18}H_{22}O_4Se_4Mo$: C, 30.27; H, 3.11%. ^{1}H NMR ($CDCl_3$): 2.02(s) (6[H], SeMe uncoord), 2.46(s) (6[H], SeMe coord), 3.86(s) (4[H], CH_2 uncoord), 3.87(s) (4[H], CH_2 coord), 7.01(s) (2[H], aromatic) ppm. $^{13}C\{^1H\}$ NMR (CH_2Cl_2/$CDCl_3$): 6.6 (SeMe uncoord), 17.4 (SeMe coord), 19.1 (CH_2 uncoord), 29.6 (CH_2 coord), 133.5, 136.0, 137.9 (aromatic), 211.4, 216.5 (CO) ppm. $^{77}Se\{^1H\}$ NMR (CH_2Cl_2): 151.8 (SeMe uncoord), 154.9 (SeMe coord) ppm. ^{95}Mo NMR (CH_3CN): −1384 ppm. IR (CH_2Cl_2): υ(CO) 2024, 1917, 1895, 1856 cm^{-1}.

$[Mo(CO)_4\{\mu$-1,2,4,5-$C_6H_2(CH_2SeMe)_4\}Mo(CO)_4]$

$[Mo(CO)_4(nbd)]$ (0.22 g, 0.78 mmol) was dissolved in toluene (20 mL) and 1,2,4,5-$C_6H_2(CH_2SeMe)_4$ (0.2 g, 0.39 mmol) in toluene (20 mL) added. The mixture was stirred at 110 °C for 3 h. cooled and stirred overnight, the solvent was removed *in vacuo*. The yellow solid was washed in CH_2Cl_2 (3 × 20 mL) and dried in vacuo. Yield: 45%. Anal. Found: C, 29.09; H, 2.20. Calc. for $C_{22}H_{20}O_8Se_4Mo_2$: C, 28.72; H, 2.19%. ^{1}H NMR ($CDCl_3$): 2.39(s) (6[H], SeMe coord), 3.80(s) (4[H], CH_2 coord), 7.21(s) (2[H], aromatic) ppm. $^{13}C\{^1H\}$ NMR (MeCN): (v. poorly soluble) 14.7 (SeMe), 24.8 (CH_2 coord), 132.8, 136.3 (aromatic), 205.2, 217.7 (CO) ppm. $^{77}Se\{^1H\}$ NMR (CH_2Cl_2): 151.9(s) ppm. ^{95}Mo NMR (MeCN): −1411 ppm. IR (CH_2Cl_2): υ(CO) 2025, 1914, 1893, 1829 cm^{-1}.

$[Mo(CO)_4\{C(CH_2SMe)_4\}]$

$[Mo(CO)_4(nbd)]$ (0.10 g, 0.33 mmol) was placed in 20 mL Young's ampoule and dissolved in dry toluene (10 mL). A solution of $C(CH_2SMe)_4$ (2.1 mL of 40 mg/mL solution) in toluene are added slowly *via* syringe. The reaction mixture was placed under partial vacuum and heated overnight at 110 °C. Volatiles were removed *in vacuo* and the yellow solid was extracted in petroleum ether (60–80), and filtered through Celite. The solution

was reduced to about 4 mL and cooled to –30 °C to produce a yellow precipitate which was isolated from the mother-liquor by filtration and dried under vacuum. A second crop was collected by reducing the volume of the mother-liquor and cooling at –30 °C. Overall yield: 0.10 g, 65%. Anal. Found: C, 33.10; H, 4.33. Calc. for $C_{13}H_{20}O_4S_4Mo$: C, 33.61; H, 4.34%. ^{1}H NMR ($CDCl_3$): 2.19(s) (6[H], SMe uncoord), 2.51(s) (6[H], SMe coord), 2.74(s) (4[H], CH_2 uncoord), 2.85(s) (4[H], CH_2 coord) ppm. $^{13}C\{^1H\}$ NMR ($CH_2Cl_2/CDCl_3$): 17.8 (SMe uncoord), 27.6 (SMe coord), 42.2 (CH_2 uncoord), 43.8 ($C_{quaternary}$), 48.5 (CH_2 coord), 206.4 and 217.0 (CO) ppm. ^{95}Mo NMR (CH_2Cl_2): –1384 ppm. IR (Nujol): υ(CO) 2026, 1921, 1857 cm^{-1}.

$[W(CO)_4\{C(CH_2SMe)_4\}]$

This was prepared as for the molybdenum complex (section 3.5.12) from $[W(CO)_4(piperidine)_2]$ and $C(CH_2SMe)_4$ in toluene. Yield: 67%. Anal. Found: C, 28.54; H, 3.79. Calc. for $C_{13}H_{20}O_4S_4W$: C, 28.27; H, 3.65%. ^{1}H NMR ($CDCl_3$): 2.20(s) (6[H], SMe uncoord), 2.68(s) (6[H], SMe coord), 2.75(s) (4[H], CH_2 uncoord), 3.08(s) (4[H], CH_2 coord) ppm. $^{13}C\{^1H\}$ NMR ($CH_2Cl_2/CDCl_3$): 17.8 (SMe uncoord), 29.5 (SMe coord), 42.2 (CH_2 uncoord), 43.8 ($C_{quaternary}$), 48.9 (CH_2 coord), 202.1 and 208.0 (CO) ppm. IR (Nujol): υ(CO) 2010, 1900(sh), 1890, 1843 cm^{-1}. Crystals were grown from a CH_2Cl_2 solution layered with hexane and stored at –18 °C.

$[(CO)_4Mo\{\mu\text{-}C(CH_2SMe)_4\}Mo(CO)_4]$

A Young's ampoule was charged with $[Mo(CO)_4(nbd)]$ (0.080 g, 0.26 mmol) in dry toluene (5 mL) and a solution of $C(CH_2SMe)_4$ in toluene (0.9 mL, 0.14 mmol of a 40 mg/ml solution). The ampoule was placed under partial vacuum and the mixture left stirring overnight. Volatiles were removed in vacuo, and the yellow solid was washed with hot hexane to remove the 1:1 complex. The residue was taken up in CH_2Cl_2, filtered through Celite and volatiles were removed under vacuum. The solid was further washed with hexane and dried under vacuum. Yield: 0.03 g, 34%. Anal. Found: C, 30.22; H, 3.09. Calc. for $C_{17}H_{20}S_4Mo_2O_8$: C, 30.36; H, 3.00%. ^{1}H NMR ($CDCl_3$): 2.56(s) (12[H], SMe), 2.9(s) (8[H], CH_2) ppm. $^{13}C\{^1H\}$ NMR ($CH_2Cl_2/CDCl_3$): 27.6 (SMe), 42.2 ($C_{quaternary}$), 48.7 (CH_2), 206.2 and 216.4 (CO) ppm. IR (Nujol): υ(CO) 2024, 1919, 1860; (CH_2Cl_2):

υ(CO) 2024, 1911, 1899, 1860 cm^{-1}. Crystals were grown by layering a CH_2Cl_2 solution of the complex with hexane.

$[Mn(CO)_3Cl\{C(CH_2SMe)_4\}]$

This was prepared with a method analogous to the $[W(CO)_4\{C(CH_2SMe)_4\}]$ (section 3.4.13) complex starting from $[Mn(CO)_5Cl]$ (0.08 g, 0.35 mmol), $C(CH_2SMe)_4$ (2.2 mL of a 40 mg/mL solution) in toluene. Yield: 0.10 g, 66%. Anal. Found: C, 33.13; H, 4.24. Calc. for $C_{12}H_{20}ClMnO_3S_4$: C, 33.45; H, 4.68%. ^1H NMR ($CDCl_3$): 2.16(s) (6[H], SMe uncoord), 2.48(s) (6[H], SMe coord), 2.67(s) (4[H], CH_2 uncoord), 3.12(s) (4[H], CH_2 coord) ppm. $^{13}C\{^1H\}$ NMR (CH_2Cl_2/$CDCl_3$): 18.0 (SMe uncoord), 22.9 (SMe coord), 40.6 (CH_2 uncoord), 41.2 (CH_2 coord), 43.3 ($C_{quaternary}$), 207.6, 217.6 (CO) ppm. ^{55}Mn NMR (CH_2Cl_2): –40 ppm $w_{½}$= 12000 Hz. IR (Nujol): υ(CO) 2027, 1941, 1909 cm^{-1}. Crystals were grown by cooling a hexane solution of the compound at –30 °C.

$[Mo(CO)_4\{C(CH_2SeMe)_4\}]$

$[Mo(CO)_4(nbd)]$ (0.14 g, 0.45 mmol) was dissolved in toluene (10 mL) and $C(CH_2SeMe)_4$ (0.2 g, 0.45 mmol) in toluene (5 mL) added. The mixture was stirred at 75 °C for 3 h, cooled and stirred overnight, when the toluene was removed *in vacuo*. The residue was dissolved in hot $CHCl_3$ (5 mL), filtered through Celite and n-pentane (10 mL) added. The flask was placed in the freezer overnight which gave a dark yellow solid, which was filtered off, rinsed with n-pentane and dried in vacuo. Yield 0.14g, 48 %.Anal. Found: C, 23.33; H, 3.09. Calc. for $C_{13}H_{20}MoO_4Se_4$: C, 23.93; H, 3.09 %. ^1H NMR ($CDCl_3$): 2.08(s) ([6H], SMe uncoord), 2.48(s) ([6H], SMe coord), 2.85(s) ([4H], CH_2 uncoord), 2.89(s) ([4H], CH_2 coord) ppm. $^{13}C\{^1H\}$ NMR (CH_2Cl_2/$CDCl_3$): 6.2(s) (MeSe uncoord), 25.3 (MeSe coord), 41.0 (CH_2 uncoord), 44.0 ($C_{quaternary}$), 47.6 (CH_2 coord), 209.1, 215.1, (CO) ppm. ^{95}Mo NMR (CH_2Cl_2): –1450 ppm. $^{77}Se\{^1H\}$ NMR (CH_2Cl_2): 16.0(s) (MeSe coord), 23.1(s) (MeSe uncoord) ppm. IR (Nujol): υ(CO) 2020, 1904, 1883, 1851 cm^{-1}.

3.5.2 X-Ray Crystallography Experimental

Structure solution and refinement were straightforward[13-15] except $[Mo(CO)_4\{\mu\text{-}1,2,4,5\text{-}C_6H_2(CH_2SMe)_4\}Mo(CO)_4]$ which showed disorder and was modelled by Dr. M. Webster. $[Mo(CO)_4\{\mu\text{-}1,2,4,5\text{-}C_6H_2(CH_2SMe)_4\}Mo(CO)_4]$ had two

centrosymmetric molecules in the cell, the second of which showed disorder at S4. This was modelled as two sites (A and B (sofs: 0.63, 0.37)) and also the bonded C(H_3) was identified in the difference electron-density map (C18A/B). C16 and C18A are on opposite sides of the Mo2/S3/S4A plane, whereas C16 and C18B are on the same side as the Mo2/S3/S4B plane (i.e. *DL* and *meso* isomers). The compound [$Mo(CO)_4${1,2,4,5-$C_6H_2(CH_2SeMe)_4$}] likewise shows disorder at the uncoordinated Se3, modelled as two sites (A/B) along with C12A/B. The compound [$W(CO)_4${$C(CH_2SMe)_4$}] ($P2_1$/n form) showed a large peak ca. 1 Å away from W1. This was added to the model as a fractional (refined) W1B atom which resulted in a large decrease in R1 and the identification of three potential (fractional) S atoms all about 1 Å away from S1, S2 and S3. The geometry of these sites gave bond lengths in good agreement with the major component, however the common refined site occupancy factor for these atoms (0.11) was such as to make identification of O and C atoms unlikely, and this was the case. The major component is shown in Fig. 3.16. Selected bond lengths and angles are given in tables 3.15 and 3.16.

3.6 References

1. W. Levason, S. D. Orchard and G. Reid, *Coord. Chem. Rev.*, 2002, **225**, 159.
2. W. Levason and G. Reid, *Comprehensive Coordination Chemistry II*, Elsevier, vol. 3, 2004.
3. F. K. Gormley, J. Gronbach, S. M. Draper and A. P. Davis, *Dalton Trans.*, 2000, 173.
4. A. J. Barton, W. Levason and G. Reid, *J. Organomet. Chem.*, 1999, **579**, 235.
5. J. Connelly, M. K. Davies and G. Reid, *J. Chem. Soc. Dalton Trans.*, 1998, 3833.
6. W. Levason, B. Patel, G. Reid and A. J. Ward, *J. Organomet. Chem.*, 2001, **619**, 218.
7. D. J. Darensbourg and R. L. Kump, *Inorg. Chem.*, 1978, **17**, 2680.
8. R. B. King, Academic Press, New York, 1965.
9. A. J. Barton, W. Levason and G. Reid, *J. Organomet. Chem.*, 1999, **579**, 235.
10. W. Levason, M. Nirwan, R. Ratnani, G. Reid, N. Tsoureas and M. Webster, *J. Chem. Soc. Dalton Trans.*, 2007, 439.
11. W. Levason, S. D. Orchard and G. Reid, *Organometallics*, 1999, **18**, 1275.
12. J. Mason, *Multinuclear NMR*, Plenum Press, New York, 1987.
13. G. M. Sheldrick, *SHELXS-97 Program for Crystal Structure Solution, University of Göttingen, Germany*, 1997.
14. G. M. Sheldrick, *SHELXL-97, Program for Crystal Structure Refinement, University of Göttingen, Germany*, 1997.
15. H. D. Flack, *Acta Crystallogr., Sect. A,*, 1983, **39**, 876.

CHAPTER 4

Synthesis and properties of mono- and heterobimetallic complexes based on $\{(\eta^6\text{-arene})RuCl\}^+$ and $\{(\eta^6\text{-arene})OsCl\}^+$ fragments with tetrathioether and tetraselenoether ligands

4.1 Introduction

Chapter 3 described a range of substituted metal carbonyl complexes based upon the four ligands $C(CH_2SMe)_4$, $C(CH_2SeMe)_4$, 1,2,4,5-$C_6H_2(CH_2SMe)_4$ and 1,2,4,5-$C_6H_2(CH_2SeMe)_4$ coordinated κ^2 or $\kappa^2\kappa'^2$ to one or two metal centres respectively.

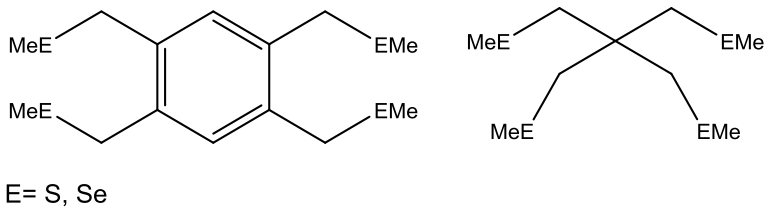

Figure 4.1 Structure of ligands studied in this chapter.

This chapter describes studies of the four tetradentates ligands $C(CH_2SMe)_4$, $C(CH_2SeMe)_4$, 1,2,4,5-$C_6H_2(CH_2SMe)_4$ and 1,2,4,5-$C_6H_2(CH_2SeMe)_4$ with arene-ruthenium(II) and -osmium(II) centres and some homo- and hetero-bimetallic derivatives. Ruthenium and osmium *p*-cymene centres were produced by reacting 0.5 equivalents of corresponding metal dimer (figure 4.2) with a chosen ligand.

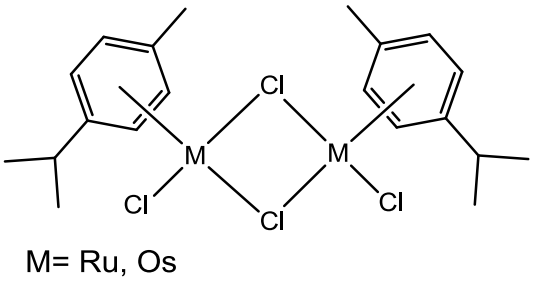

Figure 4.2 Structure of ruthenium and osmium *p*-cymene dimer.

Osmium and ruthenium *p*-cymene precursors were chosen as they are robust organometallic centres and some examples of thioether complexes had been previously isolated.[1] However, no examples with selenium based ligands have been reported.

Bidentate thioether ligands and ruthenium *p*-cymene have been shown to form a complexes by stirring *o*-$C_6H_4(CH_2SMe)_2$ and 1 eq. of $\{RuCl_2(\eta^6\text{-}p\text{-cymene})\}_2$ in CH_2Cl_2 at room temperature for 24 h.[2] The product, $[\{RuCl_2(\eta^6\text{-}p\text{-cymene})\}_2\{o\text{-}C_6H_4(CH_2SMe)_2\}]$ was structurally characterised (see figure 4.3).

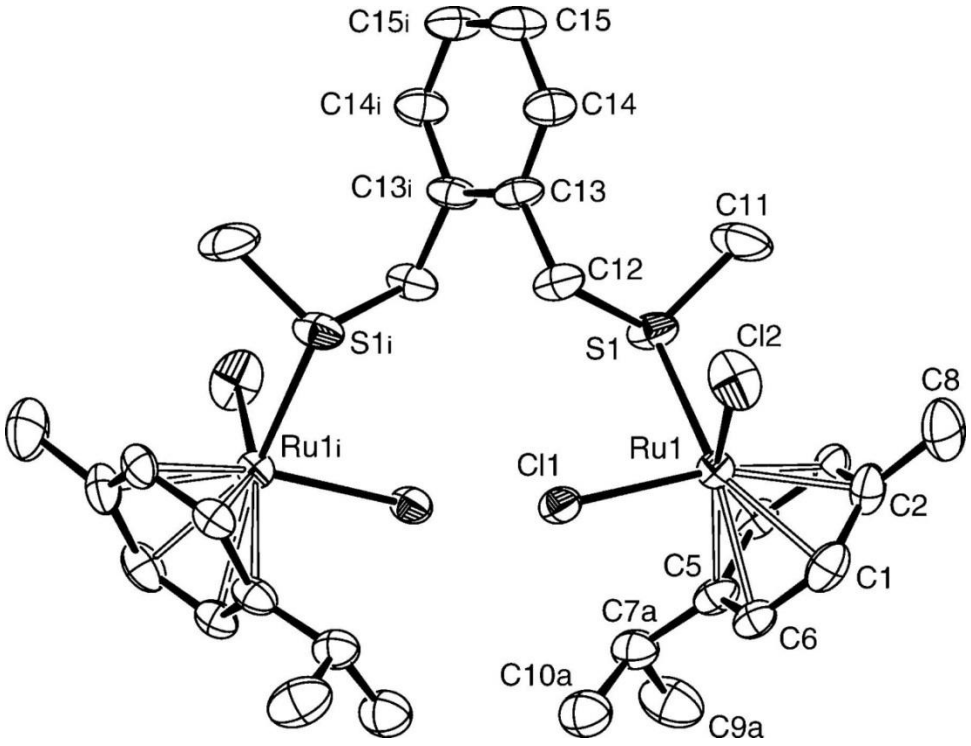

Figure 4.3 Structure of $[\{RuCl_2(\eta^6\text{-}p\text{-cymene})\}_2\{o\text{-}C_6H_4(CH_2SMe)_2\}]$. Ellipsoids are drawn at the 50% probability level and H atoms have been omitted for clarity.[2]

The complex exhibits two-fold symmetry with the dithioether ligand functioning as a bridging bidentate, through coordination *via* one thioether sulfur atom to each of the two ruthenium atoms. This forms a distorted pseudo-octahedral geometry through the *p*-cymene ligand, one thioether sulfur donor atom and two mutually *cis* Cl atoms.[3]

Synthesis of heterobimetallic species requires the complex to be κ^2 coordinated. Monodentate interactions on tetradentate ligands would lead to a mixture of products so consequently are unsuitable for production of heterobimetallic species. In order to maintain the Ru(II) oxidation state addition of a counter ion such as $[NH_4][PF_6]$ is required to produce a κ^2 coordinated complex. Addition of a counter ion also provided greater control

during the reaction, as the complex, insoluble in ethanol would precipitate producing a product containing little, if any starting material. Implementing this method produced several examples of κ^2 coordinated complexes of ruthenium and osmium, with sulfur and selenium containing ligands. Selected monometallic complexes were then reacted further to attempt to produce heterobimetallic species.

Complexes containing $AgPF_6$ and a similar thioether ligands to the tetrabenzyl type produced in Chapter 2, 1,2,4,5-tetrakis(3-pyridylmethylsulfanylmethyl)benzene (see figure 4.4) have been produced and characterised.[4] Although these systems have slight structural differences the geometry around the metal centre (distorted tetrahedral) is the same after coordination and should be considered when discussing spectroscopic data.

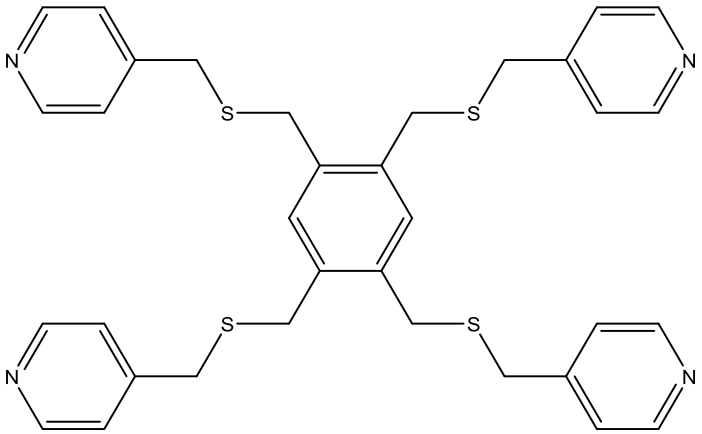

Figure 4.4 Structure of 1,2,4,5-tetrakis(3-pyridylmethylsulfanylmethyl)benzene (4_N-tet).

Heterobimetallic complexes

Metal carbonyls complexes described in chapter 3 proved be susceptible to rearrangement or displacement of the first metal centre when reacting with a second different metal. Consequently, they were not considered to be suitable candidates for production of mixed metal complexes. Although less soluble, osmium and ruthenium *p*-cymene groups should be less sensitive when compared to the labile carbonyl systems previously studied. Complexes containing spirocyclic ligands ($C(CH_2SMe)_4$ and $C(CH_2SeMe)_4$) were found to be more soluble than other ligand systems, so will be the main focus for synthesis of mixed metal complexes.

4.2 Results

4.2.1 General Synthesis

Reacting two molar equivalents of each ligand with $[Ru(\eta^6\text{-}p\text{-cymene})Cl_2]_2$ in ethanol, followed by addition of $[NH_4][PF_6]$, produced good yields of the monometallic species as yellow solids. Addition of $[NH_4][PF_6]$ allowed greater control of reaction conditions than preparations used with metal carbonyl compounds in Chapter 3. The addition of counter ion produces a less soluble product and allows control of the amount of time the reactants may react in solution. Isolating the product as a solid prevents rearrangements that may occur during the reaction promoting the formation a monometallic species.

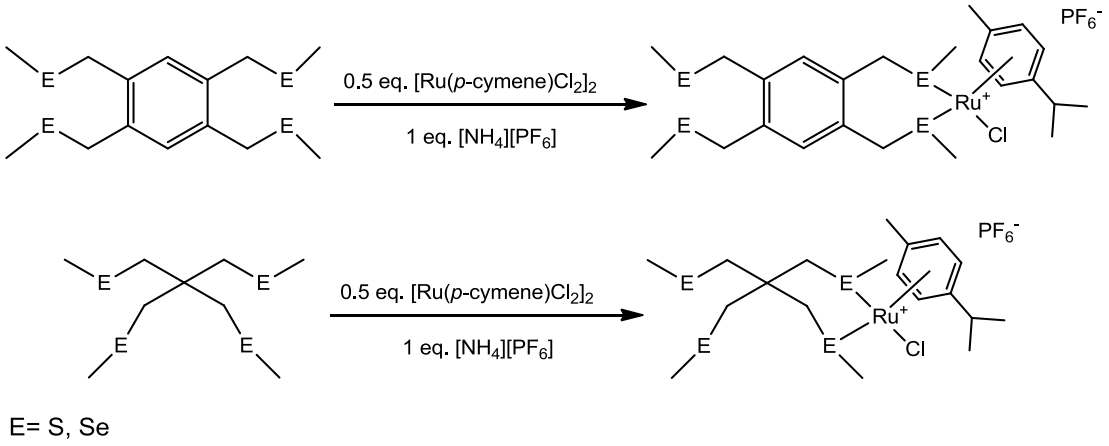

Figure 4.5 Formation of monometallic ruthenium complexes.

Bimetallic complexes with $C(CH_2SMe)_4$ can be produced in high purity, either by treating a mono-metallic complex with 0.5 equivalents of $[Ru(\eta^6\text{-}p\text{-cymene})Cl_2]_2$, or directly by reacting $[Ru(\eta^6\text{-}p\text{-cymene})Cl_2]_2$ with $C(CH_2SMe)_4$ in a 1:1 molar ratio. This produced the corresponding diruthenium species $[\{RuCl(\eta^6\text{-}p\text{-cymene})\}_2\{\kappa^2\kappa'^2\text{-}C(CH_2SMe)_4\}][PF_6]_2$ (see figure 4.6).

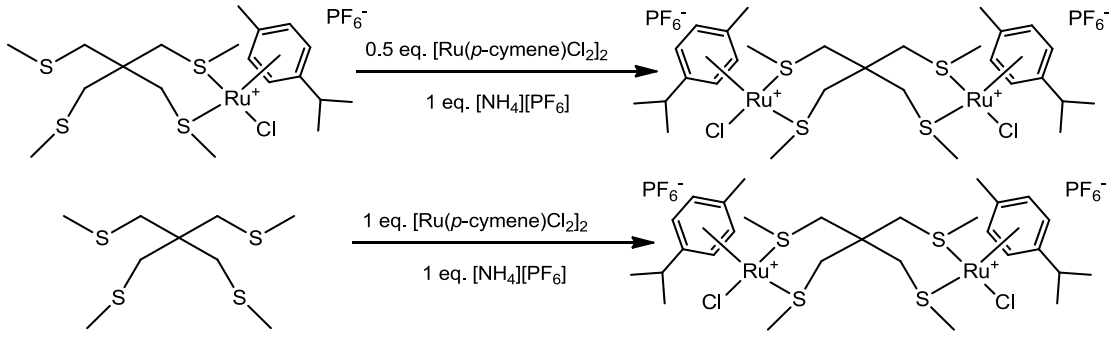

Figure 4.6 Stepwise addition and direct synthesis of diruthenium complexes.

A more limited number of osmium(II) complexes was produced, to explore any differences between the corresponding 4d and 5d metal centres. In fact the osmium compounds proved key to the successful production of heterobimetallics (see Section 4.5). All the complexes were air-stable solids with relatively poor solubility in chlorocarbons or acetone.

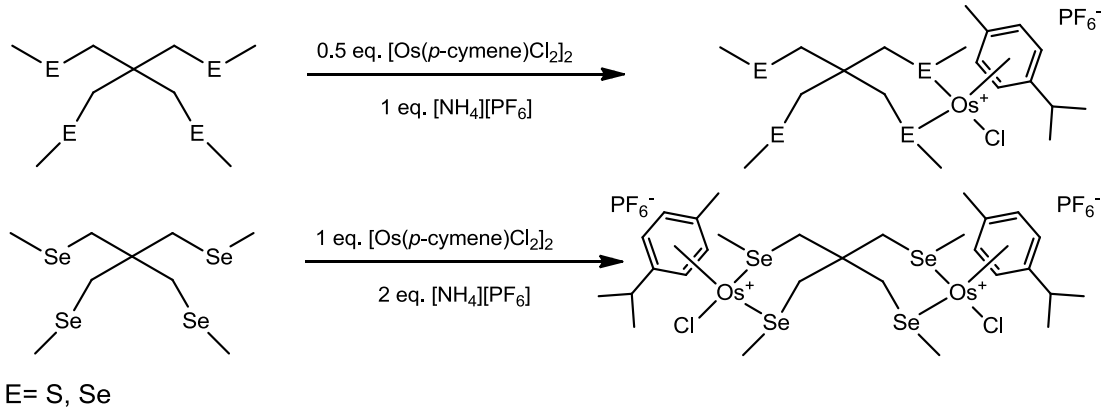

Figure 4.7 Formation of mono- and bimetallic osmium complexes.

Stepwise addition of a second 0.5 equivalents of $[Os(\eta^6\text{-}p\text{-cymene})Cl_2]_2$, to $[\{OsCl(\eta^6\text{-}p\text{-cymene})\}\{\kappa^2\text{- }C(CH_2SeMe)_4\}][PF_6]$ also produced a diosmium species.

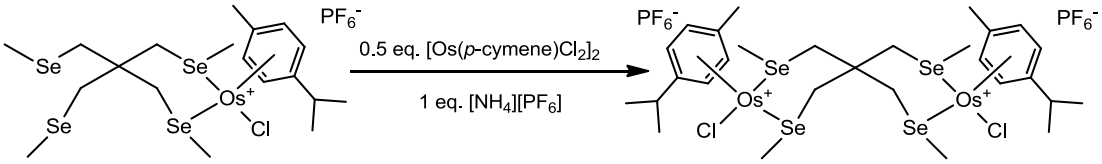

Figure 4.8 Stepwise addition 0.5 eq. $[Os(\eta^6\text{-}p\text{-cymene})Cl_2]_2$ to monometallic osmium complexes.

As expected bimetallic compounds were far less soluble than corresponding monometallic compounds, complexes with the spirocyclic ligands were markedly more soluble than compounds with an aromatic backbone. Similar behaviour was observed in carbonyl complexes (See chapter 3).

Using a different counter ion also affects solubility, replacing the $[PF_6]^-$ with $[BPh_4]^-$ increases solubility, this approach was implemented for some complexes to enable full characterisation. Some ruthenium complexes were also isolated as Cl^- salts by omitting the large anion, however these were not obtained analytically pure. The ^1H NMR spectra of the latter suggest a equilibrium in solution, with the chloride anion partially displacing a thio- or seleno-ether group from the ruthenium, as observed in the $[RuCl(\eta^6\text{-}p\text{-cymene})(R_2S)_2]Cl$ complexes.[5]

An overview of reactions and complexes produced is shown below for each ligand and details of reaction conditions are reported in the experimental section 4.6.

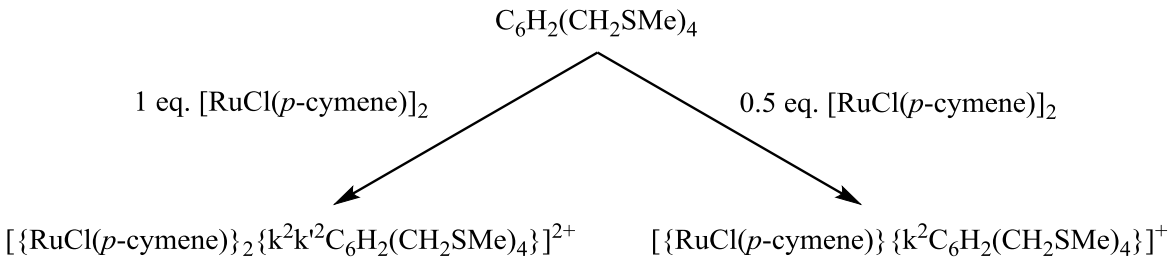

Figure 4.9 General reaction scheme for complexes with thioether tetrabenzyl ligand.

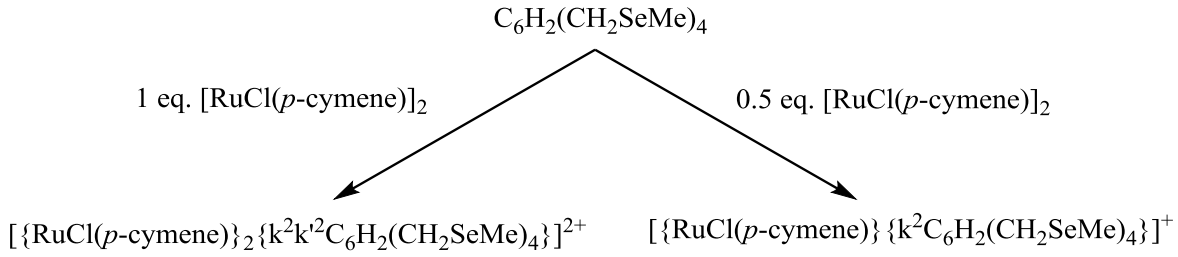

Figure 4.10 General reaction scheme for complexes with selenoether tetrabenzyl ligand.

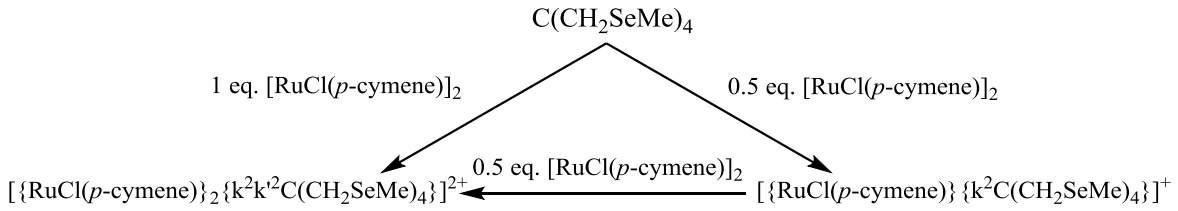

Figure 4.11 General reaction scheme for complexes with the selenoether spirocyclic ligand.

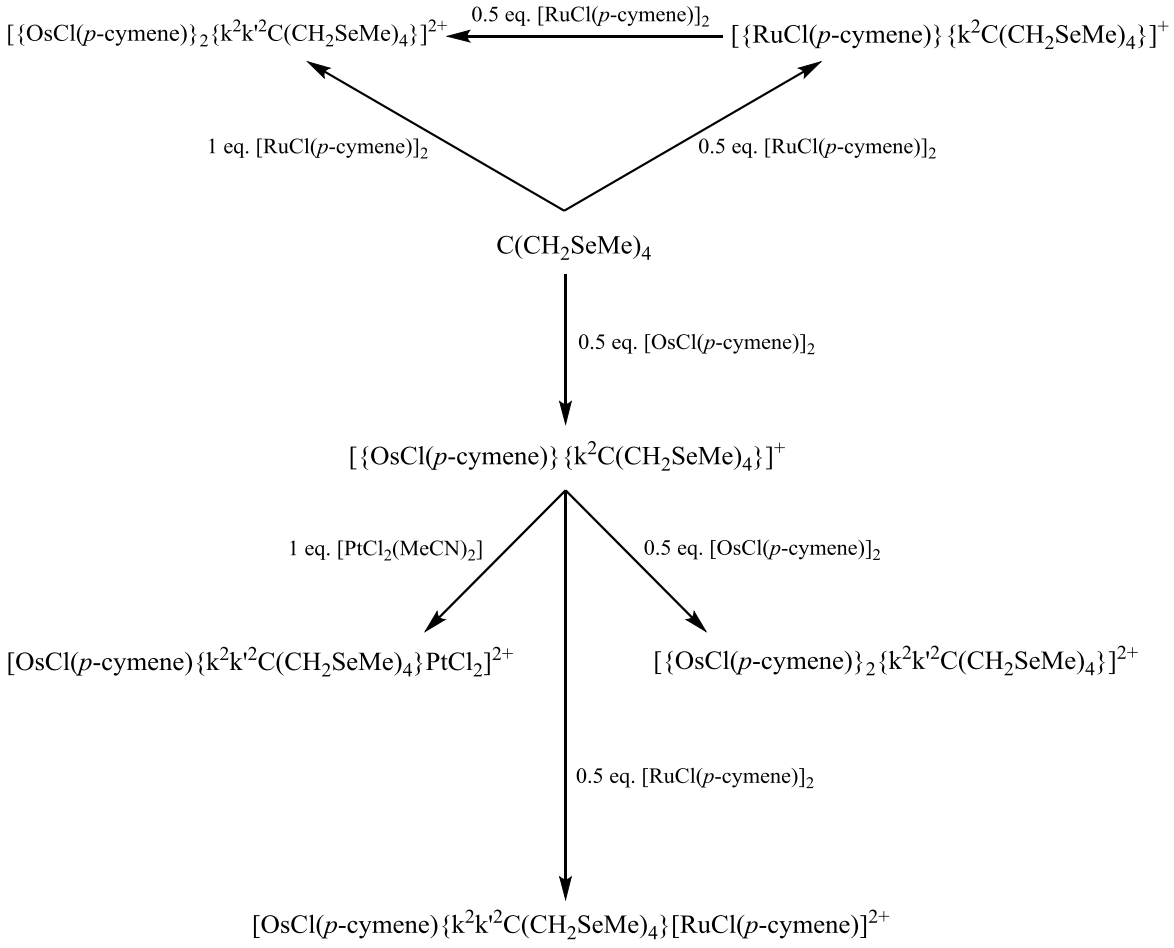

Figure 4.12 General reaction scheme for complexes with the selenoether spirocyclic ligand.

4.2.2 Characterisation

Each complex produced was characterised with a variety techniques however, poor solubility made some methods more challenging.

Infared spectra were recorded on all complexes. In each case a M-Cl stretch was observed at ~305 cm^{-1} and all complexes containing a $[PF_6]^-$ anion showed strong absorptions at ~839 and 557 cm^{-1} (PF_6 stretch and PF_6 bend respectively). This compares well with the reported PF_6 stretch reported for $[AgPF_6\{4_N\text{-tet}\}]$ at 840 cm^{-1}.[4] Although only confirming the presence of $[PF_6]^-$ anion the poor solubility of these compounds meant solid state spectroscopy (Nujol mull) was a useful technique in determining if a reaction had occurred. An example of a spectrum is shown below.

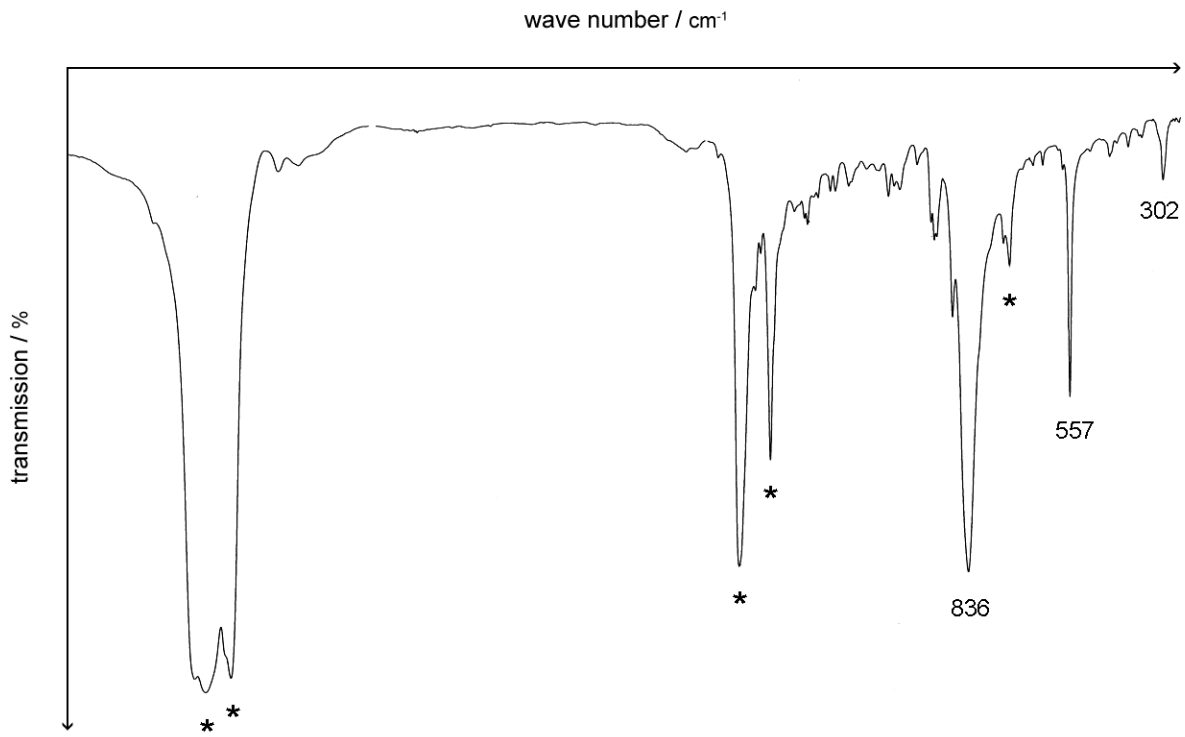

* Absorptions assigned to Nujol

Figure 4.13 Shows the Infared spectrum of [RuCl(η^6-*p*-cymene){κ^2-C($CH_2SMe)_4$}][PF_6] (Nujol mull).

ES^+ mass spectrometry (MeCN) was performed on all complexes synthesised. All homo mono- and bi-metallic compounds showed an ion multiplet corresponding to the parent cation with no other significant ions observed in the spectrum. The hetero-bimetallic compounds were more complicated and are discussed later. Each isotope pattern for homo mono- and bi-metallic compounds matched the predicted pattern, which seemed to conflict with the complicated NMR spectra observed. Micro analysis later confirmed the purity of each complex. This knowledge, together with the crystallographic data, allowed NMR spectra to be correctly interpreted.

Single crystals were obtained from most complexes synthesised. Conditions for growing crystals are detailed in Experimental Section 4.6. Single crystal X-ray diffraction was fundamental for the correct interpretation of data collected from these complexes. The low symmetry and the presence of several stereoisomers (invertomers) lead to complicated NMR spectra. The data collected from each compound are individually discussed below.

[MCl(η^6-*p*-cymene){κ^2-C($CH_2EMe)_4$}][PF_6] (M= Ru/Os, E= S/Se)

Crystals of the [RuCl(η^6-*p*-cymene){κ^2-C($CH_2SMe)_4$}]$^+$ and [RuCl(η^6-*p*-cymene){κ^2-C($CH_2SeMe)_4$}]$^+$ cation salts were grown and their structures determined. The structures were found to be isomorphous. Figure 4.14 shows the cation [RuCl(η^6-*p*-cymene){κ^2-C($CH_2SMe)_4$}]$^+$ and selected bond lengths and angles from both complexes are shown in table 4.5. The atom numbering for both the thio- and seleno-ether complexes is consistent to allow comparison.

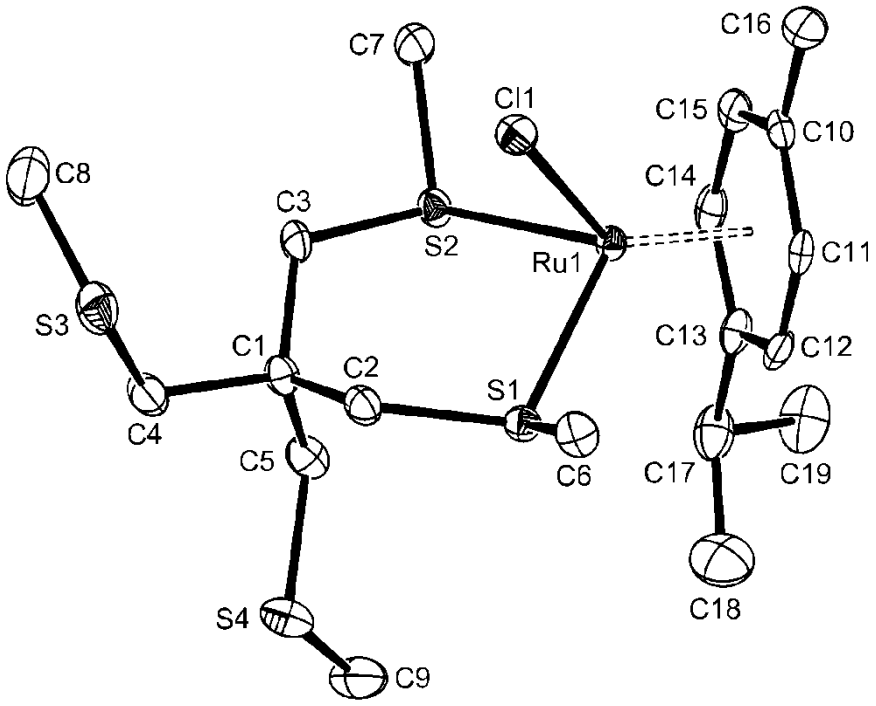

Figure 4.14 Structure of the cation in [RuCl(η^6-*p*-cymene){κ^2-C($CH_2SMe)_4$}][PF_6] showing the numbering scheme adopted. Ellipsoids are drawn at the 50% probability level and H atoms have been omitted for clarity.

	E = S	E = Se
Ru1–C(arene)	2.176(3)–2.267(3)	2.175(9)–2.225(9)
Ru1–Cl1	2.3891(8)	2.391(2)
Ru1–E1	2.3702(8)	2.4806(12)
Ru1–E2	2.3666(8)	2.4776(11)
E1···E2	3.344(1)	3.472(1)
E3···E4	4.849(1)	5.063(2)
E1–Ru1–E2	89.80(3)	88.89(4)
E1–Ru1–Cl1	88.19(3)	88.58(6)
E2–Ru1–Cl1	88.11(3)	88.63(6)
C2–E1–C6	97.4(2)	94.7(4)
C3–E2–C7	96.8(2)	94.5(4)
C4–E3–C8	102.8(2)	94.2(5)
C5–E4–C9	98.4(2)	100.8(5)

Table 4.1 Selected bond lengths (Å) and angles (°) for $[RuCl(\eta^6\text{-}p\text{-cymene})\{\kappa^2\text{-}C(CH_2EMe)_4\}][PF_6]$, (E = S or Se).

Both structures contain pseudo six-coordinate ruthenium with the arene formally occupying one triangular face of the octahedron. The chalcogenoether and chloride ligand are coordinated to the second triangular face completing the octahedron. Both κ^2–chalcogenoethers are *meso* invertomers with the EMe (E= S, Se) groups on the same side of the RuE_2 plane as the chlorine and *anti* to the *p*-cymene ^{i}Pr group. The spirocyclic ligand forms a six membered chelate ring and in both cases the bite angle (E−Ru−E) for the thio and selenoether ligand is slightly less than 90°. The distances between donor atoms within the chelate ring are S···S 3.344(1) Å and Se···Se 3.472(1) Å, contrasting with the uncoordinated donor atoms in both ligands which are ~1.5 Å greater due to the substituents being directed away from each other to minimise lone pair repulsions. There is little difference between the Ru−C and Ru−Cl bond lengths in the two complexes.

The ES^+ mass spectrum of $[OsCl(\eta^6\text{-}p\text{-cymene})\{\kappa^2\text{-}C(CH_2SMe)_4\}][PF_6]$ is shown in figure 4.15.

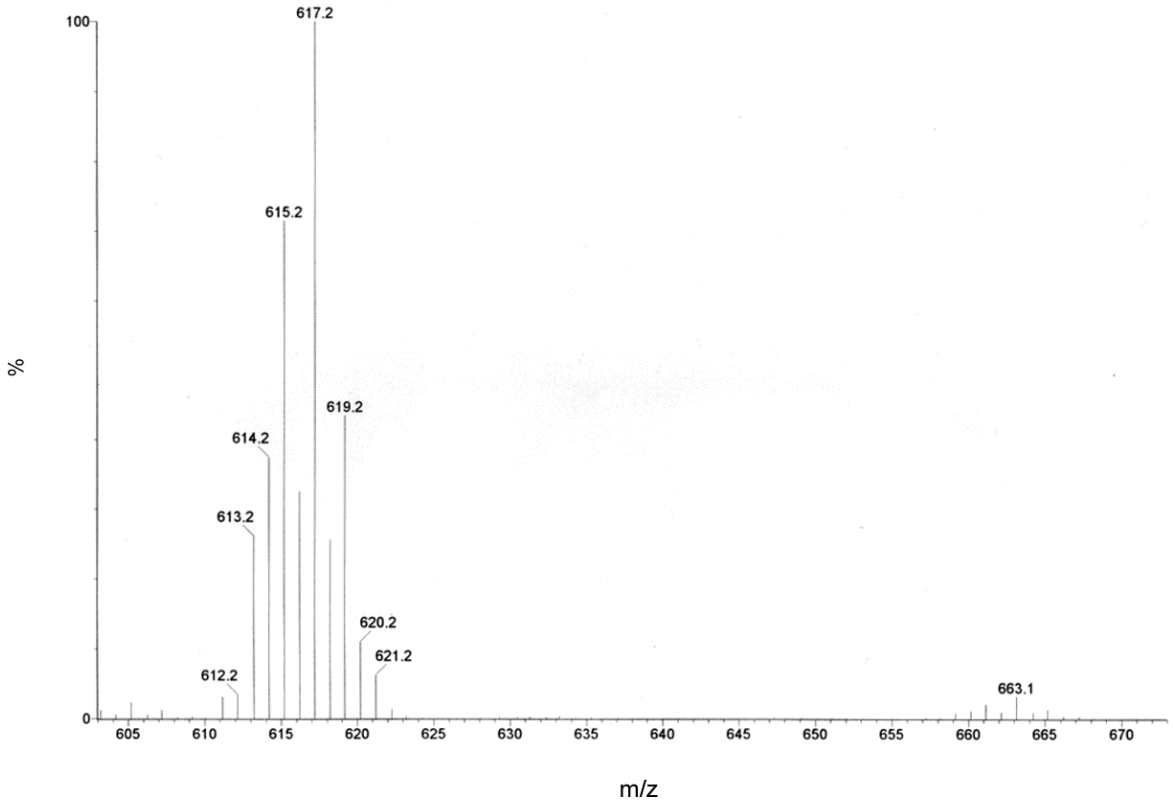

Figure 4.15 ES^+ mass spectrum of $[OsCl(\eta_6\text{-}p\text{-cymene})\{\kappa^2\text{-}C(CH_2SMe)_4\}]^+$ recorded in MeCN.

Mono-metallic complexes with $C(CH_2SMe)_4$ and $C(CH_2SeMe)_4$ are coordinated equatorially to two donor atoms in six-membered chelate rings. The ruthenium atom has no axial symmetry, which means three possible invertomers can be observed: a *DL* form and two *meso* forms; with the MeE (E= S/Se) groups *syn* or *anti* to the RuCl group.

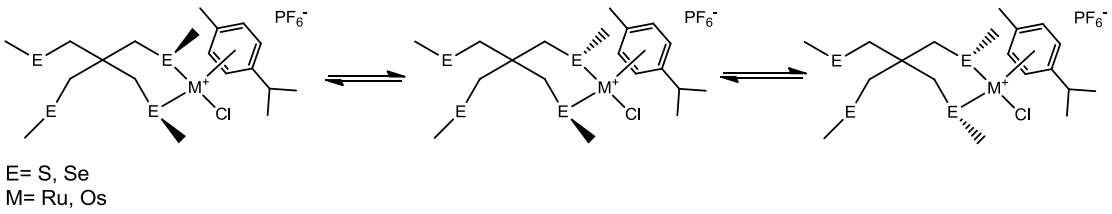

Figure 4.16 Shows three possible invertomers of monometallic complexes due to inversion.

Despite this, only one EMe (E= S/Se) resonance is observed in the ^{1}H, ^{13}C{^{1}H} and ^{77}Se{^{1}H} NMR spectra. The presence of the *DL* form would lead to two resonances of equal intensity, due to the lack of axial symmetry at the metal. Consequently the single observed resonance suggests either fast pyramidal inversion or with the presence of only one of the *meso* forms in the sample. Low temperature studies were limited due to the modest solubility and by the mp (-48°C) of CD_3CN/MeCN. Apart from small temperature drifts in the chemical shifts of the ^{77}Se{^{1}H} NMR spectra, the spectra of those complexes were unchanged on cooling.

The ^{1}H NMR spectrum of [RuCl(η^6-*p*-cymene){κ^2-C($CH_2SMe)_4$}]$^+$ shows the η^6-*p*-cymene group as two doublets at δ 6.03 and 6.22 ppm, $^{3}J_{HH}$ = 6 Hz, assigned to the four aromatic protons, a doublet at δ 1.37 ppm, $^{3}J_{HH}$ = 7 Hz for CH(C*H*$_3$)$_2$, and a septet at δ 2.95 ppm for C*H*(CH_3)$_2$. The three singlets of equal intensity at δ 2.22, 2.25, 2.30 ppm are assigned to the *p*-cymene Me group and uncoordinated SMe groups. The uncoordinated methyl groups are inequivalent, due to the lack of axial symmetry at the ruthenium, and tetrahedral disposition of the CH_2SMe groups about the quaternary carbon present in the ligand backbone. Consequently, each group is *syn* or *anti* to the arene. The remaining two coordinated SMe groups were assigned to the single resonance at δ 2.82. ^{13}C{^{1}H} NMR data are also fully consistent with the presence of a single invertomer or fast pyramidal inversion.

The assignment of the ^{1}H NMR spectrum of [RuCl(η^6-*p*-cymene){κ^2-C($CH_2SeMe)_4$}]$^+$ ^{1}H NMR spectrum follows that of the thioether analogue (details of assignments are reported in the experimental, section 4.6). The ^{77}Se{^{1}H} NMR spectrum shows two resonances at δ 24.5, 25.0 ppm for each uncoordinated MeSe group and a singlet at 115.6 ppm assigned to the coordinated SeMe groups. The spectra of both complexes were carefully examined but failed to reveal any weak resonances which could be attributed to other invertomers.

The NMR spectra of osmium complexes with C($CH_2SMe)_4$ and C($CH_2SeMe)_4$; [OsCl(η^6-*p*-cymene){κ^2-C($CH_2EMe)_4$}]$^+$ (E= S, Se) are generally similar to the ruthenium analogues, ^{1}H NMR only shows very small differences in chemical shift when compared to the corresponding ruthenium compounds. However, three very weak features are observed in the ^{77}Se{^{1}H} NMR spectra of [OsCl(η^6-*p*-cymene){κ^2-C($CH_2SeMe)_4$}]$^+$ with an overall intensity of ~5% compared with the major resonance at δ = 72.2 ppm. The presence of

very small amounts of the *DL* and the second *meso* invertomer could explain the presence of these minor resonances see figure 4.17.

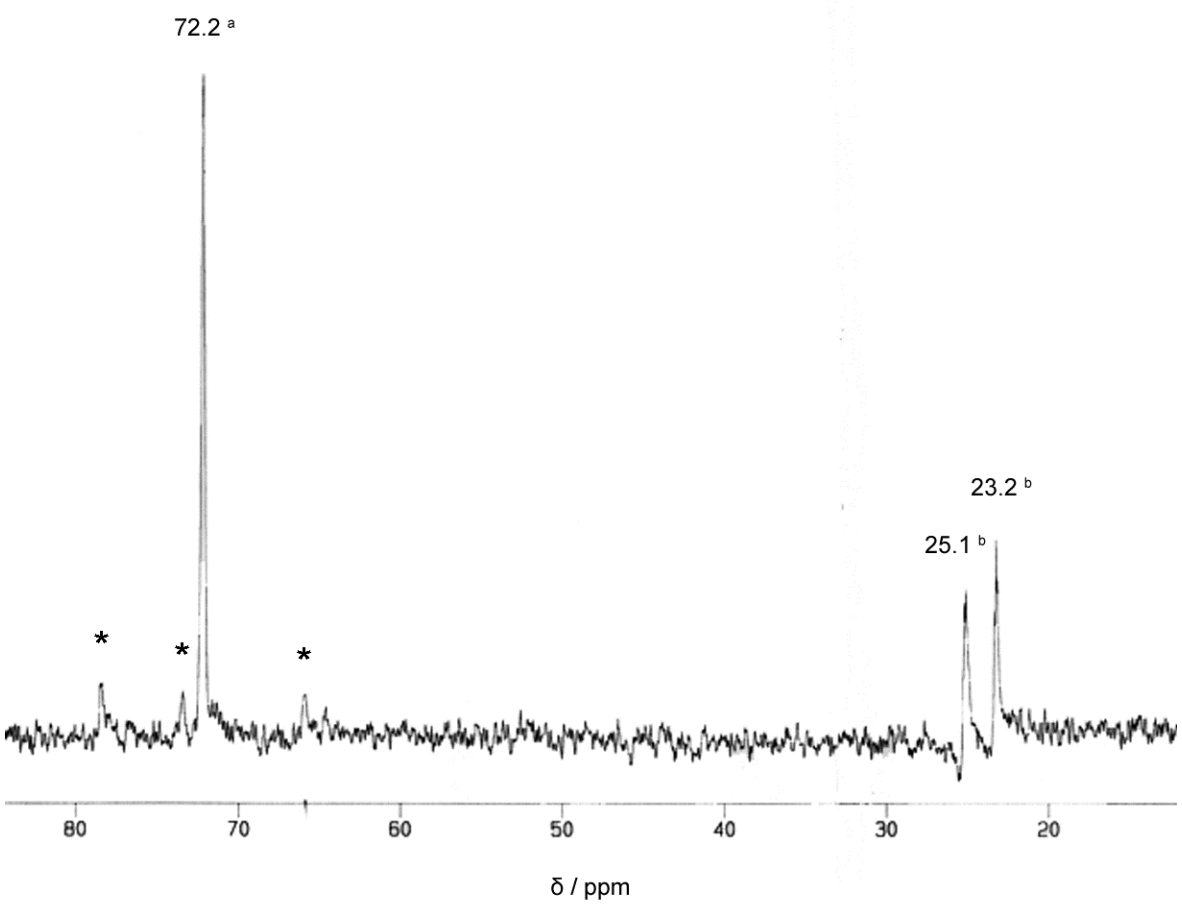

* Resonances assigned to invertomers

[a] Assigned to coordinated SeMe

[b] Assigned to uncoordinated SeMe

Figure 4.17 $^{77}Se\{^{1}H\}$ NMR spectrum of $[OsCl(\eta^{6}\text{-}p\text{-cymene})\{\kappa^{2}\text{-}C(CH_2SeMe)_4\}]^{+}$ recorded in MeCN at ambient temperature.

Smaller coordination shifts are observed in the $^{77}Se\{^{1}H\}$ NMR of the osmium complexes when compared to the ruthenium analogue; this reflects the usual trends between 4d and 5d metal centres.[1]

Weak features very close to the major resonance can be seen in ^{1}H NMR spectrum of $[OsCl(\eta^{6}\text{-}p\text{-cymene})\{\kappa^{2}\text{-}C(CH_2SeMe)_4\}]^{+}$, which can also be attributed to small amounts of the *DL* and the second *meso* invertomers. However, specific assignments are not possible. In contrast, the ^{1}H NMR spectrum of $[OsCl(\eta^{6}\text{-}p\text{-cymene})\{\kappa^{2}\text{-}C(CH_2SMe)_4\}]^{+}$

shows larger amounts (<10% overall) of the other invertomers are observed, but due to the complexity of the spectra specific invertomers cannot be assigned.

[RuCl(η^6-*p*-cymene){κ^2-1,2,4,5-$C_6H_2(CH_2EMe)_4$}][BPh_4] (E= S/Se)

Crystals of [RuCl(η^6-*p*-cymene){κ^2-1,2,4,5-$C_6H_2(CH_2SMe)_4$}][PF_6] and [RuCl(η^6-*p*-cymene){κ^2-1,2,4,5-$C_6H_2(CH_2SeMe)_4$}][PF_6] cations were grown and their structures determined. The structures of both complexes were shown to be isomorphous, with very similar bond lengths and angles. A view of [RuCl(η^6-*p*-cymene){κ^2-1,2,4,5-$C_6H_2(CH_2SMe)_4$}]$^+$ and selected bond angles from both complexes are shown in figure 4.18 and table 4.5. The atom numbering for both the thio- and seleno-ether complexes are consistent to allow comparison.

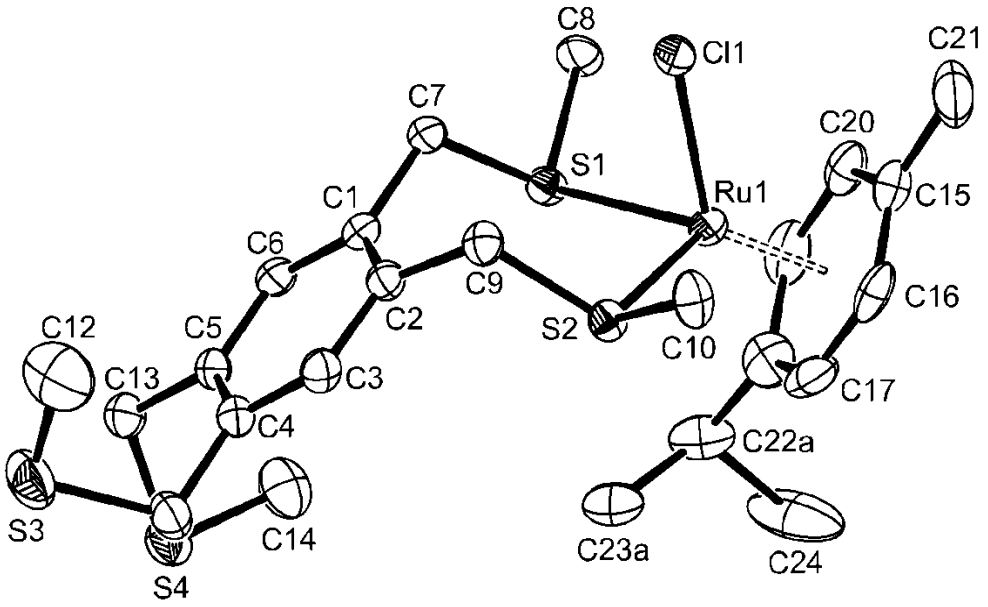

Figure 4.18 Structure of [RuCl(η^6-*p*-cymene){κ^2-1,2,4,5-$C_6H_2(CH_2SMe)_4$}][BPh_4] showing the numbering scheme adopted. Ellipsoids are drawn at the 50% probability level and H atoms have been omitted for clarity.

	E = S	E = Se
Ru1–C(arene)	2.167(4)–2.253(4)	2.174(9)–2.246(10)
Ru1–Cl1	2.3752(9)	2.382(2)
Ru1–E1	2.3766(9)	2.5138(15)
Ru1–E2	2.4044(9)	2.4799(15)
E1···E2	3.518(1)	3.637(2)
E3···E4	4.556(2)	4.765(2)
E1–Ru1–E2	94.75(3)	93.49(4)
Cl1–Ru1–E2	87.51(3)	87.91(7)
Cl1–Ru1–E1	87.40(3)	88.07(7)

Table 4.2 Selected bond lengths (Å) and angles (°) for [RuCl(η^6-*p*-cymene){κ^2-1,2,4,5-$C_6H_2(CH_2EMe)_4$}][BPh_4] (E = S or Se).

The only significant difference between the two structures is a larger covalent radius when comparing selenium to sulfur. The aromatic ligand type (1,2,4,5-$C_6H_2(CH_2SMe)_4$ and 1,2,4,5-$C_6H_2(CH_2SeMe)_4$) form seven-membered chelate rings, which results in wider E–Ru–E angles (by ~6°) compared the spirocyclic-backboned analogues. The EMe (E= S, Se) groups are *meso* invertomers, so both occupying the same side of the E−Ru−E plane. The six-coordinate ruthenium has two EMe groups and chlorine occupying one face of the octahedron and the ^{i}Pr group of the *p*-cymene *anti* to the EMe groups occupying the other face.

The presence of a planar aromatic linker in these complexes means the ^{1}H NMR spectrum differs from those of the spirocyclic ($C(CH_2SMe)_4$ and $C(CH_2SeMe)_4$) linked ligands, due to the lack of a tetrahedrally coordinated quaternary carbon. Consequently, the uncoordinated SMe groups are now equivalent by symmetry and produce a single resonance. The ^{1}H NMR spectrum of [RuCl(η^6-*p*-cymene){κ^2-1,2,4,5-$C_6H_2(CH_2SMe)_4$}]$^+$ shows a singlet at δ 2.01 ppm for the uncoordinated SMe group and a singlet at δ 2.46 ppm for the coordinated SMe group. In the $^{13}C\{^1H\}$ NMR spectrum these groups are observed as single resonances at δ 15.56 ppm and 30.89 ppm respectively.

^{1}H and ^{13}C{^{1}H} NMR data for [RuCl(η^{6}-*p*-cymene){κ^{2}-1,2,4,5-$C_6H_2(CH_2SeMe)_4$}]$^{+}$ show similar behaviour. Two resonances were seen in the ^{77}Se{^{1}H} NMR spectrum at δ 157.7 ppm and 183.9 ppm due to uncoordinated and coordinated SeMe groups. These results agree with the previous observations made in chapter 3 on metal carbonyl complexes.[5] The ^{77}Se{^{1}H} NMR coordination shifts of the complexes containing an aromatic backbone are much smaller compared to complexes with a spirocyclic linker. This can be attributed to the larger chelate ring formed by the aromatic containing complexes. The simpler NMR spectra suggest fast inversion in both complexes, which is expected to be a low energy process in seven-membered chelate rings.[6]

[{MCl(η^{6}-*p*-cymene)}$_2${κ^{2}κ'^{2}-1,2,4,5-$C_6H_2(CH_2EMe)_4$}][PF_6]$_2$ (M= Ru/Os, E= S/Se)

Crystals of [{RuCl(η^{6}-*p*-cymene)}$_2${κ^{2}κ'^{2}-1,2,4,5-$C_6H_2(CH_2SMe)_4$}][PF_6]$_2$ were grown and the structure determined. An image of the dication and selected bond angles are shown in figure 4.19 and table 4.6.

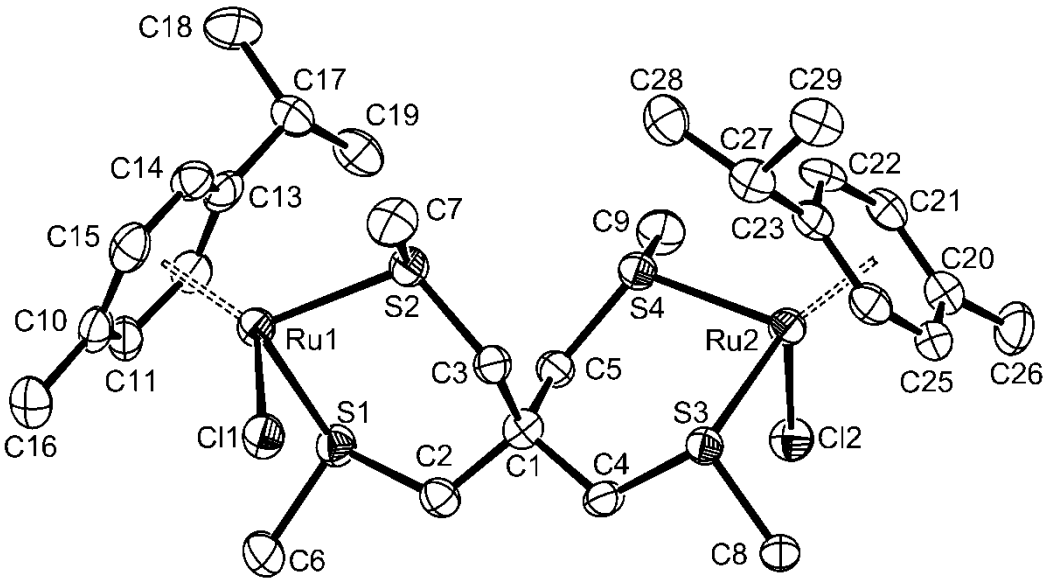

Figure 4.19 Structure of the cation in [{RuCl(η^{6}-*p*-cymene)}$_2${κ^{2}κ'^{2}-1,2,4,5-$C_6H_2(CH_2SMe)_4$}][PF_6]$_2$ showing the numbering scheme adopted. Ellipsoids are drawn at the 50% probability level and H atoms have been omitted for clarity.

Ru1–C(arene)	2.179(8)–2.218(8)	Ru2–C(arene)	2.175(8)–2.252(8)
Ru1–S1	2.366(2)	Ru2–S3	2.368(2)
Ru1–S2	2.363(2)	Ru2–S4	2.373(2)
Ru1–Cl1	2.402(2)	Ru2–Cl2	2.392(2)
S1···S2	3.323(3)	S3···S4	3.362(3)
S1–Ru1–S2	89.28(7)	S3–Ru2–S4	90.31(7)
S1–Ru1–Cl1	89.17(8)	S3–Ru2–Cl2	88.65(7)
S2–Ru1–Cl1	87.70(8)	S4–Ru2–Cl2	87.02(7)

Table 4.3 Selected bond lengths (Å) and angles (°) for $[\{RuCl(\eta^6\text{-}p\text{-cymene})\}_2\{\kappa^2\kappa'^2\text{-}1,2,4,5\text{-}C_6H_2(CH_2SMe)_4\}][PF_6]_2$

Although the two halves of the molecule $[\{RuCl(\eta^6\text{-}p\text{-cymene})\}_2\{\kappa^2\kappa'^2\text{-}1,2,4,5\text{-}C_6H_2(CH_2SMe)_4\}]^{2+}$ are not related by crystallographic symmetry, they are very similar. Both contain six-coordinate ruthenium centres with a *fac* arrangement of one chloride and a chelating dithioether unit, again with *meso* SMe groups *syn* to the chloride. The *p*-cymene is bonded η^6 to complete the octahedron. Bond lengths are not significantly different when compared to the monometallic complex.

The ES^+ mass spectrum of $[\{RuCl(\eta^6\text{-}p\text{-cymene})\}_2\{\kappa^2\kappa'^2\text{-}1,2,4,5\text{-}C_6H_2(CH_2SMe)_4\}][PF_6]_2$ shows ions with the correct isotope structure at half-mass for the cations as expected due to the dipositive charge.

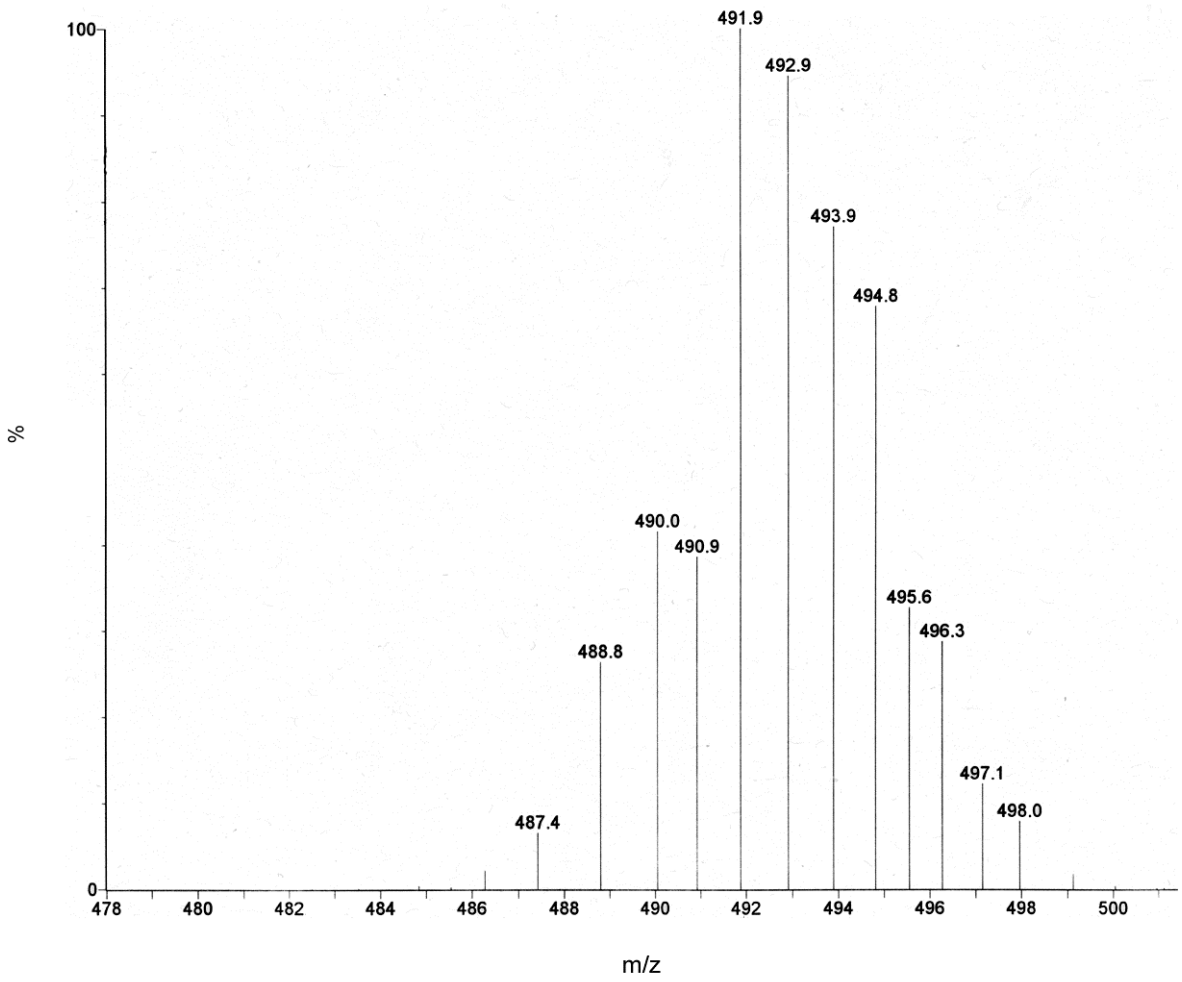

Figure 4.20 ES^+ mass spectrum of $[\{RuCl(\eta^6\text{-}p\text{-cymene})\}_2\{\kappa^2\kappa'^2\text{-}1,2,4,5\text{-}C_6H_2(CH_2SeMe)_4\}]^{2+}$ recorded in MeCN.

The NMR spectra of $[\{RuCl(\eta^6\text{-}p\text{-cymene})\}_2\{\kappa^2\kappa'^2\text{-}1,2,4,5\text{-}C_6H_2(CH_2SeMe)_4\}]^{2+}$ are again consistent with the presence of one major invertomer, indicating the presence of *meso* EMe groups. However, the symmetry of the complex makes the EMe resonances within the two chelate rings inequivalent. The ^1H NMR spectrum of $[\{RuCl(\eta^6\text{-}p\text{-cymene})\}_2\{\kappa^2\kappa'^2\text{-}1,2,4,5\text{-}C_6H_2(CH_2SeMe)_4\}]^{2+}$ showed inequivalent methyl resonances in the *p*-cymene ^{i}Pr group, possibly indicating restricted rotation. This effect however, is not evident in either of the selenoether complexes.

Two closely spaced resonances of equal intensity are observed in the $^{77}Se\{^1H\}$ NMR spectrum of $[\{RuCl(\eta^6\text{-}p\text{-cymene})\}_2\{\kappa^2\kappa'^2\text{-}1,2,4,5\text{-}C_6H_2(CH_2SeMe)_4\}]^{2+}$, which correlates

with the two SeMe resonances in the ^{1}H NMR spectrum. A image of the $^{77}Se\{^{1}H\}$ NMR spectrum is shown in figure 4.21.

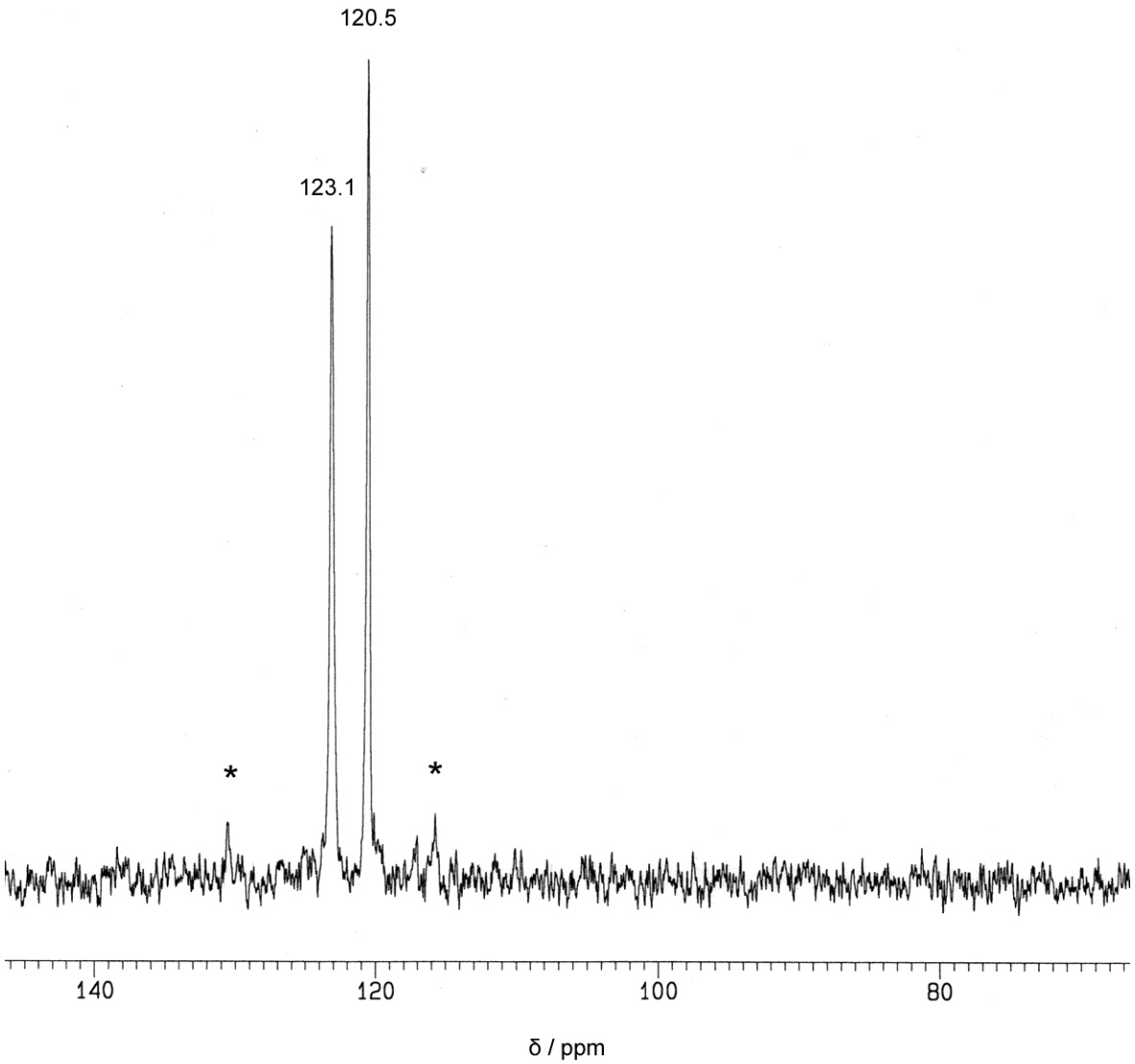

* Assigned to minor amounts of other invertomers

Figure 4.21 $^{77}Se\{^{1}H\}$ NMR spectrum of $[\{RuCl(\eta^{6}\text{-}p\text{-cymene})\}_2\{\kappa^2\kappa'^2\text{-}1,2,4,5\text{-}C_6H_2(CH_2SeMe)_4\}]^{+2}$ in MeCN recorded at ambient temperature.

The $^{77}Se\{^{1}H\}$ NMR spectrum of $[\{OsCl(\eta^{6}\text{-}p\text{-cymene})\}_2\{\kappa^2\kappa'^2\text{-}1,2,4,5\text{-}C_6H_2(CH_2SMe)_4\}]^{2+}$ showed a broad single

resonance with a clear shoulder – this can be attributed to near coincidence of the signals. Similar to the monometallic osmium analogues, the bimetallic species also showed very weak features in the spectra attributable to minor amounts of the other invertomers. These features are particularly evident in the $^{77}Se\{^{1}H\}$ NMR spectra of the two tetraselenoether osmium complexes (See figure 4.21). These minor resonances cannot have occurred from small quantities of the monometallic species as the chemical shifts, although in the same region, do not correspond to data previously collected and no resonance was observed for the uncoordinated SeMe group.

$[\{RuCl(\eta^6\text{-}p\text{-cymene})\}_2\{\kappa^2\kappa'^2\text{-}1,2,4,5\text{-}C_6H_2(CH_2EMe)_4\}]\,[PF_6]_2$ (E= S/Se)

Crystals of $[\{RuCl(\eta^6\text{-}p\text{-cymene})\}_2\{\kappa^2\kappa'^2\text{-}1,2,4,5\text{-}C_6H_2(CH_2SMe)_4\}]^{2+}$ cations were grown and the structures determined. An image of the dication and selected bond angles are shown in figure 4.22 and table 4.6.

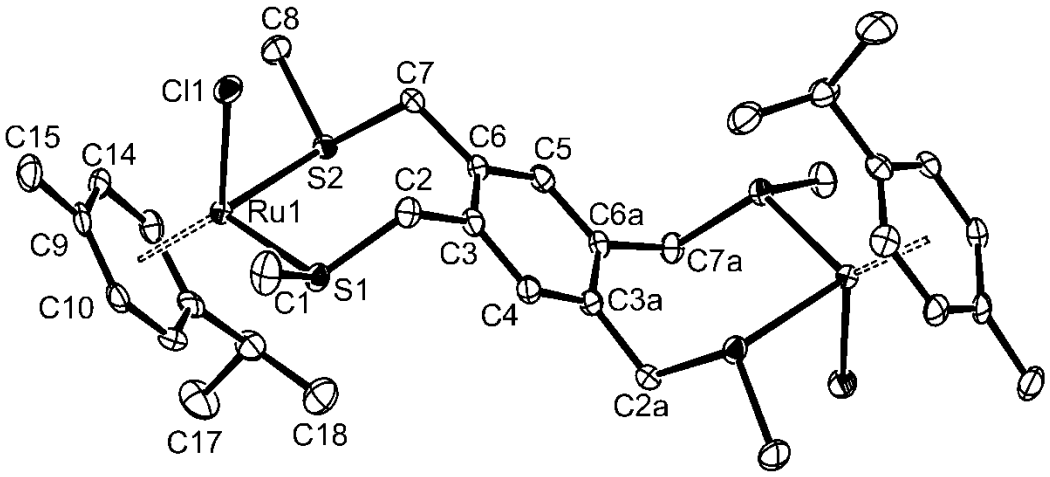

Figure 4.22 Structure of the cation in $[\{RuCl(\eta^6\text{-}p\text{-cymene})\}_2\{\kappa^2\kappa'^2\text{-}1,2,4,5\text{-}C_6H_2(CH_2SMe)_4\}][PF_6]_2$ showing the numbering scheme adopted. Ellipsoids are drawn at the 50% probability level and H atoms have been omitted for clarity.

Ru1–C(arene)	2.182(4)–2.237(4)	Ru1–S1	2.3925(10)
Ru1–Cl1	2.3915(9)	Ru1–S2	2.3934(9)
S1···S2	3.579(1)		
S1–Ru1–S2	96.80(3)	Cl1–Ru1–S2	87.52(3)
Cl1–Ru1–S1	87.43(3)		

Table 4.4 Selected bond lengths (Å) and angles for $[\{RuCl(\eta^6\text{-}p\text{-cymene})\}_2\{\kappa^2\kappa'^2\text{-}1,2,4,5\text{-}C_6H_2(CH_2SMe)_4\}][PF_6]_2\cdot 2MeCN$.

The crystal structure of the tetrathioether complex shows the same geometry at the metal centre seen in all other ruthenium structures discussed. The two metal centres are related by a two-fold rotation axis lying through the central aromatic unit (C4–C5). The bond lengths are unexceptional when compared with other structures.

The ^1H NMR spectrum of $[\{RuCl(\eta^6\text{-}p\text{-cymene})\}_2\{\kappa^2\kappa'^2\text{-}1,2,4,5\text{-}C_6H_2(CH_2SMe)_4\}]^{2+}$ showed one SMe resonance at room temperature, probably due to fast pyramidal inversion and there was no detectable amount of the monometallic complex present in the sample. $[\{RuCl(\eta^6\text{-}p\text{-cymene})\}_2\{\kappa^2\kappa'^2\text{-}1,2,4,5\text{-}C_6H_2(CH_2SeMe)_4\}]^{2+}$ was very poorly soluble even in CD_3CN, consequently, NMR data could not obtained. However, the microanalysis, ES^+ mass spectrum and the IR spectrum were consistent with the formulation.

4.2.3 Heterobimetallic complexes

These results have established that monometallic complexes can be produced in high purity with the tetradentate ligands; homo-bimetallic complexes can also be obtained by stepwise introduction of the metals. Using this approach the synthesis of several heterobimetallic complexes was explored. Complexes containing tetraselenoether ligands were considered to be the best candidates. Although slightly less soluble than the corresponding thioethers and with ^1H NMR spectroscopy of limited use due to low symmetry, $^{77}Se\{^1H\}$ NMR provides a very useful spectroscopic probe to follow the stepwise reaction.

$[RuCl(\eta^6\text{-}p\text{-cymene})\{\kappa^2\text{-}1,2,4,5\text{-}C_6H_2(CH_2SeMe)_4\}][PF_6]$ and $[RuCl(\eta^6\text{-}p\text{-cymene})\{\kappa^2\text{-}C(CH_2SeMe)_4\}][PF_6]$ were each reacted with 0.5 mol. eq. of

[{Os(η^6-*p*-cymene)Cl_2}$_2$], in ethanol. Although reaction conditions for producing mono- and bimetallic species had been explored with these systems, insertion of a second different metal required a new range of reaction conditions and times. In both cases the reaction was heated to 40 °C and stirred for 48 h before recrystallising from MeCN and Et_2O to yield an orange solid. Characterisation of these products by ES^+ mass spectrometry showed three clusters of peaks for the mixed RuOs species as well as substantial amounts of diruthenium and diosmium complexes, indicating that a rearrangement occurred during the reaction. An image of the ES^+ mass spectrum is shown in figure 4.23.

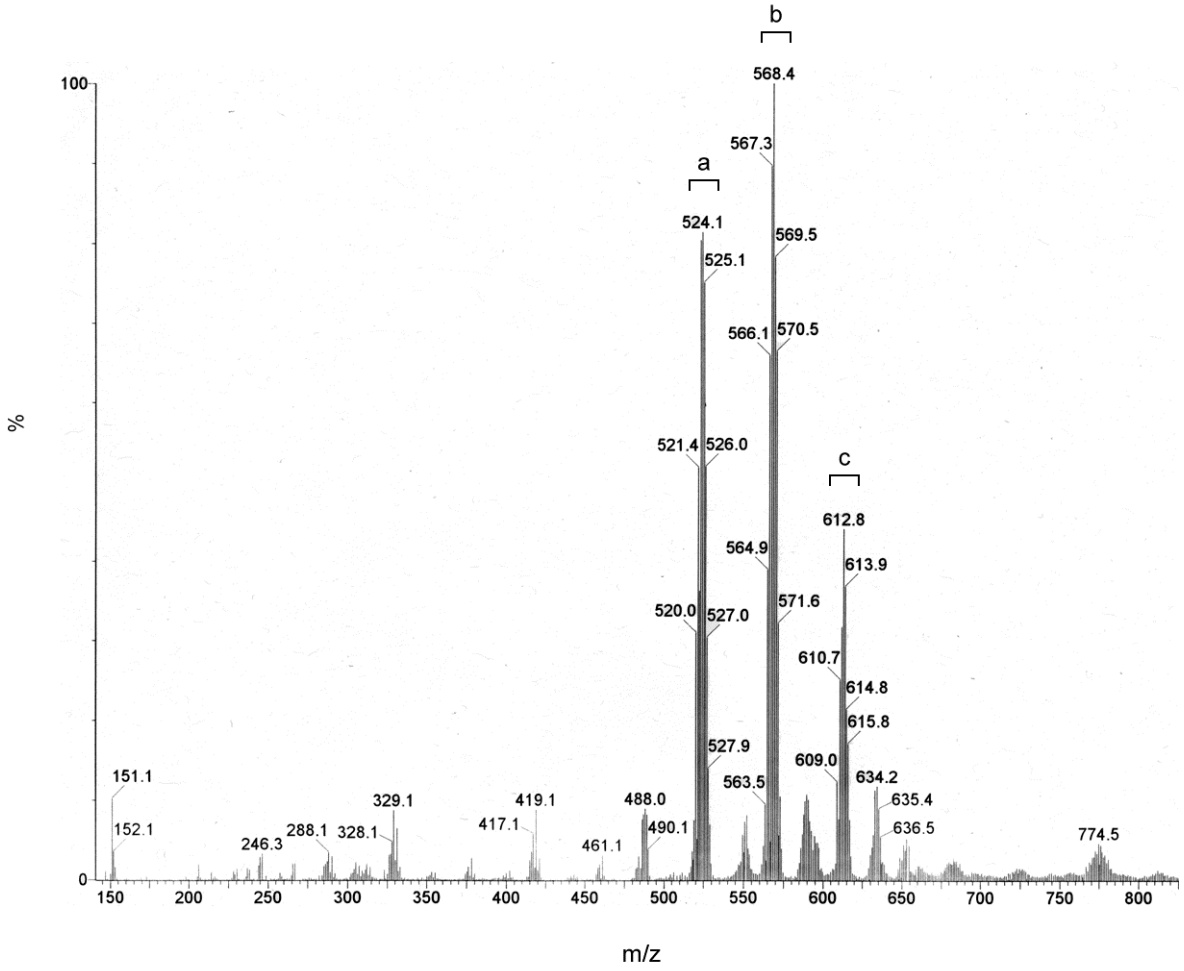

[a] Assigned to ruthenium, ruthenium homo bimetallic species

[b] Assigned to osmium, ruthenium hetero bimetallic species

[c] Assigned to osmium, osmium homo bimetallic species

Figure 4.23 ES^+ mass spectrum of [{RuCl(η^6-*p*-cymene)} {OsCl(η^6-*p*-cymene} {$\kappa^2\kappa'^2$-$C(CH_2SeMe)_4$}]$^{2+}$ in MeCN.

Due to the poor solubility of products containing the aromatic ligands (1,2,4,5-$C_6H_2(CH_2SMe)_4$ and 1,2,4,5-$C_6H_2(CH_2SeMe)_4$), subsequent efforts focused upon the spirocyclic tetraselenoether ($C(CH_2SeMe)_4$). Osmium(II) ($5d^6$) should be less labile than ruthenium(II) ($4d^6$) and consequently, less susceptible to displacement, so reversing the order of introduction of the metals could favour the formation of a single heterobimetallic product. Using the same reaction conditions, [OsCl(η^6-*p*-cymene){κ^2-$C(CH_2SeMe)_4$}][PF_6] was reacted with 0.5 eq. of [{Ru(η^6-*p*-cymene)Cl_2}$_2$], producing an orange solid which showed [{OsCl(η^6-*p*-cymene)}{RuCl(η^6-*p*-cymene)}{$\kappa^2\kappa'^2$-$C(CH_2SeMe)_4$}][PF_6]$_2$ as the dominant species in the ES^+ mass spectrum. The $^{77}Se\{^1H\}$ NMR spectrum showed strong resonances of equal intensity at 124.9 ppm and 116.9 ppm which were assigned to the SeMe groups bound to ruthenium, and a broad feature of twice the intensity at 76.8 ppm assigned to the osmium-bound SeMe groups. Although two resonances are expected for osmium bound SeMe groups it was assumed that they are near coincident and not resolved. This behaviour however, was also observed in the $^{77}Se\{^1H\}$ NMR spectrum of [{OsCl(η^6-*p*-cymene)}$_2${$\kappa^2\kappa'^2$C$(CH_2SeMe)_4$}][PF_6]$_2$. Weaker resonances at 130.1, 121.0, 77.9 and 73.2 ppm were also present in the spectrum which can be attributed to minor amounts of other invertomers. None of these resonances correlate to homobimetallic or monometallic complexes, indicating they are not present in significant quantities. The micro analysis and ^1H NMR spectrum is consistent with the formulation, but as predicted, the latter is very complicated due to low symmetry and near coincidence of some resonances.

Based upon the successful synthesis of [{OsCl(η^6-*p*-cymene)}{RuCl(η^6-*p*-cymene)}{$\kappa^2\kappa'^2$-$C(CH_2SeMe)_4$}][PF_6]$_2$, a reaction was attempted to incorporate a different metal combination in which the monometallic spirocyclic tetraselenoether complexes were reacted with [$PtCl_2(MeCN)_2$] see figure 4.24.

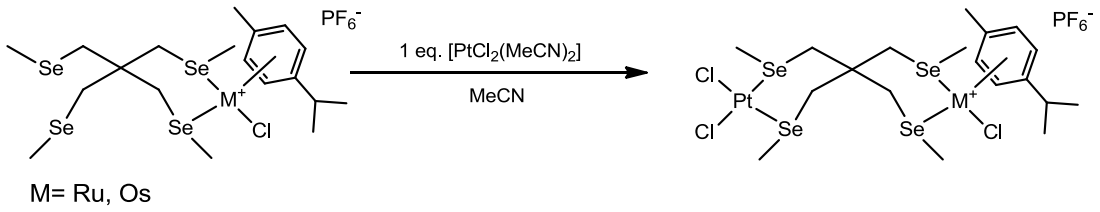

Figure 4.24 Shows synthesis of [{MCl(η^6-*p*-cymene)}{$PtCl_2$}{κ^2,κ'^2-$C(CH_2SeMe)_4$}][PF_6] (M= Ru/Os).

[OsCl(η^6-*p*-cymene){κ^2-C($CH_2SeMe)_4$}][PF_6] was reacted with [$PtCl_2(MeCN)_2$] in MeCN and produced a dark yellow solid in good yield, shown to be [{OsCl(η^6-*p*-cymene)}{$PtCl_2$}{κ^2,κ'^2-C($CH_2SeMe)_4$}][PF_6] *via* a ion multiplet at 1073 a.m.u. present in the ES^+ mass spectrum. The complex was insoluble in chlorocarbons and very poorly soluble in MeCN making characterisation challenging. After long accumulation the ^{195}Pt NMR spectrum contained a single broad peak at δ= –3686, consistent with chemical shift for a planar $PtSe_2Cl_2$ group.[7] The ^{77}Se{^{1}H} NMR spectrum showed resonances at δ = 82.5 ppm and 75.0 ppm assigned to osmium bound SeMe groups and resonances at δ = 167.1 ppm and 162.9 ppm with ^{195}Pt satellites ($^1J_{Pt\text{-}Se}$ = 572 and 467 Hz respectively) attributable to platinum bound SeMe. A number of other weak resonances are observed in the spectrum which could be due to the presence of minor invertomers as they do not correspond to [OsCl(η^6-*p*-cymene){κ^2-C($CH_2SeMe)_4$}]$^+$. Attempts to combine [RuCl(η^6-*p*-cymene){κ^2-C($CH_2SeMe)_4$}][PF_6] with [$PtCl_2(MeCN)_2$] produced many insoluble yellow products which could not be separated or identified.

4.3 Conclusions

A series of Ru(II) and Os(II) complexes containing κ^2-coordinated tetrathioether and tetraselenoether ligands have been synthesised and characterised spectroscopically and structurally.

Osmium complexes containing the spirocyclic ligands C($CH_2ECH_3)_4$ (E= S/Se) show slow pyramidal inversion. The distribution of each invertomer is unequal with the dominant form being *meso*, most probably the form present in the crystal structures. NMR spectra for ruthenium complexes indicate that either only one invertomer is present in detectable amounts or the inversion is fast and only averaged resonances are observed. The disparate distribution of invertomers seen in osmium complexes may well be due to steric factors in the crowded molecules.

Ruthenium homo-bimetallic complexes can be produced either directly or stepwise in high purity, attempts to introduce a second different metal centre Os(II) or Pt(II) to a monometallic Ru(II) complex were unsuccessful. However, osmium complexes with the same ligands can produce both homo- and hetero-bimetallic complexes with $\kappa^2\kappa'^2$-coordination. The successful production of heterobimetallics when the osmium is

introduced first, almost certainly results from the slower substitution kinetics at the 5d metal.

Dr. Tsoureas (University of Southampton) previously attempted to incorporate CoI_2 into a heterobimetallic to produce an example of a 4d-3d metal combination. However, yellow solids isolated from reacting anhydrous CoI_2 in $^{n}BuOH$ with $[RuCl(\eta^6\text{-}p\text{-cymene})\{\kappa^2\text{-}C(CH_2SMe)_4\}][PF_6]$ and $[RuCl(\eta^6\text{-}p\text{-cymene})\{\kappa^2\text{-}1,2,4,5\text{-}C_6H_2(CH_2SMe)_4\}][BPh_4]$ were both identified as the ruthenium starting materials[5] indicating the difficulties arising from use of labile 3d metal ions.

Complex	[RuCl(η⁶-*p*-cymene){κ²-C(CH₂SMe)₄}][PF₆]	[RuCl(η⁶-*p*-cymene){κ²-C(CH₂SeMe)₄}][PF₆]	[RuCl(η⁶-*p*-cymene){κ²-C₆H₂(CH₂SMe)₄}][BPh₄]	[RuCl(η⁶-*p*-cymene){κ²-C₆H₂(CH₂SeMe)₄}][BPh₄]
Formula	$C_{13}H_{24}ClF_6PRuS_4$	$C_{13}H_{24}ClF_6PRuSe_4$	$C_{48}H_{48}BClRuS_4$	$C_{48}H_{48}BClRuSe_4$
M	672.19	859.79	908.50	1096.10
Crystal system	Orthorhombic	Orthorhombic	Monoclinic	Monoclinic
Space group (no.)	$Pna2_1$ (#33)	$Pna2_1$ (#33)	$P2_1/n$ (#14)	$P2_1/n$ (#14)
a (Å)	12.957(2)	13.0594(15)	9.4108(10)	9.378(2)
b (Å)	12.2813(15)	12.4383(15)	22.201(3)	22.445(7)
c (Å)	16.5845(15)	16.893(3)	21.410(2)	21.649(7)
α (°)	90	90	90	90
β (°)	90	90	91.900(6)	91.056(18)
γ (°)	90	90	90	90
U (Å³)	2639.1(6)	2744.1(6)	4470.6(8)	4556(2)
Z	4	4	4	4
μ(Mo Kα) (mm⁻¹)	1.122	6.081	0.630	3.630
F(000)	1368	1656	1896	2184
Total no. of reflections	31011	20742	94451	49348
Unique reflections	5992	4978	10248	8917
R_{int}	0.049	0.064	0.119	0.121
No. of parameters, constraints	303, 11	279, 1	522, 6	503, 0
R_1[b] [$I_o > 2\sigma(I_o)$]	0.029	0.046	0.054	0.088
R_1 (all data)	0.039	0.059	0.096	0.146
wR_2[b] [$I_o > 2\sigma(I_o)$]	0.054	0.093	0.105	0.143
wR_2 (all data)	0.057	0.100	0.118	0.167

Table 4.5 X-ray crystallography data and structure refinement details[a].

Complex	[{RuCl(η⁶-*p*-cymene)}₂{κ²κ²-C(CH₂SMe)₄}][PF₆]₂	[{RuCl(η⁶-*p*-cymene)}₂{κ²κ²-C₆H₂(CH₂SMe)₄}][PF₆]₂·2MeCN
Formula	$C_{28}H_{48}Cl_2F_{12}P_2Ru_2S_4$	$C_{32}H_{48}Cl_2F_{12}N_2P_2Ru_2S_4$
M	1087.89	1232.07
Crystal system	Triclinic	Monoclinic
Space group (no.)	P-1 (#2)	C2/c (#15)
a (Å)	10.047(3)	25.274(3)
b (Å)	12.941(4)	9.9679(10)
c (Å)	16.904(5)	19.698(3)
α (°)	71.299(15)	90
β (°)	79.89(2)	95.144(6)
γ (°)	80.07(2)	90
U (Å³)	2033.6(10)	4942.4(10)
Z	2	4
μ(Mo Kα) (mm⁻¹)	1.236	1.029
F(000)	1092	2488
Total no. of reflections	34367	27475
Unique reflections	7906	5666
θ_{max}	0.077	0.060
No. of parameters, constraints	470, 0	283, 0
R_1[b] [$I_o > 2\sigma(I_o)$]	0.068	0.045
R_1 (all data)	0.113	0.060
wR_2[b] [$I_o > 2\sigma(I_o)$]	0.121	0.101
wR_2 (all data)	0.144	0.109

[a] Common items: temperature = 120 K; wavelength (Mo-Kα) = 0.71073 Å; θ(max) = 27.5°.
[b] $R_1 = \Sigma||F_o| - |F_c||/\Sigma|F_o|$. $wR_2 = [\Sigma w(F_o^2 - F_c^2)^2/\Sigma wF_o^4]^{1/2}$.

Table 4.6 X-ray crystallography data and structure refinement details[a].

4.4 Experimental

All preparations were carried out under a N_2 atmosphere. The tetrathioether and tetraselenoether ligands were made as described[5] and [{Ru(η⁶-*p*-cymene)Cl_2}$_2$] and [{Os(η⁶-*p*-cymene)Cl_2}$_2$] were prepared by literature methods.[8, 9]

4.4.1 Synthesis

[RuCl(η^6-*p*-cymene){κ^2-C(CH$_2$SMe)$_4$}][PF$_6$]

[Ru(η^6-*p*-cymene)Cl$_2$]$_2$ (0.100 g, 0.16 mmol) was dissolved in dry ethanol (20 mL). To this was added the tetrathioether (0.082 g, 0.32 mmol) in dry ethanol (15 mL). The reaction mixture was refluxed for 2 h. The reaction vessel was removed from the oil bath and while still hot, a solution of [NH$_4$][PF$_6$] (0.052 g, 0.32 mmol) in 10 mL ethanol was added. The mixture turned from dark orange to yellow and a yellow precipitate formed instantly. The reaction mixture was cooled to room temperature and stirred overnight. The yellow suspension was cannula filtered under nitrogen to leave a yellow solid which was washed twice in diethyl ether (50 mL) filtered, and dried *in vacuo*. Yield: 0.140 g, 66%. Anal. Calc. for C$_{19}$H$_{34}$ClF$_6$PRuS$_4$: C, 34.0; H, 5.1. Found: C, 33.4; H, 5.4%. ES$^+$: *m/z*= 527 [RuCl(η^6-*p*-cymene){κ^2-C(CH$_2$SMe)$_4$}]$^+$. IR (Nujol)/cm^{-1}: 836 (PF stretch), 557 (PF bend). ^{1}H NMR (d^6-acetone): 1.37 (d, 6[H], $^3J_{HH}$ = 7.0 Hz, CH(C*H*$_3$)$_2$), 2.22, 2.25, 2.30 (3 × s each [3H], 2 × SC*H*$_3$ uncoord, aromatic C*H*$_3$), 2.61, 2.90 (2 × s each [2H], C*H*$_2$ uncoord), 2.75–3.05 (AB quartet, [4H], C*H*$_2$ coord), 2.82 (s, [6H], coord SC*H*$_3$), 2.95 (septet, [1H], $^3J_{HH}$ = 7.0 Hz, C*H*(CH$_3$)$_2$), 6.03 (d, [2H], $^3J_{HH}$ = 6 Hz, aromatic C*H*), 6.22 (d, [2H], $^3J_{HH}$ = 6 Hz, aromatic C*H*) ppm. ^{13}C{^{1}H} NMR (d^6-acetone): 17.53, 18.06, 18.37 (2 × S*C*H$_3$ uncoord, *p*-cymene *C*H$_3$), 22.42 CH(*C*H$_3$)$_2$), 28.48 (coord S*C*H$_3$), 31.48 (*C*H(CH$_3$)$_2$), 38.82, 40.22 (2 × uncoord *C*H$_2$), 43.90 (C$_{quaternary}$), 46.40 (coord *C*H$_2$), 88.04, 88.62 (2 × aromatic *C*H), 107.84, 109.57 (2 × *C*$_{ipso}$) ppm. Yellow crystals were grown by slow evaporation of an acetone solution of the complex.

[RuCl(η^6-*p*-cymene){κ^2-C(CH$_2$SeMe)$_4$}][PF$_6$]

Prepared as described for the thioether analogue above, from [Ru(η^6-*p*-cymene)Cl$_2$]$_2$ (0.08 g, 0.125 mmol) and the ligand (0.11 g, 0.25 mmol) in ethanol (15 mL). Addition of [NH$_4$][PF$_6$] (0.04 g, 0.25 mmol) in ethanol (10 mL), followed by stirring overnight gave a yellow precipitate. Yield 0.18 g, 83%. Anal. Calc. for C$_{19}$H$_{34}$ClF$_6$PRuSe$_4$: C, 26.5; H, 4.0 Found: C, 26.6; H, 3.7%. ES$^+$:*m/z*= 714 [RuCl(η^6-*p*-cymene){κ^2-C(CH$_2$SeMe)$_4$}]$^+$. IR (Nujol)/cm^{-1}: 836 (PF stretch), 557 (PF bend). ^{1}H NMR (CDCl$_3$): 1.31 (d, [6H], $^3J_{HH}$ = 7.0 Hz, CH(C*H*$_3$)$_2$), 2.07, 2.11 (2 × s each [3H], SeC*H*$_3$ uncoord), 2.23 (s, [3H], aromatic C*H*$_3$), 2.47, 2.66 (2 × s each [2H], SeC*H*$_2$ uncoord), 2.54 (s, [6H] SeC*H*$_3$ coord), 2.74–3.05 (AB

quartet, [4H], SeC*H*$_2$ coord), 2.78 (septet, [1H], C*H*(CH$_3$)$_2$), 5.69 (d, [2H], $^3J_{HH}$ = 6 Hz, aromatic C*H*), 5.80 (d, [2H], $^3J_{HH}$ = 6 Hz, aromatic C*H*) ppm. ^{77}Se{^{1}H} NMR (MeCN/CD$_3$CN, 25ºC): 24.5, 25.0 (s, un-coordinated Se), 115.6 (s, coordinated Se) ppm. Yellow crystals suitable for X-ray diffraction studies were grown by slow evaporation of a chloroform solution.

[OsCl(η^6-*p*-cymene){κ^2-C(CH$_2$SMe)$_4$}][PF$_6$]

[Os(η^6-*p*-cymene)Cl$_2$]$_2$ (0.077 g, 0.097 mmol) in dry degassed ethanol (50 mL) was added dropwise over 1 h to a flask fitted with reflux apparatus, containing C(CH$_2$SMe)$_4$ (0.05 g, 0.2 mmol) in dry CH$_2$Cl$_2$ (50 mL). The dark yellow solution was then refluxed for 1 h. [NH$_4$][PF$_6$] (0.032 g, 0.19 mmol) in dry degassed ethanol (15 mL) was added, the solution was then stirred overnight before filtering to remove small amounts of insoluble material. The filtrate was evaporated to dryness and the product recrystallised from acetonitrile-diethyl ether. The yellow solid deposited was filtered off, washed with ether (2 × 5 mL) and dried *in vacuo*. Yield: 0.054 g, 35%. Anal. Calc. for C$_{19}$H$_{34}$ClF$_6$OsPS$_4$·CH$_2$Cl$_2$: C, 28.3; H, 4.3. Found: C, 28.2; H, 4.3%. ES$^+$:*m/z*= 617 [OsCl(η^6-*p*-cymene){κ^2-C(CH$_2$SMe)$_4$}]$^+$. IR (Nujol)/cm^{-1}: 836 (PF stretch), 557 (PF bend). ^{1}H NMR (d^6-acetone): 1.275 (d, 6[H], $^3J_{HH}$ = 8.0 Hz, CH(C*H*$_3$)$_2$), 2.13, 2.17, 2.19 (3 × s each [3H], 2 × SC*H*$_3$ uncoord, aromatic C*H*$_3$), 2.65, 2.71 (2 × s each [2H], C*H*$_2$ uncoord), 3.01–3.34 (AB quartet, [4H], C*H*$_2$ coord), 2.72 (s, [6H], coord SC*H*$_3$), 2.75 (septet, [1H], $^3J_{HH}$ = 7.0 Hz, C*H*(CH$_3$)$_2$), 5.79 (d, [2H], $^3J_{HH}$ = 6 Hz, aromatic C*H*), 6.03 (d, [2H], $^3J_{HH}$ = 6 Hz, aromatic C*H*) ppm. Much weaker resonances often nearly coincident with the peaks listed above (<5% intensity of the major peaks) were observed and are attributed to other invertomers, but it is not possible to assign these to specific forms.

[OsCl(η^6-p-cymene){κ^2-C(CH$_2$SeMe)$_4$}][PF$_6$]

[Os(η^6-*p*-cymene)Cl$_2$]$_2$ (0.089 g, 0.11 mmol) in dry degassed ethanol (50 mL) was added to a stirred solution of C(CH$_2$SeMe)$_4$ (0.10 g, 0.23 mmol) in dry degassed ethanol (50 mL). The dark yellow solution was then refluxed for 1 h. [NH$_4$][PF$_6$] (0.037 g, 0.23 mmol) in dry ethanol (15 mL) was added, the solution was then stirred overnight before filtering to remove small amounts of insoluble material. The solution was then evaporated to dryness and the product recrystallised from acetonitrile-diethyl ether. The yellow solid deposited

was filtered off, washed with ether (2 × 5 mL) and dried *in vacuo*. Yield 0.069 g, 32%. Anal. Calc. for $C_{19}H_{34}ClF_6OsPSe_4$: C, 24.1; H, 3.6. Found: C, 24.2; H, 3.5%. ES^+:*m/z*= 809 [OsCl(η^6-*p*-cymene){κ^2-C($CH_2SeMe)_4$}]$^+$. IR (Nujol)/cm^{-1}: 836 (PF stretch), 557 (PF bend). ^{1}H NMR ($CDCl_3$): 1.26 (d, [6H], $^3J_{HH}$ = 7.0 Hz, CH(C*H*$_3$)$_2$), 2.05, 2.09 (2 × s each [3H], SeC*H*$_3$ uncoord), 2.17 (s, [3H], aromatic C*H*$_3$), 2.56, 2.69 (2 × s each [2H], SeC*H*$_2$ uncoord), 2.48 (s, [6H] SeC*H*$_3$ coord), 2.63–3.28 (AB quartet, [4H], SeC*H*$_2$ coord), 2.68 (septet, [1H], C*H*(CH_3)$_2$), 5.81 (d, [2H], $^3J_{HH}$ = 6 Hz, aromatic C*H*), 6.03 (d, [2H], $^3J_{HH}$ = 6 Hz, aromatic C*H*) ppm. ^{77}Se{^{1}H} NMR (MeCN/CD_3CN, 25 ºC): 23.2, 25.1 (s, un-coordinated Se), 72.2 (s, coordinated Se); (–40 ºC): 19.8, 20.7, 71.5 ppm. Three very minor ^{77}Se resonances were observed at 66.0, 73.4 and 78.4 ppm with an overall intensity ~5% of the major resonance at 72.2 ppm and are tentatively attributed to minor amounts of the other invertomers. There are also associated weak features in the ^{1}H NMR spectrum (see text).

[RuCl(η^6-*p*-cymene){κ^2-1,2,4,5-$C_6H_2(CH_2SMe)_4$}][BPh_4]

A Schlenk tube was charged with [Ru(η^6-*p*-cymene)Cl_2]$_2$ (0.10 g, 0.16 mmol) and the contents were degassed. The orange solid was then dissolved in dry CH_2Cl_2 (5 mL), 1,2,4,5-$C_6H_2(CH_2SMe)_4$ (0.11 g, 0.32 mmol) in dry ethanol (15 mL) added and the mixture refluxed for 30 min. The reaction mixture was then removed from the oil bath and while still hot, an EtOH solution of Na[BPh_4] (0.11 g, 0.32 mmol) was added. The solution immediately turned from pale orange to yellow and a yellow precipitate formed. Stirring was continued for an hour at ambient temperature. Volatiles were removed on a rotary evaporator and the orange solid was dissolved in CH_2Cl_2 (20 mL) and filtered through a Celite pad. The solvent was removed under vacuum and the yellow oil was washed with n-pentane. It was then re-dissolved in CH_2Cl_2 (3 mL), n-pentane (50 mL) was added slowly to precipitate a yellow solid that was isolated by filtration. Yield: 0.15 g, 51%. Anal. Calc. for $C_{48}H_{56}BClRuS_4 \cdot 1/2C_5H_{12}$: C, 64.2; H, 6.3. Found: C, 64.2; H, 6.7%. ES^+:*m/z*= 589 [RuCl(η^6-*p*-cymene){κ^2-1,2,4,5-$C_6H_2(CH_2SMe)_4$}]$^+$. ^{1}H NMR (CD_2Cl_2): 0.95 (d, [6H], $^3J_{HH}$ = 7 Hz, CH(C*H*$_3$)$_2$), 2.00 (s, [3H] p-cymene C*H*$_3$) 2.01 (s, [6H] SC*H*$_3$ uncoord), 2.46 (s, [6H], SC*H*$_3$ coord.), 2.95 (septet [H], $^3J_{HH}$ = 7.0 Hz, C*H*(CH_3)$_2$), 3.33 (d, [2H], $^2J_{HH}$ = 12 Hz, C*H*$_2$S coord.), 3.78 (s, [4H], C*H*$_2$S uncoord.), 4.41 (d, [2H], $^2J_{HH}$ = 12 Hz, C*H*$_2$S coord.), 5.01 (d, [2H], $^3J_{HH}$ = 8 Hz, *p*-cymene aromatics), 5.08 (d, [2H] $^3J_{HH}$ = 8 Hz, *p*-cymene aromatics), 6.89 (m, [4H], aromatics), 7.02 (m, [8H], aromatics), 7.17 (s, [2H],

1,2,4,5-$C_6H_2(CH_2SMe)_4$), 7.35 (br, [8H], aromatics) ppm. $^{13}C\{^1H\}$ NMR (CD_2Cl_2): 15.56 (S*C*H_3 uncoord), 18.47 (aromatic-*C*H_3), 22.22 CH(*C*$H_3)_2$), 30.89 (S*C*H_3 coord), 31.28 (*C*H$(CH_3)_2$), 35.56 (*C*H_2 uncoord), 37.22 (*C*H_2 coord), 86.98, 88.81 (2 × aromatic *C*H), 107.84, 109.57 (2 × C_{ipso}), 122.73, 126.51, 132.26, 134.23, 136.80, 139.35 (aromatics), 164.80 (quartet B–C_{ipso} $^1J(^{11}B–^{13}C)$ = 50 Hz) ppm. Yellow crystals suitable for X-ray diffraction study were grown by layering a CH_2Cl_2 solution with hexane.

[RuCl(η^6-*p*-cymene){κ^2-1,2,4,5-$C_6H_2(CH_2SeMe)_4$}][BPh_4]

[Ru(η^6-*p*-cymene)$Cl_2]_2$ (0.10 g, 0.16 mmol) was dissolved in dry $CHCl_3$ (5 mL) and added by syringe to the selenoether (0.16 g, 0.32 mmol) dissolved in dry ethanol (15 mL).. The reaction mixture was refluxed for 30 min removed from the oil bath and whilst hot, Na[BPh_4] (0.11 g, 0.32 mmol) was added in one portion. The solution immediately turned from pale orange to yellow and a yellow precipitate formed. The reaction mixture was cooled to room temperature and stirred overnight. The yellow suspension was concentrated under nitrogen to leave a yellow solid which was dried *in vacuo*. Yield: 0.17g, 48%. Anal. Calc. for $C_{49}H_{60}BClRuSe_4 \cdot CHCl_3$: C, 50.2; H, 5.1. Found: C, 49.1, H, 5.0%. ES^+:*m/z*= 778 [RuCl(η^6-*p*-cymene){κ^2-1,2,4,5-$C_6H_2(CH_2SeMe)_4$}]$^+$. ^{1}H NMR ($CDCl_3$): 1.09 (d, [6H], J = 7 Hz, CH(C*H*$_3)_2$), 1.90 (s, [3H], aromatic C*H*$_3$) 1.95 (s, 6[H], SeC*H*$_3$ uncoord), 2.64 (s, [6H], SeC*H*$_3$ coord), 3.50 (m, [H], C*H*$(CH_3)_2$), 3.52, 4.68 (AB quartet, 4[H], $^2J_{HH}$ = 9 Hz, C*H*$_2$Se coord), 3.81 (s, C*H*$_2$Se uncoord), 5.56, 5.70 (2 × d each [2H] *p*-cymene aromatics), 6.84 (m), 6.99 (m), 7.27 (m), (total [22H], aromatic CH) ppm. $^{77}Se\{^1H\}$ NMR (MeCN/CD_3CN, 25ºC): 157.7 (s, Se uncoord), 183.9 (s, coord Se) ppm. Yellow crystals suitable for X-ray diffraction study were grown by slow evaporation of a chloroform solution.

[{RuCl(η^6-*p*-cymene)}$_2${κ^{2}κ'^{2}-C$(CH_2SMe)_4$}][PF_6]$_2$

A Schlenk tube was charged with [Ru(η^6-*p*-cymene)$Cl_2]_2$ (0.15 g, 0.24 mmol) suspended in dry ethanol (15 mL) and C$(CH_2SMe)_4$ (0.06 g, 0.24 mmol) in ethanol (10 mL) was added. The mixture was refluxed for 30 min, and [NH_4][PF_6] (0.08 g, 0.49 mmol) was added to the hot solution. The mixture was allowed to cool, stirred overnight at room temperature, and the yellow precipitate removed by filtration, and dried *in vacuo*. Yield: 0.21 g, 80%. Anal. Calc. for $C_{29}H_{48}Cl_2F_{12}P_2Ru_2S_4$: C, 32.0; H, 4.5. Found: C, 31.3; H, 4.0%. ES^+:*m/z*=

399 [{RuCl(η^6-*p*-cymene)}$_2${$\kappa^2\kappa'^2$-C($CH_2SMe)_4$}]$^{2+}$. IR (Nujol)/cm^{-1}: 836 (PF stretch), 557 (PF bend). ^{1}H NMR (d^6-acetone): 1.35, 1.37 (2 × d each [6H], $^3J_{HH}$ = 7.0 Hz, CH(C*H*$_3)_2$), 2.29 (br s, [3H], aromatic C*H*$_3$), 2.76, 2.83 (2 × s each [3H] SC*H*$_3$), 2.87–2.90 (m, [H], C*H*($CH_3)_2$), 2.93–3.12 (overlapping m, [4H], C*H*$_2$), 6.03 (m, [2H], aromatic C*H*), 6.25 (m, [2H], aromatic C*H*) ppm. Much weaker resonances (<5%) at 2.27(s), 2.78(s), 2.82(s) ppm are believed to be the aromatic C*H*$_3$ and SC*H*$_3$ resonances of other invertomer(s), other expected resonances are obscured by those of the major invertomer.

[{RuCl(η^6-*p*-cymene)}$_2${$\kappa^2\kappa'^2$-C($CH_2SeMe)_4$}][PF_6]$_2$

Prepared as for the tetrathioether analogue above. Yield: 83%. Anal. Calc. for $C_{29}H_{48}Cl_2F_{12}P_2RuSe_4$: C, 27.2; H, 3.8. Found: C, 27.3; H, 3.8%. ES$^+$: *m/z*= 493 [{RuCl(η^6-*p*-cymene)}$_2${$\kappa^2\kappa'^2$-C($CH_2SeMe)_4$}]$^{2+}$. IR (Nujol)/cm^{-1}: 840 (PF stretch), 557 (PF bend). ^{1}H NMR (CD_3CN): 1.26 (br, d [6H], $^3J_{HH}$ = 6.0 Hz, CH(C*H*$_3)_2$), 2.17 (br s, [3H], aromatic C*H*$_3$), 2.45, 2.55, (2 s each [3H] SeC*H*$_3$), 2.72–2.90 (m, [H], C*H*($CH_3)_2$), 2.88–3.01 (br AB quartet, [4H], C*H*$_2$), 5.73 (m, [2H], aromatic C*H*), 5.85 (m, [2H], aromatic C*H*) ppm. ^{77}Se{^{1}H} NMR (CH_3CN/CD_3CN, 25 ºC): 120.5, 123.1 (coord. Se) ppm. Again, the spectra show very minor additional resonances near to those of the major form, including very weak resonances in the ^{77}Se{^{1}H} NMR spectrum at 115.7 ppm and 130.6 ppm, tentatively attributed to other invertomer(s).

[{OsCl(η^6-*p*-cymene)}$_2${$\kappa^2\kappa'^2$-C($CH_2SeMe)_4$}][PF_6]$_2$

Method 1: [Os(η^6-*p*-cymene)$Cl_2]_2$ (0.178 g, 2.25 mmol) in dry degassed ethanol (50 mL) was added to a flask containing C($CH_2SeCH_3)_4$ (0.10 g, 2.25 mmol) in dry degassed ethanol (50 mL). The dark yellow solution was then stirred at 70 °C for 1 h. [NH_4][PF_6] (0.073 g, 4.5 mmol) in dry degassed ethanol (15 mL) was added, the solution was then stirred overnight before filtering to remove small amounts of insoluble material. The filtrate was taken to dryness and recrystallised from acetonitrile-diethylether. The yellow solid deposited was filtered off, washed with ether (2 × 5 mL) and dried *in vacuo*. Yield: 0.02 g, 63%.

Method 2: [OsCl(η^6-*p*-cymene){κ^2-C($CH_2SeMe)_4$}][PF_6] (0.05 g, 0.052 mmol) in dry degassed ethanol (50 mL) was added to a flask containing [Os(η^6-*p*-cymene)$Cl_2]_2$ (0.02 g, 0.026 mmol) in dry degassed ethanol (50 mL). The dark yellow solution was then stirred at

70 °C for 1 h. $[NH_4][PF_6]$ (0.01 g, 0.06 mmol) in dry degassed ethanol (15 mL) was added, the solution was then stirred overnight before filtering to remove small amounts of insoluble material. The filtrate was taken to dryness and the product recrystallised from acetonitrile-diethyl ether. The yellow solid deposited was filtered off, washed with ether (2 × 5 mL) and dried *in vacuo*. Yield: 0.04 g, 53%. The products from the two routes were spectroscopically identical. Anal. Calc. for $C_{29}H_{48}Cl_2F_{12}Os_2P_2Se_4$: C, 24.0; H, 3.3. Found: C, 24.3; H, 3.5%. ES^+ (m/z): 581 $[\{OsCl(\eta^6\text{-}p\text{-cymene})\}_2\{\kappa^2\kappa'^2\text{-}C(CH_2SeMe)_4\}]^{2+}$. IR (Nujol)/$cm^{-1}$: 840 (PF stretch), 557 (PF bend). ^1H NMR (CD_3CN): 1.28 (d, [6H], $^3J_{HH}$ = 7.0 Hz, $CH(CH_3)_2$), 2.26 (s, [3H], aromatic CH_3), 2.61, 2.66 (2 × s each [3H] $SeCH_3$), 2.80–3.15 (AB quartet, [4H], $SeCH_2$), 2.82 (m, [H], $CH(CH_3)_2$), 6.12 (br d, [2H], $^3J_{HH}$ = 6 Hz, aromatic CH), 6.34 (br d, [2H], $^3J_{HH}$ = 6 Hz, aromatic CH) ppm. $^{77}Se\{^1H\}$ NMR (CH_3CN/CD_3CN, 25ºC): 66.6 (br s), 66.5(sh) ppm. As above, minor resonances in the ^1H NMR at 2.23, 2.60 and 2.65 ppm are respectively aromatic CH_3 and $SeCH_3$ of other forms, and these have associated very weak resonances in the $^{77}Se\{^1H\}$ NMR spectrum at 69.6 ppm and 66.1 ppm.

$[\{RuCl(\eta^6\text{-}p\text{-cymene})\}_2\{\kappa^2\kappa'^2\text{-}1,2,4,5\text{-}C_6H_2(CH_2SMe)_4\}][PF_6]_2$

A Schlenk tube was charged with $[Ru(\eta^6\text{-}p\text{-cymene})Cl_2]_2$ (0.38 g, 0.62 mmol) suspended in dry ethanol (15 mL) and the tetrathioether (0.2 g, 0.62 mmol) in ethanol (10 mL) added. The mixture was refluxed for 30 min, and $[NH_4][PF_6]$ (0.20 g, 1.25 mmol) added to the hot solution. The mixture was allowed to cool, stirred overnight at room temperature, and the yellow precipitate removed by filtration, and dried *in vacuo*. Yield: 0.66 g, 91%. Anal. Calc. for $C_{34}H_{50}Cl_2F_{12}P_2Ru_2S_4\cdot C_2H_5OH$: C, 36.2; H, 4.7. Found: C, 36.8; H 4.3%. ES^+: *m/z*= 430 $[\{RuCl(\eta^6\text{-}p\text{-cymene})\}_2\{\kappa^2\kappa'^2\text{-}1,2,4,5\text{-}C_6H_2(CH_2SMe)_4\}]^{2+}$. IR (Nujol)/$cm^{-1}$: 840 (PF stretch), 557 (PF bend). ^1H NMR (CD_3CN): 0.99 (d, [6H], $^3J_{HH}$ = 9 Hz, $CH(CH_3)_2$), 2.10 (s, [3H] *p*-cymene CH_3), 2.67 (s, [6H], SCH_3), 2.85 (m [H], $^3J_{HH}$ = 9.0 Hz, $CH(CH_3)_2$), 3.44 (d, [2H], $^2J_{HH}$ = 12 Hz, CH_2S), 4.36 (d, [2H], $^2J_{HH}$ = 12 Hz, CH_2S), 5.52 (d, [2H], $^3J_{HH}$ = 8 Hz, *p*-cymene aromatics), 5.66 (d, [2H] $^3J_{HH}$ = 8 Hz, *p*-cymene aromatics), 7.32 (s, [H], 1,2,4,5-$C_6H_2(CH_2SMe)_4$) (and EtOH resonances at 1.12 (t), 3.54 (q) 2.63 (s)) ppm.

$[\{RuCl(\eta^6\text{-}p\text{-cymene})\}_2\{\kappa^2\kappa'^2\text{-}1,2,4,5\text{-}C_6H_2(CH_2SeMe)_4\}][PF_6]_2$

A Schlenk tube was charged with [Ru(η^6-p-cymene)Cl_2]$_2$ (0.075 g, 0.12 mmol) and dry ethanol (15 mL) added, followed by a solution of the tetraselenoether (0.060 g, 0.12 mmol) in ethanol (10 mL). The mixture was refluxed for 30 min and the [NH_4][PF_6] (0.04 g, 0.24 mmol) added. The mixture was allowed to cool and stirred overnight. The yellow precipitate was filtered off and dried *in vacuo*. Yield: 0.12 g, 75%. Anal. Calc. for $C_{34}H_{50}Cl_2F_{12}P_2Ru_2Se_4$: C, 30.5; H, 3.8. Found: C, 30.1, H, 4.1%. ES$^+$:*m/z*= 523 [{RuCl(η^6-*p*-cymene)}$_2${$\kappa^2\kappa'^2$-1,2,4,5-$C_6H_2(CH_2SeMe)_4$}]$^{2+}$. IR (Nujol)/cm^{-1}: 836 (PF stretch), 557 (PF bend). The complex proved to be too poorly soluble for NMR studies.

[{RuCl(η^6-*p*-cymene)}{OsCl(η^6-*p*-cymene}{$\kappa^2\kappa'^2$-C($CH_2SeMe)_4$}][PF_6]$_2$

[OsCl(η^6-*p*-cymene){κ^2-C($CH_2SeMe)_4$}][PF_6] (0.053 g, 0.056 mmol) was dissolved in ethanol (80 mL), [Ru(η^6-*p*-cymene)Cl_2]$_2$ (0.017 g, 0.028 mol) dissolved in ethanol (50 mL) was added dropwise over 1 h. The solution was then heated to 40 ºC for 2 h. [NH_4][PF_6] (0.01 g, 0.06 mmol) in ethanol was added to the warm solution and stirred for 48 h. The resulting solution was taken to dryness in vacuum and the residue recrystallised from MeCN and Et_2O to yield an orange solid. Crystals were grown from a solution of MeCN at room temperature. Yield: 0.047 g, 62%. Anal. Calc. for $C_{29}H_{48}Cl_2F_{12}OsP_2RuSe_4$: C, 25.5; H, 3.7. Found: C, 25.5, H, 3.6%. ES$^+$:*m/z*= 538 [{RuCl(η^6-*p*-cymene)}{OsCl(η^6-*p*-cymene}{$\kappa^2\kappa'^2$-C($CH_2SeMe)_4$}]$^{2+}$. IR (Nujol)/cm^{-1}: 842 (PF stretch), 577 (PF bend). ^{1}H NMR (CD_3CN): 1.27 (br, d [12H], $^3J_{HH}$ = 6.0 Hz, CH(C*H*$_3$)$_2$), 2.18, 2.20 (2 × br s, each [3H], aromatic C*H*$_3$), 2.45, 2.46, 2.55, 2.57, (4 × s, each [3H], SeC*H*$_3$), 2.72–2.90 (m, [2H], C*H*(CH_3)$_2$), 2.72–3.21 (br multiplets, [8H], C*H*$_2$), 5.72 (m, [2H], aromatic C*H*), 5.86 (m, [4H], aromatic C*H*), 6.06 (m, [2H], aromatic C*H*). ^{77}Se{^{1}H} NMR (CH_3CN/CD_3CN, 25ºC): 124.0, 117.0, 76.9 (sh), 78.8 (minor features at 80.0, 73.1) ppm.

[{OsCl(η^6-*p*-cymene)}{$PtCl_2$}{$\kappa^2\kappa'^2$-C($CH_2SeMe)_4$}][PF_6]

$PtCl_2$ (0.013 g, 0.05 mol) was suspended in MeCN (50 mL) and refluxed for 1.5 h, then the solution was allowed to cool to room temperature. [OsCl(η^6-*p*-cymene){κ^2-C($CH_2SeMe)_4$}][PF_6] (0.05 g, 0.052 mmol) dissolved in MeCN (50 mL) was added dropwise over 10 min, and the mixture was stirred for 48 h. The resulting solution was the taken to dryness in vacuum and the residue recrystallised from MeCN and Et_2O to yield a dark yellow solid. Yield: 0.022 g, 46%. Anal. Calc. for C; 21.0, H, 3.3. Found: C, 20.6, H,

3.3%. ES^+:*m/z*= 1072 [{OsCl(η^6-*p*-cymene)}{$PtCl_2$}{$\kappa^2\kappa'^2$-$C(CH_2SeMe)_4$}]$^+$, also *m/z*= 803 [M–$PtCl_2$]$^+$. IR (Nujol)/cm^{-1}: 840 (PF stretch), 577 (PF bend). ^{195}Pt NMR (CH_3CN/CD_3CN, 25ºC): –368 (minor resonances at –3667, –3753). ^{77}Se{^{1}H} NMR (CH_3CN/CD_3CN, 25ºC): 167.1 ($^1J_{PtSe}$ = 572 Hz), 162.9 ($^1J_{PtSe}$ = 467 Hz), 82.5, 75.0 (minor resonances at 83.2, 72.1) ppm.

4.4.2 X-ray crystallography experimental

Details of the crystallographic data collection and refinement are given in tables 4.1 and 4.2. Structure solution and refinement were straightforward,[10-12] except as described below, and H atoms were introduced into the model in calculated positions using the default C–H distances. [RuCl(η^6-*p*-cymene){κ^2-1,2,4,5-$C_6H_2(CH_2SMe)_4$}][BPh_4] had a disordered *i*-propyl group on the cymene residue which was modelled as two sites (A/B) with a refined population and the use of DFIX commands to control C–C distances. The major component (A, 0.68) is shown in figure 4.17. In [RuCl(η^6-*p*-cymene){κ^2-$C(CH_2SMe)_4$}][PF_6] the adp values of the anion F atoms used EADP constraints on *trans* F atoms, together with a common refined P–F distance (DFIX/FVAR).

4.5 References

1. W. Levason, G. Reid and S. D. Orchard, *Coord. Chem. Rev.*, 2002, **225**, 159.
2. W. Levason, M. Nirwan, R. Ratnani, G. Reid, N. Tsoureas and M. Webster, *Dalton Trans.*, 2007, 439.
3. W. Levason and T. Kemmitt, *Organometallics*, 1989, **8**, 1303.
4. D. B. Cordes and L. R. Hanton, *Inorg. Chem.*, 2007, **46**, 1634.
5. W. Levason, L. P. Ollivere, G. Reid, N. Tsoureas and M. Webster, *J. Organomet. Chem.*, 2009, **694**, 2299.
6. C. J. Anderson and M. J. Webb, *Chem. Rev.*, 1999, **99**, 2219.
7. G. Bandoli, A. Dolmella, F. Tisato, M. Porchia and F. Refosco, *Coord. Chem. Rev.*, 2009, **253**, 56.
8. D. E. Reichert, J. S. Lewis and C. J. Anderson, *Coord. Chem. Rev.*, 1999, **184**, 3.
9. J. A. Cabeza and P. M. Maitlis, *J. Chem. Soc., Dalton Trans.*, 1985, 573.
10. G. M. Sheldrick, SHELXS-97, Program for Crystal Structure Solution, University of Göttingen, Germany, 1997.
11. G. M. Sheldrick, SHELXL-97, Program for Crystal Structure Refinement, University of Göttingen, Germany, 1997.
12. H. D. Flack, *Acta Crystallogr.*, 1983, **39**, 876.

CHAPTER 5

Synthesis and complexation of dichalcogenoethers with cyclopropyl backbones, $(CH_2)_2C(CH_2EMe)_2$ (E = Se or Te)

5.1 Introduction

Two cyclopropyl-backboned ligands, 1,1-bis(methylselenomethyl)cyclopropane and 1,1-bis(methyltelluromethyl)cyclopropane, were isolated the during synthesis of the spirocyclic ligands under the experimental conditions detailed in chapter 2. This chapter describes the synthesis and characterisation of cyclopropyl ligand complexes with several different metal centres.

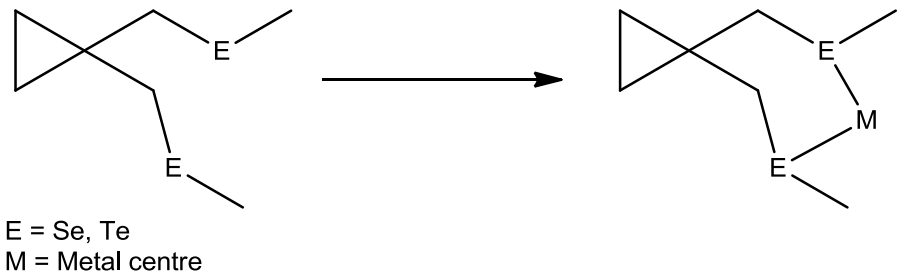

Figure 5.1 Chelation of a cyclopropyl ligand to a metal centre.

Detailed studies have shown that neutral selenium and tellurium donor ligands (chalcogenoethers R_2E, E = Se or Te) are better donors than the corresponding sulfur analogues. These ligands also exhibit ready oxidation at the heteroatom, and cleavage of the weaker and more reactive E–C bonds, properties less commonly found with thioethers.[1-3] The less reactive E–C bonds present in thioether ligands means that cleavage of an E-C bond does not occur during the ligand preparation and consequently, the cyclopropyl thioether ligand was never observed.

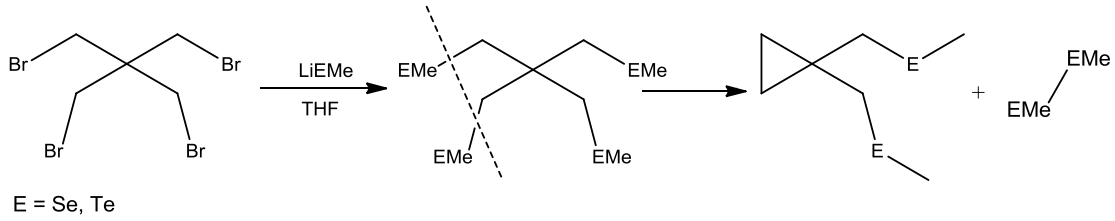

Figure 5.2 Formation of a cyclopropyl backboned ligand during synthesis.

Synthesis of these cyclopropyl ligands $(CH_2)_2C(CH_2EMe)_2$ E= Se/Te is detailed chapter 2.[4] These studies showed that when E = Se, the reaction of MeSeLi with $C(CH_2Br)_4$ produces either $C(CH_2SeMe)_4$ or $(CH_2)_2C(CH_2SeMe)_2$ depending upon the reaction conditions. The corresponding $(CH_2)_2C(CH_2TeMe)_2$ was mentioned some years ago in a paper dealing with the synthesis of ditelluroethers,[5] but the reaction was not investigated in detail.

This chapter describes the synthesis of the cyclopropyl ligand complexes with ruthenium(II)- and osmium(II)-(η^6-*p*-cymene) and manganese(I) carbonyl centres. Metal carbonyl complexes of the tetradentates 1,2,4,5-$C_6H_2(CH_2EMe)_4$ (E = S or Se) and $C(CH_2EMe)_4$ were discussed in chapter 3 and provide useful comparative data,[4] similarly ruthenium and osmium(II) complexes with the same ligands were discussed in chapter 4.[6]

The use of selenium compounds, mostly based upon selenoalkenes, as reagents for the formation of cyclopropyl rings in organic synthesis, is well established.[7, 8] Although these bidentate ligands are not capable of producing heterobimetallic complexes, bidentate group 16 ligands bound to early and late transition metals have been studied extensively.[2] However, the presence of a highly strained C_3 ring could lead to interesting secondary reactions. Ring opening and ring enlargement reactions are possible and have been explored in depth.[8] However, no reactions at the C_3 ring were observed during this study. Ring opening reactions with these compounds could provide a useful technique for functionalising organic compounds with chalcogenoether bound to a metal centre.

5.2 Results

5.2.1 Preparations

Manganese(I) carbonyl complexes

Reacting $Mn(CO)_5Cl$ with the seleno- and tellurocyclopropyl ligands in hot chloroform gave orange-red solids shown to be *fac*-$[Mn(CO)_3Cl\{(CH_2)_2C(CH_2EMe)_2\}]$ as the sole product in each case.

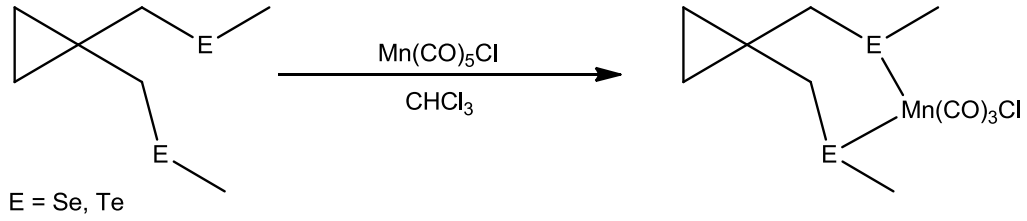

Figure 5.3 Chelation of a cyclopropyl ligand to manganese carbonyl chloride.

Complexes of cyclopropyl ligands form six-membered chelate rings. Hence the data from these compounds are directly comparable to complexes of $MeE(CH_2)_3EMe$ (E = Se, Te). Comparison of IR and NMR data (detailed comparison discussed in section 5.22) shows very similar trends, indicating the cyclopropyl unit in the ligand backbone has minimal effects at the metal centre, and there is no evidence in these systems of any reaction at the three-membered ring.[9-11]

Ruthenium and Osmium Complexes

Reacting 0.5 equivalents of $[\{MCl_2(\eta^6\text{-}p\text{-cymene})\}_2]$ (M= Ru^{II} or Os^{II}) with $(CH_2)_2C(CH_2EMe)_2$ (E = Se,Te) in ethanol, followed by addition of 1 equivalent of $[NH_4][PF_6]$ produced orange and red solids in good yield for the seleno- and telluro-ethers respectively.

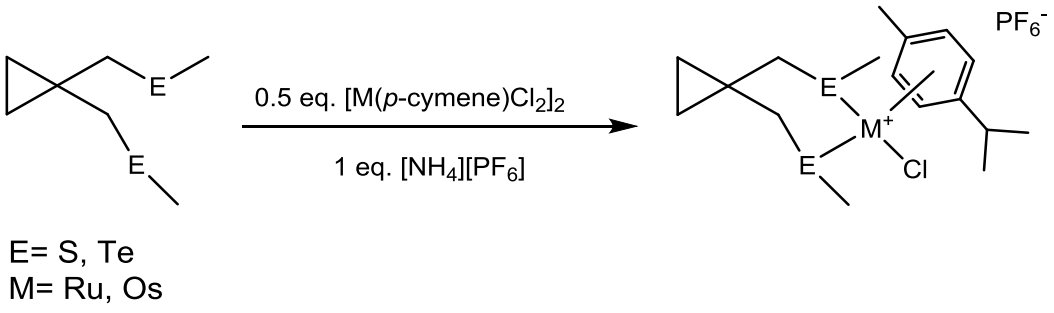

Figure 5.4 Chelation of a cyclopropyl ligand to M(*p*-cymene)Cl_2 dimer.

These complexes are directly comparable to the spirocyclic compounds discussed in chapter 4.

5.2.2 Characterisation

The characterisation of each group of compounds is discussed separately in this section. Crystallography was a fundamental technique, as the NMR data from ruthenium and osmium containing complexes were complicated due to the low symmetry of the complexes. In contrast, infrared and NMR spectroscopy were key in characterising manganese carbonyl complexes due to the presence of C=O groups and the higher symmetry of the complexes.

fac-[Mn(CO)$_3$Cl{(CH$_2$)$_2$C(CH$_2$EMe)$_2$}] (E= Se/Te)

Crystals of *fac*-[Mn(CO)$_3$Cl{(CH$_2$)$_2$C(CH$_2$TeMe)$_2$}] were grown from CHCl$_3$ and the structure determined. An image of the complex and selected lengths and bond angles are shown in figure 5.5 and table 5.1.

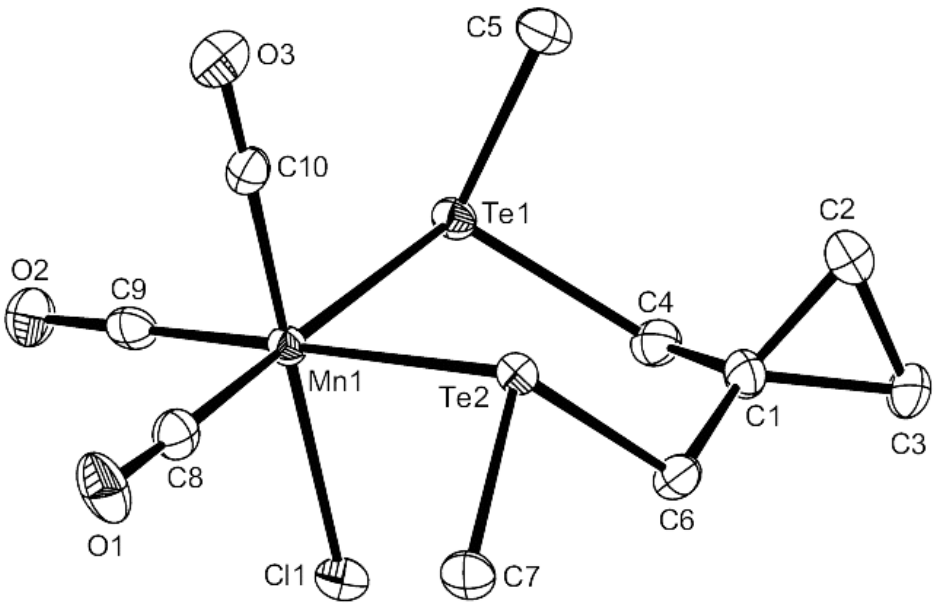

Figure 5.5 Structure of *fac*-[Mn(CO)$_3$Cl{(CH$_2$)$_2$C(CH$_2$TeMe)$_2$}] shows the numbering scheme adopted. Ellipsoids are drawn at the 50% probability level and H atoms have been omitted for clarity.

Mn1–Te1	2.6394(7)	Mn1–C8	1.813(4)
Mn1–Te2	2.6285(8)	Mn1–C9	1.806(4)
Mn1–Cl1	2.4053(11)	Mn1–C10	1.785(4)
Te1···Te2	3.712(1)	C–O	1.139(5)–1.150(5)
Te1–Mn1–Te2	89.62(2)	Cl1–Mn1–Te1	88.65(3)
C8–Mn1–Cl1	91.03(13)	Cl1–Mn1–Te2	89.98(3)
C9–Mn1–Cl1	88.96(13)	C8–Mn1–Te2	89.13(12)
C9–Mn1–Te1	89.42(12)	C10–Mn1–Te2	90.26(12)
C10–Mn1–Te1	90.20(12)	C–Mn1–C	90.1(2)–91.8(2)

Table 5.1 Selected bond lengths (Å) and angles (°) for *fac*-$[Mn(CO)_3Cl\{(CH_2)_2C(CH_2TeMe)_2\}]$.

The structure (figure. 5.5, table 5.1) showed the angles around the octahedral manganese centre to be very close to idealised 90°. The TeMe groups are present in the *DL* form with one methyl group above and one below the Te−Mn−Te plane. The Mn–C bond length *trans* to Cl (1.785(4) Å) is shorter than those *trans* to Te (1.806(4), 1.813(4) Å). Very similar Mn–Te bond lengths are observed in other structurally characterised manganese carbonyl telluroether complexes such as *fac*-$[Mn(CO)_3Cl\{o\text{-}C_6H_4(TeMe)_2\}]$ and *fac*-$[Mn(CO)_3\{MeC(CH_2TeMe)_3\}][CF_3SO_3]$.[12, 13] The bond angle of C2−C1−C3 is 59.7° due to the constrained geometry of the cyclopropane ring; this is compensated for by a relatively wide C4−C1−C6 bond angle (116.7°), leading to Te–Mn–Te = 89.62(2)°.

Assuming the ligand is considered planar and *cis* coordinated, then each complex will have C_s local symmetry. Three strong absorptions were seen for both complexes centred at *ca*. 2020, 1946, 1910 cm^{-1} consistent with the predictions from the point group (2A' + A"). Table 5.2 gives solution IR data for each complex. The carbonyl region of a typical spectrum is shown below.

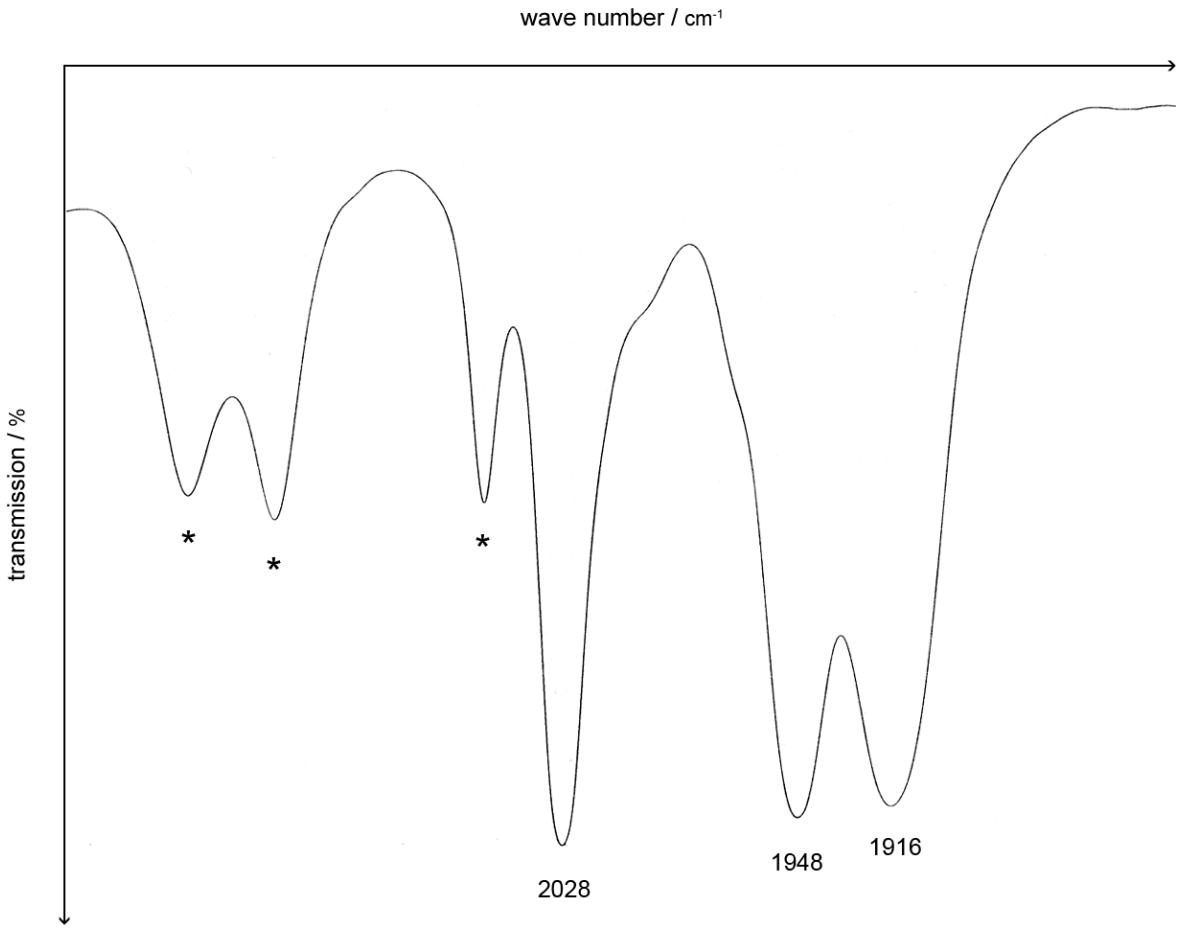

* Absorptions assigned to CH_2Cl_2

Figure 5.6 The carbonyl region (1600-2200 cm^{-1}) IR spectrum of $[Mn(CO)_3Cl\{(CH_2)_2C(CH_2SeCH_3)_2\}]$ in CH_2Cl_2

Compound	ν_{CO}/cm^{-1}
$[Mn(CO)_3Cl\{(CH_2)_2C(CH_2SeCH_3)_2\}]$[a]	2028, 1948, 1916
$[Mn(CO)_3Cl\{(CH_2)_2C(CH_2TeCH_3)_2\}]$[a]	2012, 1943, 1904
$[Mn(CO)_3Cl\{CH_3SeCH_2CH_2CH_2SeCH_3\}]$[b]	2032, 1955, 1917
$[Mn(CO)_3Cl\{CH_3TeCH_2CH_2CH_2TeCH_3\}]$[b]	2021,1949, 1906

[a] Recorded in CH_2Cl_2.

[b] Comparative data from literature, in $CHCl_3$.[10]

Table 5.2 Solution IR spectroscopic data of C≡O region.

Literature data of $[Mn(CO)_3Cl\{CH_3ECH_2CH_2CH_2ECH_3\}]$ (E= Se, Te) provide a useful comparison for these complexes, as they both form a 6-membered ring after chelation to a metal centre. Each absorption is comparable with the literature data, with the greatest difference in frequency being 10 cm^{-1} which can be largely attributed to different solvent systems.

Multinuclear NMR spectroscopy was fundamental in characterising manganese(I) complexes. $^{13}C\{^1H\}$ and ^1H NMR spectra show extensively broadened resonances in manganese carbonyl halides, due to the quadrupolar ^{55}Mn nucleus. Consequently little useful data were obtained with these techniques. However, the ^{55}Mn NMR spectra showed relatively sharp resonances and, as a result, provided useful structural data regarding pyramidal inversion.

Fac-$[Mn(CO)_3Cl\{(CH_2)_2C(CH_2EMe)_2\}]$ (E= Se, Te) complexes showed slow pyramidal inversion at the chalcogen centres. Both compounds show three ^{55}Mn NMR resonances of varied intensities, corresponding to the three invertomers *meso-1*, *meso-2* and *DL* shown below; a typical spectrum is shown in figure 5.8.

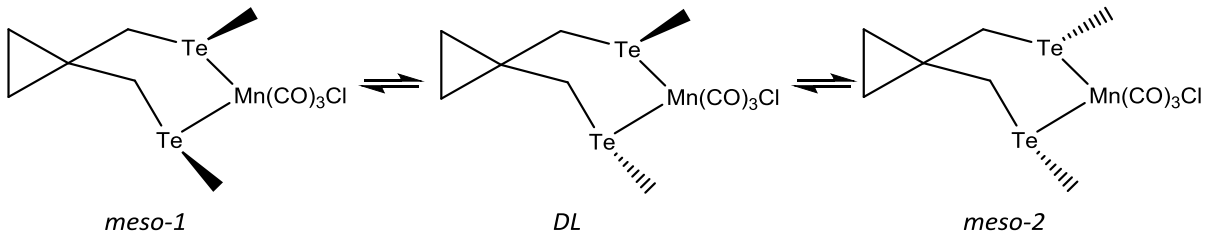

Figure 5.7 Possible invertomers of Fac-$[Mn(CO)_3Cl\{(CH_2)_2C(CH_2TeMe)_2\}]$.

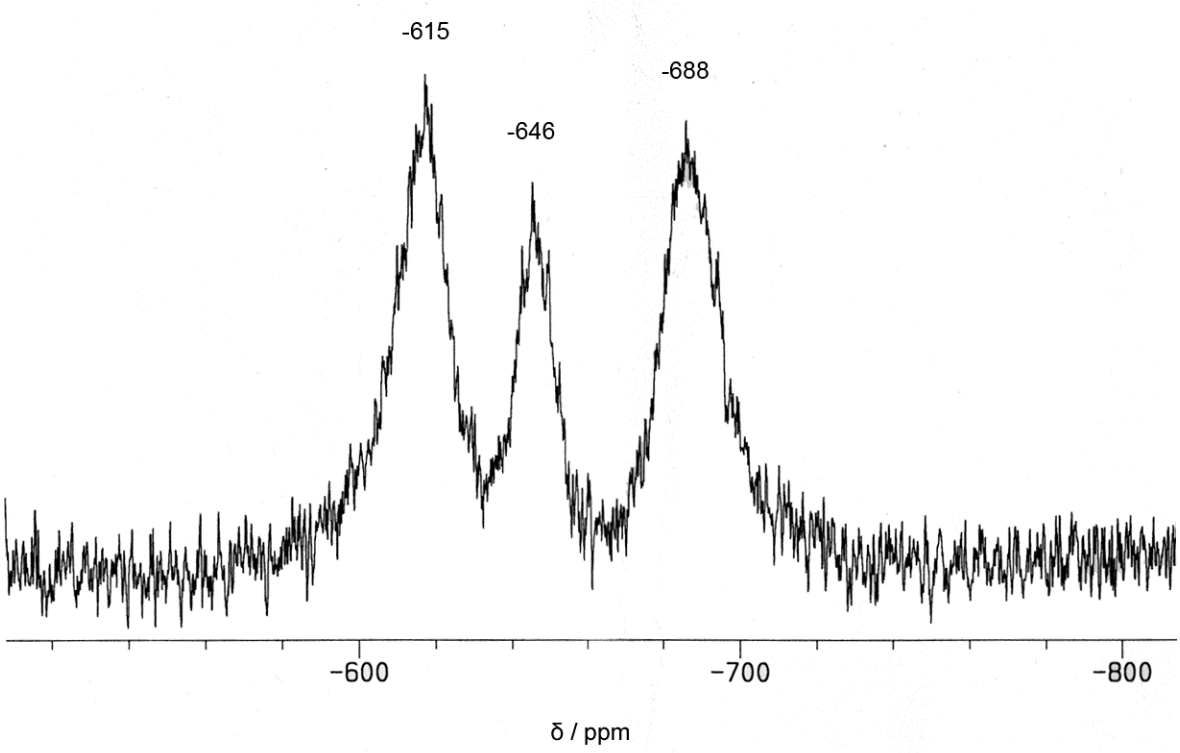

Figure 5.8 ^{55}Mn NMR spectrum of *fac*-[Mn(CO)$_3$Cl{(CH$_2$)$_2$C(CH$_2$TeMe)$_2$}] recorded at 295 K in CD_2Cl_2/CH_2Cl_2.

Four resonances are seen in the ^{77}Se{^{1}H} and ^{125}Te{^{1}H} NMR spectra, two corresponding to the *meso* invertomers, where the SeMe/TeMe groups are either both *syn* or *anti* to the Mn–Cl unit. The remaining two equally intense resonances are assigned to the *DL* invertomer.[9-11]

Compound	δ^{77}Se{^{1}H}, ^{125}Te{^{1}H}/ ppm	Coordination shift[a]/ ppm
[Mn(CO)$_3$Cl{(CH$_2$)$_2$C(CH$_2$SeMe)$_2$}]	74.4, 76.7, 108.9, 136.5	15.8, 18.1, 50.3, 77.9
[Mn(CO)$_3$Cl{(CH$_2$)$_2$C(CH$_2$TeMe)$_2$}]	45.2, 61.1 (major), 183.8, 194.5	-17.9, 2.0, 120.7, 131.4
[(CH$_2$)$_2$C(CH$_2$SeMe)$_2$][b]	58.6	
[(CH$_2$)$_2$C(CH$_2$TeMe)$_2$][b]	63.1	

[a] Coordination shift = $\delta_{(complex)} - \delta_{(ligand)}$.

[b] Comparative data from chapter 2.

Table 5.3 ^{77}Se{^{1}H} and ^{125}Te NMR spectroscopic data recorded in CH_2Cl_2 at ambient temperatures.

[MCl(η^6-*p*-cymene){$(CH_2)_2C(CH_2EMe)_2$}][PF_6] (E= Se/Te) (M= Ru/Os)

Crystals of two Ru and one Os complexes were obtained and structurally characterised. An image of [RuCl(*p*-cymene){$(CH_2)_2C(CH_2SeMe)_2$}]$^+$ and selected bond angles are displayed below (figure 5.9, table 5.4); additional crystallographic data shown in table 5.6. The atom numbering is consistent for each complex to allow comparison.

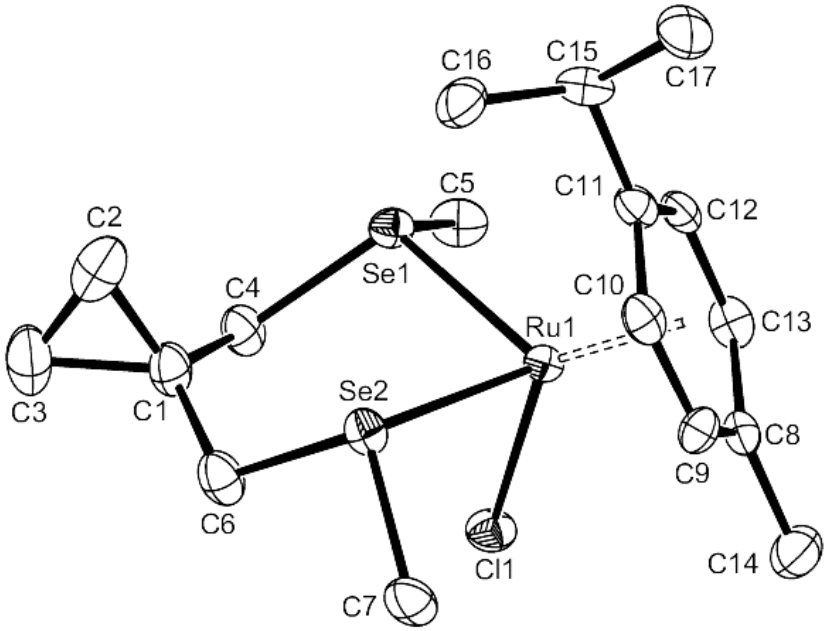

Figure 5.9 Structure of the cation in [RuCl(*p*-cymene){$(CH_2)_2C(CH_2SeMe)_2$}][PF_6] showing the numbering scheme adopted. Ellipsoids are drawn at the 50% probability level and H atoms have been omitted for clarity.

M = Ru, E = Se		M = Ru, E = Te		M = Os, E = Se	
Ru1–Se1	2.4856(5)	Ru1–Te1	2.6222(6)	Os1–Se1	2.4954(7)
Ru1–Se2	2.4972(6)	Ru1–Te2	2.6231(7)	Os1–Se2	2.5034(7)
Ru1–Cl1	2.396(1)	Ru1–Cl1	2.4097(15)	Os1–Cl1	2.4041(14)
Ru1–C_{ring}	2.178(4)–2.238(4)	Ru1–C_{ring}	2.188(7)–2.251(6)	Os1–C_{ring}	2.181(6)–2.231(6)
Se1–Ru1–Se2	87.87(2)	Te1–Ru1–Te2	88.17(2)	Se1–Os1–Se2	87.70(2)
Cl1–Ru1–Se2	88.58(3)	Cl1–Ru1–Te2	88.67(4)	Cl1–Os1–Se2	87.83(4)
Cl1–Ru1–Se1	88.36(3)	Cl1–Ru1–Te1	88.33(4)	Cl1–Os1–Se1	87.90(4)

Table 5.4 Selected bond lengths (Å) and angles (°) for $[MCl(p\text{-cymene})\{(CH_2)_2C(CH_2EMe)_2\}]^+$ (M = Ru or Os, E = Se; M = Ru, E = Te).

The structures were shown to be isomorphous ($P2_12_12_1$). The EMe groups were *meso* in the complex, with both Me groups on the same side of the E−M−E plane and the *i*-propyl group in the *p*-cymene on the opposite side. These features are consistent with structural data discussed in chapter 4.

As previously mentioned the NMR spectra are very complicated for compounds containing a [MCl(η^6-*p*-cymene)] unit, but despite this both the ^{1}H NMR and the ^{77}Se/^{125}Te NMR spectra are fully consistent with slow pyramidal inversion at the coordinated chalcogen donor atoms. The major form observed is a *meso* invertomer (probably the form seen in X-ray structures, figure 5.9). Minor amounts of the *DL* and second *meso* form are present in some spectra for example, $[OsCl(\eta^6\text{-}p\text{-cymene})\{(CH_2)_2C(CH_2TeMe)_2\}]^+$ shows four ^{125}Te resonances. The major peak is assigned to a *meso* invertomer at δ = 159.5, two weak singlets at 185.4 and 164.5 ppm due to the *DL* form and another weak resonance at 58.0 ppm for the second *meso* form.

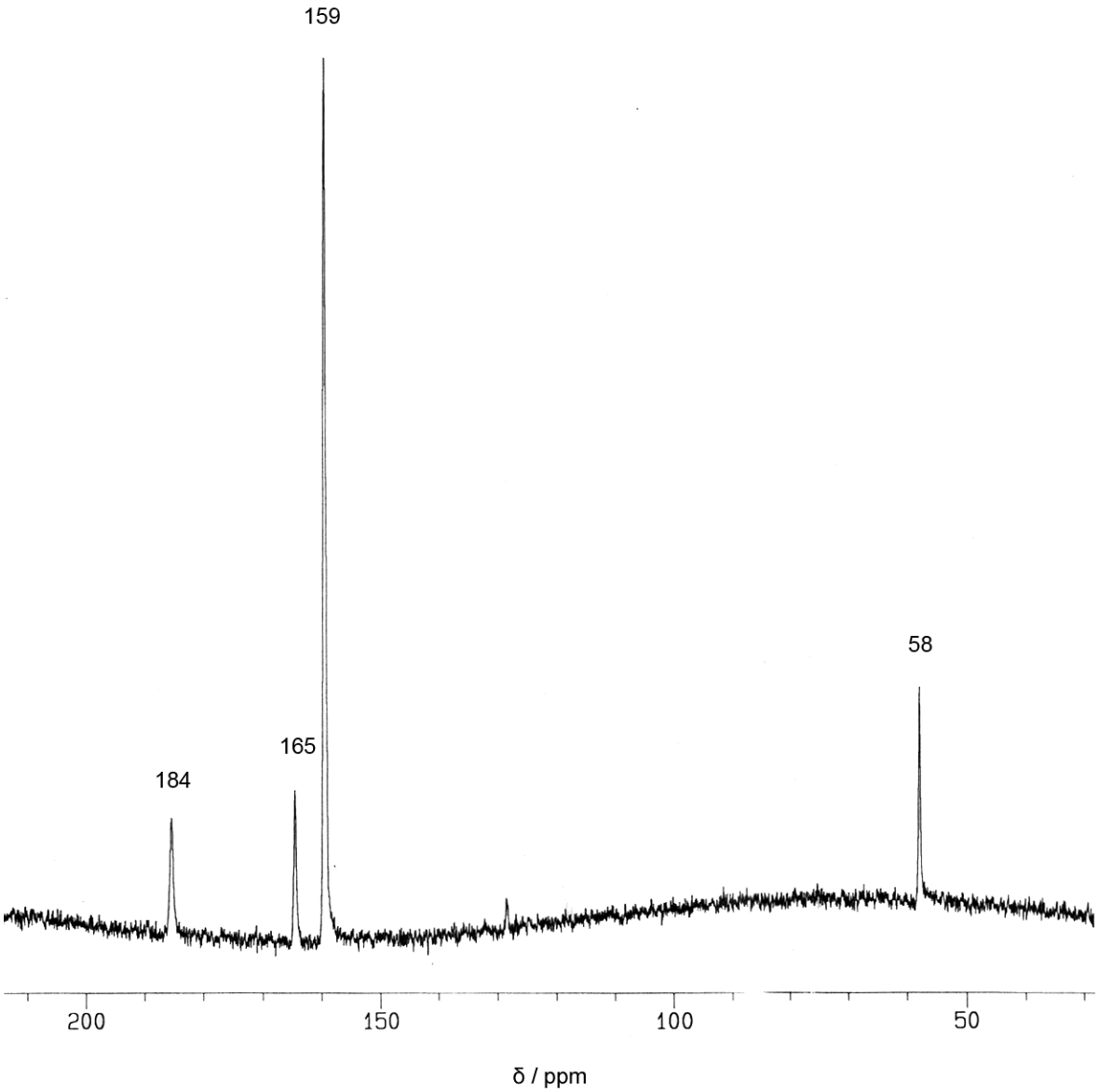

Figure 5.10 ^{125}Te NMR spectrum of [OsCl(η^6-*p*-cymene){$(CH_2)_2C(CH_2TeMe)_2$}]$^+$ in CH_3CN at ambient temperatures.

A considerable chemical shift range is observed for the stereoisomers,which is attributed the orientations of the EMe groups with respect to the *p*-cymene and Cl ligands. These chemical shifts are also moderately solvent dependent, for example in the ^{77}Se{^{1}H}NMR spectrum of [RuCl(η^6-*p*-cymene){$(CH_2)_2C(CH_2SeMe)_2$}]$^+$ the chemical shifts are ~7 to 10 ppm to lower frequency in CH_3CN compared to CH_2Cl_2 solution. A greater coordination shift (the difference in chemical shift between free ligand and complex) was

observed in ^{77}Se and ^{125}Te NMR spectra of analogous ruthenium complexes compared to osmium as expected.[2]

Data collected with other spectroscopic techniques were fully consistent with the predicted product. Infrared spectra of all ruthenium and osmium complexes showed two strong absorptions present at 839 and 557 cm^{-1} assigned to the PF_6^- stretch and bend respectively. ES^+ mass spectroscopy was collected on each osmium and ruthenium containing compound. All spectra showed the presence of a single product with a parent ion that matched the predicted isotope pattern. An image of the collected *vs* predicted data is shown in figure 5.11.

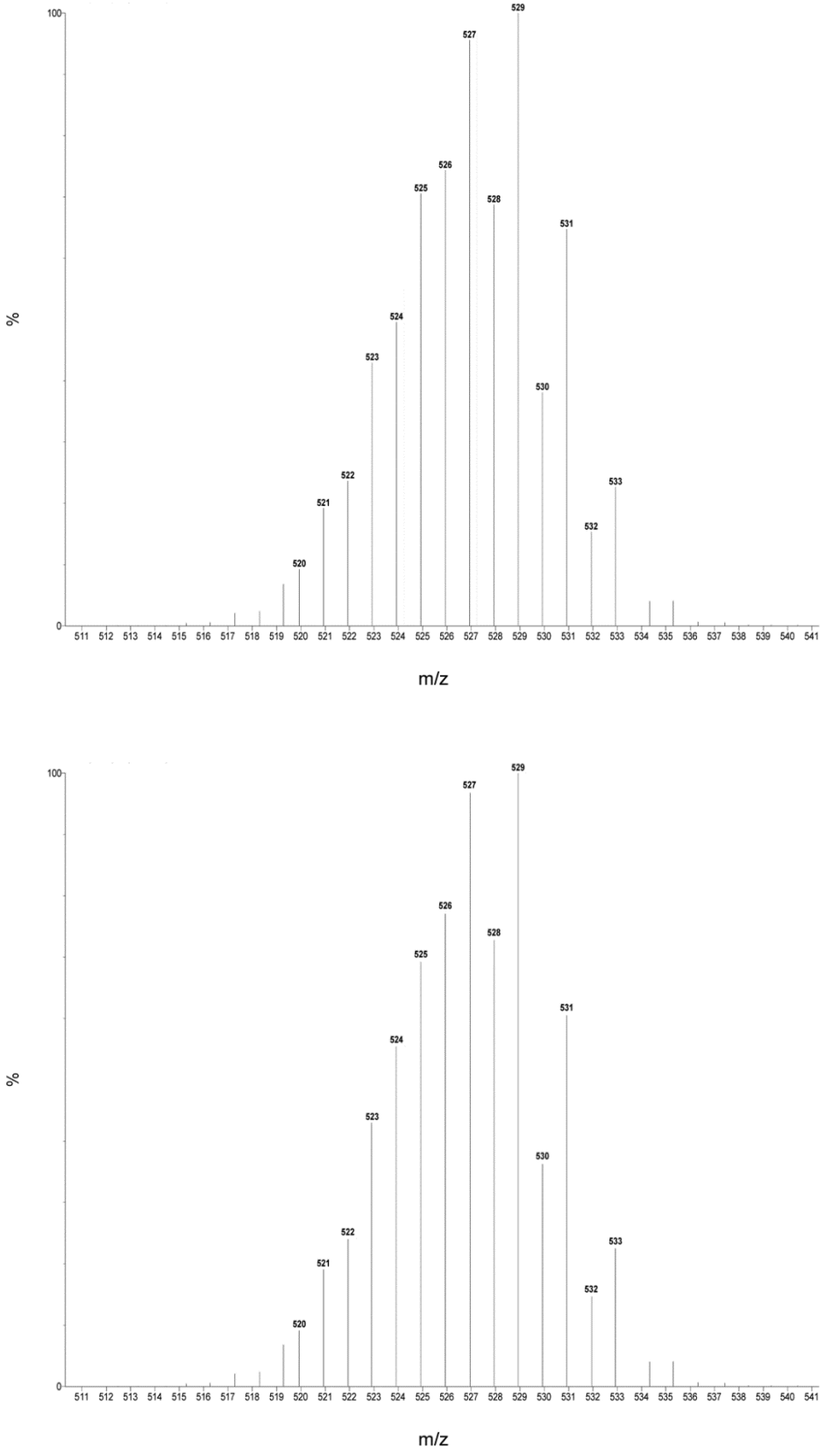

Figure 5.11 ES^+ spectrum of $[RuCl(\eta^6\text{-}p\text{-cymene})\{(CH_2)_2C(CH_2SeMe)_2\}]^+$ in CH_3CN with predicted isotope pattern beneath.

5.2.3 Cyclic voltammetry

Cyclic voltammetry measurements were undertaken on solutions of [MCl(η^6-*p*-cymene){$(CH_2)_2C(CH_2EMe)_2$}][PF_6] in 0.1 moldm^{-3} $^nBu_4NBF_4$ in dry MeCN. However, the osmium telluroether complex was not sufficiently soluble in the base electrolyte solution.

The voltammograms showed an irreversible oxidation for each complex (see table 5.5)

[RuCl(η^6-*p*-cymene){$(CH_2)_2C(CH_2SeMe)_2$}][PF_6]	+0.90 V
[RuCl(η^6-*p*-cymene){$(CH_2)_2C(CH_2TeMe)_2$}][PF_6]	+1.01 V
[OsCl(η^6-*p*-cymene){$(CH_2)_2C(CH_2SeMe)_2$}][PF_6]	+1.10 V

Table 5.5 Irreversible oxidation of complexes *vs* $[Fe(Cp)_2]/[Fe(Cp)_2]^+$ at a scan-rate of 0.1 V s^{-1}

These observed processes are attributed to irreversible $M^{II/III}$ couples. Electrochemical data are available for several Ru and Os complexes with seleno- and telluroether ligands. Most of the literature data recorded are from *trans*-[MX_2(dichalcogenoether)$_2$],[14] and [RuX_2(tetraselenoether)].[15] These species usually exhibit reversible II/III redox couples with $E_{1/2}$ values around 0 to +0.2 V *vs* $[Fe(Cp)_2]/[Fe(Cp)]_2]^+$, with the $E_{1/2}$ values largely insensitive to chalcogen type and halide.

The oxidation of the *p*-cymene complexes was shown to be irreversible. This was also observed for [RuCl(*p*-cymene)$(SMe_2)_2]^{+/2+}$,[16] possibly reflecting stabilisation of the low spin d^6 configuration, due to the presence of the arene co-ligand.

5.3 Conclusions

The reactions of a novel telluroether ligand with a cyclopropyl backbone and its selenium analogue have been the studied with selected metal reagents. Several new organotellurium and -selenium compounds have been thoroughly characterised. The cyclopropyl ring appears to be unreactive during and after metal complexation. Crystallographic data were collected, and structures determined from two selenium and two tellurium containing compounds with different metal centres. The cyclopropyl ring in the ligand backbone

opens up the C–C–C angle within the chelate ring, when compared with trimethylene linked analogues.

Complex	[Ru(*p*-cymene)Cl {(CH$_2$)$_2$C(CH$_2$SeMe)$_2$}][PF$_6$]	[Ru(*p*-cymene)Cl {(CH$_2$)$_2$C(CH$_2$TeMe)$_2$}][PF$_6$]	[Os(*p*-cymene)Cl {(CH$_2$)$_2$C(CH$_2$SeMe)$_2$}][PF$_6$]
Formula	$C_{17}H_{22}ClF_6PRuSe_2$	$C_{17}H_{22}ClF_6PRuTe_2$	$C_{17}H_{22}ClF_6OsPSe_2$
M	671.80	769.08	760.93
Crystal system	orthorhombic	orthorhombic	orthorhombic
Space group (no.)	$P2_12_12_1$ (#19)	$P2_12_12_1$ (#19)	$P2_12_12_1$ (#19)
a (Å)	12.3668(15)	12.5305(15)	12.363(2)
b (Å)	12.4682(10)	12.5472(10)	12.4710(14)
c (Å)	15.028(2)	15.2251(10)	15.056(2)
α (°)	90	90	90
β (°)	90	90	90
γ (°)	90	90	90
U (Å^3)	2317.2(5)	2393.7(4)	2321.3(6)
Z	4	4	4
μ(Mo Kα) (mm^{-1})	4.051	3.270	8.862
F(000)	1312	1456	1440
Total no. of reflections	15487	21520	20612
Unique reflections	5104	5219	5282
β_{int}	0.034	0.038	0.056
No. of parameters, constraints	254, 0	241, 6	258, 0
R_1[b] [$I_o > 2\sigma(I_o)$]	0.028	0.034	0.032
R_1 (all data)	0.031	0.038	0.037
wR_2[b] [$I_o > 2\sigma(I_o)$]	0.062	0.080	0.064
wR_2 (all data)	0.064	0.083	0.065

[a] Common items: temperature = 120 K; wavelength (Mo-Kα) = 0.71073 Å; θ(max) = 27.5°.

[b] $R_1 = \Sigma||F_o| - |F_c||/\Sigma|F_o|$. $wR_2 = [\Sigma w(F_o^2 - F_c^2)^2/\Sigma wF_o^4]^{1/2}$.

Table 5.6 Crystal data and structure refinement details.[a]

5.4 Experimental

All preparations were carried out under a N_2 atmosphere. $[Mn(CO)_5Cl]$,[17] $[\{RuCl_2(\eta^6\text{-}p\text{-cymene})\}_2]$ and $[\{OsCl_2(\eta^6\text{-}p\text{-cymene})\}_2]$[18] were made by literature methods.

5.4.1 Synthesis

[Chloro{1,1-bis(methylselenomethyl)cyclopropane}(η^6-*p*-cymene)ruthenium(II)] hexafluorophosphate

$[Ru(\eta^6\text{-}p\text{-cymene})Cl_2]_2$ (0.12 g, 0.19 mmol) in dry ethanol (10 mL) was added to $(CH_2)_2C(CH_2SeMe)_2$ (0.10 g, 0.39 mmol) in dry ethanol (5 mL) and refluxed for 2 h. $[NH_4][PF_6]$(0.065 g, 0.4 mmol) in dry degassed ethanol (5 mL) was added, the solution was then allowed to cool and stirred overnight. The pale orange precipitate was filtered off, washed with cold ethanol (2 ×5 mL) and dried *in vacuo*. Yield: 0.17 g (65%). Crystals were grown by refrigerating the filtrate. Anal: Calc. for $C_{17}H_{28}ClF_6PRuSe_2$: C, 30.4; H, 4.2. Found: C, 30.3; H, 4.3%. ^{1}HNMR (CD_3CN): 0.62 (m, [2H], $CH_{2cyclopropyl}$), 0.80 (m, [2H], $CH_{2cyclopropyl}$), 1.32 (d, [6H], J = 7Hz, $CH(CH_3)_2$), 2.24 (s, [3H], cymene-CH_3), 2.28, 2.45, 2.48 (major), 2.55 (4 × s, [6H], SeMe), 2.80 (m, [H], CH), 3.37, 3.41, 3.50 (major), 3.53 (major), 3.75, 3.79 (6 × s, [4H], CH_2Se), 5.60–5.84 (overlapping d, [4H], $CH_{aromatic}$) ppm.^{77}Se{^{1}H} NMR (CH_2Cl_2):147.8, 123.8, 117.7(major), 71.8; (CH_3CN): 135.1, 113.7, 110.3 (major), 62.5 ppm. IR (Nujol, cm^{-1}): 839 υ(PF), 557 δ(PF). ES$^+$-MS: *m/z* = 527 $[C_{17}H_{28}ClRuSe_2]^+$.

[Chloro{1,1-bis(methyltelluromethyl)cyclopropane}(η^6-*p*-cymene)ruthenium(II)] hexafluorophosphate

$[Ru(\eta^6\text{-}p\text{-cymene})Cl_2]_2$ (0.086 g, 0.14 mmol) in THF (10 mL) was added to a Schlenk tube containing $(CH_2)_2C(CH_2TeMe)_2$ (0.10 g, 0.28 mmol) in dry degassed ethanol (10 mL). The dark red solution was then stirred at room temperature for 2 h. $[NH_4][PF_6]$ (0.05 g, 0.3 mmol) in dry degassed ethanol (5 mL) was added and the solution was stirred for a further 1h before filtering to remove small amounts of insoluble material. The filtrate was then reduced in volume by 50% and placed in the freezer overnight. The bright red solid deposited was filtered off, washed with hexane (2 × 5 mL) and dried *in vacuo*. Yield 0.165 g (76%). Crystals were grown by refrigerating the filtrate. Anal. Calc. for

$C_{17}H_{28}ClF_6PRuTe_2$: C, 26.6; H, 3.7. Found: C, 26.6; H, 3.4%. ^{1}HNMR (CD_3Cl_3): 0.51, 0.77, 1.00 (3 × m, [4H], $CH_{2\ cyclopropyl}$), 1.27 (overlapping d, [6H], $CH(CH_3)_2$), 2.19 (s, [3H], cymene-CH_3), 2.24, 2.25, 2.27, 2.30 (4 × s, [6H], TeMe), 2.76 (m, [H], CH), 3.10, 3.14, 3.46 (major), 3.50 (major), 3.67, 3.71 (6 × s [4H], CH_2Te), 5.50–5.90 (overlapping m, [4H], $CH_{aromatic}$). ^{125}Te{^{1}H} NMR (CH_2Cl_2): 283.1, 265.8 (major), 264.0. IR (Nujol, cm^{-1}): 839 υ(PF), 557 δ(PF). ES$^+$-MS: *m/z* = 627 $[C_{17}H_{28}ClRuTe_2]^+$.

[Chloro{1,1-bis(methylselenomethyl)cyclopropane}(η^6-*p*-cymene)osmium(II)] hexafluorophosphate

$[Os(\eta^6\text{-}p\text{-cymene})Cl_2]_2$ (0.15 g, 0.20 mmol) in dry degassed ethanol (30 mL) was added to a Schlenk tube containing$(CH_2)_2C(CH_2SeMe)_2$ (0.10 g, 0.39 mmol) in dry degassed ethanol (10 mL). The dark yellow solution was then stirred at 70 °C for 1 h. $[NH_4][PF_6]$ (0.031 g, 0.20 mmol) in dry degassed ethanol (15 mL) was added, the solution was then stirred overnight before filtering to remove small amounts of insoluble material. The filtrate was reduced in volume by 50% and placed in the freezer overnight. The yellow solid deposited was filtered off, washed with hexane (2 × 5 mL) and dried *in vacuo*. Yield: 0.21 (71%). Crystals were grown from the filtrate at −18 °C. Anal: Calc. for $C_{17}H_{28}ClF_6OsPSe_2$: C, 26.8; H, 3.7. Found: C, 25.4; H, 3.4%. ^{1}HNMR (CD_3CN): 0.58–0.72 (m, [4H], $CH_{2cyclopropyl}$), 1.27 (major), 1.30 (2 × d, [6H], $CH(CH_3)_2$), 2.16 (major), 2.19 (2 × s, [3H], cymene-CH_3), 2.27, 2.40 (major), 2.58 (4 × s, [6H], SeMe), 2.90 (m, [H], CH), 3.46, 3.50, 3.62 (major), 3.65 (major), 3.82, 3.86 (6 × s, [4H], CH_2Se), 5.76–6.05 (overlapping d, [4H],$CH_{aromatic}$) ppm. ^{77}Se{^{1}H} NMR (CH_3CN): 92.9, 68.4, 65.8 (major), 47.2 ppm. IR (Nujol, cm^{-1}): 839 υ(PF), 557 δ(PF). ES$^+$-MS: *m/z* = 617 $[C_{17}H_{28}ClOsSe_2]^+$.

[Chloro{1,1-bis(methyltelluromethyl)cyclopropane}(η^6-*p*-cymene)osmium(II)] hexafluorophosphate

$[Os(\eta^6\text{-}p\text{-cymene})Cl_2]_2$ (0.11 g, 0.14 mmol) in dry degassed ethanol (30 mL) was added to a Schlenk tube containing $(CH_2)_2C(CH_2TeMe)_2$ (0.10 g, 0.28 mmol) in dry degassed ethanol (10 mL). The orange solution was then stirred at 50 °C for 1 h. $[NH_4][PF_6]$ (0.023 g, 0.14 mmol) in dry degassed ethanol (15 mL) was added, the solution was then stirred overnight before filtering to remove small amounts of insoluble material. The filtrate was then reduced in volume by 50% and placed in the freezer overnight. The orange solid was

filtered, washed with hexane (2 × 5 mL) and dried *in vacuo*. Yield: 0.07 g. (57%). ^{1}HNMR (CD_3CN): (see text) 0.50–0.91 (overlapping m, [4H], $CH_{2cyclopropyl}$), 1.24–1.29 (3 overlapping d, [6H], $CH(CH_3)_2$), 2.15, 2.16 (2 × s, [3H], cymene-CH_3), 2.25, 2.29, 2.37, 2.41 (4 × s, [6H], TeMe), 2.6–2.8 (m, [H], CH), 3.14, 3.18, 3.42, 3.52, 3.53 (major), 3.56 (major), 3.69, 3.73 (6 × s, [4H], CH_2Te), 5.67–6.10 (overlapping m, [4H], $CH_{aromatic}$) ppm. ^{125}Te{^{1}H} NMR (CH_3CN): 185.4, 164.5, 159.5 (major), 58.0 ppm. IR (Nujol, cm^{-1}): 839 υ(PF), 557 δ(PF). ES^{+}-MS: *m/z* = 715 $[C_{17}H_{28}ClOsTe_2]^{+}$.

Chlorotricarbonyl{1,1-bis(methylselenomethyl)cyclopropane}manganese(I)

$[Mn(CO)_5Cl]$ (0.09 g, 0.38 mmol) was dissolved in $CHCl_3$ (50 mL) and $(CH_2)_2C(CH_2SeMe)_2$ (0.10 g, 0.38 mmol) in $CHCl_3$ (20 mL) added. The mixture was refluxed for 3 h, cooled, and the solvent removed *in vacuo*. The residue was washed with hot $CHCl_3$ (3 × 20 mL) and the bright orange solid was dried *in vacuo.* Yield: 0.11 g (68%). Anal. Calc. for $C_{10}H_{14}ClMnO_3Se_2 \cdot 0.5CHCl_3$: C, 26.7; H, 3.1. Found: C, 26.2; H, 3.7%. ^{1}H NMR ($CDCl_3$): peaks too broad to assign.^{13}C{^{1}H} NMR ($CH_2Cl_2/CDCl_3$): 10.88, 11.43, 12.77, 13.46, 14.61 ($CH_{2cyclopropyl}$), 15.16, 17.56, 18.00, 19.05 (MeSe), 21.65, 30.02 ($C_{quaternary}$), 32.50, 34.60, 35.10, 39.17 (CH_2Se), 219 (vbr) CO ppm.^{77}Se{^{1}H} NMR (CH_2Cl_2): 74.4, 76.7, 108.9, 136.5 ppm. ^{55}Mn NMR (CH_2Cl_2): –205, –230, –290 ppm. IR (CH_2Cl_2, cm^{-1}): υ(CO) 2028, 1948, 1916.

Chlorotricarbonyl{1,1-bis(methyltelluromethyl)cyclopropane}manganese(I)

$[Mn(CO)_5Cl]$ (0.09 g, 0.38 mmol) was dissolved in dry $CHCl_3$ (50 mL) and$(CH_2)_2C(CH_2TeMe)_2$ (0.14 g, 0.38 mmol) in $CHCl_3$ (20 mL) was added. The mixture was heated at 40 °C for 3 h, cooled, and the solvent removed *in vacuo*. The residue was washed with hot $CHCl_3$ (3 × 20 mL). The resulting red solid was filtered and then dried *in vacuo*. Yield: 0.14 g (68%). Anal. Calc. for $C_{10}H_{14}ClMnO_3Te_2$: C, 22.8; H, 2.7. Found: C, 23.6; H, 2.3%.^{1}H NMR ($CDCl_3$): very broad, see text.^{13}C{^{1}H} NMR ($CH_2Cl_2/CDCl_3$): –21.73, –13.17, –10.67,–10.30 (TeMe),16.66, 17.98, 19.17, 20.87, 22.77, 24.68 (CH_2Te + $CH_{2\ cyclopropyl}$), 220 (vbr) CO ppm.^{125}Te{^{1}H} NMR (CH_2Cl_2): 194.5, 183.8, 61.1 (major),45.2 ppm. ^{55}Mn NMR (CH_2Cl_2): –615, –646, –688 ppm. IR (CH_2Cl_2. cm^{-1}): υ(CO) 2012, 1943, 1904.

5.4.2 X-Ray crystallography experimental

Details of the crystallographic data collection and refinement parameters are given in table 5.7. The crystallisation details are provided under the section for each compound. Structure solution and refinement were straightforward,[19-21] except as described below, H atoms were introduced into the models in calculated positions using the default C–H distances. The diffraction data for [Ru(*p*-cymene)Cl{$(CH_2)_2C(CH_2TeMe)_2$}][PF_6] was modelled by Dr. M. Webster, the sample was initially collected for a tetragonal system ($a \approx b$), but a solution only emerged in an orthorhombic space group. The anion showed large adp values for the F atoms, and this was modelled using the EADP command on *trans* F atoms and restraining all the P–F distances to be the same (DFIX/FVAR).

5.5 References

1. W. Levason and G. Reid, *Handbook of Chalcogen Chemistry*, RSC, 2007.
2. W. Levason, G. Reid and S. D. Orchard, *Coord. Chem. Rev.*, 2002, **225**, 159.
3. E. G. Hope and W. Levason, *Coord. Chem. Rev.*, 1993, **122**, 109.
4. W. Levason, L. P. Ollivere, G. Reid, N. Tsoureas and M. Webster, *J. Organomet. Chem.*, 2009, **694**, 2299.
5. E. G. Hope, T. Kemmitt and W. Levason, *Organometallics*, 1988, **7**, 78.
6. W. Levason, C. Marshall and L. P. Ollivere, *J. Organomet. Chem.*, 2010, **695**, 2039.
7. C. Paulmier, *Selenium Reagents and Intermediates in Organic Synthesis*, Pergamon, Oxford, 1986.
8. Z. Rappoport, *The Chemistry of the Cyclopropyl Group*, Wiley, New York, 1987.
9. W. Levason, S. D. Orchard and G. Reid, *J. Chem. Soc., Dalton Trans.*, 1999, 823.
10. W. Levason, S. D. Orchard and G. Reid, *Organometallics*, 1999, **18**, 1275.
11. J. Connolly, M. K. Davis and G. Reid, *J. Chem. Soc., Dalton Trans.*, 1998, 3833.
12. W. Levason, S. D. Orchard and G. Reid, *Organometallics*, 1999, **18**, 1275.
13. W. Levason, S. D. Orchard and G. Reid, *J. Chem. Soc. Dalton Trans.*, 1999, 823.
14. N. R. Campness, W. Levason, S. R. Preece and M. Webster, *Polyhedron*, 1994, **13**, 881.
15. W. Levason, J. J. Quirk, G. Reid and S. M. Smith, *J. Chem. Soc., Dalton Trans.*, 1997, 3719.
16. J. Cubrilo, I. Hartenbach, F. Lissner, T. Schleid, M. Niemeyer and R. F. Winter, *J. Organomet. Chem.*, 2007, **692**, 1496.
17. K. J. Reimer and A. Shaver, *Inorg. Synth.*, 1979, **19**, 159.
18. J. P. Flackler, *Inorg. Synth.*, 1982, **21**, 75.
19. H. D. Flack, *Acta Crystallogr.*, 1983, **39**, 876.
20. G. M. Sheldrick, SHELXL-97, Program for Crystal Structure Refinement, University of Göttingen, Germany, 1997.
21. G. M. Sheldrick, SHELXS-97, Program for Crystal Structure Solution, University of Göttingen, Germany, 1997.

CHAPTER 6

Synthesis and characterisation of gallium(III) and indium(III) chloride complexes with geometrically constrained thio- and seleno-ether ligands

6.1 Introduction

This chapter explores a quite different area of coordination chemistry, a series of gallium(III) and indium(III) complexes has been produced by reacting the appropriate Group 13 trihalide with the relevant bi- or tetra-dentate Group 16 ligands. The chapter particularly focuses on how a small difference in ligand architecture can cause significant differences to the complex formed.

The coordination chemistry of p-block elements has different properties affecting their coordination geometries that are not present in d-block metal complexes. Firstly, the lack of vacant d-orbitals means that coordination to different ligand types is less predictable. Consequently, formation of complexes is based upon s and p-orbital interactions.[1] Fewer examples of p-block complexes with Group 16 ligands are available in the literature, these tend to exhibit a wide range of coordination numbers with less regular geometries and different ligand substitution chemistry compared to transition metal analogues.[1-3]

Several factors affect the bonding of Group 13 compounds and in many cases the octet rule is exceeded. Consequently, these compounds require a different bonding model. This topic has attracted much debate in recent years.[4]

Earlier bonding models involving d-orbitals suggested an octahedral central atom with sp^3d^2 bonding. However, this model is less favoured as *n*d orbitals are now considered to be too diffuse and too high in energy.[5] Consequently, this model has been replaced by either donor acceptor bonding or electron rich multi centre bonding.

The donor acceptor bonding model consists of polarised M–X σ bonds (M = Ga or In, X = Cl). The σ-orbitals are polarised towards the more electronegative halide and the M–X σ* antibonding orbital polarised towards M, a schematic of the bonding model is shown below.

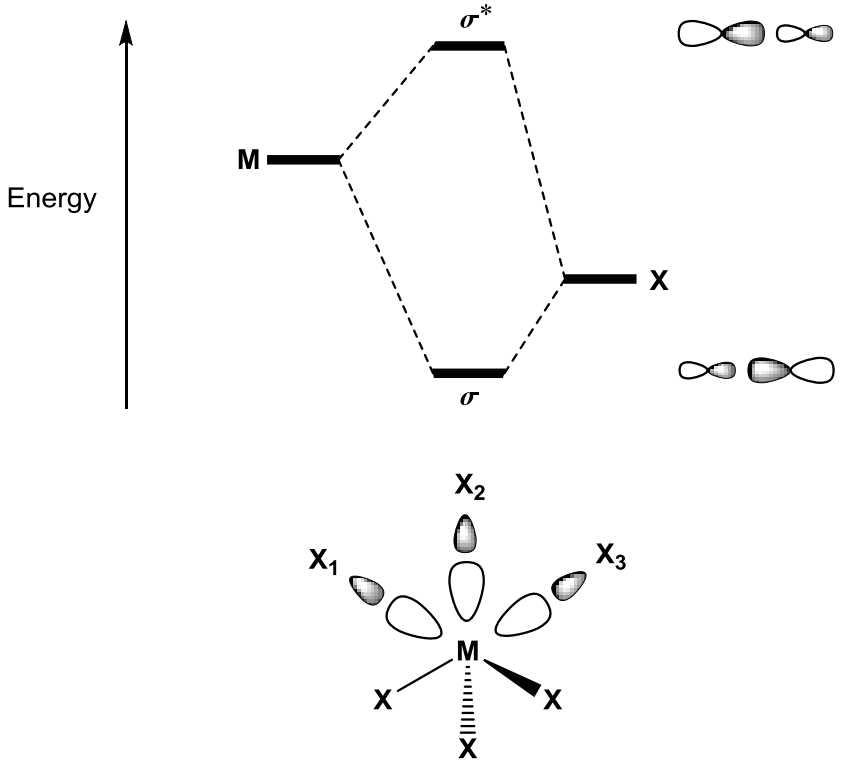

Figure 6.1 Schematic of donor acceptor bonding model.[4]

When the σ* antibonding orbital lies at a low enough energy, it may act as an acceptor orbital and bridge a halide from another monomer unit, or interact with a Lewis base such as a chalcogeno-ether ligand.

Electron rich multi centre bonding,[6] in this case three centre four electron bonds (3c-4e) consist of linear four electron bonds, for example the Cl-In-Cl sub-unit is considered to be one bond containing four electrons however, two of the electrons are in the non-bonding orbitals. A schematic for the bonding of a Cl-In-Cl sub-unit is shown below.

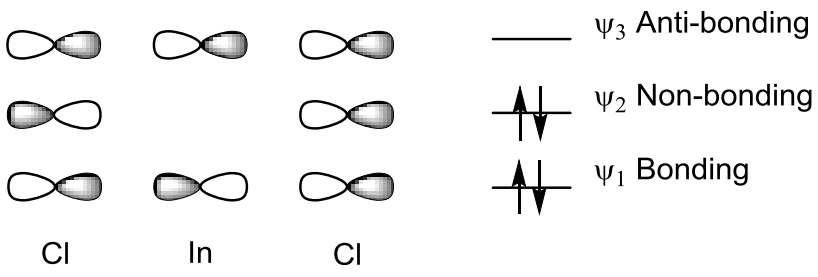

Figure 6.2 Schematic of 3c-4e bonding model of Cl-In-Cl sub-unit.[6]

The bonding and non-bonding orbitals contain two electrons each, an octahedral complex contains three of these sub-units, so in total contains six bonding and six non-bonding electrons. Bond order (the number of bonds between pairs of atoms) is defined as:

$$\text{Bond order} = \left(\frac{\text{No. of bonding electrons}}{\text{No. of non-bonding electrons}} \right) / 2$$

So the bond order for each In-Cl bonds is equal to 1/2 meaning each Cl-In-Cl sub-unit is considered to be a single bond. While both the donor acceptor and electron rich multi centre models can be applied to these systems current option is that the electron rich multi centre model is most likely.[1]

Another important factor in these systems is secondary bonding, first introduced in 1972.[7] This concept recognises that many p-block compounds show directional interaction shorter than van der Waals interactions but longer than primary bonds. The only conclusive method for determining secondary bonds is crystallography, throughout this chapter secondary interactions are given the notation of three dashes (M- - -X) and primary or normal bonds are shown with a single dash (M–X). The strength of secondary bonding interactions is dependent on mismatch in orbital size and electronegativity of M and X, both of which determine in the energy of M–X σ*.

The atomic properties of boron, aluminium, gallium and indium are shown below.

Property	B	Al	Ga	In
Atomic number	5	13	31	49
Atomic weight	10.81	26.98	69.72	114.82
Electronic configuration	$[He]2s^2 2p^1$	$[Ne]3s^2 3p^1$	$[Ar]3d^{10} 4s^2 4p^1$	$[Kr]4d^{10} 5s^2 5p^1$
Ionic radius/pm (6-coordinate) III	27	53.5	62.0	80.0

Table 6.1 Atomic properties of selected Group 13 elements.[8]

Ionic radii increase down Group 13. Consequently, Al(III) and Ga(III) are most commonly found as four-coordinate complexes. Some examples of five- and six-coordinate species have been reported with hard anionic mixed N/O-donor systems, but are less common.[9] An example of six coordinate gallium with a O_3N_3 donor set is shown below, other octahedral gallium complexes with bi-, tri- and tetra-dentate N/O donors have also been described in the same review.[9]

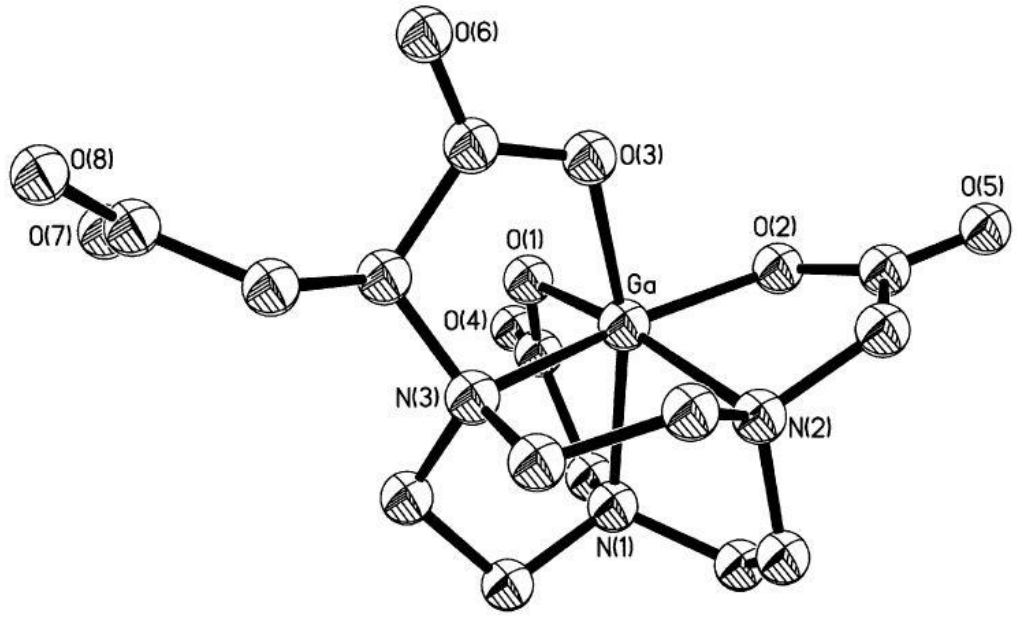

Figure 6.3 Structure of a six coordinate gallium complex with a hexadentate mixed donor ligand.[9]

More recently, some gallium(III) macrocyclic systems with sulfur or selenium donors have also been found to adopt different geometries.[1] The larger indium(III) ion however, is more commonly found as in five- or six-coordinate complexes, such as $[InCl_3(Se(CH_3)_2)_2]$[10] and $[In_2Cl_6\{CH_3Se(CH_2)_2SeCH_3\}_2]$[11].

6.1.1 Ga(III) halide complexes with thio- and seleno-ether ligands

Levason, Reid and co-workers have shown that thio- and seleno-ether complexes of gallium trihalides form readily in anhydrous conditions.[12] Selected mono-, bi- and tri-dentate (tripodal) ligands with different linking carbon backbones and terminal substituents were reacted with GaX_3 and InX_3. A more limited set of telluroether complexes were also

reported in this work.[4] Products were characterised with single crystal X-ray diffraction, vibrational and multinuclear (^{1}H, ^{71}Ga, ^{77}Se, ^{125}Te) NMR spectroscopy. The gallium complexes produced in most cases only contained neutral Ga(III) adopting a distorted tetrahedral geometry (X_3E donor set, E = S, Se or Te), irrespective of ligand type.

Reacting the monodentate $E(CH_3)_2$ with $GaCl_3$ produces $[GaCl_3(E(CH_3)_2)]$; X-ray diffraction on the selenoether derivative shows the structure contains Ga(III) present as a distorted tetrahedron.[12] Using flexible bidentate ligands such as $^{n}BuSeCH_2CH_2Se^{n}Bu$ also produces a tetrahedral gallium-containing complex shown in figure 6.4, this time in a 2:1 Ga:ligand stoichiometry.

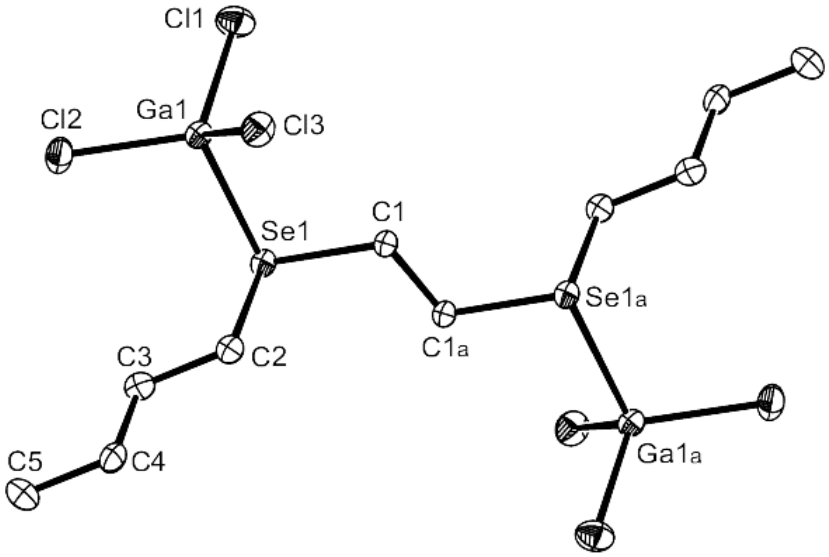

Figure 6.4 Structure of $[(GaCl_3)_2(^{n}BuSeCH_2CH_2Se^{n}Bu)]$.[12]

Despite the presence of the diselenoether ligand, $[(GaCl_3)_2(^{n}BuSeCH_2CH_2Se^{n}Bu)]$ has the same donor set and coordination environment as the monodentate ligand, and does not show substitution of halide. Other acyclic bidentate chalcogenoethers give analogous complexes, suggesting this is the favoured geometry for GaX_3 complexes with simple thio- and selenoether ligands.[12] This is very different behaviour compared to d-block chemistry discussed in earlier chapters, where the presence of vacant d-orbitals allows metal centres to form other geometries with ligands containing more than one donor atom. However, Ga(III) complexes have been shown to adopt other geometries depending upon the steric

and electronic properties. Very recent work by Levason, Reid and co-workers reported several macrocyclic gallium(III) complexes with geometries other than a distorted tetrahedral. Both trigonal bipyramidal and octahedral coordination geometries at Ga(III) have both been reported.[13, 14]

The structure of the $[GaCl_3([14]aneS_4]$ complex, produced by stirring $GaCl_3$ with 1 mol. eq. of $[14]aneS_4$ in anhydrous CH_2Cl_2 for 45 minutes at room temperature, is shown below.

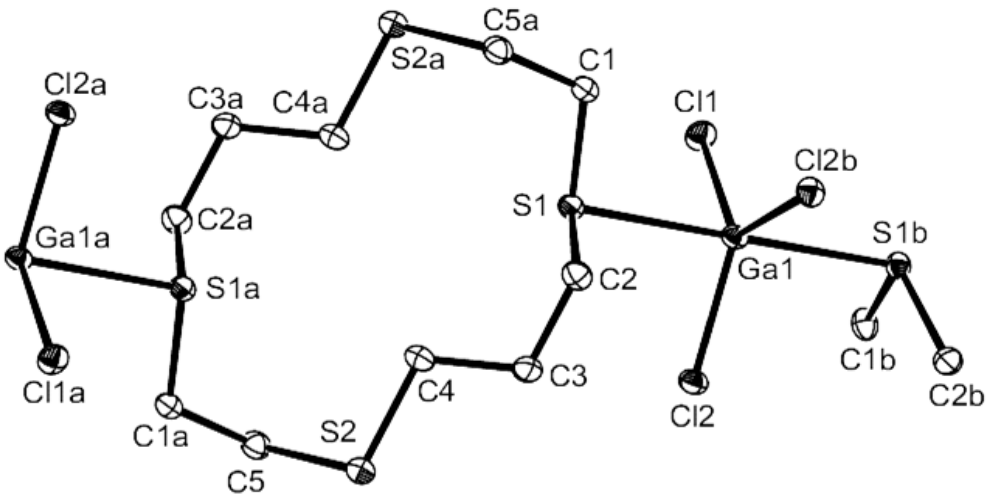

Figure 6.5 View of the structure of a section of the chain polymer of $[GaCl_3([14]aneS_4)]$.[13]

The structure in figure 6.5 shows $GaCl_3$ coordinated to $[14]aneS_4$ in a 1:1 ratio forming an infinite chain polymer. The gallium centre has a five-coordinate trigonal bipyramidal coordination geometry from the three (planar) Cl ligands and two axial sulfur donor atoms from bridging macrocyclic rings producing the chain structure.

Using the larger 16-membered ring tetra thio crown produces $[GaCl_2([16]aneS_4)][GaCl_4]$ from stirring a solution of $[16]aneS_4$ and 2 mol. eq. of $GaCl_3$ in a CH_2Cl_2 and CH_3CN mixed solvent. The structure of the complex cation is shown in figure 6.6.

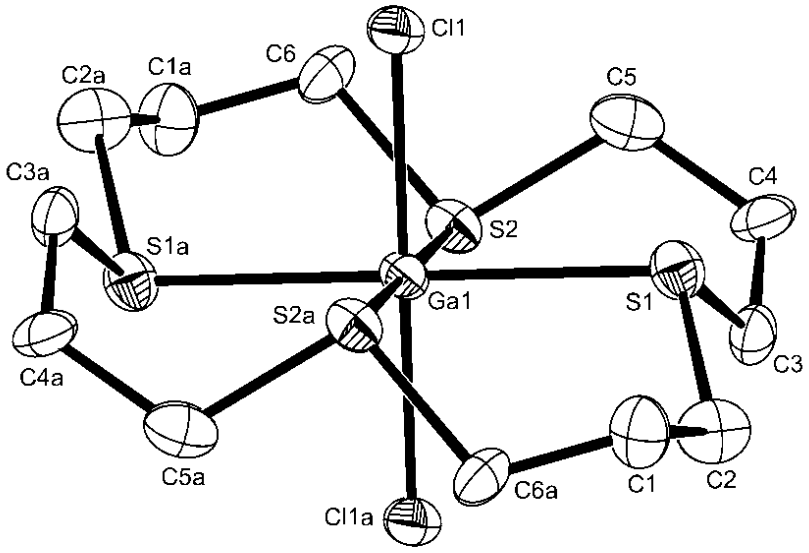

Figure 6.6 View of the cation in $[GaCl_2([16]aneS_4)][GaCl_4]$.[13]

The structure in figure 6.6 shows the gallium occupying the ring with an octahedral coordination geometry formed *via* four sulfur donor atoms and two *trans* Cl ligands, giving the S_4Cl_2 donor set. The analogous product was also obtained using $[16]aneSe_4$.[1]

Reacting 2 mol. eq. of $GaCl_3$ with $[8]aneSe_2$ in CH_2Cl_2 has been found to produce a highly air sensitive white solid. Spectroscopic data showed the product to be $[(GaCl_3)_2([8]aneSe_2)]$, most likely containing Ga(III) coordinated to each selenium with tetrahedral geometry.

Bubbling O_2 gas though the product dissolved in CH_2Cl_2 produced a red precipitate, crystals of this red product were isolated and structurally characterised.[1] The crystals were shown to be $[\{[8]aneSe_2\}_2][GaCl_4]_2$. The structure showed oxidation had occurred with one selenium atom in each macrocycle had undergoing a one electron oxidation followed by a radical coupling to produce a dimer.

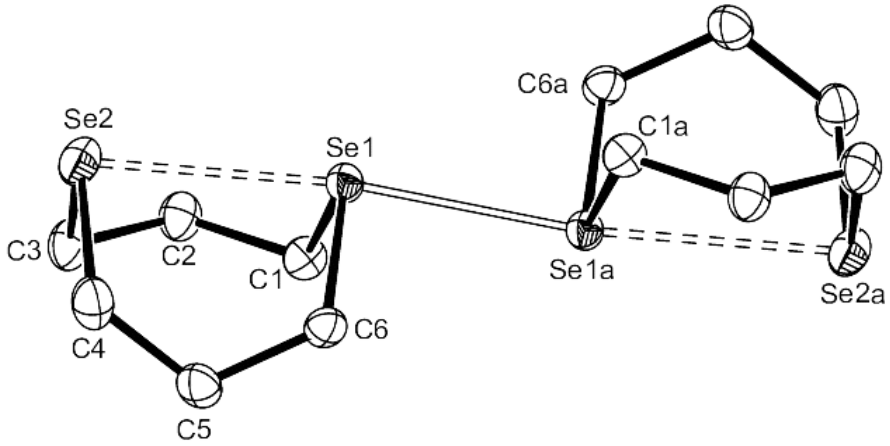

Figure 6.7 Structure of the dimeric cation in $[\{[8]aneSe_2\}_2][GaCl_4]_2$.[1]

Addition of acetone to the red precipitate in CH_2Cl_2 initially causes the precipitate to dissolve before initially turning then bright yellow then pale yellow after a few minutes. These colour changes suggest further oxidation is occurring, crystals of the yellow product were also isolated and structurally characterised.[1] The yellow crystals were identified as $[\{[8]aneSe_2Cl\}][GaCl_4]$, with both selenium atoms undergoing oxidation, an image of the structure is shown below.

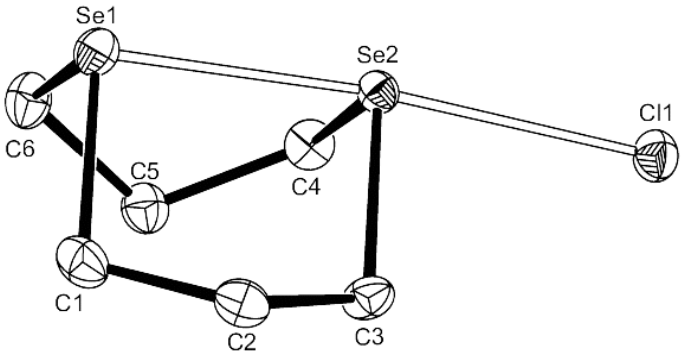

Figure 6.8 Structure of the cation in $[\{[8]aneSe_2Cl\}][GaCl_4]$.[1]

$[8]aneSe_2$ is not air-sensitive and can be stored over of several months without oxidation occurring, this suggests that these reactions are promoted by the $GaCl_3$.

6.1.2 In(III) halide complexes with thio- and selenoether ligands

InX_3 complexes with chalcogenoethers are much more structurally diverse than for GaX_3 and InX_3 show a much wider coordination chemistry when reacted with the same set of ligands.[1, 11] Examples of indium complexes with distorted tetrahedral and octahedral geometries have been observed, as well as compounds containing different ratios of ligand to metal.[10, 11] Chelating bidentate chalcogenoether ligands have been shown to form three structure types, neutral halide-bridged dimers, octahedral cations and distorted tetrahedral species.[11] Examples of a chloro-bridged dimer and a mononuclear octahedral cation are shown in figures 6.9 and 6.10 respectively. These results demonstrate how small structural changes to the ligand structure can produce very different products in this part of the periodic table.

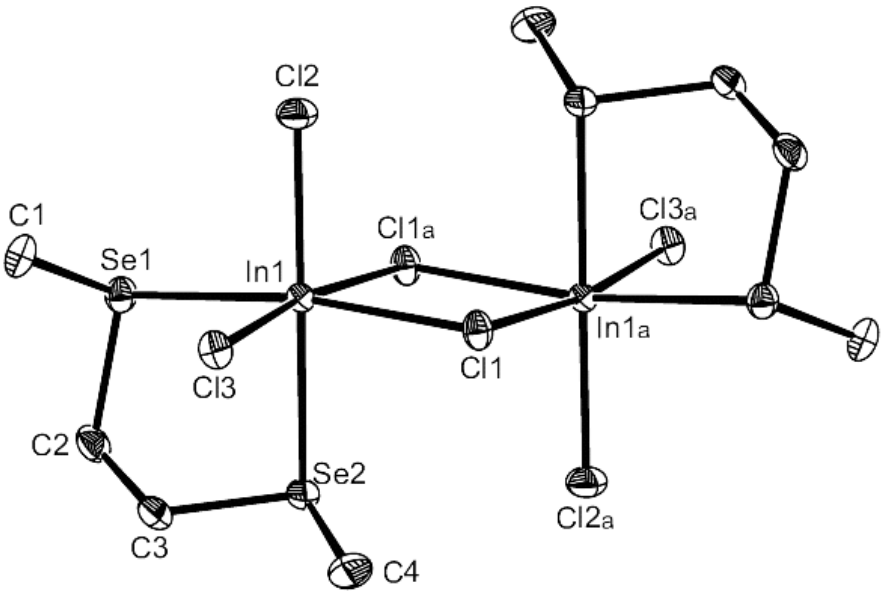

Figure 6.9 Structure of $[In_2Cl_6\{CH_3Se(CH_2)_2SeCH_3\}_2]$.[11]

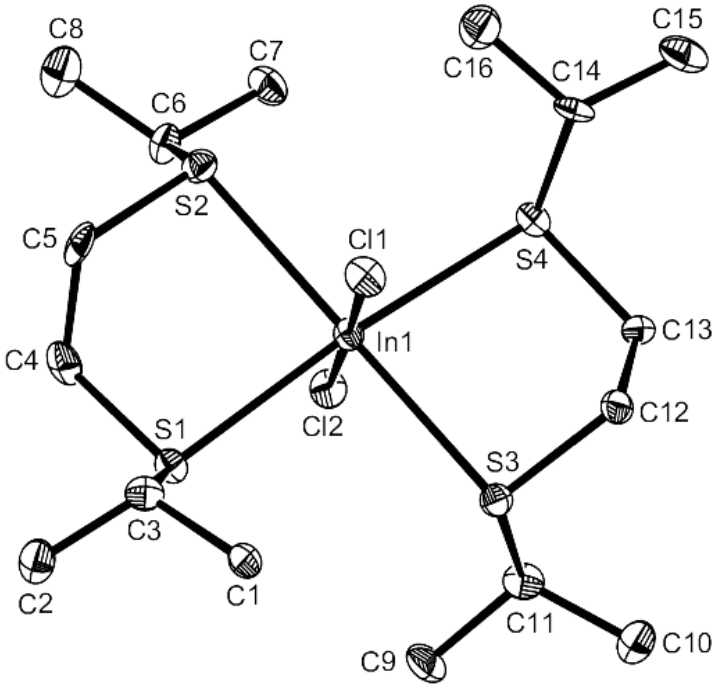

Figure 6.10 Structure of the *trans*-$[InCl_2\{^iPrS(CH_2)_2S^iPr\}_2]^+$ cation (isolated as its $[InCl_4]^-$ salt).[11]

In order to develop further the coordination chemistry and explore the factors affecting the formation and structures of Ga(III) and In(III) complexes, each of the thio- and seleno-ether ligands synthesised in Chapter 2 were reacted with gallium and indium halides then characterised with a variety of spectroscopic and structural techniques.

6.2 Results and discussion

Synthesis of each complex was typically performed under a dry nitrogen atmosphere in anhydrous CH_2Cl_2 solution to prevent hydrolysis and coordination of the solvent. MeCN (weak donor solvent) was added in some cases to increase solubility during the reaction, particularly in the reactions of $InCl_3$, to increase yield and purity.

Full characterisation of the products required several spectroscopic and analytical techniques. Microanalyses allowed the identification of the products stoichiometries, while IR and Raman spectroscopy were performed on each sample to determine the presence or

absence of $[MCl_4]^-$ ion[15, 16] or a S/Se coordinated to MCl_3, by comparison with literature data.[10-12]

^{1}H NMR spectroscopic studies provided only limited structural information due to the lability of the Ga(III) and In(III) complexes in solution. However, where possible, ^{77}Se, ^{71}Ga NMR studies were performed to provide supporting evidence.

X-ray crystallographic studies were performed on a range of examples for which single crystals were obtained; this enabled definitive identification of their structures and comparisons with the earlier work in the area.

6.2.1 Bidentate thio- and selenoether ligand complexes

A range of simple mono- and bi-dentate thio- and seleno-ethers complexes with $GaCl_3$ and $InCl_3$ have been described in earlier studies.[11, 12] As part of this project ligands with greater geometric and/or steric constraints have been used to investigate the effect of different ligand architectures. The bidentate ligands shown in figure 6.11 were selected for study with $GaCl_3$ and $InCl_3$.

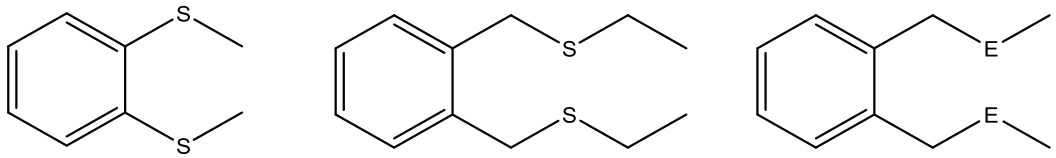

Figure 6.11 The rigid *o*-$C_6H_4(SCH_3)_2$ and semi-rigid *o*-$C_6H_4(CH_2ECH_2CH_3)$, *o*-$C_6H_4(CH_2ECH_3)$ (E = S or Se) ligands used in this work.

Reactions with $(CH_2)_2C(CH_2SeCH_3)_2$

The cyclopropyl-linked ligand $[(CH_2)_2C(CH_2SeCH_3)_2]$ was reacted with 2 mol. eq. of $GaCl_3$ and 1 mol. eq. of $InCl_3$. The reaction with indium produced an intractable mixture of species. Reacting $GaCl_3$ with $[(CH_2)_2(CH_2SeCH_3)_2]$ in anhydrous CH_2Cl_2 led to fragmentation at C–Se, forming a yellow oil containing a complex mixture of species including the selenonium cation, $[(CH_2)_2C(CH_2)_2SeCH_3]^+$ identified by positive ion ESMS (*m/z* = 163) and $[GaCl_4]^-$ anion (*m/z* = 211).

Synthesis of $[(GaCl_3)_2\{o\text{-}C_6H_4(SCH_3)_2\}]$ and $[InCl_3\{o\text{-}C_6H_4(SCH_3)_2\}]$

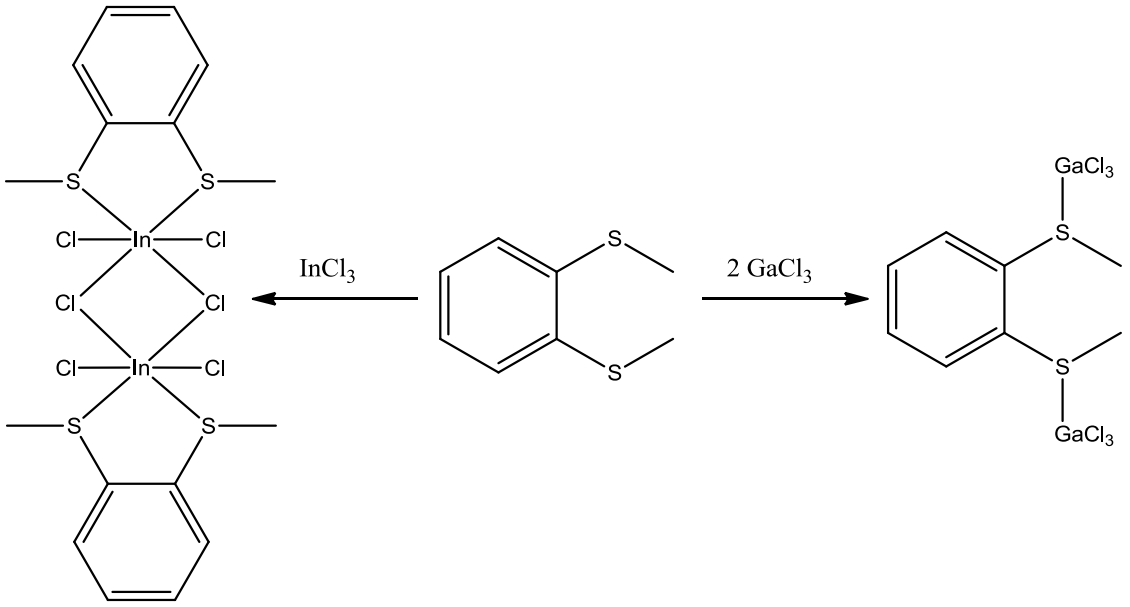

Figure 6.12 Scheme showing reaction of *o*-$C_6H_4(SCH_3)_2$ with MCl_3 (M = Ga or In).

Reacting 1 mol. eq. of $InCl_3$ with *o*-$C_6H_4(SCH_3)_2$ in CH_2Cl_2 produces a white solid with a 1:1 stoichiometry which is most likely to be a chloro-bridged dimer with a distorted octahedral Cl_4S_2 donor set. Indium trihalide complexes with similar ligands, such as $[(InCl_3)_2\{CH_3Se(CH_2)_2SeCH_3\}_2]$, have been shown to form chloro-bridged dimers.[11] Comparison of the far-IR data show absorptions at 302 and 257 cm^{-1} which compare well with literature data for $[(InCl_3)_2\{CH_3Se(CH_2)_2SeCH_3\}_2]$ (300 and 247 cm^{-1}) additionally, there is no spectroscopic data for the presence of $[MCl_4]^-$. Microanalysis data is consistent with a 1:1 stoichiometry suggesting the formation of a chloro-bridged dimer is likely, however, the absence of crystallographic evidence makes this formulation is uncertain.

Reacting *o*-$C_6H_4(SCH_3)_2$ with 2 mol. eq. of $GaCl_3$ in CH_2Cl_2 produces a pale orange solid, ^1H NMR data shows a coordination shift of 0.47 ppm to high frequency at the terminal methyl group, comparison of the far-IR data shows broad peak at 395 cm^{-1} which compares well the data collected for $[(GaCl_3)_2\{o\text{-}C_6H_4(CH_2SEt)_2\}]$ (394 cm^{-1}). Microanalytical data are ~1 % high for carbon and hydrogen, probably due to the sensitivity of the product; with this in mind the product is tentatively formulated as

[$(GaCl_3)_2${*o*-$C_6H_4(SCH_3)_2$}] with Ga(III) adopting a distorted tetrahedral Cl_3S coordination geometry.

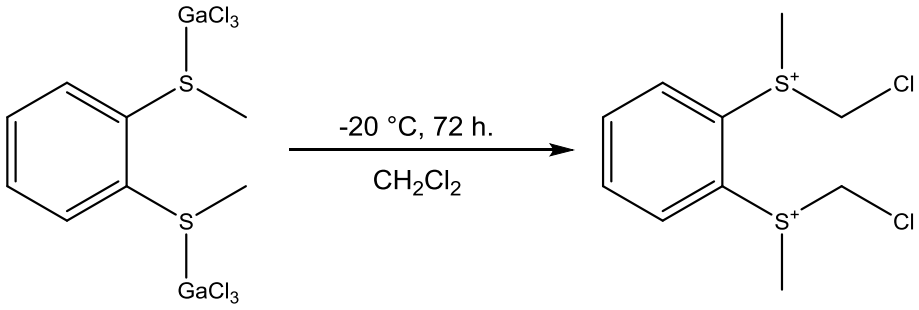

Figure 6.13 Formation of [*o*-$C_6H_4(SCH_3CH_2Cl)_2$][$GaCl_4$]$_2$.

Crystals were grown from a CH_2Cl_2 solution of [$(GaCl_3)_2${*o*-$C_6H_4(SCH_3)_2$}] left at –20 ^oC (freezer) for several days. The structural data indicate that these conditions led to further reaction with the CH_2Cl_2 solvent (see figure 6.13). Crystallographic analysis showed the product to be [*o*-$C_6H_4(SCH_3CH_2Cl)_2$][$GaCl_4$]$_2$, containing discrete bis-sulfonium dications (figure 6.14) and tetrahedral $[GaCl_4]^-$ anions. IR spectroscopy confirms the presence of $[GaCl_4]^-$ and did not show any other absorptions observed in [$(GaCl_3)_2${*o*-$C_6H_4(SCH_3)_2$}]. $[GaCl_4]^-$ is the only significant anion present in the negative ion ESMS (MeCN). Several species are observed in the positive ion ESMS; $[o\text{-}C_6H_4(SCH_3)(SCH_3CH_2Cl)]^+$ is the major species (*m/z* = 219), while a weaker feature consistent with $[o\text{-}C_6H_4(SCH_3)(SCH_3)]^+$ is also clearly evident (*m/z* = 185). All attempts to crystallise the neutral gallium complex from MeCN were unsuccessful. The formation of the sulfonium dication is likely to occur from a nucleophilic attack of the thioether sulfur onto the CH_2Cl_2 and its formation is very unusual, as the dithioether itself is stable in CH_2Cl_2 solution. It is therefore likely that the reaction is promoted by the $GaCl_3$ polarising the C-Cl bond in CH_2Cl_2.

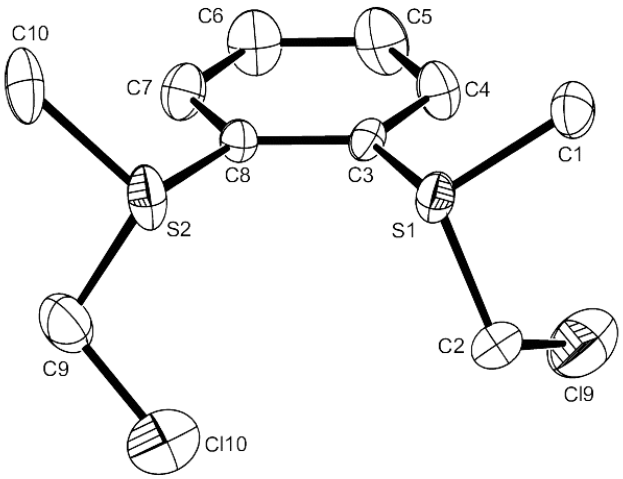

Figure 6.14 View of the structure of the sulfonium dication in [*o*-$C_6H_4(SCH_3CH_2Cl)_2$][$GaCl_4$]$_2$ with atom numbering scheme. Ellipsoids are shown at the 50% probability level and H atoms are omitted for clarity.

S1–C1 = 1.786(8)	S2–C8 = 1.790(7)
S1–C2 = 1.820(8)	S2–C9 = 1.821(9)
S1–C3 = 1.779(7)	S2–C10 = 1.812(9)
C1–S1–C2 = 101.3(4)	C8–S2–C9 = 101.1(4)
C1–S1–C3 = 104.9(4)	C8–S2–C10 = 104.0(4)
C2–S1–C3 = 103.5(4)	C9–S2–C10 = 100.7(4)

Table 6.2 Selected bond lengths (Å) and angles (°) for [*o*-$C_6H_4(SCH_3CH_2Cl)_2$][$GaCl_4$]$_2$.

[($GaCl_3$)$_2${*o*-$C_6H_4(CH_2SCH_2CH_3)_2$}]

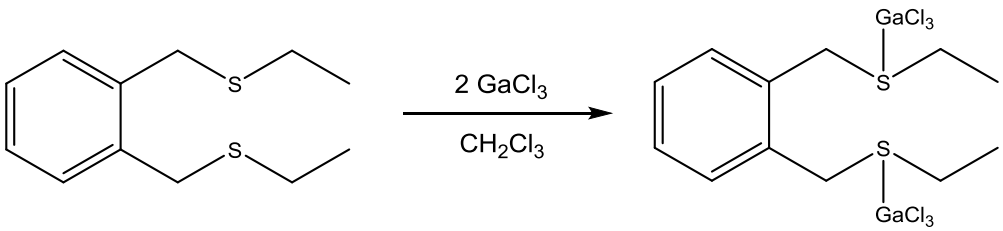

Figure 6.15 Scheme showing the reaction of *o*-$C_6H_4(CH_2SCH_2CH_3)_2$ with $GaCl_3$.

Reacting [*o*-$C_6H_4(CH_2SEt)_2$] with 2 mol. eq. of $GaCl_3$ under similar conditions to those already described gives a pale yellow solid. The product, like the other gallium complexes discussed in this chapter, was highly moisture sensitive. However, crystals were grown by placing the reaction filtrate in the freezer for several days. The structure shows a dinuclear complex, [$(GaCl_3)_2${*o*-$C_6H_4(CH_2SEt)_2$}] as shown in figure 6.16.

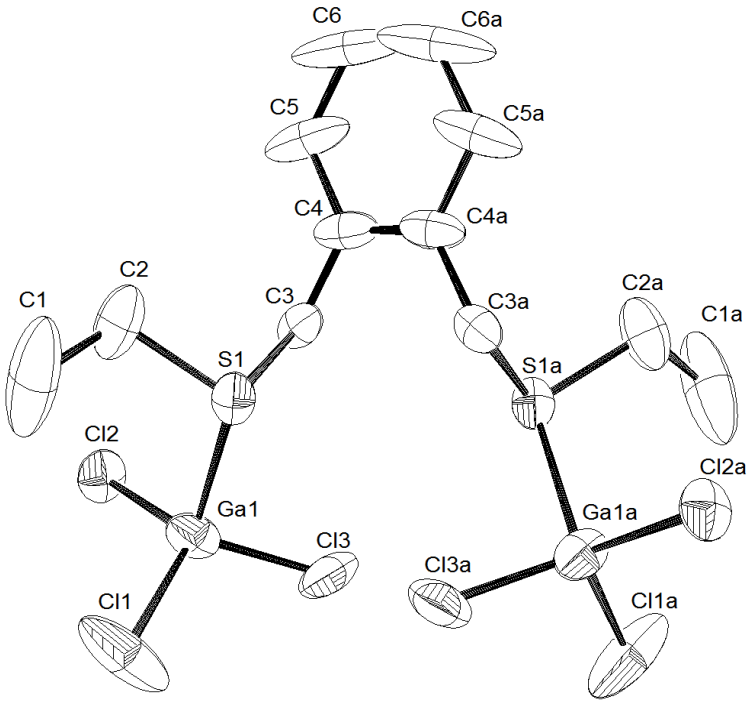

Figure 6.16 View of the structure of [$(GaCl_3)_2${*o*-$C_6H_4(CH_2SEt)_2$}] with atom numbering scheme. Ellipsoids are shown at the 50% probability level and H atoms are omitted for clarity. Symmetry operation: a = 1–x, y, ½ – z.

S1–Ga1 = 2.351(2)	Ga1–Cl1 = 2.132(3)
Ga1–Cl2 = 2.158(3)	Ga1–Cl3 = 2.156(3)

Cl1–Ga1–S1 = 107.27(7)	Cl1–Ga1–Cl2 = 113.4(1)
Cl2–Ga1–S1 = 105.78(8)	Cl1–Ga1–Cl3 = 114.3(1)
Cl3–Ga1–S1 = 103.07(9)	Cl2–Ga1–Cl3 = 111.9(1)

Table 6.3 Selected bond lengths (Å) and angles (°) for [$(GaCl_3)_2${*o*-$C_6H_4(CH_2SEt)_2$}].

The bond lengths and angles are unexceptional when compared to other similar structures from the literature.[12, 14] The complex contains two distorted tetrahedral gallium atoms, with Cl_3S coordination at Ga and with the S substituents *anti*. Microanalysis data is consistent with a 2:1 stoichiometry, two peaks are present in the far-IR region 394 cm^{-1} and 357 cm^{-1} and no absorption that can be assigned to $[MCl_4]^-$. The ^1H NMR spectrum is simple with resonances shifted to high frequency from the free ligand. The ^{71}Ga resonance (233 ppm) is consistent with other similar gallium halide complexes from literature.[12]

$[(InCl_3)_4\{o\text{-}C_6H_4(CH_2SCH_2CH_3)_2\}_3]$

When $InCl_3$ was reacted with $[o\text{-}C_6H_4(CH_2SCH_2CH_3)_2]$ in a 1:1 ratio, a colourless crystalline complex was produced. Microanalysis data unexpectedly showed the product contained a 4:3 In : dithioether ratio with no tetrachloroindate anion evident in the far IR region.

The crystal structure (figure 6.17) and microanalysis shows the complex to be $[(InCl_3)_4\{o\text{-}C_6H_4(CH_2SEt)_2\}_3]$, a discrete tetranuclear moiety with mirror symmetry. The central indium atom (In3) is coordinated octahedrally to six bridging chlorine atoms. The three other indium atoms (In1, In2 and In2a) are coordinated octahedrally via two bridging chlorines, two terminal chlorines and two mutually *trans* sulfur donor atoms from different ligands.

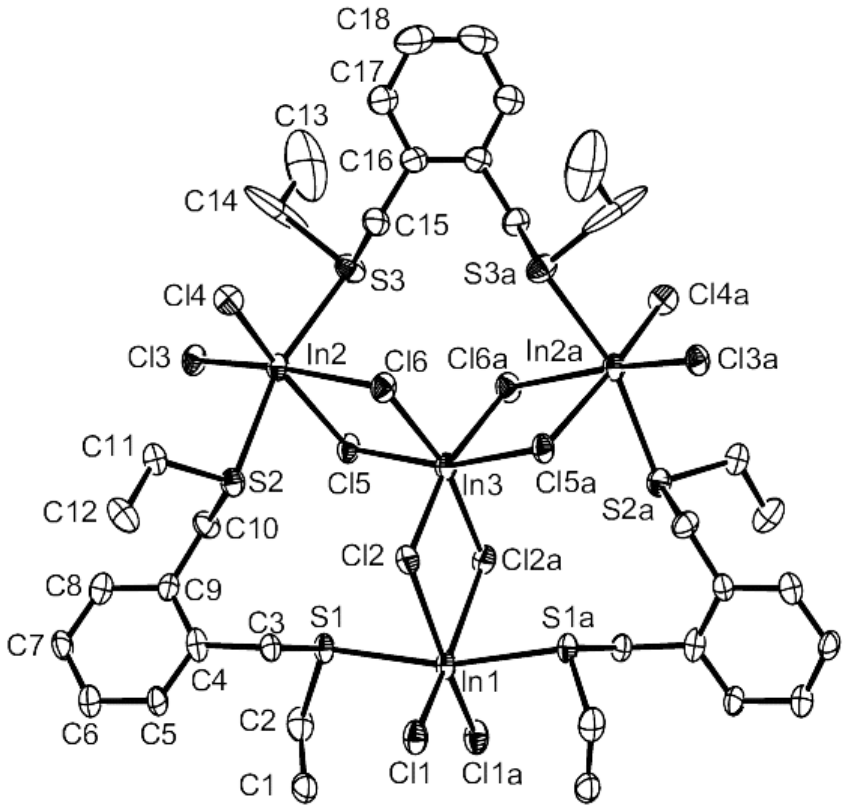

Figure 6.17 View of the structure of $[(InCl_3)_4\{o\text{-}C_6H_4(CH_2SEt)_2\}_3]$ with atom numbering scheme. Ellipsoids are shown at the 50% probability level and H atoms are omitted for clarity. Symmetry operation: a = –x, y, ½ – z.

In1–Cl1	2.396(3)	In1–Cl2	2.693(3)
In1–S1	2.646(2)	In2–Cl3	2.408(2)
In2–Cl4	2.407(3)	In2–Cl5	2.658(3)
In2–Cl6	2.639(2)	In2–S2	2.655(3)
In2–S3	2.657(3)	In3–Cl2	2.509(3)
In3–Cl5	2.496(2)	In3–Cl6	2.546(3)
Cl1a–In1–Cl1	105.25(14)	Cl1a–In1–S1	92.87(8)
Cl1–In1–S1	96.10(8)	S1–In1–S1a	165.20(12)
Cl1–In1–Cl2a	164.03(9)	S1–In1–Cl2a	88.38(8)
Cl1–In1–Cl2	89.77(9)	S1–In1–Cl2	79.93(8)
Cl2a–In1–Cl2	75.89(11)	Cl4–In2–Cl3	100.67(9)
Cl4–In2–Cl6	90.76(9)	Cl3–In2–Cl6	168.49(9)
Cl4–In2–S2	96.18(9)	Cl3–In2–S2	93.17(8)
Cl6–In2–S2	86.87(8)	Cl4–In2–S3	93.83(9)
Cl3–In2–S3	94.47(9)	Cl6–In2–S3	83.33(9)
S2–In2–S3	166.07(9)	Cl4–In2–Cl5	168.99(8)
Cl3–In2–Cl5	90.14(8)	Cl6–In2–Cl5	78.49(8)
S2–In2–Cl5	80.97(8)	S3–In2–Cl5	87.37(9)
Cl5a–In3–Cl5	163.13(13)	Cl5a–In3–Cl2	90.01(8)
Cl5–In3–Cl2	102.72(8)	Cl2a–In3–Cl2	82.63(12)
Cl5a–In3–Cl6	86.17(8)	Cl2a–In3–Cl6	167.02(8)
Cl5–In3–Cl6	83.30(8)	Cl5a–In3–Cl6	86.17(8)
Cl2a–In3–Cl6	167.02(8)	Cl2–In3–Cl6	87.99(9)
Cl6a–In3–Cl6	102.58(13)	In1–Cl2–In3	100.74(9)
In2–Cl5–In3	99.49(8)	In2–Cl6–In3	98.71(8)

Table 6.4 Selected bond lengths (Å) and angles (°) for $[(InCl_3)_4\{o\text{-}C_6H_4(CH_2SEt)_2\}_3]\cdot 2CH_2Cl_2$.

Symmetry operation: a = –x, y, ½ – z.

The structure was very unexpected and only one other similar example can be found in the literature, $[(BiCl_3)_4\{o\text{-}C_6H_4(CH_2SCH_3)_2\}_3]$, in which the thioether also incorporates the large *o*-xylyl linkage.[17] This suggests that the arrangement in which the ligand bridges two metals produces a more stable species compared to the formation of a seven membered chelate ring. This differs from the majority of other transition metal complexes containing this ligand architecture, where bidentate chelation typically occurs, with E–M–E angles significantly greater than 90°.[18, 19]

Bond lengths for In–S and In–Cl are comparable to other indium thioether complexes,[11] the In–S bond distances (*ca.* 2.65 Å) are approximately 0.25 Å longer than the terminal In–Cl bonds despite sulfur and chlorine being neighbouring elements in the periodic table, suggesting weak, secondary In- - -S coordination.

6.2.2 Tetradentate thio- and selenoether ligand complexes

The tetradentate ligands $C(CH_2SCH_3)_4$, $C(CH_2SeCH_3)_4$ and $1,2,4,5\text{-}C_6H_2(CH_2SCH_3)_4$ were reacted with MCl_3 (M = Ga or In) to investigate the effect of ligand architecture upon the product obtained.

$[\{GaCl_3\}_4\{1,2,4,5\text{-}C_6H_2(CH_2SCH_3)_4\}]$

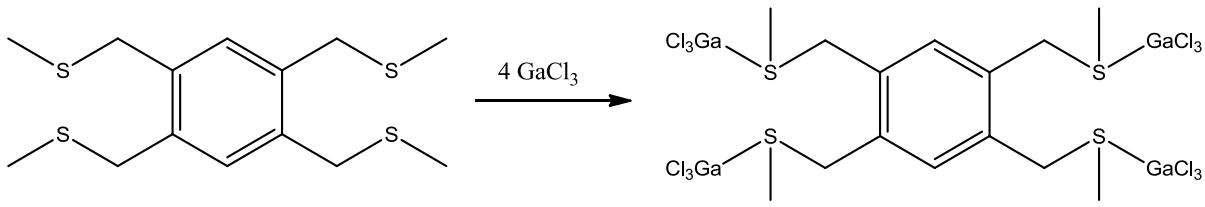

Figure 6.18 Scheme showing reaction of $1,2,4,5\text{-}C_6H_2(CH_2SCH_3)_4$ with $GaCl_3$.

Reacting four equivalents of $GaCl_3$ with $1,2,4,5\text{-}C_6H_2(CH_2SCH_3)_4$ in CH_2Cl_2 produces a pink, highly sensitive solid; the product has poor solubility in non-donor solvents which is unsurprising as most complexes involving the tetrabenzyl ligand framework are poorly soluble when compared to the saturated ligands used in this work. Microanalytical data were consistent with the product shown in figure 6.18. IR spectroscopy showed a broad

peak at 374 cm^{-1} which compares well with the literature data for $[(GaCl_3)_2\{o\text{-}C_6H_4(CH_2SCH_3)_2\}]$ (370 cm^{-1}).[12] ^1H NMR spectroscopy showed resonances at 2.41 ppm (CH_3) and 4.11 ppm (CH_2) giving a coordination shifts of 0.36 ppm and 0.30 ppm to high frequency respectively.

Reaction of $InCl_3$ with 1,2,4,5-$C_6H_2(CH_2SCH_3)_4$

Using either 2 or 4 mol. eq. of $InCl_3$ with 1,2,4,5-$C_6H_2(CH_2SCH_3)_4$ in CH_2Cl_2 gave a highly moisture sensitive white solid with very poor solubility in both cases. Although no $[InCl_4]^-$ was detected in the IR spectrum, microanalysis and mass spectroscopy showed addition $InCl_3$ leads to a mixture of species with no major identifiable product.

$[\{GaCl_3\}_4\{C(CH_2SCH_3)_4\}]$

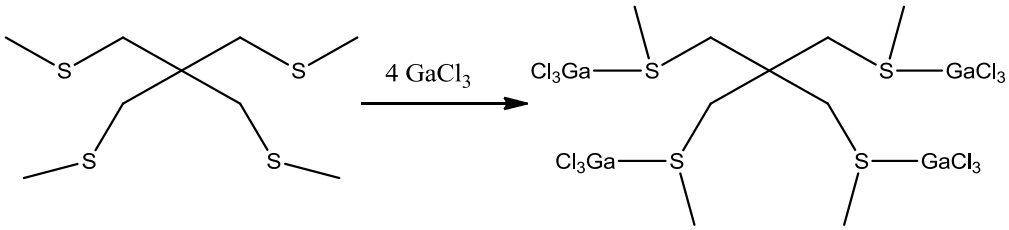

Figure 6.19 Scheme showing the reaction of $C(CH_2SCH_3)_4$ with $GaCl_3$.

Reacting 4 mol. eq. of $GaCl_3$ with $C(CH_2SCH_3)_4$ in anhydrous CH_2Cl_2 produced a highly moisture sensitive dark yellow oil with a 4:1 ratio of $GaCl_3$ to ligand (based upon the microanalytical data), probably with the structure shown in figure 6.19. The infrared spectrum showed a broad peak at 390 cm^{-1} and a second shoulder peak at 360 cm^{-1}, which not an exact match to the literature data for $[(GaCl_3)_2\{o\text{-}C_6H_4(CH_2SCH_3)_2\}]$ (370 cm^{-1})[12] the difference could be attributed to differences in the ligand structure however this seems unlikely. $[GaCl]_4^-$ shows a single sharp absorption in a similar region (386 cm^{-1})[20] however, no sharp peak was observed at 386 cm^{-1} when lowering the concentration in the Nujol mull during an attempt to further resolve the two recorded absorptions. ^1H NMR spectroscopy ($CDCl_3$) showed a high frequency coordination shift of 0.25 ppm for the resonance assigned to the terminal methyl groups, while the resonance assigned to CH_2 showed a low frequency coordination shift of 0.14 ppm. Microanalysis also confirmed the

stoichiometry and purity of the product. As the product is an oil, collection of crystallographic data was not possible. The ^{71}Ga NMR spectrum showed a resonance at +251 ppm, which correlates well with +252 ppm reported for $[(GaCl_3)_3\{CH_3C(CH_2SCH_3)_3\}]$,[12] suggesting the product adopts the same distorted tetrahedral geometry at gallium.

Reaction of $InCl_3$ with $C(CH_2SCH_3)_4$

Reacting 2 mol. eq. of $InCl_3$ with $C(CH_2SCH_3)_4$ in CH_2Cl_2 produced a moisture sensitive insoluble white the solid. No ^{1}H NMR or mass spectrometry data could be collected as the product appeared to completely insoluble. Microanalysis confirmed the 1:1 stoichiometry of the product and as no other species were observed in either ^{1}H NMR or mass spectrometry, therefore it may assumed this is not a mixture of species, but a single insoluble product. Infrared spectroscopy showed three absorptions at 324, 308 and 241 cm^{-1} with no absorptions correlating to $[InCl_4]^-$. This in mind the product is most likely a polymer with indium coordinated by sulfur atoms in an infinite chain however, the absence of crystallographic evidence makes this formulation uncertain.

Reaction of $(GaCl_3)_4$ with $C(CH_2SeCH_3)_4$

The tetraselenoether $C(CH_2SeCH_3)_4$, fragments at the C–Se units when reacted with 4 mol, eq. of $GaCl_3$. The product is a yellow oil which contained a mixture of selenonium species, most of which were unidentifiable. However, the selenonium cation, $[(CH_2)_2C(CH_2)_2SeCH_3]^+$ was identified by positive ion ESMS (*m/z* = 163). Infrared spectroscopy showed single sharp absorption at 387 cm^{-1} identified as $[GaCl_4]^-$ ion, literature data (386 cm^{-1})[20]. Mass spectrometry also confirmed the presence $[GaCl_4]^-$ (*m/z* = 211).

6.3 Conclusions

A series of $GaCl_3$ and $InCl_3$ complexes containing multi-dentate chalcogeno-ether ligands have been synthesised and characterised spectroscopically and structurally. Crystallographic and other spectroscopic data in this chapter has shown that gallium and indium complexes with Group16 ligands can form diverse range of geometries, unlike

previous studies where distorted tetrahedral and octahedral geometries were usually observed.

Several Ga(III) complexes produced contained four coordinate gallium in presumably with distorted tetrahedral geometry and Cl_3E (E= S or Se) donor set. Despite sensitivity of the complexes preventing X-ray crystallography of most complexes, $[(GaCl_3)_2\{o\text{-}C_6H_4(CH_2SEt)_2\}]$ was structurally characterised. The highly Lewis acid properties of $GaCl_3$,[1, 3] were also shown to promote unique reaction chemistry demonstrated during the reaction of $GaCl_3$, $o\text{-}C_6H_4(SCH_3)_2$ and CH_2Cl_2 where a sulfonium cation was produced during attempts to crystallise $[(GaCl_3)_2\{o\text{-}C_6H_4(SCH_3)_2\}]$.

In(III) compounds produced were often highly insoluble with making characterisation challenging, most complexes produced were presumed to contain octahedral indium. However, slightly variations in ligand architecture can produce very different products, the reaction of $o\text{-}C_6H_4(CH_2SCH_3)_2$ with $InCl_3$, produces a white solid presumed to be a chloro-bridged dimer. Whereas, the same reaction conditions with the ethyl analogue of the same ligand produced the tetranuclear $[(InCl_3)_4\{o\text{-}C_6H_4(CH_2SEt)_2\}_3]$. This tetranuclear structure is very unusual, similar structures have not been reported in d-block chalcogenoether chemistry.

Compound	[{o-$C_6H_4(SCH_3CH_2Cl)_2$}$_2$]$(GaCl_4)_2$]	[$(GaCl_3)_2${o-$C_6H_4(CH_2SEt)_2$}]	[$(InCl_3)_4${o-$C_6H_4(CH_2SEt)_2$}$_3$]·$2CH_2Cl_2$
Formula	$C_{10}H_{14}Cl_{10}Ga_2S_2$	$C_{12}H_{18}Cl_6Ga_2S_2$	$C_{38}H_{58}Cl_{16}In_4S_6$
M	692.27	578.52	1733.68
crystal syst.	monoclinic	monoclinic	monoclinic
Space group	$P2_1/c$ (no. 14)	C2/c (no. 15)	C2/c (no. 15)
a [Å]	9.4813(15)	18.561(4)	24.016(5)
b [Å]	14.009(3)	10.809(3)	18.726(5)
c [Å]	18.403(3)	13.495(3)	14.995(4)
α [deg]	90	90	90
β [deg]	104.377(10)	126.201(5)	114.76(2)
γ [deg]	90	90	90
U [Å^3]	2367.9(6)	3.384	6123(3)
Z	4	4	4
μ(Mo Kα) [mm^{-1}]	3.576	3.384	2.419
total no. reflns	27701	11619	69930
unique reflns	5415	2500	7092
R_{int}	0.066	0.0425	0.1492
no. of params, restraints	217, 0	100, 0	290, 0
R_1[b] [$I_o > 2\sigma(I_o)$]	0.073	0.074	0.083
R_1 [all data]	0.099	0.103	0.123
wR_2[b] [$I_o > 2\sigma(I_o)$]	0.181	0.126	0.146
wR_2 [all data]	0.199	0.140	0.160

[a] Common items: temperature = 120 K; wavelength (Mo Kα) = 0.71073 Å; θ(max) = 27.5°.
[b] $R_1 = \Sigma||F_o| - |F_c||/\Sigma|F_o|$. $wR_2 = [\Sigma w(F_o^2 - F_c^2)^2/\Sigma wF_o^4]^{1/2}$.

Table 6.5 Crystal data and structure refinement details[a].

6.4 Experimental

All preparations were performed under an atmosphere of dry N_2 using Schlenk techniques, and spectroscopic samples were prepared in a dry N_2-purged glove box.

6.4.1 Synthesis

$[(GaCl_3)_2\{o\text{-}C_6H_4(SCH_3)_2\}]$

$GaCl_3$ (0.22 g, 1.24 mmol) was dissolved in CH_2Cl_2 (5 mL) and *o*-$C_6H_4(SCH_3)_2$ (0.11 g, 0.62 mmol) was added dropwise with constant stirring. The solution was stirred for a further 10 mins., and then concentrated *in vacuo*, yielding a pale orange precipitate. The product was filtered off, washed with hexane (3 mL) and dried *in vacuo.* Yield: 0.22 g, 68%. Anal. Calcd for $C_8H_{10}Cl_6Ga_2S_2$: C 18.4, H 1.9. Found: C 19.0, H 2.4%. IR (cm^{-1}, Nujol): 395(br), 366(sh). ^1H NMR ($CDCl_3$, 295 K): 2.92 (s, [6H], Me), 7.6–7.7 (m, [4H], aromatic CH) ppm. ^{71}Ga {^1H} NMR: (CH_2Cl_2, 295 K): 250 ($w_{1/2}$ = 1100 Hz) ppm.

$[o\text{-}C_6H_4(SCH_3CH_2Cl)_2][GaCl_4]_2$

A solution of $[(GaCl_3)_2\{o\text{-}C_6H_4(SCH_3)_2\}]$ in anhydrous CH_2Cl_2 was left to stand at –20 °C under an inert atmosphere for *ca.* one week, furnishing a small number of pale yellow crystals shown by X-ray crystallographic analysis to be $[o\text{-}C_6H_4(SCH_3CH_2Cl)_2\}][GaCl_4]_2$. Positive ion ESMS (MeCN) on the crystals: found *m/z* = 219 $[o\text{-}C_6H_4(SCH_3)(SCH_3CH_2Cl)]^+$; negative ion ESMS (MeCN): found *m/z* = 211$[GaCl_4]^-$. IR (cm^{-1}, Nujol): 381 (s).

$[(InCl_3)_2\{o\text{-}C_6H_4(SCH_3)_2\}_2]$

$InCl_3$ (0.22 g, 1.0 mmol) was suspended in CH_2Cl_2 (7 mL) and *o*-$C_6H_4(SCH_3)_2$ (0.17 g, 1.0 mmol) was added dropwise with constant stirring. The solution was stirred for a further 1 h, filtered and the solid was washed with CH_2Cl_2 (5 mL). The product was then dried *in vacuo* to yield a white solid. Yield: 0.20 g, 51%. Anal. Calcd for $C_8H_{10}Cl_3InS_2$: C, 24.5; H, 2.6. Found: C, 24.3; H, 2.6%. IR (cm^{-1}, Nujol): 302 (s), 257 (s). Raman (cm^{-1}): 307 (s), 280 (s). ^1H NMR ($CDCl_3$, 295 K): 2.50 (s, [6H], Me), 7.1–7.4 (m, [4H], aromatic CH) ppm.

[$(GaCl_3)_2${*o*-$C_6H_4(CH_2SEt)_2$}]

$GaCl_3$ (0.22 g, 1.24 mmol) was dissolved in CH_2Cl_2 (5 mL) and *o*-$C_6H_4(CH_2SEt)_2$ (0.14 g, 0.62 mmol) was added dropwise. The solution was stirred for a further 10 mins and then concentrated *in vacuo*, yielding a pale yellow precipitate. The product was filtered off, washed with cold CH_2Cl_2 (3 mL) and dried *in vacuo.* Yield: 0.23 g, 64%. Crystals were grown from the filtrate stored at –20 °C for 2 days. Anal. Calcd for $C_{12}H_{18}Cl_6Ga_2S_2$: C 24.9, H 3.1. Found: C 24.5, H 2.5%. IR (cm^{-1}, Nujol): 394 (s), 357 (m). ^{1}H NMR (d_6-acetone, 295 K): 1.23 (t, [6H], ^3J = 6 Hz, CH_2CH_3), 2.50 (q, [4H], CH_2CH_3), 3.94 (s, [4H], SCH_2Ar), 7.2–7.4 (m, [4H], aromatic CH) ppm. ^{71}Ga {^{1}H} NMR: (CH_2Cl_2, 295 K): 233 ($w_{1/2}$ = 10 000 Hz) ppm.

[$(InCl_3)_4${*o*-$C_6H_4(CH_2SEt)_2$}$_3$]

$InCl_3$ (0.22 g, 1.0 mmol) was suspended in CH_2Cl_2 (7 mL) and *o*-$C_6H_4(CH_2SEt)_2$ (0.23 g, 1.0 mmol) was added dropwise with constant stirring. After 1 h the solid was filtered to remove undissolved $InCl_3$, and the filtrate was placed in the freezer at –18 °C for 2 weeks to give colourless crystals. Yield: 0.043 g, 10%. Anal. Calcd for $C_{36}H_{54}Cl_{12}In_4S_6 \cdot 2CH_2Cl_2$: C, 26.3; H, 3.4. Found: C, 26.1; H, 3.8. IR (cm^{-1}, Nujol): 341(s), 330(s), 307(s). ^{1}H NMR (CD_2Cl_2, 295 K): 1.28 (t, [6H], ^3J = 6 Hz, CH_2CH_3), 2.54 (q, [4H], CH_2CH_3), 3.94 (s, [4H], SCH_2Ar), 7.2–7.4 (m, [4H], aromatic CH) ppm.

[{$GaCl_3$}$_4${1,2,4,5-$C_6H_2(CH_2SCH_3)_4$}]

$GaCl_3$ (0.22 g, 1.24 mmol) was dissolved in CH_2Cl_2 (5 mL) and 1,2,4,5-$C_6H_2(CH_2SCH_3)_4$ (0.10 g, 0.31 mmol) was added dropwise with constant stirring. The solution was stirred for a further 10 min., concentrated *in vacuo*, yielding a pink precipitate. The product was filtered off, washed with cold CH_2Cl_2 (3 mL) and dried *in vacuo.* Yield: 0.16 g, 53%. Anal. Calcd for $C_{14}H_{22}S_4Ga_4Cl_{12}$: C 16.4, H 2.2. Found: C 15.3, H 2.3%. IR (cm^{-1}, Nujol): 374 (br). Raman (cm^{-1}): 362. ^{1}H NMR ($CDCl_3$ 295 K) 2.41 (s, [6H]), 4.11 (s, [4H]), 7.3 (s, [2H]) ppm.

[{$GaCl_3$}$_4${$C(CH_2SCH_3)_4$}]

$GaCl_3$ (0.22 g, 1.24 mmol) was dissolved in CH_2Cl_2 (5 mL) and $C(CH_2SCH_3)_4$ (0.08 g, 0.31 mmol) was added dropwise with constant stirring. After 10 min., the solvent was

removed *in vacuo*, yielding a dark yellow oil. 0.15 g, 50%. Anal. Calcd for $C_9H_{20}S_4Ga_4Cl_{12}$: C 11.3, H 2.8. Found: C 11.2, H 2.9%. IR (cm^{-1}, Nujol): 390 (vbr), 360(sh). Raman (cm^{-1}): 390(sh), 360(br). ^1H NMR ($CDCl_3$ 295K) 2.37 (s, [12H]), 2.95 (s, [8H]) ppm. ^{71}Ga {^1H} NMR: (CH_2Cl_2 295K) 251 ppm.

[{$InCl_3$}$_2${$C(CH_2SCH_3)_4$}]

$InCl_3$ (0.22 g, 1 mmol) was suspended in CH_2Cl_2 (7 mL) and $C(CH_2SCH_3)_4$ (0.13 g, 0.5 mmol) was added dropwise with constant stirring. The solution was stirred for a stirred for a further 1 h., filtered and the solid washed with CH_2Cl_2 (5 mL). The product was then dried *in vacuo* to yield a white solid. Yield: 0.26 g, 76%. Anal. Calcd for $C_9H_{20}S_4In_2Cl_6$: C 15.5, H 2.9. Found: C 14.6, H 2.9%. IR (cm^{-1}, Nujol): 324, 308, 241. Raman (cm^{-1}): 313, 302, 254.

6.4.2 X-ray crystallography experimental

Details of the crystallographic data collection and refinement parameters are given in Table 1. Crystals were obtained as described above. Structure solution and refinement were generally routine,[17, 18] except as described below, with hydrogen atoms on C added to the model in calculated positions and using the default C–H distance. The diffraction data for [$(GaCl_3)_2${*o*-$C_6H_4(CH_2SEt)_2$}] and [$(InCl_3)_4${*o*-$C_6H_4(CH_2SEt)_2$}$_3$] were modelled by Dr. M. Light. [$(GaCl_3)_2${*o*-$C_6H_4(CH_2SEt)_2$}] display characteristics indicative of a modulated structure. Indexing was possible using most reflections and a large cell (*a* = 13.4632, *b* = 53.8898, *c* = 15.1497 Å, β = 99.554^o (P)) but this did not lead to a solution. Indexing was also possible using a smaller C-centred monoclinic cell and a modulation vector 0.0069, –0.6039, –0.0036 up to order 1. Using this cell and conventional data reduction, ignoring the modulation, leads to the solution presented here. The data for [$(InCl_3)_4${*o*-$C_6H_4(CH_2SEt)_2$}$_3$] were originally collected as triclinic (P), and later transformed to the monoclinic (C) cell presented here. The crystal quality for [$(InCl_3)_4${*o*-$C_6H_4(CH_2SEt)_2$}$_3$] was modest, and the structure refinement revealed some disorder of the C atoms of the Et substituents associated with S3 (and S3a) (elongated thermal ellipsoids) possibly suggesting that the molecule is disordered across the crystallographic mirror plane.

6.5 References

1. W. Levason, G. Reid and W. Zhang, *Dalton Trans.*, 2011, **40**, 8491.
2. W. Levason, S. Maheshwari, R. Ratnani, G. Reid, M. Webster and W. Zhang, *Inorg. Chem.*, 2010, **49**, 9036.
3. S. Dagorne and S. Bellmin-Laponnaz, *Group 13 Metals Aluminium, Gallium, Indium and Thallium*, Eds. Aldridge, S.; Downs, A. J., 2nd Edn. Blackie, London, UK, 2011, Chapter 11, p. 654
4. W. Levason and G. Reid, *Dalton Trans.*, 2001, 2953.
5. A. E. Reed and P. V. R. Schleyer, *J. Am. Chem. Soc.*, 1990, **112**, 1434.
6. R. E. Rundle, *J. Am. Chem. Soc.*, 1963, **85**, 112.
7. N. W. Alcock, *Adv. Inorg. Chem. Radiochem.*, 1972, **15**, 1.
8. *The Chemistry of Aluminium, Gallium, Indium and Thallium*, Ed. Downs A. J., Blackie, First Edn. London, UK, 1993, Chapter 1, p. 3.
9. G. Bandoli, A. Dolmella, F. Tisato, M. Porchia and F. Refosco, *Coord. Chem. Rev.*, 2009, **253**, 56.
10. S. Mishra, E. Jeanneau and S. Daniele, *Polyhedron*, 2010, **29**, 500.
11. C. Gurnani, M. Jura, W. Levason, R. Ratnani, G. Reid and M. Webster, *Dalton Trans.*, 2009, 1611.
12. C. Gurnani, W. Levason, R. Ratnani, G. Reid and M. Webster, *Dalton Trans.*, 2008, 6274.
13. K. George, M. Jura, W. Levason, M. E. Light, L. P. Ollivere and G. Reid, *Inorg. Chem.*, 2012, **51**, 2231.
14. W. Levason and G. Reid, *Comprehensive Coordination Chemistry II*, ed. J. A. McCleverty and T. J. Meyer, Elsevier, Oxford, 2004, vol. 1, p. 399.
15. W. Levason and T. Kemmitt, *Organometallics*, 1989, **8**, 1303.
16. R. J. Batchelor, F. W. B. Einstein, I. D. Gay, J.-H. Gu, B. D. Johnston and B. M. Pinto, *J. Am. Chem. Soc.*, 1989, **111**, 6582.
17. G. M. Sheldrick, SHELXS-97, Program for Crystal Structure Solution, University of Göttingen, Germany, 1997.
18. G. M. Sheldrick, SHELXL-97, Program for Crystal Structure Refinement, University of Göttingen, Germany, 1997.
19. W. Levason, M. Nirwan, R. Ratnani, G. Reid, N. Tsoureas and M. Webster, *Dalton Trans.*, 2007, 439.
20. K. Nakamoto, *IR Spectra of Inorganic and Coordination Compounds*, Wiley, New York, 2nd edn, 1970.
1. K. Brodersen, W. Roelz, G. Jordan, R. Gerbeth and J. Ellerman, *Chem. Ber.*, 1978, **111**, 132.

2. D. J. Gulliver, E. G. Hope, W. Levason, S. G. Murray, D. M. Potter and G. L. Marshall, *J. Chem. Soc., Perkin Trans. II*, 1984, 429.

3. E. G. Hope, T. Kemmitt and W. Levason, *Organometallics*, 1988, **7**, 78.

4. W. Levason, M. Nirwan, R. Ratnani, G. Reid, N. Tsoureas and M. Webster, *Dalton Trans.*, 2007, 439.

5. W. Levason and T. Kemmitt, *Organometallics*, 1989, **8**, 1303.

6. W. Levason, L. P. Ollivere, G. Reid, N. Tsoureas and M. Webster, *J. Organomet. Chem.*, 2009, **694**, 2299.

7. D. H. O'Brien, N. Deren, C. K. Huang, K. J. Irgolic and F. F. Knapp, *Organometallics*, 1983, **2**, 305.

8. N. P. Luthra and J. D. Odom, eds. S. Patai and Z. Rappoport, Wiley, NY, 1986, vol. 1, p. 189.

9. R. K. Chadha and J. E. Drake, *J. Organomet. Chem.*, 1986, **299**, 331.

10. Z.-L. Zhou, Y.-Z. Huang, Y. Tang, Z.-H. Chen, L.-P. Shi, X.-L. Jin and Q.-C. Yang, *Organometallics*, 1994, **13**.

11. N. J. Hill, W. Levason, G. Reid and A. J. Ward, *J. Organomet. Chem.*, 2002, **642**, 186.

12. R. J. Shine, in *Organic Selenium Compounds*, eds. D. L.Klayman and W. H. H. Gunther, Wiley, NY, 1973, ch. 6.

13. W. McFarlane and R. J. Wood, *J. Chem. Soc.*, 1972, 1397.

14. R. Pietschnig, S. Spirk, G. N. Rechberger and K. Merz, *Inorg. Chim. Acta.*, 2008, **361**, 1958.

15. S. D. Reid, A. L. Hector, W. Levason, G. Reid, B. J. Waller and M. Webster, *Dalton Trans.*, 2007, 4769.

16. C. Gurnani, W. Levason, R. Ratnani, G. Reid and M. Webster, *Dalton Trans.*, 2008, 6274.

17. W. Levason, B. Patel, G. Reid and A. J. Ward, *J. Organomet. Chem.*, 2001, **619**, 218.

18. A. J. Barton, W. Levason and G. Reid, *J. Organometal. Chem.*, 1999, **579**, 235.

19. G. M. Sheldrick, SHELXS-97, Program for Crystal Structure Solution, University of Göttingen, Germany, 1997.

20. G. M. Sheldrick, SHELXL-97, Program for Crystal Structure Refinement, University of Göttingen, Germany, 1997.

21. H. D. Flack, *Acta Crystallogr.*, 1983, **39**, 876.

CHAPTER 7

Conclusions and further work

The results presented in this thesis have shown that stepwise addition of two different metal centres to a tetradentate Group 16 ligand, is a possible synthetic route for the production hetero bimetallic molecules.

In order to complete this study a series of novel tetradentate chalcogenoether ligands were produced and characterised including some telluroether ligands. During the synthesis of $C(CH_2SeCH_3)_4$ the cyclopropyl ligand $(CH_2)_2C(CH_2SeMe)_2$ was found to be a major by product. The quantity the cyclopropyl ligand produced was shown to be dependant of molar ratio of reactants. In contrast, the same reaction with tellurium only produced the product.

Monometallic and homo-bimetallic complexes were prepared and characterised from each of these ligands. Metal carbonyl centres ($Mo(CO)_4$, $W(CO)_4$ and $Mn(CO)_3Cl$) were first investigated and although monometallic carbonyls could be produced in high purity they were shown to dissociate in solution and subsequent reactions. Consequently, a different metal system needed to be explored in order to allow the insertion of a second metal. A series of monometallic and homo-bimetallic Ru^{II} and Os^{II} *p*-cymene complexes were produced and found not to be susceptible to dissociation in solution, also homo-bimetallic complexes could be produced from addition of a metal precursor to a monometallic species.

The ligand type also played an important role when selecting appropriate candidates for further reactions. Spirocyclic ligand complexes were more soluble than the aromatic linked systems, so appeared to be more suitable for producing hetero-bimetallic species.

Homo-bimetallic ruthenium complexes with the spirocyclic ligand can be produced either directly or stepwise. However, attempts to introduce a second metal such as Os^{II} or Pt^{II} produced several mixed metal species. Addition of a metal precursor to a monometallic osmium complex with the same ligand was successful suggesting that osmium is less susceptible to substitution.

As discussed in chapter 1 the bimetallic molecules are of considerable interest in the catalysis industry while these complexes my not be directly relevant to a particular catalytic process. Further research could be performed with the view to producing bimetallic materials from precursors produced with this synthetic route. While this study

focused on specific ligand types and donor atoms, the methods and synthetic strategies developed in this work could be employed in the development of bimetallic moles with different metal combinations and donor types.

Appendix

Infrared spectra were recorded as Nujol mulls between CsI plates using a Perkin-Elmer Spectrum100 spectrometer over the range 4000–200 cm^{-1}. Raman spectra were obtained using a Perkin-Elmer FT2000R with a Nd:YAG laser. Significant bands in the range 400–200 cm^{-1} are listed below. ^{1}H NMR spectra were recorded in $CDCl_3$ or CD_2Cl_2 unless otherwise stated, using a Bruker AV300 spectrometer. Multinuclear NMR spectra were recorded using a Bruker DPX400 spectrometer references for each nucleus are given in Chapter 1. Electrospray (ES) MS data were obtained from solutions in MeCN using a VG Biotech Platform. Microanalyses were undertaken by Medac Ltd. Solvents were dried by distillation prior to use, CH_2Cl_2 from CaH_2, hexane from sodium benzophenone ketyl. Electrochemical measurements were undertaken using an Ecochemie PGStat20 with 0.1 $moldm^{-3}$ $[NBu_4][BF_4]$ in dry MeCN as electrolyte. Data collection used a Nonius Kappa CCD diffractometer fitted with monochromated (confocal mirrors) Mo–K_α X–radiation (λ = 0.71073 Å). Crystals were held at 120 K in a nitrogen gas stream.

Metal carbonyls were obtained from Aldrich and used as received. $Mn(CO)_5Cl$ was made from $Mn_2(CO)_{10}$ and Cl_2/CCl_4. *o*-$C_6H_4(CH_2SMe)_2$, *o*-$C_6H_4(CH_2SeMe)_2$ and $C(CH_2SMe)_4$ were prepared *via* the literature methods, references for each preparation are detailed in Chapter 3. Experimental details for preparations of 1,2,4,5-$C_6H_2(CH_2SMe)_4$, 1,2,4,5-$C_6H_2(CH_2SeMe)_4$ and $C(CH_2SeMe)_4$ are given in Chapter 2 section 2.4. $GaCl_3$, $InCl_3$, obtained from Aldrich and used as received.